NON-EQUILIBRIUM BEDLOAD TRANSPORT BY STEADY AND NON-STEADY FLOWS

A thesis
submitted in partial fulfilment
of the requirements for the Degree
of

Doctor of Philosophy in Civil Engineering

in the

University of Canterbury

Christchurch, N.Z.

by

ROBERT G. BELL

University of Canterbury

November 1980

TABLE OF CONTENTS

Page

ABSTRACT

The temporal and spatial response of an alluvial reach to imposed steady and non-steady flows is examined under non-equilibrium conditions, specifically the case where the bedload input at the upstream boundary is zero.

The experimental research to date in the areas of initial motion, steady flow and non-steady flow non-equilibrium bedload transport and general mathematical models for non-equilibrium alluvial conditions are reviewed. Some of the assumptions of the models are questioned, particularly the use of an equilibrium transport formula under transient conditions.

A qualitative approach to understanding the physics of the bed response is achieved by the development of conceptual models. Comparison procedures are also developed to resolve differences in bed-load transport rates, due to firstly non-equilibrium effects and secondly non-steady flow effects, from appropriate experimental data sets.

An experimental programme was designed to test the assumptions of the mathematical models by examining the bed response for different reach lengths and for both steady and non-steady flows.

The steady flow non-equilibrium transport rates were compared with comparable local equilibrium transport capacity rates at selected time intervals and spatial positions. In the comparison process, the same mean flow velocity is common to both states, enabling the transport rates to be compared. The difference between local equilibrium capacity rates and non-equilibrium rates exhibited a spatial and temporal variation, being a maximum at $x = 0^+$ and decreasing to a small value as the end of the local scour hole is approached.

The non-steady flow types tested were triangular translation waves and step changes in discharge. Non-steady flow non-equilibrium transport rates are compared with comparable steady flow non-equilibrium transport rates at selected time intervals. In this comparison process the mean stage and bed levels are equated for both states. Differences in transport rates between these two states were observed, due to a non-steady flow bed response effect. For step changes in discharge an initial transient phase is present, characterised by a temporal lag and a transport rate difference.

For translation waves, the bed response effect is more significant for the steeper waves, given the same wave peak discharge. The bed response effect is a maximum at the downstream end of the local scour hole and diminishes as the end of the general scour hole is approached. The bed response effect is intimately connected with the delayed response of the dune bedforms downstream of the local scour hole.

The performance of the mathematical model for the non-equilibrium state will be poor when the reach length is less than the general scour hole length due to the bed response effect and the use of an equilibrium transport formula.

Other aspects of reach response which receive attention include initial motion, bedforms, flow resistance and stage-discharge relations.

ACKNOWLEDGEMENTS

The research for this thesis was carried out in the Department of Civil Engineering, (University of Canterbury), whose head is Professor R. Park.

Special thanks are due to my supervisor, Dr. A.J. Sutherland, for his guidance, encouragement and helpful criticism during this study.

Appreciation is also expressed to the academic and technical staff of the Department of Civil Engineering. In particular I thank the following:

Professor I.R. Wood and Mr. P. Giddens for their helpful advice;

Messrs. A. Stokes, H. Pearce and F. Archer for assistance in the construction of equipment and the performance of experiments;

Messrs. H. Patterson, L. Gardner and H. Pearce for the photographic work; and

Mrs. Heather Crawley and Mrs. Christine Mackenzie for typing the manuscript.

I wish to thank my fellow students, particularly G.T. Proffitt, for their support and for rewarding discussions.

I appreciate my wife Ruth, for her companionship and devotion during this time.

I appreciate the interest and criticisms made by visitors to the Civil Engineering Department, namely Professor A.J. Raudkivi of the University of Auckland, Dr. W.R. White of the Wallingford Research Station, Dr. I. Beechi of the University of Florence and Dr. G.A. Griffiths of the Ministry of Works and Development.

I acknowledge the co-operation of Central Laboratories, Ministry of Works and Development, in allowing the use of their ultrasonic bed detector for experiments reported herein. For the duration of this study, the writer was supported financially by the University Grants Committee and the National Water and Soil Conservation Organisation. The latter also provided financial support for equipment and computing services. Their support is gratefully acknowledged.

LIST OF FIGURES

LIST OF PLATES

LIST OF TABLES

LIST OF SYMBOLS

(Note: Only the commonly used symbols are listed)

a,b	Constants
B	Channel width
C_d	Dune celerity
C_w	Translation wave celerity
d_{max}	Maximum local scour hole depth
D	Diameter of particles
D_{50}	Diameter of particles in a sample 50% of which is finer
e	2.7183 (Exponential constant)
e_s	Local erosion rate of particles from bed/unit width/unit time
f	Friction factor
Fr	Froude number
g	Acceleration of gravity
g_s	Bedload transport rate/unit width (dry weight)
g_{se}	Equilibrium transport rate/unit width or transport capacity rate
$g_{se}(x,t)$	Local equilibrium transport rate calculated from mean velocities/unit width
g_{se_o}	Initial equilibrium transport rate at t=0 for ST runs/unit width
g_s^*	Dimensionless bedload transport rate
G_s	Bedload yield/unit width (dry weight)
G_{se}	Equilibrium bedload yield/unit width
G_{ST}	Bedload yield at the end of the reach during the ST runs
G_{SC}	Bedload yield for the transition phase of the SC series
G_{NS}	Bedload yield for a translation wave of the NS series
G_{ST}^*	Psuedo bedload yield under the comparable steady flow non-equilibrium transport rate hydrograph

G_Y	Dimensionless bedload yield number
h	Stage level above a horizontal datum
k_s	Height of surface roughness projections
K	Constant
l	Step length of a single particle movement; length dimension
L_s	General scour hole length (approx)
n	Number of grain detachments/unit area/unit time; Manning's resistance coefficient
N	Dimensionless erosion rate
NS	Triangular Translation Wave series
p	Protruding distance of a grain into the flow above the surrounding bed; porosity
P_s	Bulk specific dry weight of sediment in the bed
q	Water discharge/unit width
q_c	Base flow/unit width at threshold conditions
q_o	Final water flow rate/unit width after a step change in discharge
q_{max}	Wave peak water discharge/unit width
r_{xy}	Correlation coefficient
R	Hydraulic radius
Re_*	Particle shear Reynolds Number
S_d	Dune Steepness - ratio of dune height to wavelength
S_f	Friction Slope
S_o	Bed Slope
S_s	Specific gravity of sediment grains, ρ_s/ρ
S_t	Strouhal Number
SC	Step Change in Discharge series
ST	Steady Flow Non-Equilibrium Transport series
t	Time
t^*	Temporal lag

T	Translation wave period
$u, \bar{u}$	Mean flow velocity
u_p	Mean velocity of sediment particles
u_{*_b}	Shear velocity on the sediment bed
V_g	Spherical volume of a single grain (mean diameter)
V_s	Transported bedload yield volume/unit width
x	Spatial coordinate in the direction of flow
x_R	Test reach length of erodible bed
y	Water depth where $y \doteq h-z$ if S_o is small
y_c	Water depth at threshold conditions
y_{max}	Water depth at the flood wave peak
Y	Shields Entrainment Function
Y_c	Threshold value of Y
z	Bed level above a horizontal datum
$\bar{z}$	Mean bed level over the reach length
Z	Relative roughness y/D_{50}
α	Proportionality; Angle between scoured bed surface and original bedlevel at the upstream end
γ_s	Submerged specific weight of sediment, $\gamma_w(S_s-1)$
γ_w	Specific weight of water, ρg
δ	Phase lag (radians); Boundary layer thickness
Δ_d	Dune height from max. crest level to min. trough level
$\Delta g_s', \Delta g_s$	Bedload transport rate deficit between actual and comparable rates due to the non-equilibrium effect (steady flow)
Δg_s^*	Bedload transport rate deficit between actual and comparable rates due to a step change in discharge (non-equilibrium)
$\Delta q, \Delta t, \Delta x$	Incremental changes in q, t, x
η	Dimensionless shear stress τ_o/τ_c
$\bar{\theta}$	Water temperature
λ	Scale ratio

λ_d	Dune wavelength
ν	Kinematic viscosity of water
ρ	Density of water
ρ_s	Density of sediment grains minus pore volume
τ_c	Shear stress at the threshold of bed motion
τ_o	Shear stress at the bed
$\emptyset$	Angle of repose of sediment

CHAPTER 1

INTRODUCTION

1.1 PROBLEM STATEMENT

Water flowing over a bed composed of cohesionless sediment exerts hydrodynamic forces on the sediment grains. If these forces are sufficiently large, a finite quantity of sediment will be entrained by the flow and transported according to the sediment load carrying capacity of the flow. The transport of sediment derived from the bed can be separated into two components : suspended sediment load where the grains were entrained into the main flow field and consequently move at the mean flow velocity; and bedload, where the grains are moved along the bed surface by rolling or sliding and occasionally by saltation into the flow near the bed, the velocity of the grains being much less than the mean flow velocity. Herein, only the bedload component of the sediment transport load will be considered.

Bed-material transport relations for alluvial channels are generally based on an equilibrium criterion. An equilibrium state for a given alluvial reach can be defined as a sediment transport input-output balance over a sufficiently long, but finite, time interval. However, conditions in natural alluvial channels are generally non-steady in either the flow phase or the sediment phase (defined as non-equilibrium) or both. Therefore channels, which are in equilibrium over long periods of time, may be subject to significant deviations or transients over much shorter time intervals. Transients in alluvial channels are commonly caused by : changes in the upstream sediment transport supply; introduction of man-made hydraulic structures e.g. sediment barriers and either inflow or outflow diversion of large

quantities of water; and non-steady flow conditions e.g. flood waves or abrupt changes from one equilibrium flow state to another.

Large, steep, gravel bed rivers are characteristic of New Zealand river systems. The stability of these rivers with regard to mitigation of floods and the effects of hydro-electric structures and irrigation diversions, is of economic importance. It is generally recognized that the bulk of the annual sediment yield of a river may be transported by only a few storm run-offs annually e.g. Waimakariri River, N.Z. {Griffiths (1979)}, and Wairoa-Waimea Rivers, N.Z. {Pemberton (1979)}. This is particularly true for coarser non-uniform gravel rivers where armouring of the bed surface can occur during sustained low to medium flows.

Modelling of the flow component, for both steady and non-steady flows, has met with a large measure of success. How the sediment phase under transient conditions is to be dealt with is, as yet, not clearly defined. Commenting on the future needs in the sediment field, Wolman (1977), suggested : (p51)

> "Both erosion and transport in natural systems vary with time. Perhaps a major need is to understand the way in which discontinuous (transient) transport processes take place in channels"

and concluded (p54)

> "... as always, we know very little in detail about the sequential microprocesses involved in erosion and sedimentation, but much about the gross impact of some climatic and flow conditions... From both a theoretical and practical point of view, more attention is needed to unsteady or transient phenomena of erosion and transportation."

Consequently, theoretical and experimental research in this area must be directed firstly; at understanding the physics of the phenomenon of non-equilibrium bedload transportation under steady and non-steady flows and secondly; at making quantitative predictions of the alluvial

system behaviour, in particular, the estimation of bedload transport rates and yields, the effects of bedforms on roughness and transport rates and the prediction of stage-discharge rating curves.

1.2 SCOPE OF THE THESIS

The work reported herein forms part of a continuing research programme aimed at understanding the spatial and temporal variation of the processes which occur during non-equilibrium conditions, subject to steady and non-steady water flows. In particular, non-equilibrium conditions within the general scour hole, which forms downstream of a fixed bed when the sediment input to the system is zero, were investigated. The fluid phase is restricted to steady flows, abrupt step changes in discharge from threshold conditions, and triangular translation or flood waves also beginning from threshold conditions. The sediment phase consists of uniform, cohesionless, gravel particles. Therefore armouring of a non-uniform gravel bed was not considered. Except for the establishment of equilibrium transport conditions, the sediment supply to the system was zero.

Threshold conditions were included as part of this study because of their importance in the determination of when scouring ceases for steady flow non-equilibrium conditions and because both the step changes in flow and the flood waves started from threshold conditions. The steady flow equilibrium transport state was studied briefly to serve as a check and a basis for comparison with the non-equilibrium state.

Chapter 2 is a review of the literature relevant to this study. It includes also a brief discussion of current mathematical models and specific problems to be examined in this thesis are posed.

In Chapter 3, the physical alluvial system is defined and its response predicted qualitatively using conceptual models for equilibrium and non-equilibrium transport conditions. Comparison procedures to

relate experimental transport rates from different states are also discussed.

Chapters 4 and 5 are devoted to a description of the design and procedures of the experimental programme and the apparatus used to obtain the relevant measurements.

Results of the experimental investigation are presented and discussed in Chapters 6,7 and 8 for the respective states listed below :

(1) Initial Motion and Equilibrium Transport
(2) Steady Flow Non-equilibrium Transport
(3) Non-steady Flow Non-equilibrium Transport

A set of conclusions and recommendations for future work are given in the final chapter.

All theoretical and experimental detail including formulae and data, not directly relevant to the thread of the main text, are relegated to the Appendices.

CHAPTER II

LITERATURE REVIEW

2.1 SYNOPSIS

A review of previous research in the fields of initial particle motion, steady and non-steady flow non-equilibrium bedload transport and non-steady bedform development is presented. The implications of the established research results relevant to the study herein are discussed, leading to specific areas of need, which have been set as a guide for the research programme.

2.2 INITIAL MOTION

A turbulent flow of water, over a non-cohesive sediment bed, exerts hydrodynamic forces on the solid grains comprising the bed surface layer. These forces fluctuate with time but conform to a certain mean value, given constant flow characteristics. For small flow intensities, most of the solid particles remain in position, because the resisting forces acting on the particles are greater than the applied hydrodynamic forces {Raudkivi (1976)}. As the flow intensity increases, greater numbers of particles are displaced by the fluctuating applied forces when their magnitude is instantaneously greater than the resisting forces, even if mean conditions do not produce movement. Hence the definition of a critical or initial motion condition by various researchers has tended to be subjective resulting in a wide array of initial motion formulae, as shown by Chien (1954), whose Figure 4 shows that predicted values of critical tractive force can differ by up to an order of magnitude for a given mean grain diameter.

The classic work on the initiation of motion is that of Shields

(1936). He showed that the process could be represented by :

$$\frac{\tau_0}{\gamma_s D_{50}} = fn\left(\frac{u_{*_b} D_{50}}{\nu}\right) \quad \ldots (2.1)$$

or $$Y = fn\ (Re_*)$$

where Y is the Shields Entrainment function and Re_* is the particle Reynolds Number. The other symbols are defined as : τ_0 = mean bed shear stress, $\gamma_s = g(\rho_s - \rho)$ which is the submerged specific weight of sediment, D_{50} = mean grain size, u_{*_b} = bed shear velocity = $(\tau_0/\rho)^{1/2}$; ν, ρ = kinematic viscosity and density of the fluid respectively and ρ_s = the density of the sediment grains.

Shields obtained the critical mean bed shear stress by an extrapolation process back to a zero transport rate. However, in practice one has no alternative but to identify the initial motion of grains by a certain degree of established sediment transport. Paintal (1971a) measured transport rates for a wide range of Shields Entrainment function below the Shields curve*, defined by equation 2.1, for $Re_* > 38$. He found that the relationship between the sediment transport rate and the entrainment function Y, for $g_s^* < 10^{-2}$, was a high 16th power correlation, where

$$g_s^* = \frac{g_s}{\rho g S_s D_{50} \left[(S_s - 1) g D_{50}\right]^{1/2}} = K\, Y^{16} \quad \ldots (2.2)$$

where $K = 6.56 \times 10^{18}$, S_s is the specific gravity of the sediment and g_s is the bedload transport rate (dry weight/unit width/unit time). Pazis and Graf (1977) obtained an 8th power correlation for equation 2.2, for $g_s^* < 5 \times 10^{-3}$. Taylor (1971) established a similar relationship to equation 2.2, with measured bedload transport rates, using $(g_v/u_{*_b} D_{50})$ instead of g_s^*, where g_v = the volumetric bedload transport rate/unit width. He found a similarly high power correlation of 17.5.

*drawn later in 1939 by H. Rouse

It is clear, despite the wide range of exponent values, that a small increase in Y, and therefore bed shear stress, causes a major change in the transport rate. There are thus real difficulties associated with the definition of a critical shear stress when the transport rate is "zero".

For initial motion conditions, what is needed is an arbitrary, flexible definition, specifying the degree of movement which is acceptable in any given situation. Neill (1968) and Neill and Yalin (1969) introduced this approach by incorporating a new parameter n, which is the number of grains detached per unit area per unit time, into equation 2.1. They showed that the following relationship obtains,

$$\frac{n\, D_{50}^3}{u_{*b}} = fn\left(\frac{u_{*b}\, D_{50}}{\nu}, \frac{\tau_0}{\gamma_s D_{50}}\right) \qquad \ldots (2.3)$$

or $$N = fn\,(Re_*, Y)$$

where N is the dimensionless erosion rate. Thus an initial motion criterion could be obtained by choosing a value of N. In this way, the subjective nature of a qualitative criterion and also the problems associated with an extrapolation process, are avoided.

One influence however, which will affect the quantitative erosion rate apporach, is the manner in which the particles are packed on the bed surface. Fenton and Abbott (1977) demonstrated that the threshold Shields Entrainment function possessed a marked dependence on the relative protrusion (p/D_{50}) of grains into the flow stream above the surrounding bed. For example, they found that the threshold value of $Y(=Y_c)$ of a spherical grain resting on the top of an otherwise plane bed of spherical grains ($p/D_{50} = .82$), was 0.01, which is considerably less than the value of 0.056 for the rough turbulent zone of the Shields curve.

2.3 STEADY FLOW, NON-EQUILIBRIUM TRANSPORT

2.3.1 Introduction

Past research of alluvial systems has centred on steady and uniform conditions with regard to both the flow and sediment phases e.g. reviews by Shen (1971), Graf (1971), Raudkivi (1976) and Yalin (1977). However, many of the dynamic processes which shape the river bed resulting in degradation or aggradation, are due to non-equilibrium transport conditions, and as such are non-steady processes even though the water discharge may be steady. After an alluvial system attains equilibrium with the upstream supply of sediment load, non-equilibrium conditions can result if a change occurs in that supply; an increase leading to deposition of sediment (aggradation) and a decrease leading to erosion of bed material (degradation). Herein, only the degradational case will be reviewed, but local scour due to obstructions and constrictions in the flow will not be considered.

The critical case for any degradation or scour process occurs when the sediment supply is practically reduced to zero due, for example, to the influence of hydraulic structures such as dams and culvert outlets. Estimation of the time development of local scour and the final equilibrium scour depth immediately below a hydraulic structure, together with estimation of the general degradation which occurs further downstream of the local scour hole, are problems continually faced by engineers. An early discussion of this problem was written by Lane (1934).

2.3.2 Experimental Research

There are many varieties of local scour systems below hydraulic structures, each with its own particular geometry and hence local scour mechanisms. Some of these geometric configurations are shown in Simons and Sentürk (1977, p702).

Experimental research with water jets and free overfalls im-

pinging on an alluvial bed, which has been prevalent because the flow could be represented simply by a constant velocity and a linear dimension, led to a clearer understanding of local scour and its development with time. Examples of such experimental research are : Laursen

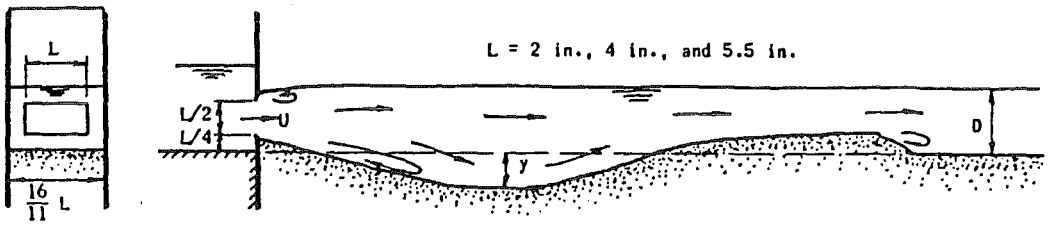

Models of Submerged Opening

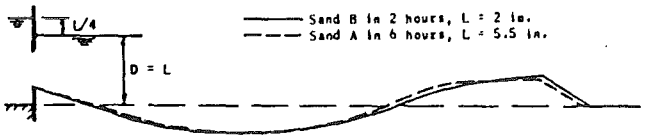

Similarity of Scoured Beds in Models of Submerged Opening

FIGURE 2.1 : Local scour hole profile resulting from the action of a submerged jet, (after Li (1955))

(1952), Rajaratnam and Berry (1977), A.S.C.E. (1975, p49-58), Li (1955) and several papers under the heading, "Erosion and Local Scour Downstream from Hydraulic Structures" in the Proceedings of the 12th Congress, Volume 3, of the I.A.H.R. (1967). A typical scour hole due to scouring by a submerged jet is shown in Figure 2.1, after Li (1955), where further downstream, threshold conditions are usually present on the original bed surface. Various stilling basin geometries and steps immediately upstream of an erodible bed have also been extensively tested e.g. Novak (1961), Schoppmann (1975) and Doddiah (1967).

Although the geometric configurations were different, some principles of local scour are common to most cases. Chuna (1975) outlined four distinct phases present during experiments of the develop-

ment of any local scour phenomenon. These may be listed as :

(1) Initial transition phase from t = 0, where $d_{max} = 0$, up to the start of the first principal phase. This initial phase is a relatively short period and one of rapid scouring. (d_{max} = maximum scour depth at any time t)

(2) Principal phase 1, where the rate of scour decreases as the bed profile is enlarged and deepened. It is usually governed by the relationship

$$\frac{d_{max}}{y} = at^b \qquad \ldots (2.4)$$

where a,b are constants describing the characteristics of the flow and bed sediment, and y is the flow depth or other suitable linear dimension.

(3) Transition phase between the two principal phases where the final principal phase is approached asymptotically.

(4) Principal phase 2, the final phase where equilibrium is reached for a given set of initial conditions and geometric properties.

Fewer experimental tests have been carried out to examine the local scour and general degradation downstream of a fixed rough plane bed or armoured protection layer, where the flow onto the erodible bed was subcritical* as distinct from supercritical flow for water jets and from free overfalls. Colaric, Pichon and Sananes (1967) and Breusers (1966) performed experiments using uniform sized sediment and found that the relationship

$$d_{max} \propto t^b$$

was relevant for the first principal phase after an initial transition

*Froude Number of the flow is less than 1.0

period. Breusers confirmed that local scour profiles with the same dimensionless maximum depth $\left(\frac{d_{max}}{y}\right)$, where approximately the same in different bed materials and found that the value of the exponent b was 0.38. Watkins (1969) also carried out local scour experiments downstream of a short plane bed, but used a roof on the flume, (i.e. effectively a rectangular conduit), to keep the depth constant. The absence of a free surface, which will introduce a different pressure distribution across the flow field, may have affected the results in comparison with free surface flows. After an initial transition phase, he obtained a relation of the form

$$d_{max} \propto \log t^{n}$$

for various gravel materials. Ettema (1980) conducted local scour experiments, where a break was made in an armoured protection layer, until a new equilibrium bed level was reached downstream of the intact upstream armour layer. He derived an approximate formula for the final equilibrium maximum scour depth d_{max_e} as

$$d_{max_e} = (y_2 - y_0)\eta \qquad \ldots (2.5)$$

where y_0 = upstream flow approach depth, y_2 = flow depth corresponding to threshold conditions on the general degraded bed further downstream from the localised scour hole and η = 1.3 to 2.6 for D_{50} > 0.7mm and η = 1.0 for D_{50} < 0.7mm, (ripple forming sediment).

The profile shape of the local scour hole, which forms downstream of a fixed rough apron, and its interaction with the general degradation downstream, are also important considerations. With time, the scour hole profile will lengthen indefinitely as the deepest section of the scour hole (or scour pit) approaches it equilibrium depth. The bedform, which the downstream extremity of the local scour hole takes, is likely to be related to the bedform regime which exists further downstream e.g. for a ripple regime a ripple bedform is present

at the end of the local scour hole, Figure 2.2, after Raudkivi (1965). This is a different situation from the local scour experiments using water jets and free overfalls shown in Figure 2.1, where downstream

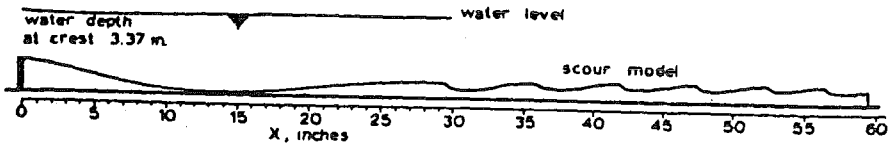

FIGURE 2.2 : Local scour hole profile due to a subcritical flow, (after Raudkivi (1965))

of the dune bedform, a plane bed exists due to the presence of threshold conditions. Padmavally et al.(1980) similarly postulated, for a fixed rough upstream apron geometry, that perhaps dunes could be present on the bed, downstream of the dune bedform at the downstream extremity of the local scour hole, although her flume length (approximately 1 m) was too short to observe this phenomenon. Besides analysis of the scour hole development and shape, measurements and observation of turbulence structures and vortex systems within the local scour hole have been made e.g. Breusers (1966), Gruat and Pichon (1971) and Raudkivi (1965). These measurements have highlighted the effect of the complex flow field within the scour hole on the shape and development of the resultant local scour. Breusers (1975) has attempted to describe mathematically this complex flow field by using the analogy of a free turbulent shear flow past a step expansion in a fixed channel floor. He obtained reasonable agreement between computed and measured velocity profiles and static pressure distributions.

2.3.3 Mathematical Models

Numerous mathematical and numerical models have been developed to estimate the local scour and general degradation, as a function of time, downstream of a sediment barrier such as a dam. As the process

of general degradation in a river occurs over a long time period, (0 {years}), most of the formulae and computational processes, understandably, apply to conditions where the discharge is assumed to be constant.

The closed equation set generally used is set out below :

Flow Phase

Non-uniform steady flow equation

$$\frac{d}{dx}\left(z + y + \frac{u^2}{2g}\right) = -S_f = -\frac{u|u|f}{8gR} \qquad \ldots (2.6)$$

where z = bedlevel above a horizontal datum, S_f = friction slope, f = friction factor and R = hydraulic radius.

Sediment Phase

Continuity equation

$$\frac{\partial z}{\partial t} + \frac{1}{P_s}\frac{\partial g_s}{\partial x} = 0 \qquad \ldots (2.7)$$

Momentum equation (transport formula)

$$g_s = fn(u,y)$$

or

$$g_s = fn(\tau_0 - \tau_c) \qquad \ldots (2.8)$$

where P_s = bulk specific dry weight of sediment in the bed and τ_c = critical or threshold shear stress.

The computational procedure using forms of the above equations has been set out by Gessler (1971) as follows :

(1) Evaluation of S_f and the water surface profile along the given alluvial reach, at intervals of (Δx), for a chosen time interval using equation 2.6.

(2) Computation of the corresponding sediment transport rate along the reach using the equilibrium

transport equation 2.8.

(3) Application of the sediment continuity equation 2.7 over the channel segments within the reach to find the degradation (Δz) of the bed.

(4) Determination of a new bed profile, $z_0 - \Delta z$.

(5) Return to (1) for the next time interval.

The final equilibrium profile is reached asymptotically as critical conditions on the bed are approached. Similar degradation models have been proposed by de Vries (1973), Cunge and Perdreau (1973), Aksoy (1971), Komura (1971), Hwang (1975), Ashida and Michiue (1971) and Hales, Shindala and Denson (1970). The authors of the latter four papers have also attempted to model the armouring process for non-uniform bed materials, which is important in almost all field applications, when degradation will cease at a much earlier stage due to the formation of an armour protection layer. All the mathematical models use a down-stream grade control in the bed such as a rock outcrop, about which the degrading bed slope rotates. Field studies of degradation below dams have been compiled by Lane (1955) and Priest and Shindala (1974).

Objections to the computational procedure of these models include the use of an equilibrium transport formula and the neglect of the bed material already in transport within each distance segment Δx. This neglect occurs if the time interval Δt, over which the computational procedure outlined above {Gessler (1971)} is carried out, is short e.g. when sediment transported in one step Δt does not have sufficient time to leave the distance segment Δx. Consequently the erosive capacity of the flow for the new time step will be reduced. Clearly non-equilibrium conditions exist immediately downstream of a hydraulic structure, as any flow requires a finite length of channel bed to erode enough sediment to meet its steady flow transport capacity. Bogardi (1965) observed that confusion between <u>equilibrium</u>

transport capacity and actual sediment load, frequently resulted in appreciable discrepancies during the calculation of sediment transport, sometimes by using an equilibrium transport formula when non-equilibrium conditions existed. Tinney (1962), used a similar degradation computation procedure as outlined by Gessler, using the experimental results of Newton (1951). The mentioned problem of transport equations was circumvented by adjusting the coefficients of an equilibrium transport formula to match the experimental bedload rates.

It can be seen that the use of an equilibrium transport rate for a non-equilibrium state, is a crucial point of the computational procedure, as noted by Gessler (1971). This objection, together with the neglect of sediment in transport if the time step is short, will lead to an overestimation of the depth of degradation. For the contrasting case of aggradation, Soni, Garde and Ranga Raju (1977) found in general, that the actual transport rate was smaller than that under uniform flow conditions for a particular mean velocity ($\bar{u}$). They also concluded, that a uniform flow resistance relationship could be used under non-uniform conditions, provided the local friction slope is used in place of the bed slope. These findings are likely to be applicable to the degradation case also.

2.4 NON-STEADY FLOW, NON-EQUILIBRIUM TRANSPORT

2.4.1 Introduction

Many cases of degradation can be treated assuming the flow is steady when the discharge-time hydrograph variations are gradual. However, there are cases in which the flow must be treated as non-steady and therefore the acceleration terms due to the changing discharge must be added to the analysis. Thus for a non-equilibrium state, the non-steady effects on the bedload phase are not only caused by a change with time of the transport capacity due to the degrading bed

level, but also by changes in the transport capacity due to the changing flow discharge. Thus the need to define this state as a non-steady flow, non-equilibrium transport condition.

2.4.2 Experimental Research

Experimental data reflecting bedload transportation by non-steady flows is extremely limited in both scope and quantity, and has lagged considerably behind the development of mathematical models.

de Vries (1965) created a long transition phase between two steady flow equilibrium transport states by a sudden step change in water level but maintaining the discharge and input sediment supply constant throughout. He found that the response of the bed was slow and thus questioned the use of an equilibrium transport formula to describe the local bedload transport during the transition phase.

Sutherland and Griffiths (1975,1977) and Griffiths (1976) using two sets of steady flow and triangular translation wave experimental results, compared the bedload transport rates at several different times during the wave period with comparable steady flow transport rates at the same time. For the non-equilibrium case, where the upstream sediment supply was zero, it was found that the bedload transport rates obtained during the translation waves were less than the comparable steady flow transport rates, which were derived by a comparison procedure. The qualitative reason put forward was that the differences between comparable steady flow and non-steady flow transport rates were caused by changes in entrainment of bed-material occurring more slowly than the changes in discharge.

2.4.3 Mathematical Models

Extensive development of mathematical models to simulate the deformation of an alluvial bed due to non-steady flows has been achieved in recent years. Essentially the work has been concerned with

formulating an analytical model where the water behaviour is described by the St. Venant Equations and the sediment behaviour by the Exner erosion equation and an equilibrium transport rate predictor. The simplest one-dimensional model takes the following form :

Flow Phase

$$\frac{1}{g}\frac{\partial u}{\partial t} + \frac{u}{g}\frac{\partial u}{\partial x} + \frac{\partial y}{\partial x} = S_o - S_f \qquad \ldots (2.9)$$

$$u\frac{\partial y}{\partial x} + y\frac{\partial u}{\partial x} + \frac{\partial y}{\partial t} = 0 \qquad \ldots (2.10)$$

Sediment Phase

$$\frac{\partial g_s}{\partial x} + P_s\frac{\partial z}{\partial t} = 0 \qquad \ldots (2.11)$$

$$g_s = fn(u,y,....) \qquad \ldots (2.12)$$

where $S_o = -\partial z/\partial x$ = bedslope. Usually the equilibrium transport predictor (in lieu of a sediment momentum equation) is given in the simplified form

$$g_s = a\,\bar{u}^{\,b} \qquad \ldots (2.13)$$

where $\bar{u} = q/y$ = mean flow velocity and a,b are constants. However, equation 2.13 must necessarily be applied as a piecewise function, as the equilibrium transport rate relation curves downwards on a logarithmic plot, as threshold conditions are approached.

Attempts at modelling the non-steady flow, non-equilibrium transport state, by various researchers, based on equations 2.9-2.12, have been made in a variety of ways, as shown in Figure 2.3. de Vries (1965) presented a graphical representation of the three characteristic celerities obtained from the governing equations; two for the water flow and one for the bed phase. He concluded that for flows in which the Froude Number was less than 0.6, or if low transport rates were

present, then the characteristic celerities of the fluid flow may be assumed to tend to infinity in comparison with the bed celerity. On the basis of this simplification, several mathematical models, (Figure 2.3), were proposed in which the flow was regarded as steady during each time step i.e. the inflow discharge hydrograph was transformed into a series of stepped constant discharges. The governing equations then reduce to the steady flow equation set, 2.6-2.8, for each time step. This approach has been dealt with in two ways; firstly the uncoupled mode where the flow and the bedlevel computations are completed sequentially and the required flow depth adjustments made for each time step, or secondly, the coupled mode where the governing equations are solved simutaneously when the bed deformations are assumed to be large during the time step.

The other approach has been to solve the complete dynamic equation set, 2.9-2.12, particularly if the system is subject to changes in discharge where the local acceleration terms $\frac{\partial y}{\partial t}$ and $\frac{\partial u}{\partial t}$ are significant, over each time step. The mathematical models in this category employ one of two numerical schemes, (Figure 2.3), the characteristics or the finite difference methods. The latter method can once again be coupled or uncoupled with regard to the water flow and bed level computations, depending on whether

$$\left.\frac{\partial y}{\partial t}\right|_{z = \text{const.}} >> \left.\frac{\partial y}{\partial t}\right|_{q = \text{const.}}$$

, {Miloradov et al. (1971)}.

A hybrid simulation model was developed by Sakhan, Riley and Renard (1972). They employed a systems engineering approach to solve a generalised version of equations 2.9-2.11 for ephemeral streams, combined with a stochastic sediment transfer equation which included the bedload and suspended sediment fractions.

Few of the mathematical models e.g. Bennett et al.(1977) and

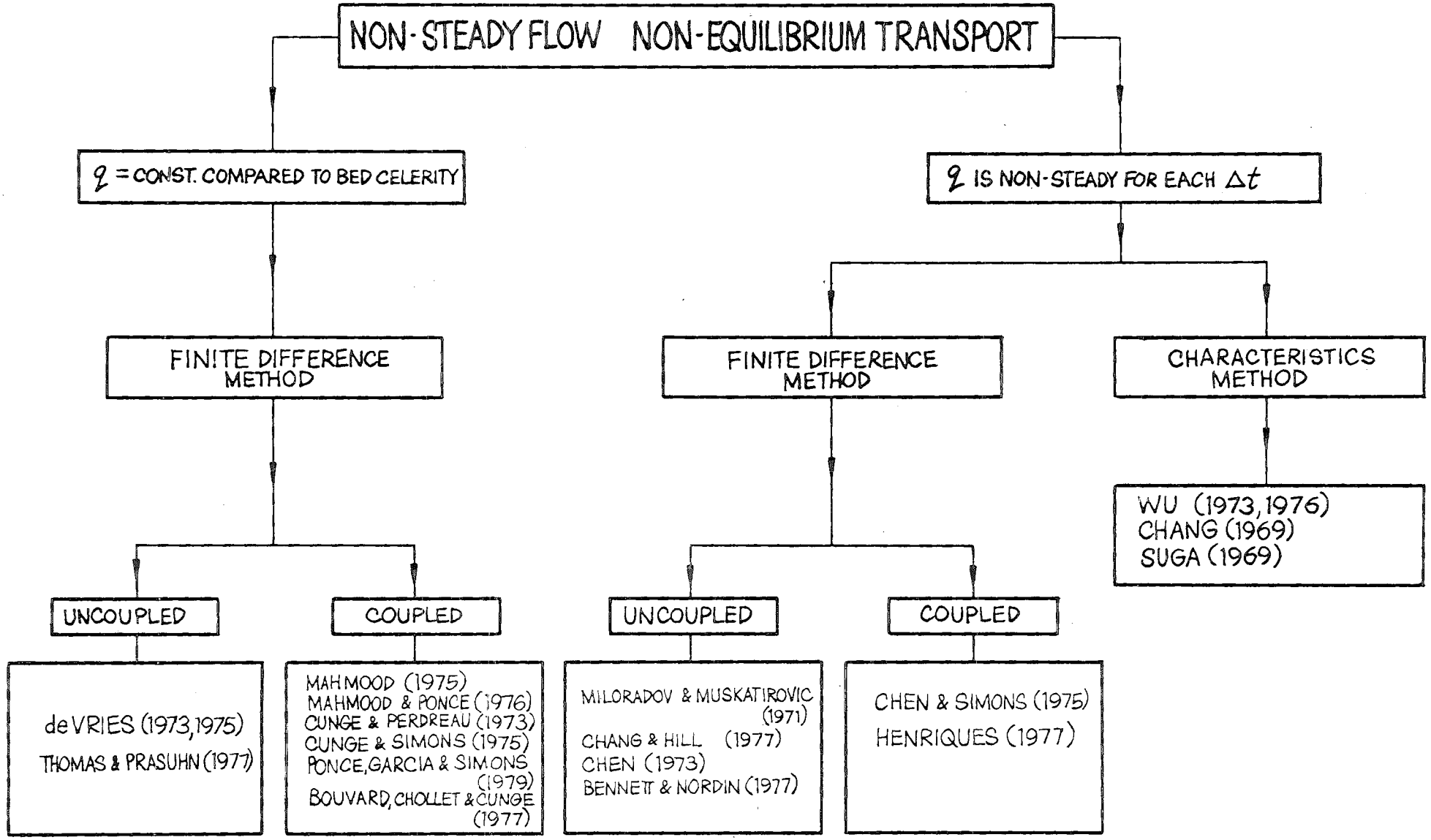

FIGURE 2.3 : Non-steady Flow Mathematical Models

Chen (1973), included the effect of the armouring process during degradation. For high flood flows, armouring is unlikely to be significant until the advent of the slowly falling recession curve.

For fixed bed cases, the non-steady water flow computation based on the St. Venant equations, has proved highly successful in the prediction of transient flows; Gunaratnam and Perkins (1970) and the review by Mahmood and Yevjevich (1975). For the movable bed model, where sediment motion is considered, Chen (1973) states that the mathematical model may reasonably describe the bed deformation, provided the sediment load and the armouring effect can be accurately determined. As stated previously in section 2.3.3, the use of an equilibrium transport predictor may be suspect for certain steady flow, non-equilibrium states. If the changes in bedload entrainment occur more slowly than changes in discharge, then the uncertainty associated with the use of an equilibrium formula in a non-steady flow, non-equilibrium transport state will be compounded. Padmavally (1977) has made an unjustifiable development of the mathematical model by introducing a general momentum equation for the bedload layer in place of an equilibrium transport formula. She then proceeded to assume that the shear stress and the mean bed particle velocity, at any point x and time t, were the same as if the transport rate there was steady and uniform, because of a lack of non-steady flow data.

2.5 BEDFORMS

2.5.1 Experimental and Field Research

Researchers have achieved some success in describing empirically the realationship of various bedform types and their geometric properties with gross parameters describing the steady flow hydraulic conditions e.g. reviews by Yalin (1977), Simons and Şentürk (1977), Raudkivi (1976) and Graf (1971). Herein, only the lower tranquil reg-

ime, with regard to the bedform type of Simons and Richardson (1961) will be considered.

Field and experimental observations during non-steady flows have shown that the development of bedforms can deviate considerably from steady state predictions, using the instantaneous hydraulic parameters.

Field observations of bedforms which experience a temporal lag behind corresponding changes in discharge have been documented, predominantly on sand bed rivers e.g. in the Red River by Neill (1969), the tidal reaches of the Weser River by Nasner (1973) and in the Mississippi River by Carey and Keller (1957). The latter authors noted that sand dunes on the Mississippi River were "smaller than they should be" on the rising limb of a flood wave and "larger than they should be" on the receding limb. Nasner (1973) found that for a dune configuration in the Weser River :

(1) The bedform height varied more than its length

(2) There was a phase lag between a change in discharge and a change in bedform height

(3) The stage of equilibrium was reached sooner for an increasing discharge than for a decreasing discharge

Experimental evidence for the temporal lag associated with the imperfect adjustment of bedforms to changes in flow has been obtained by; Simons, Richardson and Haushild (1962), Jensen (1973) and Griffiths (1976) for flood waves; Gee (1975), Raichlen and Kennedy (1965) and Yalin (1975) for step changes in discharge or for an initial artificial plane bed; and Bayazit (1969) for reversing or periodic flows. Simons et al. (1962) found that the type of bedform, consistent with a certain discharge, did not have the required time to develop fully before the imposition of a new discharge produced from a stepped triangular hydro-

graph. Thus they concluded that the resistance to flow also lagged behind. Bayazit (1969) likewise found that non-steadiness in reversing flows had an influence on the resistance because of the temporal delay required by ripples to adapt to the new flow conditions.

Jensen (1973) and Griffiths (1976) measured the geometric properties of dunes under triangular translation waves using polystyrene balls (D_{50} = 1.5mm) and gravel (D_{50} = 4.02mm) respectively. The dune height was found to follow the water hydrograph, but with a certain lag, while the dune wavelength continued to increase throughout the wave passage. Gee (1975) examined bedform response by forcing an alteration in dune characteristics between two discrete steady flow equilibrium states using sand-sized sediment. The principal conclusions he arrived at, were that dune growth proceeded at a greater efficiency than dune destruction and that the bedload transport is a necessary condition for changes to occur in dune dimensions. Raichlen et al. (1965) and Yalin (1975) studied the growth of sand dunes from a plane bed and found that the change in bedform size is initially rapid, followed by a period of slower growth as the equilibrium state was approached.

2.5.2 Mathematical Models

Mathematical models to determine the response of dunes to non-steady flows have been attempted by Allen (1976a,b), Fredsøe (1979) and Puls, Sundermann and Vollmers (1977). Allen (1976b) separated the response of dune into two categories, in the first of which the response occurs at a much faster rate :

(1) Change due to modification of individual bedforms

(2) Change due to a creation-destruction process, where the original dunes are replaced by others more suited to the new flow conditions.

To formulate the rate of change of the dune configuration with time,

Allen introduced several empirical constants and assumptions. One assumption being that the discharge was strictly periodic with a long base period e.g. one year. Thus short term fluctuations due to individual storm runoffs were ignored. This assumption will be more severe for gravel rivers, where the bulk of the bedload yield, and thus the greatest rate of change of bedforms, occurs in these individual storm runoffs.

Fredsøe (1979) modelled the response of dunes to sudden step changes in flow, where the change of the bedform configuration was by modification of the individual bedforms. Incorporating the changing resistance to flow during the transition period, he compared his model with results from the experiments of Gee (1975) and obtained satisfactory agreement. By linearising his general equation set, Fredsøe determined typical phase lags and response time scales for the water depth, grain resistance and dune steepness for weakly periodically varying flow, where small changes in discharge were assumed.

Puls et al. (1977) based their model of non-steady bedform propagation on the general two dimensional Navier-Stokes equations and a transport rate computation scheme. The transport rate computation, which modelled the sediment transfer processes of erosion, transport and sedimentation and the effects of turbulence, was assumed to be more suitable for bedform analysis than an equilibrium transport formula.

The transport of bedload and bedform propagation are intimately connected, when bedforms are present on the bed. With the advent of the sonic bed sounder, several formulae have been proposed for the computation of the bedload transport rate from the bedform configuration of the form

$$g_s = P_s \frac{\bar{C}_d \bar{\Delta}_d}{2} \quad \text{(N/s/m)} \qquad \ldots (2.14)$$

for a triangular shaped bedform, where $\bar{C}_d$ and $\bar{\Delta}_d$ are the mean celerity

and height of the dunes respectively; Simons, Richardson and Nordin (1965). A similar form has been derived by stochastic methods for a random bedform configuration by Hubbell and Sayre (1964) and Shen and Cheong (1977). Therefore a lag in the response of dune bedforms to non-steady flows may induce a lag in the response of the bedload, (the reverse is also true where the bedload response affects the bedform response), provided the combination of the dune celerity and height magnitudes also lags behind.

2.6 RESISTANCE AND STAGE-DISCHARGE RELATIONS

2.6.1 Introduction

The relevance of the experimental bedform research in this context is, that if dunes do appear and undergo different development from that in comparable steady flows, then loops will be produced in the stage-discharge curves. Furthermore, the flow resistance, whether assessed in terms of total shear stress or total friction factor, will be overestimated on the rising limb of a flood wave, and underestimated on the falling stage compared with the equilibrium state, as found by Simons et al. (1962).

2.6.2 Resistance

Several methods have been devised to determine the total resistance offered to the flow by the erodible sediment bed; reviews by Simons and Şentürk (1977), Graf (1971) and Raudkivi (1976). The total resistance, assessed by shear stress, friction slope or friction factor, can be separated into two components as first proposed by Einstein (1950). The first component described the grain roughness or surface drag and the second component represented the bedform roughness or form drag, thus

$$f = f' + f'' \quad \text{or} \quad \tau_o = \tau_o' + \tau_o'' \qquad \ldots (2.15)$$

where f is the friction factor and the superscripts (′), (″) refer to the grain and form roughness respectively. Commonly used methods, incorporating formulations for both resistance components, to compute the total resistance to flow, are those of Einstein and Barbarossa (1952) and Engelund and Hansen (1967), although considerable scatter of data from experiments and natural channels has been shown.

These two methods have been incorporated into the non-steady flow mathematical model, Cunge and Simons (1975) and Bouvard et al. (1977), to replace the commonly used single valued Manning relationship. Thus changes in resistance to flow, due to variations in the development of bedforms with discharge, are taken into consideration by the more complex resistance predictors, and will lead to a more realistic simulation of the flow phase. The comparison of the model of Cunge et al. (1975) with experimental flow results was satisfactory for the flow phase, but the comparison of the sediment transport rate was once again poor, due to the use of an equilibrium transport formula, which overestimated the sediment transport concentration.

2.6.3 Stage-Discharge Relations

In natural channels, the stage-discharge rating curve, at a particular site, is not necessarily single valued, particularly for sand bed rivers where discontinuities may occur. Richardson and Simons (1973) state that shifts in the rating curve and hysteresis effects can occur due to scour and fill of the bed and/or banks, changes of the energy slope and changes in resistance to the flow resulting from changes in bedform configuration. Changes resulting from scour and fill can be eliminated by using a depth-discharge relation. The other two factors mentioned by Richardson et al. (1973) will cause loops or a hysteresis effect in the depth-discharge rating curve.

Many stage-discharge rating prediction methods, using various

resistance formulations, have been developed for steady flows in alluvial channels, {A.S.C.E. (1975), p126-152}. The methods give different estimates and the user is invariably left to make a judgement as to the most appropriate value for his particular situation.

Simons et al. (1962) also examined the variation of the depth-discharge relation resulting from changes in bedform type and size, by routing a stepped hydrograph through a sand bed flume. The following observations were noted for the lower flow regime, where ripples and dunes were present :

(1) For the rising stage, the resistance lagged the increase in discharge, because the bedform roughness also lagged behind. Hence the depth was less than it would have been, if the bedforms could respond perfectly.

(2) The opposite was true of the falling stage, where the dunes were larger (and therefore the resistance) than required for equilibrium conditions. Therefore the depth was higher than that obtained for the same discharge on the rising stage.

(3) The magnitude of spread of this hysteresis effect was found to be dependent primarily on the variation of bed roughness which was influenced by the rate of change of discharge with time as well as other sediment and flow parameters.

Henderson (1966) also points out that the hysteresis effect on the stage-discharge relation can also be caused by the dynamic effects of the flood wave motion. The reason is that slope terms other than the bedslope, S_o, prescribe that the discharge is not a single-valued function of depth. Sensitivity of these dynamic effects to the size and shape of the stage-discharge loop have also been investigated numerically by Ivanova (1967).

2.7 IMPLICATIONS FOR THIS STUDY

This literature survey indicates areas in which research work would be most useful. Of the many, the need for experimental data must be a high priority. Specific aspects are :

(1) Further work is needed to test the usefulness of Neill's (1968) quantitative definition of initial motion. More data is also required to firmly establish the power correlation between the dimensionless transport rate and the shear stress.

(2) It appears that the properties and response of mathematical models for the steady flow, non-equilibrium state have been reasonably well explored theoretically. What is required now is more experimental and field data to determine the range of applicability of the assumptions made in the derivation of the models. This particularly applies to the use of an equilibrium sediment transport predictor in a non-equilibrium situation e.g. degradation, as similarly investigated by Soni et al. (1977) for aggradation.

Further experimental research is also required so that the dynamic processes and the shape of the local scour hole, which forms downstream of a solid fixed apron, may be more clearly understood.

(3) The mathematical model for the non-steady flow, non-equilibrium state has also been reasonably well explored theoretically in terms of computational procedures. However, the experimental and field data base for bedload transportation under non-steady flow conditions has lagged considerably behind the theoretical development of the model.

The same comments in (2) apply with regard to the use of an equilibrium transport formula, and will be reinforced if the bedload response lags the rate of change of discharge with time, as found by Griffiths (1976).

The experimental data base for non-steady non-equilibrium transport conditions must be extended before improvements can be made to the mathematical model. What is unknown are the temporal and spatial variations of the bedload response to various transient flows.

(4) The development of bedforms under non-steady flows and its connection with the resistance to flow, transport rates and stage-discharge relations has been explored tentatively, mainly with regard to sand bed-material. What the situation might be for coarser gravel materials and steep flood waves remains relatively unexplored.

Thus, although the theory is well substantiated for steady flow equilibrium transport situations, there are difficulties in its application to natural rivers, because seldom does the simplified steady state exist. It is believed that this study makes a contribution by seeking to comprehend the specific points outlined above.

CHAPTER III

THEORETICAL CONCEPTS AND COMPARISON MODELS

3.1 SYNOPSIS

In this chapter the physical alluvial system examined in this thesis is defined. Conceptual models and bedload transportation principles, relevant to the physical system, are discussed to gain an insight into the bed response as a background for the quantitative experiments which are discussed in the following chapters. Analytic models for alluvial systems are reviewed and an experimental model presented so that comparisons between steady and non-steady flows can be accomplished.

3.2 ALLUVIAL SYSTEM RESPONSE

3.2.1 Definition of the System and Internal Interactions

The physical system considered is a constant width, finite length channel with a constant initial slope and a bed composed of fine uniform gravel particles ($D_{50}^{*} =$ 2mm). The erodible section is set longitudinally between two fixed lengths of roughened bed which act as buffers to prevent flow non-uniformities entering the system. The system is operated in an open circuit fashion where sediment, which may or may not be added at the upstream end, is completely removed and measured at the downstream end. Three types of flow input to the system will be considered; steady uniform flow, gradually varied non-steady flows with linear changes in discharge with time, and rapidly varied flow with sudden step changes in discharge. The two types of sediment input considered are an equilibrium transport rate and zero input. The boundary and initial conditions for the physical system

(Figure 3.1) with combinations of the above inputs are summarised below :

($g_s(x,t)$ is the bedload transport rate/unit time/unit width and $q(x,t)$ is the water discharge/unit width.)

(1) Equilibrium Transport

Sediment : $g_s(o,t) = \bar{g}_s(x_R,t) = \text{constant}$

Water : $q(o,t) = q(x_R,t) = \text{constant}$

(where x_R is the reach length)

(2) Non-Equilibrium Transport

(a) Steady Flow

Sediment : $g_s(o,t<o) = \text{constant}$, $g_s(o,t>o) = 0$

$g_s(x_R,t) \neq \text{constant}$

Water : $q(o,t) = q(x_R,t) = \text{constant}$

(b) Triangular Translation Wave Imposed on a Threshold Baseflow (q_c)

Sediment : $g_s(o,t) = 0$

$g_s(x_R,t) \neq \text{constant}$

Water : $q(o,o) = q(x_R,0) = q_c$

$q(0,0<t<T/2) = q_c + K_1 t$

$q(0,T/2\leq t<T) = q_c + K_2(T-t)$

$q(0,t>T) = q_c$

where K_1, K_2 are constants

(c) Step Change in Discharge from q_c to q_o

Sediment : $g_s(o,t) = 0$

$g_s(x_R,t>o) \neq \text{constant}$

Water : $q(o,o) = q(x_R,o) = q_c$

$q(o,t>o) = q_c + \Delta q = q_o$

The fundamental aspects of alluvial mechanics are concerned with the inter-relationships between the water and sediment phases and the movable boundary separating the two phases. The system response is determined by the interaction of these three components shown in a simplified form in Figure 3.2, after Puls et al. (1977), and listed below :

(1) Above a definite critical mean velocity, the flow erodes material from the bed and transports it according to the applied fluid shear stress.

(2) As the bed material is eroded or deposited, the alluvial bed profile is distorted giving rise to bedforms and changes in channel slope (degradation and aggradation)

(3) The loose boundary profile then acts as a feedback mechanism altering the flow locally, where bedforms exist, and over much greater lengths for changes in channel slope

(4) The bedload behaviour is strongly controlled by the bed geometry corresponding to the hydraulic conditions e.g. for a dune bed configuration the bedload transport rate time series at a point markedly fluctuates about a mean value

(5) The final interaction is the effect of solid particles in motion on the dynamics of the fluid flow, which will be minimal for the case where suspended sediment transport is negligible and when the water depth to mean grain size ratio is large

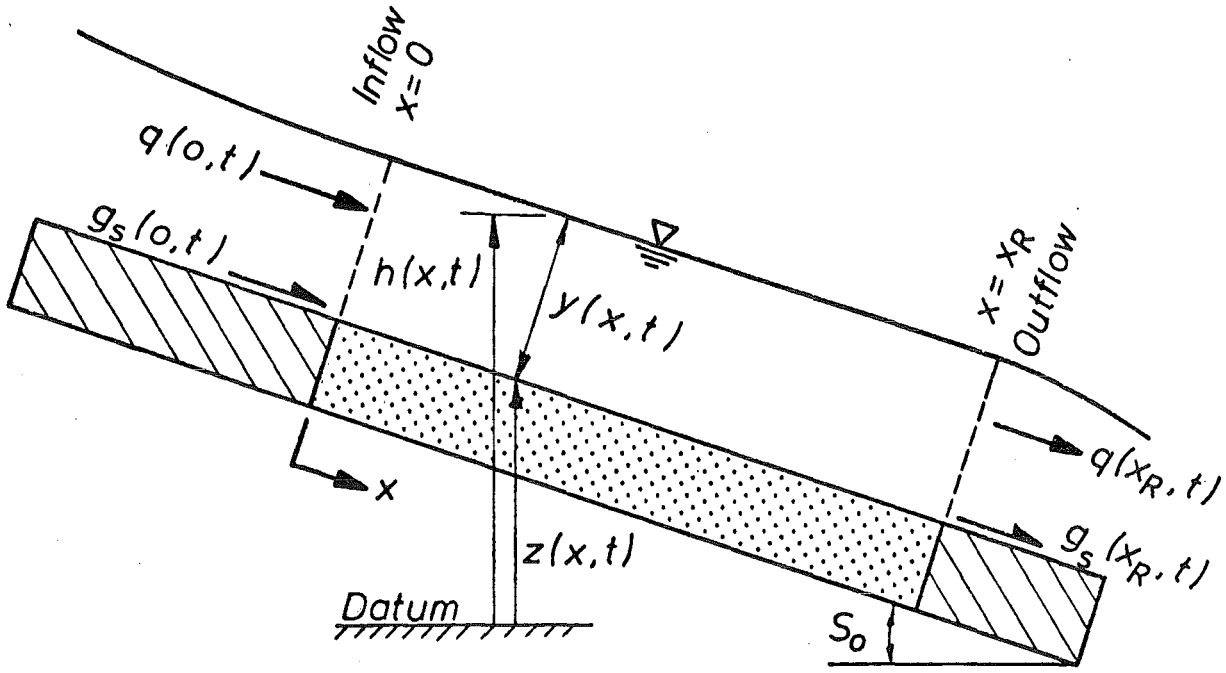

FIGURE 3.1 : Physical alluvial system

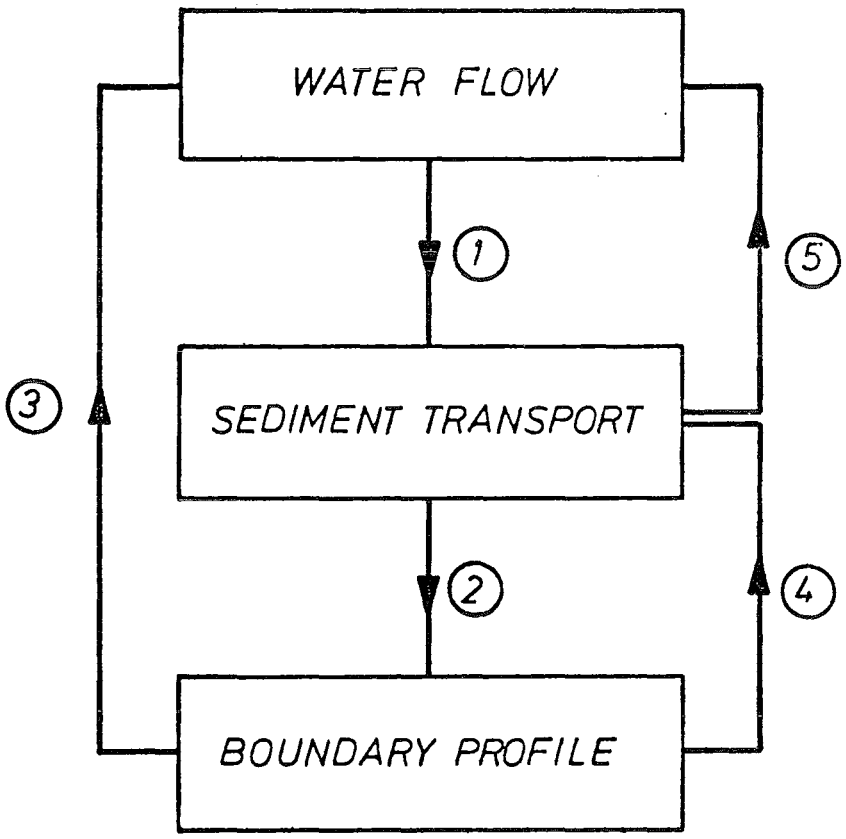

FIGURE 3.2 : Inter-relationships of the system components

These relationships are complex in detail, and the principles involved are not, as yet, fully understood especially with regard to transient sediment transport processes.

3.2.2 Steady Flow - Equilibrium Transport

The interaction between a steady uniform flow and an alluvial bed, which leads to equilibrium of the system, is the simplest state that can be considered and has therefore received extensive treatment by investigators. Simply stated, equilibrium requires that:

$$\bar{g}_s = g_{se} = \text{constant} \qquad \ldots (3.1)$$

where g_{se} and $\bar{g}_s$ are the equilibrium capacity transport rate/unit width and the mean bedload transport rate/unit width. This has resulted in a vast array of sediment transport formulae*, the best of which serve only as predictors for the likely maximum transport capacity, given a particular flow condition. The predicted maximum transport capacity does not necessarily equal the sediment transport rate that actually occurs in a natural river. One reason for this anomaly is that while the steady equilibrium transport capacity may be attained for short periods, generally the natural processes present in any river system vary with time, sometimes in an abrupt manner. One other major reason is the availability of bed material.

Bagnold (1966, pI3) defines a steady equilibrium system as follows :

> "A system which is defined as statistically steady and representative, not of conditions at a single cross section, but of average conditions along a length of channel sufficient to include all repetitive irregularities of shape, cross-section and boundary profile"

The time scale, t_s, is an important consideration in the definition of equilibrium transport conditions for an alluvial system where

*White, Milli and Crabbe (1973) investigated the predictive powers of 18 formulae.

$$\bar{g}_s = \frac{1}{t_s} \int_0^{t_s} g_s dt \qquad \ldots (3.2)$$

Observation at a point of such an equilibrium system, on a microscale, for short time periods (O[secs]), when plane bed conditions exist, reveals a continual exchange of particles between the moving bedload layer and the bed, {Luque and van Beek (1976)}. Therefore three sediment transfer mechanisms exist for localized segments of the system {Puls et al.(1977)} as follows :

(1) Detachment of grains from the bed (Synonymous with erosion or sediment pick-up)

(2) Deposition of moving grains to a stationary position on the bed. (Synonymous with sedimentation)

(3) Translation of particles at a characteristic transport velocity. (Synonymous with transportation)

However over a longer time span (or channel length for the spatial domain), the system can be viewed as in a state of equilibrium, as the rate of detachments will be equal to the deposition rate. This equality, necessary for stable bed conditions, forms the connecting link in the bedload formula of Einstein (1950). Similarly on a macroscale, conditions where bedforms develop result in regions of localised scour and fill {Foley (1975)}, but the system will be in equilibrium in a gross sense, when the time scale over which the transport rate is averaged, is of the same order as the translation period of the bedforms.

A detailed understanding of the movement of bed-material load, caused by the entrainment of particles into the flow, cannot be obtained from an equilibrium transport formula, which only yields spatially averaged transport rates for the system. Instead, the sediment transfer mechanisms can be incorporated into a simple conceptual model,(as outlined below), to gain this insight on a microscale. This model is extended later in the chapter to steady and non-steady non-

equilibrium systems to gain a greater understanding of the concepts involved in these states.

For the equilibrium transport model, the system can be viewed from different reference frames because each of the components; the flow, bedload transport and the fixed bed surface, (Figure 3.2), has a characteristic velocity. The average velocity of bedload particles (u_p) is considerably less than the local velocity of the surrounding flow. Reasons why this occurs are the finite length required for acceleration of the particles from rest, (the same applies for deceleration), due to inertial effects and the resistance offered by the bed surface, and also the loss of kinetic energy through inter-particle collisions. When bedforms are present, their celerity (C_d) is again smaller than the velocity of grains on the back slope of the bedform.

The reference frame relative to a stationary observer (or the fixed bed) was chosen for the conceptual model, shown in Figure 3.3, for the overall system in equilibrium for both plane bed and bedform configurations.

(1) Plane Bed Conditions (Figure 3.3a)

The summation of various bed material weights, for each transfer mechanism, (erosion, deposition and transportation), moved during a short time period $\Delta t'$, are represented by arrows where the width has been scaled with the equilibrium yield, $g_{se} \cdot \Delta t'$. The time interval is $\Delta t' = \Delta x/u_p$ (where Δx is a small distance travelled by a particle with velocity u_p). The following assumption is made to simplify the model; all particles which are eroded and subsequently transported, travel downstream with a constant characteristic particle velocity (u_p). The system is shown in Figure 3.3(a) at the end of the time period $\Delta t'$. The following alphabetical sections refer to the circled labels on the diagram :

|a| The accumulated weight of bed material transported into section I during the time interval $0 < t \leqslant \Delta t'$, which is equal to

G'_{se} (= $g_{se} \cdot \Delta t'$) if the sediment input boundary condition is set at the appropriate value, to maintain an equilibrium balance in the system. None of this material features in the output $|e|$ from section I until the next time period, according to the above assumption.

$|b|, |c|, |d|$ The interaction between the fluid flow and the bed results in an exchange of particles from the flow to the bed, (total quantity of deposited particles = $|d|$), and from the bed to the surrounding flow, (total quantity of detached particles = $|b| + |c|$), during the time period. The necessity for the two quantities of eroded material $|b|$ and $|c|$ stems from the spatial and temporal variations of sediment detachment within section I during the time $\Delta t'$. Only some of the eroded particles, viz. those contained in $|c|$, join the output quantity $|e|$ (shown by cross hatching), while the rest, $|b|$, will remain within the section e.g. the case when particle α is detached early in the time interval compared to the particle β which is say detached near the end of the time interval. Further, a grain eroded from the bed may well be deposited again within section I as part of $|d|$. The net sum of the quantities $|b|$, $|c|$ and $|d|$ gives the net change in transported bed-material across section I in time $\Delta t'$.

$|e|$ The input to section I in the previous time interval, $-\Delta t' < t \leqslant 0$ was also G'_{se}. However the accumulated weight output from the same section in the current time interval is now, for example, greater than G'_{se} having the benefit of a <u>net</u> excess, $|b|+|c|-|d|$, of particles derived from the bed by erosion. This output quantity is also now the input quantity of bed material for section II in the same time period.

The other sections II-V exhibit a similar pattern with spatial variations in the transported material between each section. The average of all these values will be the equilibrium transport rate which is equal to g_{se}.

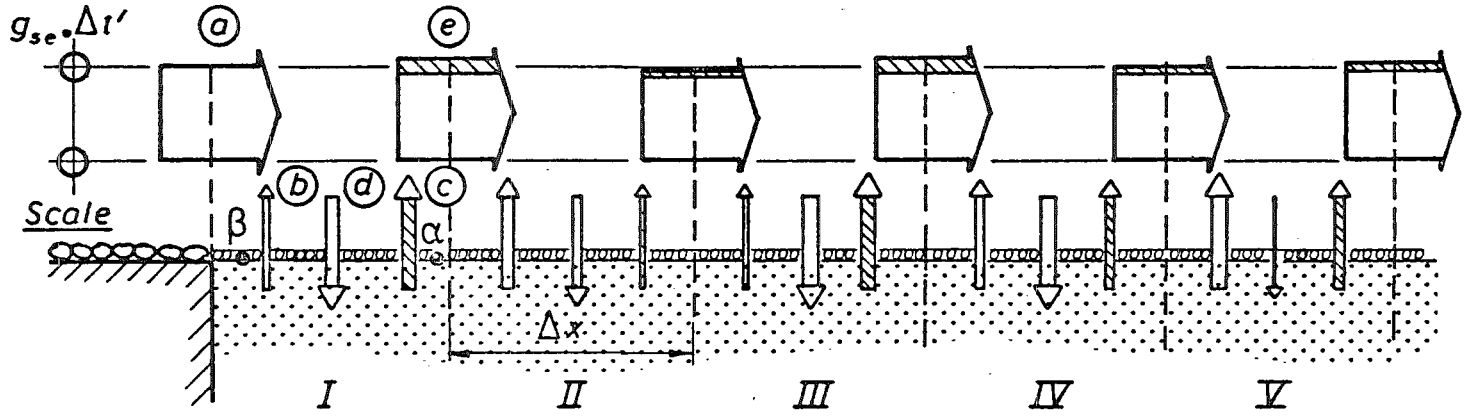

(a) Plane bed conditions

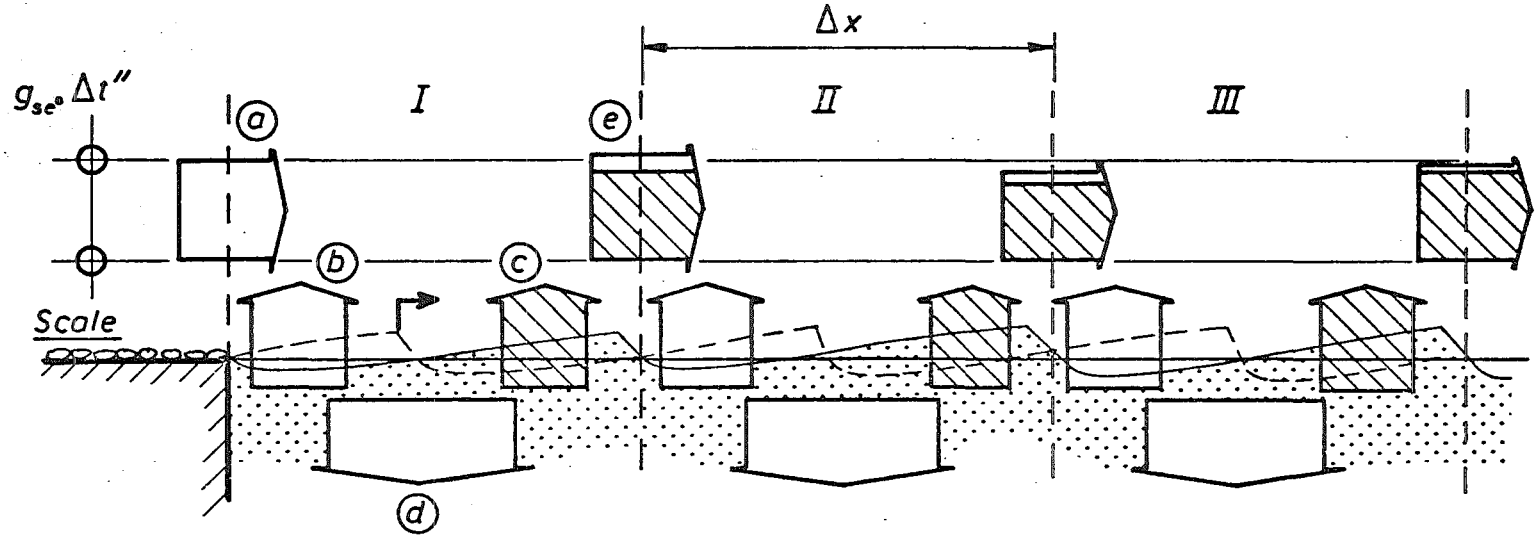

(b) Bedform configuration

FIGURE 3.3 : Equilibrium transport conceptual model

(2) Bedform Configuration (Figure 3.3b)

Again the accumulated bed material quantities, associated with each sediment transfer mechanism, moved in a time period $\Delta t"$, are represented by arrows. The arrow width is scaled relative to the equilibrium transport yield, $G"_{se} = g_{se} \cdot \Delta t"$ where $\Delta t" = \Delta x/C_d$, (where Δx is the wavelength of the bedforms which are all assumed to be propagating at a constant celerity C_d).

|a| The input quantity to the system is set at $G"_{se}$ to maintain equilibrium.

|b| |c| |d| The mechanism by which bedforms propagate downstream has been outlined by Simons and Şentürk (1977). Solid particles are eroded, |b|, and transported, |a| + |b|, rapidly on the upstream surface of the bedform, $u_p > C_d$, and the majority are subsequently deposited, |d|, in the trough region after the particles avalanche down the steep downstream face. The deposited particles will remain at rest for periods of up to $\Delta t"$, depending on the elevation at which they came to rest, before they are exposed again on the upstream surface of the bedform. On average the rest period will be $\frac{1}{2}\Delta t"$. The quantity |c|, shown with cross hatching, is eroded from the surface of the next bedform downstream and forms the bulk of the output quantity |e| from section I in the time period $\Delta t"$.

|e| The output quantity is the input to section II. The small unhatched portion is comprised of particles which continue in transport from the input, quantity |a|, having overshot the deposit region in the trough.

The bedform amplitudes will vary slightly along the reach length because of spatial and temporal variations in pick-up and deposition processes, but averaged over several bedforms, equilibrium conditions will exist.

Although the internal quantities of bedload particles deposited and eroded within each segment Δx are different between the two cases,

shown in Figure 3.3 by the quantities |b|, |d| and |c|, the spatial variation of the input and output quantities over several segments will be similar for each case. The mechanism by which particles are entrained will also be similar, and therefore any lag in the response of the bedload layer which occurs will also create a corresponding lag in the bedform configuration as shown by their interrelationship in Figure 3.2. Thus the conceptual models developed in the rest of the chapter will be limited to plane bed conditions for clarity.

3.2.3 Steady Flow - Non-Equilibrium Transport

Consider the physical system initially in equilibrium with an appropriate sediment input rate. Under these conditions, as discussed in section 3.2.2, the flow at each section is transporting the same quantity of bed material, on average, with no net change in bed elevation with time. The transport rate under these conditions is equivalent to the transport capacity of the steady flow. Suppose that the equilibrium of the system is now disturbed by a change in the upstream sediment supply, resulting in a non-equilibrium situation. An increase in the sediment input will lead to aggradation of the bed in the reach while a decrease will cause degradation of the bed. Herein, only the response of the system when the upstream sediment supply is removed will be considered.

After a step change in sediment input from equilibrium transport to zero, the flow begins to scour the erodible bed at the upstream end of the reach, in an attempt to restore the system to equilibrium and so satisfy the transport capacity of the flow. Hence the bed material in the upper reach has become the internal sediment supply to the system, for the reach downstream of the general scour hole. Over the initial scouring section, the flow will be deficient in sediment. The deficit can be expected to decrease in the downstream direction until the equilibrium transport rate is reached.

The entrainment mechanisms, resulting from the interaction of the flow field and the alluvial bed, will be similar to those operating under steady equilibrium conditions, except in that region of the scour hole from the edge of the fixed bed to the area of maximum scour depth. In this region a fluid vortex develops as observed later in section 7.2, with a noticeable reverse flow close to the bed caused by the separation of the main flow stream from the degraded bed surface. To predict accurately the entrainment and net downstream transport of sediment particles, a suitable description of the flow field within the scour hole is required. Breusers (1975) has presented a method which produces an approximate description of the velocity distribution based on the diffusion equation for flow through a sudden enlargement. However, no general relation exists relating the local velocity of the surrounding flow near the bed, in the scour hole, to the local sediment transport rate.

The interaction between the sediment transport and boundary profile components of the system can be related by the continuity equation for sediment

$$\frac{\partial g_s}{\partial x} + P_s \frac{\partial z}{\partial t} = 0 \qquad \ldots (3.3)$$

where P_s = bulk specific dry weight of the bed sediment and z is the bedlevel above a fixed horizontal datum (+ve. upwards). By the principle of continuity, the net amount of material supplied from the general scour hole, must balance the volume of the scour hole adjusted for porosity. The bedload yield G_s from the general scour hole for the period t = 0 until t = t is therefore

$$G_s = \int_0^t g_s(L_s,t)dt = P_s \int_0^{L_s(t)} |z(x,0) - z(x,t)| dx \qquad \ldots (3.4)$$

where $L_s(t)$ is the instantaneous general scour hole length taken from

$x = 0$ to the point where the mean bed profile intersects with the original bed level.

The continuity equation in a finite difference form can also be used to obtain average sediment transport rates within the scour hole if a successive series of scour hole profiles is available. For small changes in space and time, equation 3.3 can be approximated as

$$\Delta g_s = - \frac{P_s \, \Delta z \, \Delta x}{\Delta t} \cdot n_s \qquad \ldots (3.5)$$

where an additional parameter n_s is introduced to account for deviations of the experimental profiles from a two dimensional profile across the channel width. With reference to the finite difference grid, shown in Figure 3.4, equation 3.5 becomes

$$\bar{g}^{j}_{s_{i+1}} - \bar{g}^{j}_{s_{i-1}} = -P_s \frac{\Delta x}{\Delta t} \left(\bar{z}^{j+1}_{i} - \bar{z}^{j-1}_{i} \right) \cdot n_s \qquad \ldots (3.6)$$

$$\text{where} \quad \bar{z}^{j+1}_{i} = \tfrac{1}{2} \left(z^{j+1}_{i-1} + z^{j+1}_{i+1} \right)$$

$$\text{and} \quad \bar{z}^{j-1}_{i} = \tfrac{1}{2} \left(z^{j-1}_{i-1} + z^{j-1}_{i+1} \right)$$

Given the upstream boundary condition, $\bar{g}^{j}_{s_0} = 0$, the average transport rate at time $t + \frac{\Delta t}{2}$, $(g^{j}_{s_{i+1}})$, can be computed for sections $i = 1,2,\ldots,N$.

The section at which the transport rate reaches equilibrium, at the end of the general scour hole, can be visualised as lying on a characteristic curve in the x - t plane, (Figure 3.5), moving downstream indefinitely at a celerity C_s as long as the flow continues. The system downstream of the scour hole must be in equilibrium as it lies in the constant state region of Figure 3.5, which remains under the influence of the initial condition, $\bar{g}_s (x,o) = g_{se_o}$, until the disturbance arrives. The encroachment of the scour hole into the constant state region and the likely spatial distribution of trans-

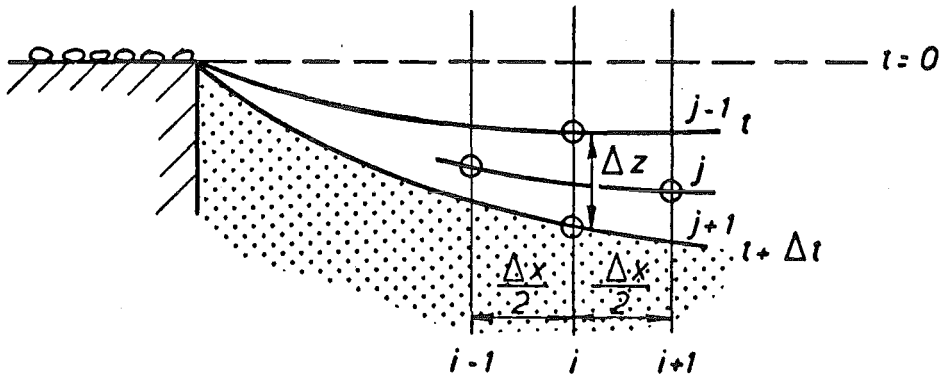

FIGURE 3.4 : Finite difference grid

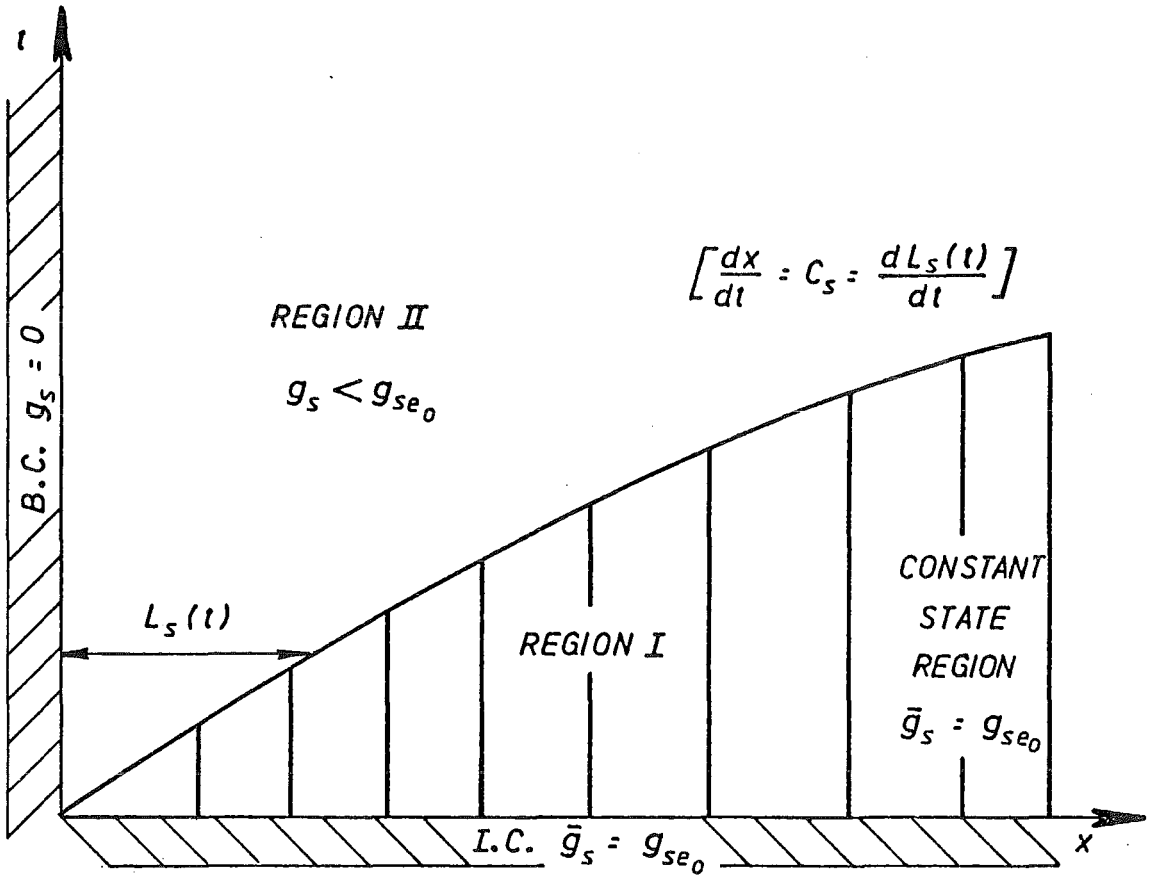

FIGURE 3.5 : Propagation of a non-equilibrium disturbance in the x-t plane

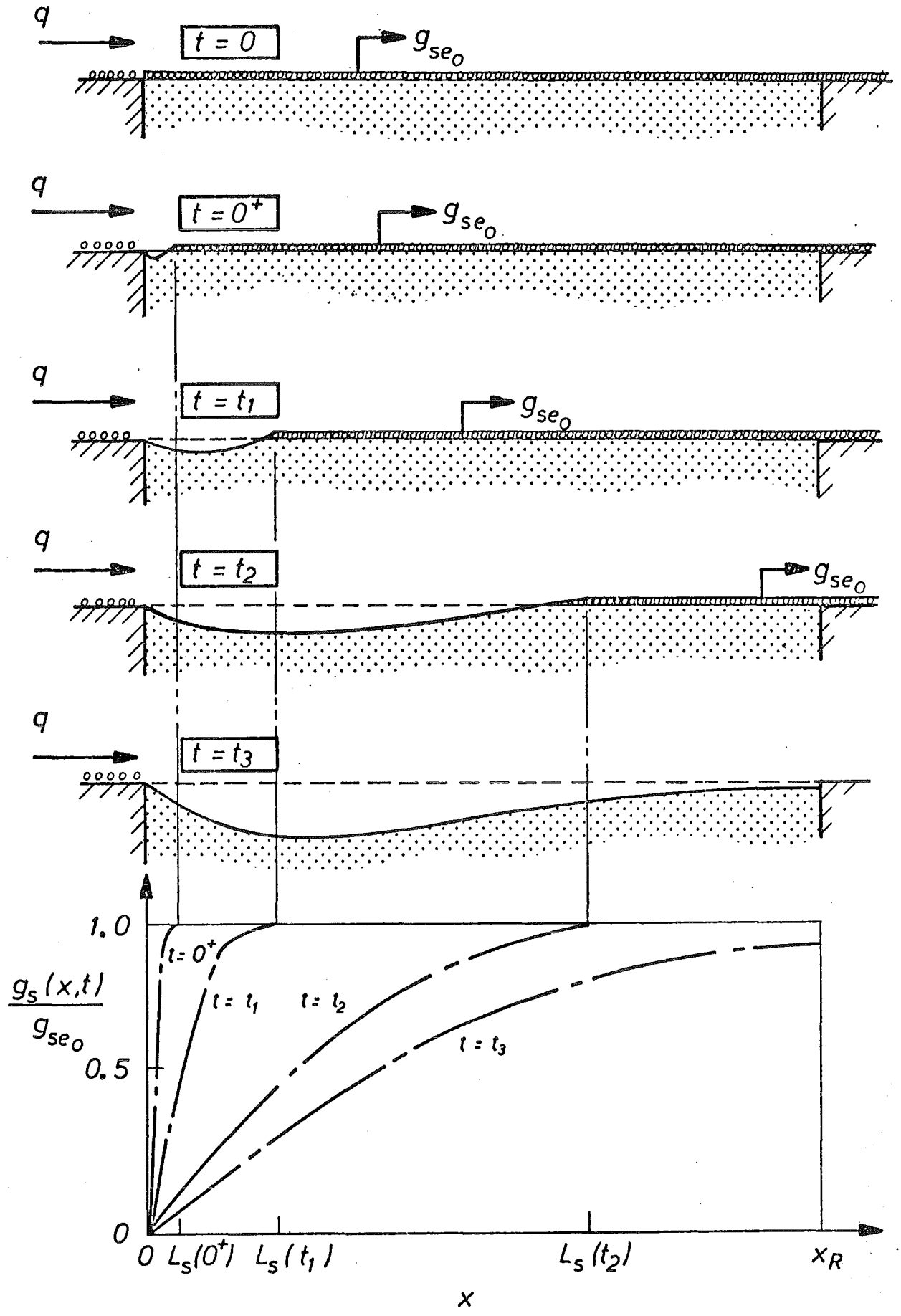

FIGURE 3.6 : Idealised general scour hole development and transport rate spatial distribution

port rate within the reach length is shown in Figure 3.6, after increasing periods of time.

A conceptual model, similar to the model discussed in section 3.2.2, can be developed for the case of steady flow non-equilibrium transport, (Figure 3.7). The moving bed material volumes accumulated over a short time period $\Delta t'$, and associated with each sediment transfer process, are again scaled according to the width of each arrow.

$$\Delta t' = \Delta x/u_p \text{ (where } u_p \text{ is the mean particle velocity)}$$

As the scour hole deepens the particle velocity decreases because of a decrease of the local fluid velocity in the vicinity of the bed and therefore the length of the section, Δx, must also decrease. The conceptual model is only considered for the case where plane bed conditions exist in the equilibrium constant state region, for the reasons given in section 3.2.2. Three different stages, representative of the response of the system to a halt in the input sediment supply, will be discussed below with reference to Figure 3.7

(1) Figure 3.7(a) $t<0$

Prior to the termination of the sediment input rate, g_{se_o}, the system is in overall equilibrium in spite of small local changes in rates of detachment and deposition at each section. This is the same as Figure 3.3a and a detailed explanation for this case can be found in section 3.2.2.

(2) Figure 3.7(b) $t = t_1$

The situation is shown at time t_1 (after the time interval $t_1 - \Delta t' < t \leq t_1$)* soon after the upstream sediment supply was severed, thus the sediment input $|a|$ to section I is zero. The accumulated weight of deposited particles $|d|$, shown for the first section, is probably small as the predominant transfer process will be detachment because of the high erosive capacity of the flow. It is phy-

*The celerity of the scour hole edge, C_s, is not equal to u_p.

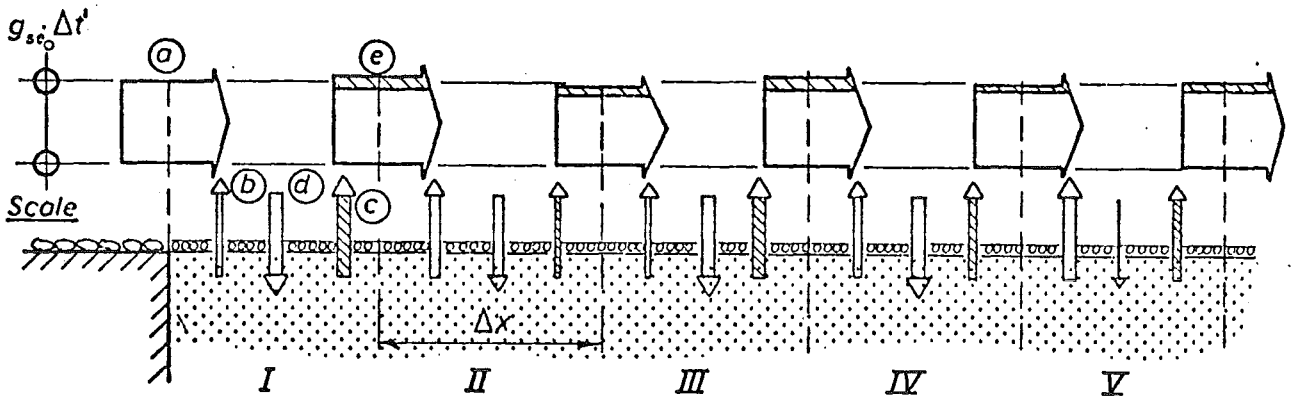

(a) Equilibrium transport (t<0)

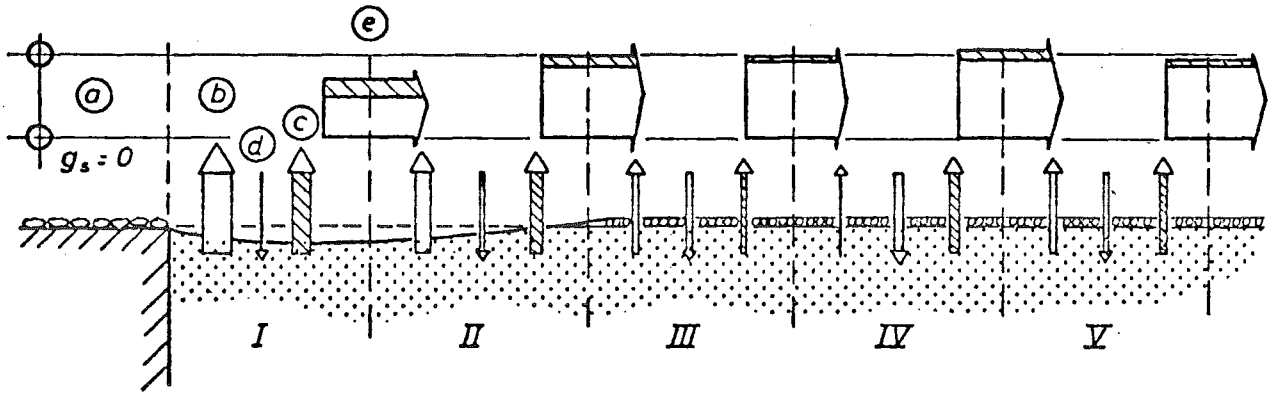

(b) $t=t_1$

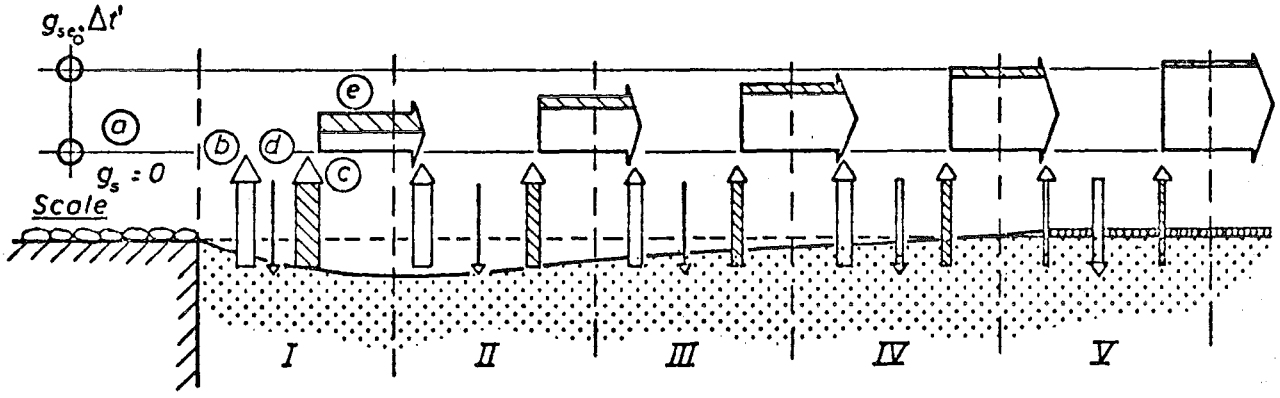

(c) $t=t_2$

FIGURE 3.7 : Steady flow non-equilibrium transport conceptual model

sically impossible for the system to respond instantaneously, creating a situation where, at x = 0, the transport rate is zero but everywhere else attains the equilibrium value. The flow requires a finite pick-up length, having to overcome friction exerted by the bed on individual grains and their inherent inertia. Therefore in section I, the total quantities of eroded material($|b|$ and $|c|$) will not completely satisfy the transporting capacity of the flow, leading to a reduction in the output from that section when compared to the output before t = 0. The quantity of eroded material $|b|$ remains in transport within section I at $t = t_1$, but will form part of the output during the next time period, provided no deposition occurs. The cross-hatched portion of the current output $|e|$ is derived from particles eroded, $|c|$, during the period just completed. The remainder of $|e|$ comes from $|b|$ of the previous time step. Section II, as distinct from the first section, receives an input $|e|$ during the time interval, and so the erosive capacity of the flow is reduced as it approaches the equilibrium sediment transport rate, which begins, for example, in section III.

(c) Figure 3.7(c) $t = t_2$

At a later time t_2, the bed has continued to degrade in the area affected by the non-equilibrium sediment transport state but the erosive capacity of the flow decreases as the flow velocity decreases due to the greater flow depth. The bed material quantities for erosion from section I, $|b|$ and $|c|$, will therefore be less than the eroded material for the situation exhibited in Figure 3.7(b). Sections I, II and III are also shorter in length because the average particle velocity decreases. The output from section I (input to section II), comprising the eroded particles $|c|$ which pass out of the section plus particles in transport from the preceding time period, is therefore reduced, providing a mechanism whereby the scour hole

length increases continuously, so that the transport capacity of the flow may be eventually satisfied. Hence equilibrium conditions begin much further downstream than was the case in Figure 3.7(b).

3.2.4 Non-Steady Flow - Non-Equilibrium Transport

The physical system is that described in section 3.2.1, with the facility to generate non-steady flow inputs. The sediment transport input to the system, for all the non-steady water flows, was zero for all time, and therefore there was no step-change in the upstream sediment supply as for the steady flow case (section 3.2.3). Under non-steady flow conditions, the transport capacity is altered due to changes in discharge, either in an abrupt step-like manner or in a continuous manner such as in a triangular translation wave.

Both the entrainment process and scour hole development will be similar to the steady flow case with zero sediment input. However, the bed response characteristics will differ if the transporting capacity of the flow varies at a rate faster than that at which the sediment transport can respond. This will cause a difference between the actual transport rate and the transport capacity of the flow. These differences, which are expected to increase as the rate of change of discharge with time increases, are in addition to those which occur for a comparable steady flow non-equilibrium transport situation (section 3.2.3). Hence two transient effects will be evident in the sediment phase; non-equilibrium effects and effects of bed response to non-steady flows.

A non-steady flow, non-equilibrium transport alluvial system is the most complex state in terms of interactions between the system components (Figure 3.2). Whenever a change is imposed on the flow field, a change in boundary resistance, towards a roughness compatible with the new flow conditions, is achieved by a change in bedform configuration. However, a change in the geometrical shape of the bed-

forms requires the transfer of bed material by transportation, which cannot occur instantaneously with a change in flow conditions. To consider the response of the bed conceptually, only the response of the bedload transport layer on a plane bed will be considered as stated in section 3.2.2.

A conceptual model presented below is based on small segments of a translation wave and is similar to the model proposed for steady non-equilibrium conditions. It does however, incorporate the variation with time of the mean particle velocity (u_p) and the mean flow velocity. The same concepts, outlined below with the aid of the conceptual model, will apply to the case of a step change in discharge, but in a more severe sense, during the initial transient phase.

For simplification, the non-steady flow may be reduced to a steady-state flow. This is achieved by superimposing a velocity equal and opposite to the wave segment celerity (C_w) on the system, which effectively changes the frame of reference from the viewpoint of a stationary observer to one moving with the wave segment. In this frame the velocities of the sediment particles and the static bed are ($u_p - C_w$) and ($-C_w$) respectively. The sediment transfer processes, which occur as a wave segment propagates through the test reach, are shown in Figure 3.8 during the rising stage of a triangular translation wave. The bed-material quantities associated with each process for wave segment II are recorded for four successive time periods $\Delta t'$ where

$$\Delta t' = \frac{\Delta x}{C_w}$$

where Δx is the distance travelled in time $\Delta t'$ by the wave segment propagating at a celerity C_w. The spatial position of wave segment II, relative to the upstream fixed bed, is shown in each diagram at the end of the specified time interval. The accumulated weight

of bed particles for each process over the time interval is represented by the thickness of an arrow scaled in proportion to the equivalent steady transport capacity of the segment II,

$$G_{se} = g_{se}(II).\Delta t'.$$

The various components of the idealised conceptual model represented by each arrow are as follows :

|A| These particles are eroded from the bed by the segment during the time interval but because the segment is propagating at a much greater velocity than the transported particles, they will be left behind thus forming a portion of the input |F| to the following wave segment III (shown by cross hatching). This does not occur in Figure 3.8(a).

|B| Particles in transport, which have either been eroded by the segment or passed on from the preceding segment I, which are deposited under segment II during the time interval.

|C| This quantity has also been eroded by the segment, but remains in transport under the segment at the end of the time interval except those particles subsequently deposited with |B|. The particles in |C| will be those eroded by the leading section of the segment and moved downstream a sufficient distance to maintain contact with the upstream section of the segment.

|D| Transported particles which are passed onto the segment from the preceding segment I, which

possesses a lower transport capacity.

$|E|$ The total transported quantity under the segment at the end of the time interval comprises particles combined in the equation

$$|E| = |D| + |C| - |B| + |e|$$

Quantity $|e|$ is composed of those particles which were transported under segment II at the end of the previous time period but have continued to maintain contact with the segment because they were formerly close to the leading edge of the segment.

$|F|$ This quantity comprises particles in transport which are passed onto the following segment III which has a higher transport capacity than segment II. The quantity is calculated from

$$|F| = |E|' - |e| + |A|$$

where $|E|'$ is the quantity $|E|$ from the previous time interval.

None of the particles overtaken by segment II, $|D|$, will form part of $|F|$ until the next time period.

Using the four diagrams in Figure 3.8, the fluid-sediment transport interaction can be explained by way of a hypothetical example where specific quantities of bed particles are prescribed for each process, shown in square brackets.

(1) Figure 3.8 (a) - time interval $t_1 < t \leq t_2$

- wave segment position shown at $t=t_2$

As the flow segment II proceeds from the fixed bed to the erodible section, it will entrain sediment particles from the bed to begin satisfying the transport capacity of the segment, which is greater than the preceding segment I. This will require the passage over a finite length of erodible bed to overcome the non-equilibrium component of the sediment transport and a finite time period for the bed to adjust to the non-steady component of the alluvial system. Therefore sediment transport rates in the present and all successive time periods will exhibit a similar spatial distribution to the steady flow non-equilibrium model (3.2.3) but will be smaller in magnitude due to the time lag associated with the delayed response of the bed.

During the initial time period as the segment passes onto the erodible reach, it receives no external input of sediment. The transport capacity of segment II for each time period is chosen as 15 units by way of example. Because the trailing edge of the segment is still in contact with the fixed bed at $t = t_2$, none of the eroded material (e.g. $|C| = 3$ units) will be passed on to segment III, ($|A| = 0$) and all that is not redeposited will remain in transport under the segment. If the segment also received particles in transport from the preceding segment, ($|D| = 5$), and deposits particles during the time interval ($|B| = 1$), the quantity of material in transport under the segment at $t = t_2$ is $|E|$ equal to 7 units.

(2) Figure 3.8(b) - time interval $t_2 < t \leq t_3$

- wave position shown at $t = t_3$

As the characteristic particle velocity is much less than the wave celerity, the particles in transport under the wave segment at $t = t_2$ will be either left behind as part of $|F|$ or remain with the segment at $t = t_3$ ($|e| = 2$) e.g. $|E|' - |e| = 7-2 = 5$ units. This quantity will be joined by some of the particles eroded during the present time period e.g. $|A| = 2$ units. Therefore the output

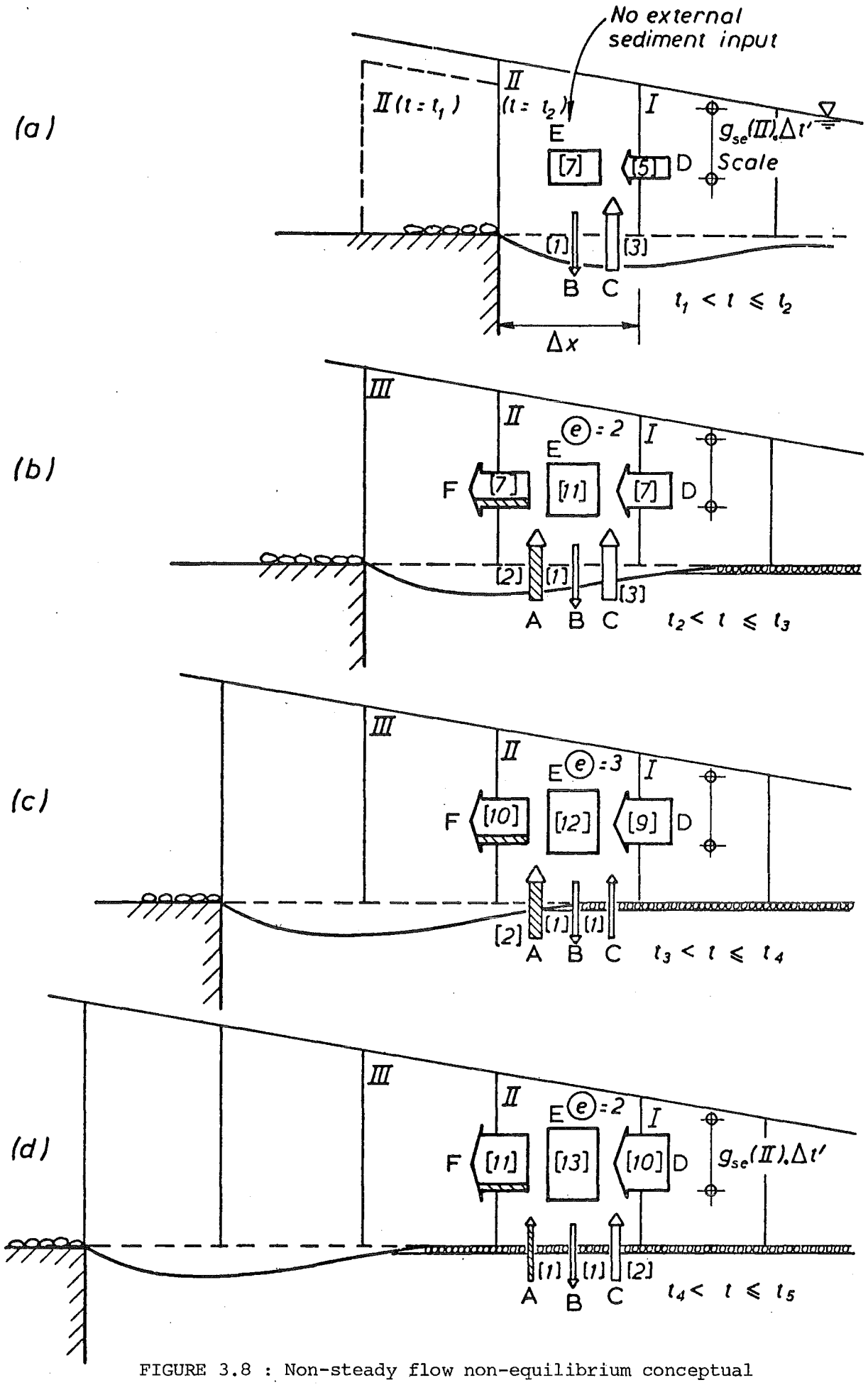

FIGURE 3.8 : Non-steady flow non-equilibrium conceptual model (rising stage of a triangular wave)

quantity $|F|$ passed on to segment III is $|E|' - |e| + |A| = 7$ units. Because the transport capacity of segment II is greater than that of segment I, the output quantity $|F|$ will likewise be greater than the transported material passed on to segment II, $|D|'$, during the previous time period e.g. compare $|F| = 7$ with $|D|' = 5$. Therefore the effect of the wave segment is to increase the momentum of the moving sediment layer by both a net erosion of more particles and an increase in the mean particle velocity (u_p) of those particles already in transport. The material in transport under segment II at $t = t_3$, ($|E| = 11$ units), has increased compared with the quantity $|E|'$ at $t = t_2$, as the wave segment moves further into the scour hole. It would be expected that this quantity is still below a comparable steady flow non-equilibrium transport rate, given the same scour hole dimensions and flow transporting capacity.

(3) Figure 3.8(c) - time interval $t_3 < t \leqslant t_4$

- wave segment position at $t = t_4$

The erosion capacity of the wave segment begins to decrease near the end of the scour hole as the sediment transport quantity ($|E| = 12$ units) becomes closer to the transport capacity, ($G_{se} = 15$ units). Therefore the eroded quantities $|A|$ and, especially, $|C|$ will be reduced.

(4) Figure 3.8(d) - time interval $t_4 < t \leqslant t_5$

- wave segment position at $t = t_5$

The non-equilibrium transport component, resulting from the upstream boundary condition ($g_s = 0$), is reduced to zero as the wave segment moves downstream from the local scour hole region. Here the non-steady flow component becomes the dominant influence which can impede the attainment of the transport capacity rate, especially when bedforms are present on the bed. This is shown in the diagram by the transport quantity under the segment ($|E| = 13$ units) which is below the potential transport capacity of 15 units per time per-

iod $\Delta t'$ for segment II. The reason stems from the transport rate magnitude difference which was present with segment I and so on for all preceding wave segments, provided the changes in flow transport capacity exceed the ability of the bed to respond to the changing flow conditions. However, the absolute quantity of particles passed on to segment III ($|F|$ = 11 units) will still be greater than the quantity passed on to segment II during the previous time interval ($|D|'$ = 9 units). The mechanism, where the number of particles passed on by the segment is greater than the number received at the same section x, as a result of the net erosion quantity, leads to degradation of the bed on the rising limb, symbolised mathematically by the sediment continuity equation (3.3). Aggradation on the falling limb of the wave will follow from the reverse of the above mechanism, provided the section is downstream of the advancing general scour hole profile, while upstream in the general scour hole, degradation will continue because of non-equilibrium effects.

3.3 EXPERIMENTAL MODEL OF ALLUVIAL SYSTEM

3.3.1 Introduction

The interactions between the various components of an alluvial system were conceptualised in the previous section, (3.2), to gain a clearer understanding of the sediment processes which occur for various flow and sediment boundary conditions. To quantify the spatial and temporal response of the alluvial bed under non-equilibrium conditions and test the validity of the conceptual models, an experimental programme was undertaken. This also enabled the more significant assumptions of the mathematical models to be tested experimentally. Separation of the non-steady flow and the non-equilibrium transport conponents of the system was achieved using the comparison procedures outlined below.

3.3.2 Comparison Procedure for Equilibrium and Non-Equilibrium Transport Rates (Steady Flow)

An equilibrium transport formula of the form,

$$g_{se} = a\,\bar{u}^{\,b} \qquad \ldots (3.7)$$

where $\bar{u}$ is the mean flow velocity = q/y, is widely used as the fourth equation to complete the mathematical formulation of a general alluvial system, discussed in section 2.3.3. The assumption, that an equilibrium transport formula is also applicable under steady flow non-equilibrium conditions, can be tested experimentally. The experimental comparison model below has been devised to compare transport rates in the system under the influence of the two different sediment input boundary conditions, given the same mean flow velocity at a particular cross section.

Equilibrium transport conditions were deemed to exist when rates of sediment inflow to the test reach matched the outflow rate and consequently the mean bed level, $\bar{z}_e$, and bed slope remained constant. The mechanics of the procedure to derive comparable transport rates from experimental data are shown in Figure 3.9. From a series of equilibrium transport experiments with different steady flow rates, a power relationship can be obtained between the equilibrium transport rate, g_{se}, and the mean flow velocity, $\bar{u}_e$, for the higher flow rates of the form, {Figure 3.9 (d)},

$$g_{se} = a\,\bar{u}_e^{\,b} \qquad \ldots (3.8)$$

At two successive times t_1 and t_2 during a steady flow (q) non-equilibrium experiment, the relevant system variables, h^{ST}(= water stage) and z^{ST}(= bed elevation), have known specific values at the end of each small segment (Δx) e.g. the segment centred at $x = x_1$ {Figure 3.9 (e) and (f)}. The spatial distribution of mean flow

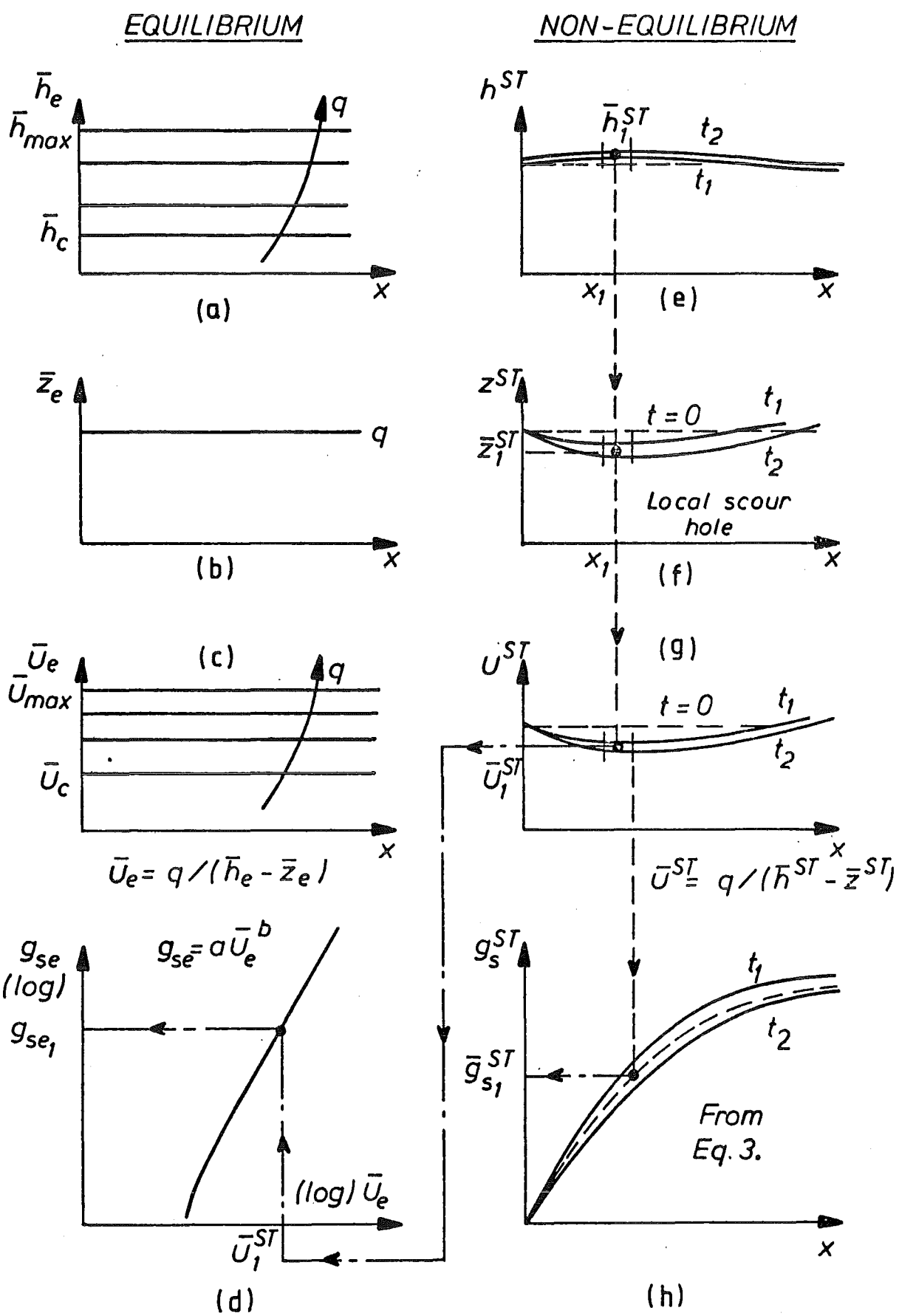

FIGURE 3.9 : Comparison procedure for transport rates under equilibrium and non-equilibrium conditions

velocity u^{ST} along the scour hole section can be otained from the equation

$$u^{ST} = \frac{q}{(h^{ST} - z^{ST})} \qquad \ldots (3.9)$$

This is shown in Figure 3.9(g). The calculation of the mean bedload transport rate at the end of each segment Δx is achieved by using the finite difference form of the continuity equation (3.6) applied to successive scour hole profiles measured at t_1 and t_2. The mean transport rate derived at the end of the example segment is $\bar{g}_{s_1}^{ST}$. The comparable steady equilibrium transport rate, g_{se_1}, is obtained by entering the value $\bar{u}_1^{ST}$ on the equilibrium transport graph, Figure 3.9(d). A plot of actual non-equilibrium transport rates ($\bar{g}_s^{ST}$) for each section as well as comparable equilibrium transport rates, (g_{se}), can be derived by considering the system at several values of t_1 and t_2, so that any differences between $\bar{g}_s^{ST}$ and g_{se} can be determined.

3.3.3 Comparison of Transport Rates for Continuous Steady Flows and Step Changes in Flow (Non-Equilibrium)

The object of the comparison procedure is to compare transport rates obtained from steady flow experiments with transport rates from experiments in which the flow rate was changed suddenly from a critical base flow (q_c) to a higher steady flow (q_o). The mechanics of the procedure to derive a comparable steady flow non-equilibrium transport rate are shown in Figure 3.10, which is similar to the process used by Griffiths and Sutherland (1977). This procedure will effectively separate the bed response due to the non-steady flow component from the non-equilibrium transport component because the non-equilibrium state is common to both sets of experiments.

A time t_1^{SC} is selected, at which the measured system variables $\bar{h}^{SC}$, $\bar{z}^{SC}$ and $\bar{g}_s^{SC}$ are known for conditions resulting from a

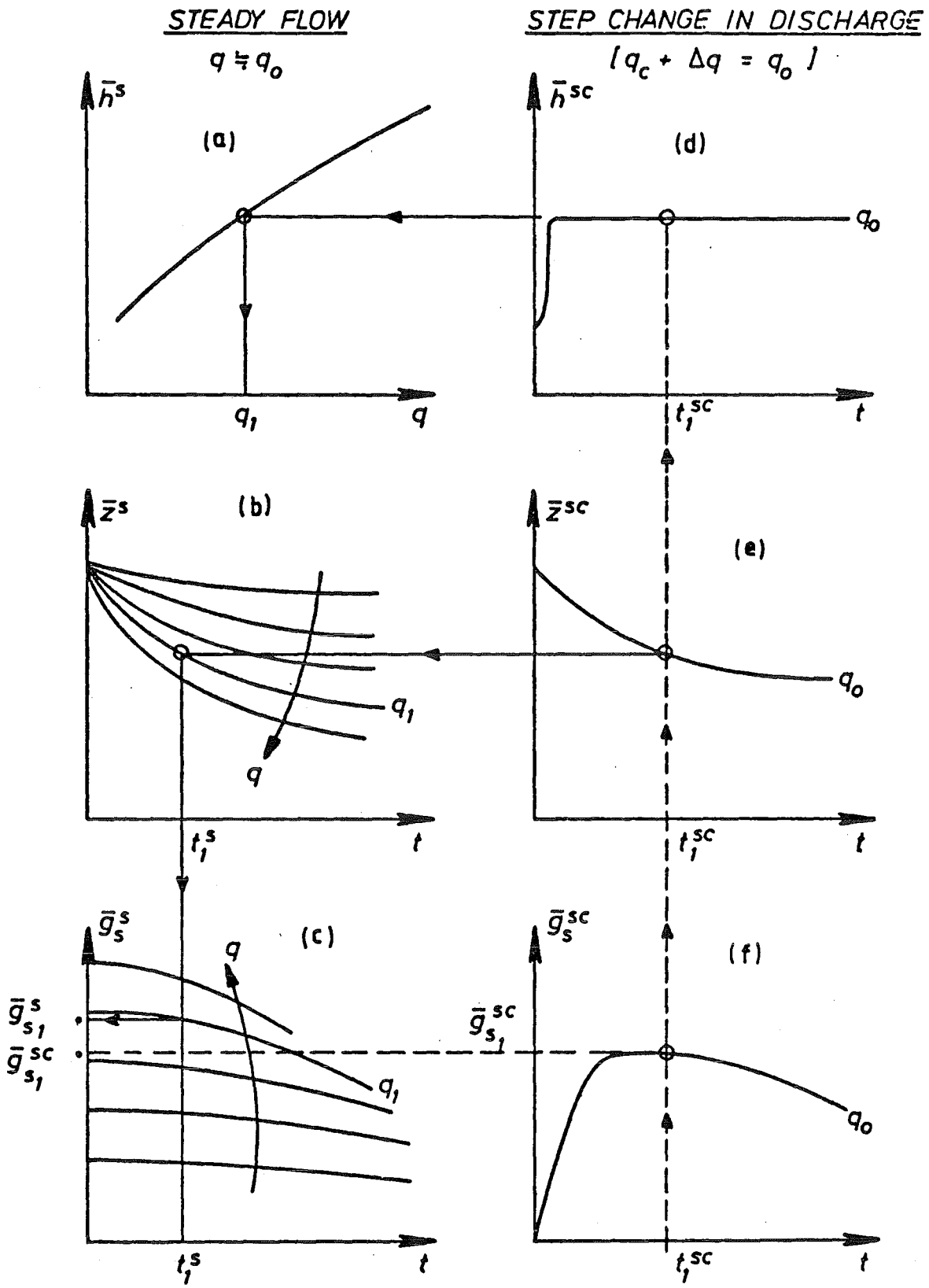

FIGURE 3.10 : Comparison procedure for transport rates for steady flows and step changes in discharge (non-equilibrium)

step change in discharge (Δq), Figure 3.10(d), (e) and (f). The variables $\bar{h}$ and $\bar{z}$ are the mean stage level and bed level respectively of measured values taken over the whole test reach, and $\bar{g}_s$ is measured at the downstream end. Corresponding to the mean stage $\bar{h}^{SC}$, the steady flow rating curve will yield a steady discharge q_1, Figure 3.10(a). Under steady flow conditions, the discharge q_1 requires a time t_1^S to reduce the mean bed level $\bar{z}^S$ to the same value $\bar{z}^{SC}$ existing at t_1^{SC}, Figure 3.10 (b). Values of t_1^S and q_1 define a comparable steady flow non-equilibrium transport rate $\bar{g}_{s_1}^S$, which can be compared with the measured rate $\bar{g}_{s_1}^{SC}$ for a step change in flow rate experiment, Figure 3.10(c). This can be repeated for several values of t_1^{SC} to build up a comparable bedload curve which will permit an assessment of the magnitude differences and the temporal lag which occur during the initial bedload transient phase. Comparable conditions can now be defined as occurring when the system variables, with the exception of q_s, approximately correspond.

3.3.4 Comparison of Transport Rates for Steady Flows and Non-Steady Translation Waves (Non-Equilibrium)

The principal object of this experimental comparison model is to compare non-equilibrium transport rates under steady flow conditions with those of a translation wave passing over the same test reach. This procedure will effectively separate the bed response due to the non-steady translation wave component from the non-equilibrium component.

The comparison of transport rates at any stage of the translation wave with transport rates under comparable steady flow conditions is equivalent to the assumption made sometimes to simplify the solution technique for non-steady flow mathematical models (section 2.4.3). That is, the translation wave can be treated as a finite succession of steady flow discharges which reproduce the

wave hydrograph as closely as possible. The validity of this assumption can be challenged if significant differences in comparable transport rates result from the comparison procedure.

These differences in experimental bedload transport rates under compared steady and non-steady flow conditions, if they occur, will be a function of some or all of the following factors :

(1) The additional slope terms of the dynamic equation of motion associated with the translation wave motion

(2) A change in the friction slope, S_f, where

$$S_f = \frac{f\,\bar{u}^2}{8gy} \qquad \ldots (3.10)$$

arising from a different friction factor (f) of the bed configuration

(3) A difference between the response of the bed to non-steady flows and the response to steady flows, under non-equilibrium conditions.

In regard to the fluid motion, the degree of approximation inherent in the comparison model, can be obtained from an estimate of the additional slope terms. Consider the momentum equation for the fluid flow

$$\frac{1}{g}\frac{\partial u}{\partial t} + \frac{u}{g}\frac{\partial u}{\partial x} + \frac{\partial y}{\partial x} = S_o - S_f \qquad \ldots (3.11)$$

where S_o = the bed slope. For steady uniform flow, the L.H.S. of equation 3.11 is zero, therefore

$$S_o = S_f = \frac{f\bar{u}|\bar{u}|}{8gy} \qquad \ldots (3.12)$$

If the translation wave and steady flow experimental series are run for the same initial bed slope, $S_o = 2 \times 10^{-3}$ chosen in section 4.4, then the differences arising from the other slope terms in

equation 3.11, for the steepest wave selected in section 4.3.1, are

$$\frac{1}{g}\frac{\partial u}{\partial t} = 3 \times 10^{-5} \quad , \quad \frac{u}{g}\frac{\partial u}{\partial x} = 2 \times 10^{-5} \quad , \quad \frac{\partial y}{\partial x} = 2 \times 10^{-4}$$

The contribution of these terms is an order of magnitude less than the bed slope. Therefore any differences resulting from the comparison process will largely be due to the bed response effects and changes in friction slope which are necessarily linked together.

Two series of non-equilibrium experiments will be considered with no upstream sediment input for all time. The first series consists of several runs with various constant water discharges ranging between the critical base flow (q_c) and the maximum peak flow (q_{max}) chosen for some of the translation waves. Triangular translation waves, released over the same test reach with different peak flows and periods, form the second series. The mechanics of the procedure to derive comparable steady flow transport rates are shown in Figure 3.11. Again $\bar{z}$ and $\bar{h}$ are mean values of measurements taken throughout the reach and $\bar{q}_s$ is measured at the end of the reach.

A steady flow discharge used for one of the steady flow runs, q_1^S ,is selected initially. The measured steady flow system variables $\bar{z}^S$ and $\bar{q}_s^S$ are known in the temporal domain for the particular run where $q = q_1^S$, Figure 3.11 (b) and (c).

For compatibility between steady flow and translation wave experiments, the first requirement is matching mean stage values

$$\bar{h}^S \equiv \bar{h}^{NS}$$

where $\bar{h}^S$ is obtained from the steady flow rating curve knowing q_1^S, Figure 3.11(a). The equivalent non-steady flow stage $\bar{h}^{NS}$, shown for example on the rising limb of the wave in Figure 3.11(d) specifies

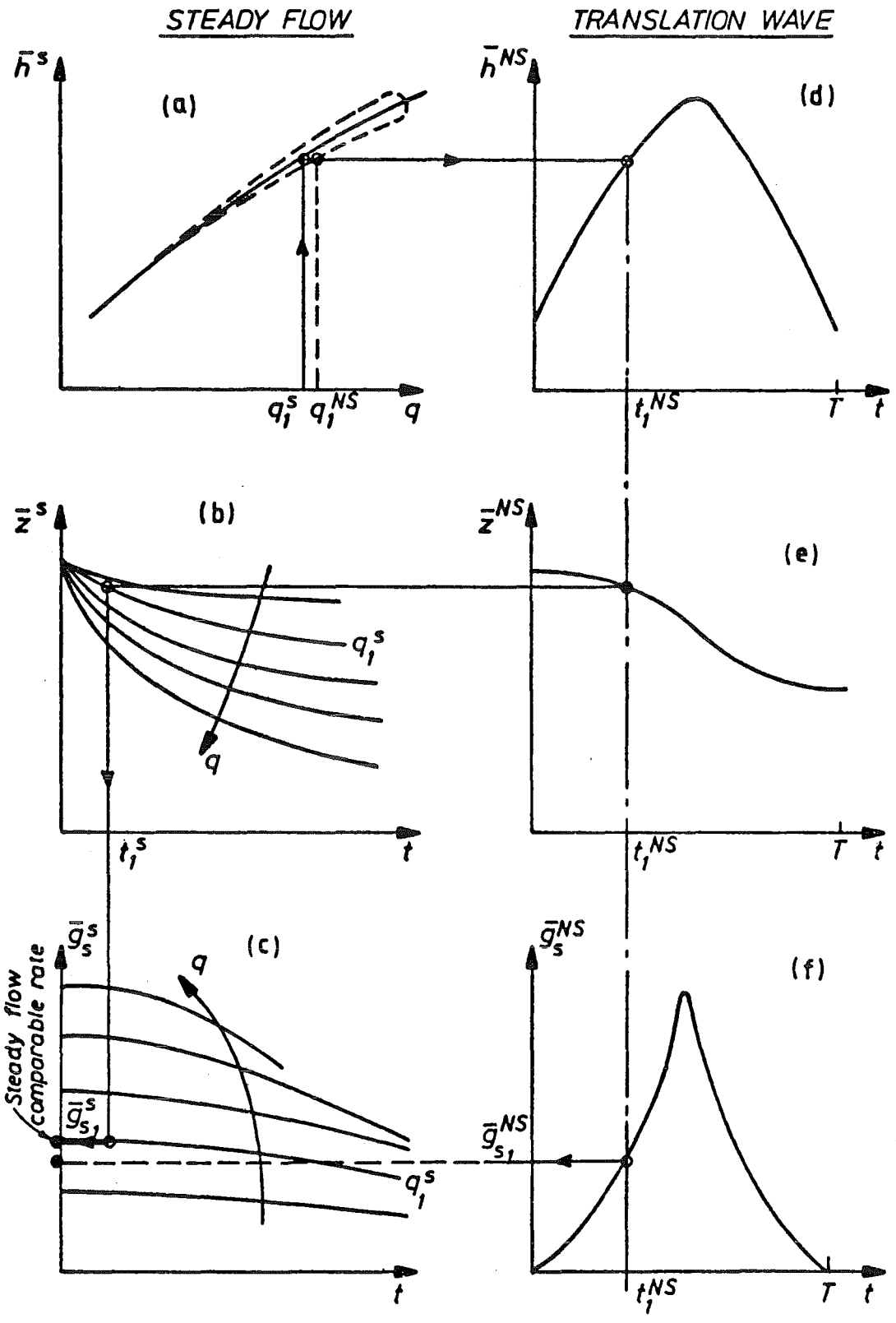

FIGURE 3.11 : Comparison procedure for transport rates for steady flows and triangular translation waves (non-equilibrium)

a time t_1^{NS} at which the measured system variables, from the translation wave experiments, $\bar{z}^{NS}$ and $\bar{g}_s^{NS}$ are known, Figure 3.11(e) and (f).

Under steady flow conditions, the discharge q_1^S requires a time t_1^S, Figure 3.11 (b), to reduce the mean bedlevel $\bar{z}^S$ to the same value $\bar{z}^{NS}$ existing at t_1^{NS}, being the second matching requirement. Using the same mean bedlevel for both sets of non-equilibrium experiments, will ensure that the general scour hole profiles in each case are approximately the same. Values of t_1^S and q_1^S define a comparable steady flow non-equilibrium transport rate $\bar{g}_{s_1}^S$, Figure 3.11(c), which can be compared with the measured non-steady flow transport rate $\bar{g}_{s_1}^{NS}$ at t_1^{NS}. Comparable conditions can now be defined as occurring when the system parameters, with the exception of the bedload transport rate, approximately correspond.

However, the stage-discharge curve for a flood wave normally forms a hysteresis loop, so a slightly different (<6%) comparable steady flow bedload transport rate will be obtained if the actual wave discharge q_1^{NS} was used instead of q_1^S. An average value of the transport rates, resulting from the use of the two flow rates, should be taken as the comparable steady flow transport rate.

Repetition of the above procedure for different constant discharges q_1^S for both the rising and falling limbs of the translation wave allows a comparable steady flow non-equilibrium transport rate hydrograph to be derived. This will serve as a comparison with the measured transport rate hydrograph for a non-steady translation wave. Any differences in magnitude can then be perceived.

CHAPTER IV

LABORATORY EXPERIMENTS : DESIGN AND APPARATUS

4.1 SYNOPSIS

This chapter describes the scaling and the design of an experimental programme in accordance with the aims presented. The equipment employed during the experiments is described in the latter half of the chapter.

4.2 INTRODUCTION AND AIMS

A series of laboratory experiments, designed to investigate various fundamental aspects of transient sediment transport processes, was conducted in the Fluid Mechanics Laboratory, University of Canterbury, during the period 1978-79. The initiation of particle motion and equilibrium transport experiments were also included in the experimental programme for the reasons given in section 1.2.

The aims of the experimental programme, which stem from the implications of the literature review (section 2.7), are as follows:

(1) To further extend the quantitative assessment of initial motion conditions on the bed.

(2) To provide quantitative experimental data for simple non-equilibrium conditions with both steady and non-steady flows, thus providing useful background data in the important field of transient sediment transport.

(3) To provide a comparison, using the experimental data, between transport rates in equilibrium and non-equilibrium steady flow conditions and between transport rates in steady flow and

non-steady flow non-equilibrium conditions.

(4) To test the predictive powers of current mathematical models which use equilibrium transport formulae for transient bedload conditions.

(5) To examine the effect of non-steady flows on bedform development and its effect on resistance to flow and stage-discharge curves.

(6) To test the hypothesis of Griffiths (1976), that the difference between actual non-steady flow non-equilibrium transport rates and comparable steady flow transport rates will diminish as the bedload sampling point is moved further downstream within the general scour hole.

To achieve these aims, an experimental programme was designed as outlined below.

4.3 EXPERIMENTAL MODEL : SCALING AND DESIGN

4.3.1 Model Scaling

For many of the rivers in New Zealand, the bed slope is steep and the bed, composed of coarse gravel, is wide. In these rivers, significant bedload transport generally occurs only in times of flood; Griffiths (1979), Pemberton (1979). Consequently the experimental model was chosen to simulate typical flow and bedload transport characteristics covering and extending the upper range of flood events observed in the field.

To achieve simulation of a typical river in an experimental model, the relevant scaling relationships must be satisfied. For

two phase phenomena where the flow phase is non-steady, Yalin (1971) derives 5 dimensionless variables which, although not unique, completely determine the alluvial system. The dimensionless variables are

$$X_1 = Re_* = \frac{u_{*_b} D}{\nu} \qquad \text{Grain Reynolds Number}$$

$$X_2 = Y = \frac{u_{*_b}^2}{(S_s - 1) g D} \qquad \text{Entrainment Function} \qquad \ldots (4.1)$$

$$X_3 = \frac{y}{D} \qquad \text{Relative Roughness}$$

$$X_4 = S_s = \frac{\rho_s}{\rho} \qquad \text{Grain Specific Gravity}$$

$$X_5 = S_t = \frac{u_{*_b} T}{y} \qquad \text{Strouhal Number}$$

where u_{*_b} is the bed shear velocity, D the mean grain size, ν , ρ the kinematic viscosity and density of water, ρ_s is the density of the sediment grains, and T is the translation wave period. The grain Reynolds number is unimportant as flow conditions in the model and prototype will be in the rough turbulent zone ($Re_* > 70$).

The prototype fluid and sediment were used in the experimental model and so S_s was the same for both. Therefore the dynamic similarity laws are

$$\lambda_{x_2} = \lambda_{x_3} = \lambda_{x_5} = 1 \qquad \ldots (4.2)$$

where

$$\lambda_x = \frac{x'}{x''} \quad \frac{\text{model}}{\text{prototype}}$$

This reduces to the following scale relationships for the system variables :

$$\lambda_y = \lambda_D = \lambda_1 = \text{undistorted length scale}$$

$$\lambda_{u*_b} = \sqrt{\lambda_1} \qquad \ldots (4.3)$$

$$\lambda_T = \sqrt{\lambda_1}$$

By using a model grain size, D_{50} = 2mm, and assuming a typical prototype size, D_{50} = 30 mm, a length scale of 1/15 is implied. Therefore

$$\lambda_D = \lambda_y = \frac{1}{15}$$

This is greater than the minimum scale criterion of Yalin (1971)

$$\lambda_1 > \left(\frac{70}{Re_*''}\right)^{2/3}$$

which for a typical New Zealand river is $\lambda_1 \geq \frac{1}{30}$. Similarly, from equation 4.3

$$\lambda_T = \lambda_{u*_b} = \lambda_u = \frac{1}{3.87}$$

The most important modelling aspect is that the rates of rise for floods should be correctly modelled. A very fast rising river may rise at 0.5 m/hr, which scales to 0.13 m/hr. using the above velocity scale. This rate was used as a guide for selecting the eight triangular translation waves of varying steepness and period. As bedload transport effects, due to non-steady flows, are more pronounced under severe conditions, rise rates ranging from 0.08 m/hr. to 0.77 m/hr. were selected for the model.

4.3.2 Design of Experiments

Methods of conducting movable bed experiments in flumes have been well established, using either a closed-circuit system (where the sediment is re-circulated) or an open-circuit system (where the gravel is added at the upstream end of the erodible reach). Most experimental runs were planned with non-equilibrium transport conditions (i.e. zero upstream sediment input). Therefore it was convenient to operate the flume in an open-circuit fashion.

The parameters of flume slope (S_o), inlet discharge per unit width (q) and the flume width (B) were chosen as independent variables. This leaves the water depth (y), velocity ($\bar{u}$), transport rate (g_s) and friction factor (f) as the dependent variables. This choice of independent variables defines a system which may be multi-valued over some ranges, {Kennedy and Brooks (1963}. However, as the Froude Number range was small, ($Fr' \simeq$ 0.55 - 0.6), the friction factor and transport rate relationships with steady discharges will be single-valued. By carefully choosing the magnitudes and ranges of the independent variables B , S_o and $q_c \leq q \leq q_{max}$, the constraints imposed by the capacity of the bedload discharge measuring device were overcome.

4.4 EXPERIMENTAL PROGRAMME

The experimental programme involved the execution of 170 different runs in the large flume. The conditions and constant parameters for each series are summarised below :

(1) Constant Parameters - 30 m long flume, B = 0.305 m wide, flume slope (S_o) = 0.0020 (unless otherwise specified) and D_{50} = 2.11 mm.

(2) Steady Flow Experiments

(a) Series IM - Initial motion studies (S_o = 0.0030 for most of these runs)

(b) Series SE - Constant discharge, equilibrium transport

(c) Series ST - Constant discharge, non-equilibrium transport

(3) Non-Steady Flow, Non-Equilibrium Transport Experiments

(a) Series NS - Symmetrical and skew triangular translation waves

(b) Series SC - step change in constant discharge from threshold conditions.

Details of the experimental programme and the procedures involved are given in the next chapter.

4.5 LABORATORY APPARATUS

4.5.1 30 m Tilting Flume

The primary laboratory component was a 30 m long tilting flume, (Plate 4.1), which has been described in detail by Hill (1967). The flume consists of adjustable side wall elements which sit on a flat steel plate deck, 28.5 m in length and has a working section of 23 m. The side wall elements were constructed of steel plate with the exception of a 10.5 m section of 19 mm thick plate glass located in the mid section of one sidewall. Stilling basins were incorporated at each end of the flume. Changes in slope were achieved by the use of screw jacks at the midpoint and upper end supports of the flume, the downstream support being freely hinged. The selected slope was set using two pointers sliding over fixed background scales. Rails attached to each edge of the steel deck allow free movement of a carriage over the length of the working section.

A 305 mm wide channel was constructed within the 610 mm wide flume using one existing flume wall and a new wall of 6 mm thick perspex, shown in Figure 4.1. To prevent buckling of the perspex wall due to hydrostatic pressures and thermal gradients, the redundant channel (Figure 4.1), was sealed off at both ends and filled with water from the mains up to the main channel stage level. The horizontal water surface in the sealed reservoir was utilised to check the flume slope with a point gauge mounted on the carriage.

The longitudinal section was designed as three different sections to prevent non-uniformities in the flow field of the test section.

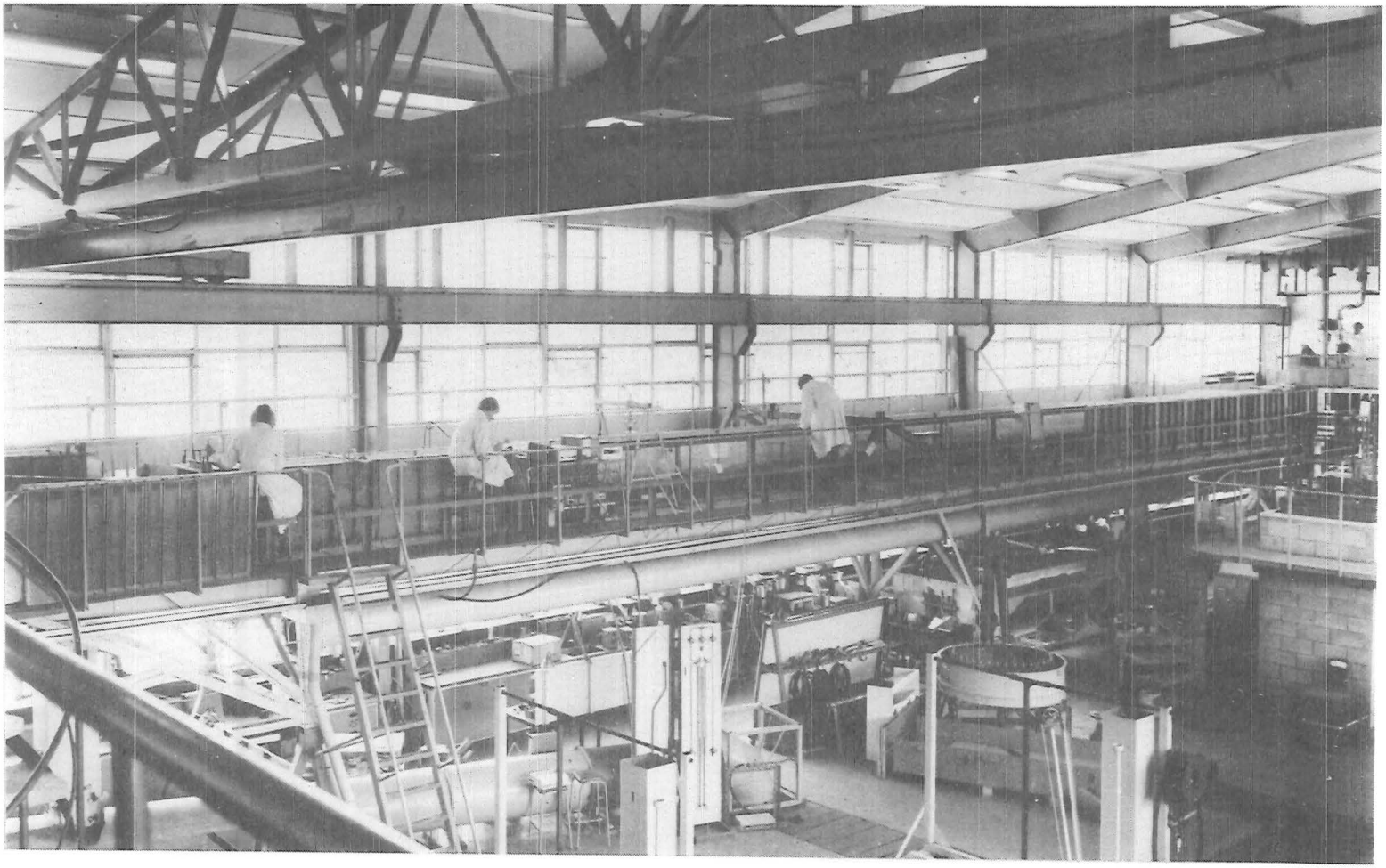

PLATE 4.1 : General view of the tilting flume during a translation wave experiment

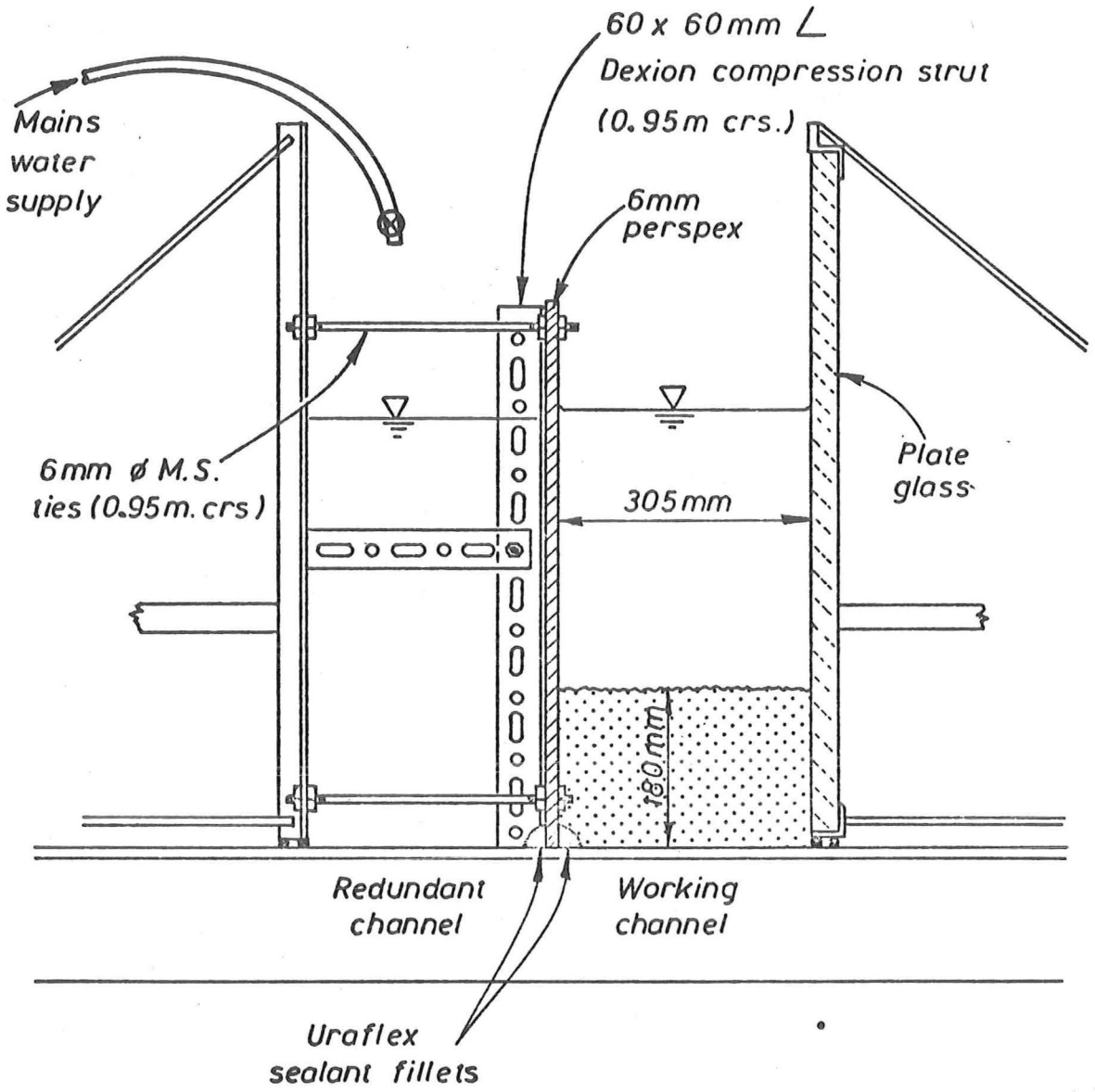

FIGURE 4.1 : Flume cross section

A schematic flume longitudinal section is shown in Figure 4.2. The essential components of these sections are as follows :

(1) Upstream Section

(a) Reception area for the piped laboratory water supply.

(b) Contracting stilling basin containing flow straightening devices.

(c) Concrete ramp leading onto a length of fixed rough bed. The roughness elements and minimum length were selected to ensure the turbulent boundary layer was fully developed before reaching the test section (see Appendix A).

(d) Sediment dispensing hopper near the beginning of the erodible section.

(2) Test Reach

A length of movable bed composed of uniform fine gravel particles to a depth of 180 mm. Two partition boards were inserted to separate the test section from the two fixed sections. (Figure 4.2)

(3) Downstream Section

(a) Bedload trap used to measure the sediment transport rate at the end of the erodible bed.

(b) Another length of rough fixed bed sufficient to accommodate any backwater effects induced by the downstream control.

(c) Water level control weir at the outflow point of the channel.

(d) Stilling basin from which water drains back into the laboratory system.

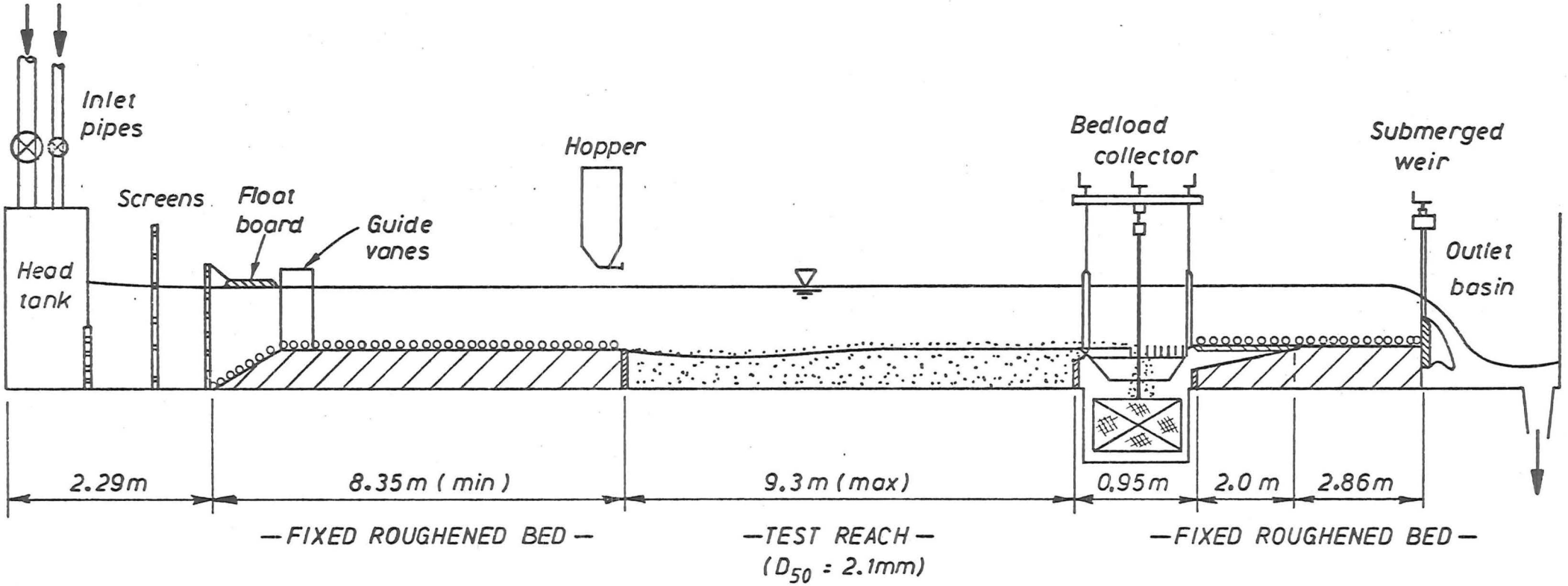

FIGURE 4.2 : Schematic flume longitudinal section

4.5.2 Water Supply and Control

Water was supplied from a constant head tower and introduced to the upstream head tank of the flume through two valve-controlled pipes of different diameter. The smaller diameter pipe (76 mm) provided a baseflow to establish critical conditions on the bed, while the larger diameter pipe (152 mm) provided the balance of flow required for steady and non-steady runs. The maximum flow obtainable from both pipes together was 0.15 m^3/s.

Prescribed non-steady flow hydrographs were generated manually by opening and closing the larger valve in small steps at predetermined times. The valve settings were derived from a steady flow calibration curve plotted from 60 flow measurements for clockwise and anticlockwise valve movement. The position of the valve was read from a fixed circular scale, divided into 144 divisions (2.5^0 of arc), with the aid of a pointer attached to the valve wheel. In practice the valve was nearly continuously moved, the time step between changes lying in the range 0.4 to 0.8 per cent of the wave period. The calibration curve was checked during each steady flow series.

A series of perforated screens (Figure 4.2) was inserted in the upstream contracting section to dampen disturbances and provide an even flow distribution across the flume. A float board (520 mm x 290 mm x 20 mm) was situated at the entrance to the 305 mm wide channel to remove wave disturbances on the water surface. A flow alignment device was also placed at the beginning of the fixed rough bed. It consisted of three (800 mm x 800 mm x 3 mm) mild steel plates at 75 mm spacing, bolted to dexion angle strips cemented in the fixed bed. This device proved necessary as without it secondary flow currents caused a ridge to develop along the centre line of the scour hole. Plate 4.2 shows the various flow smoothing devices.

At the downstream end of the channel, a submerged weir was

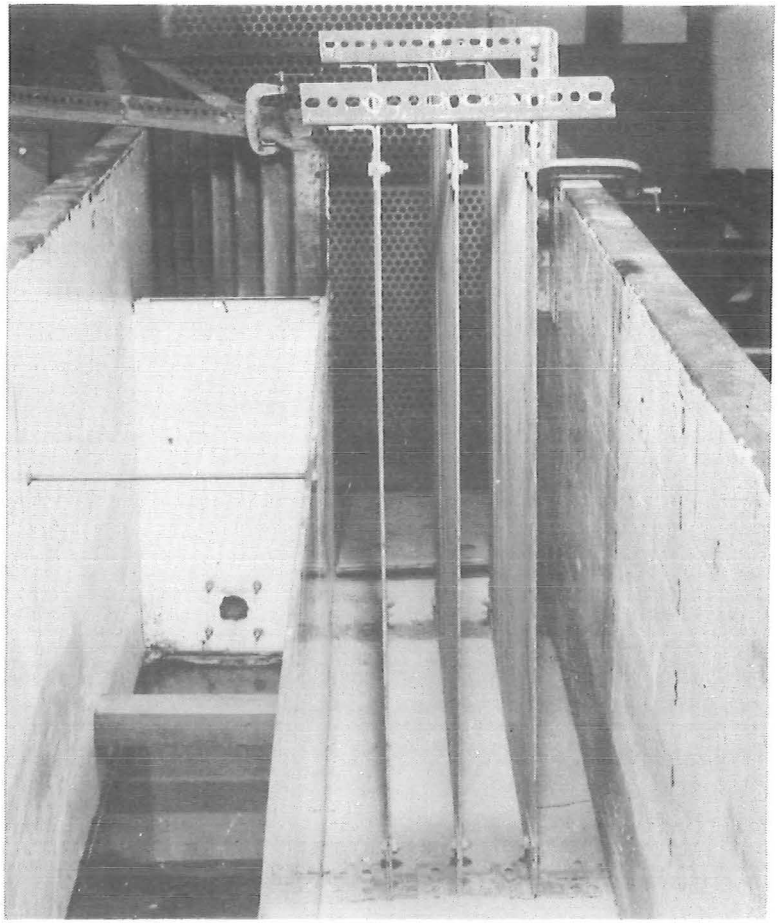

PLATE 4.2 : Flow smoothing devices

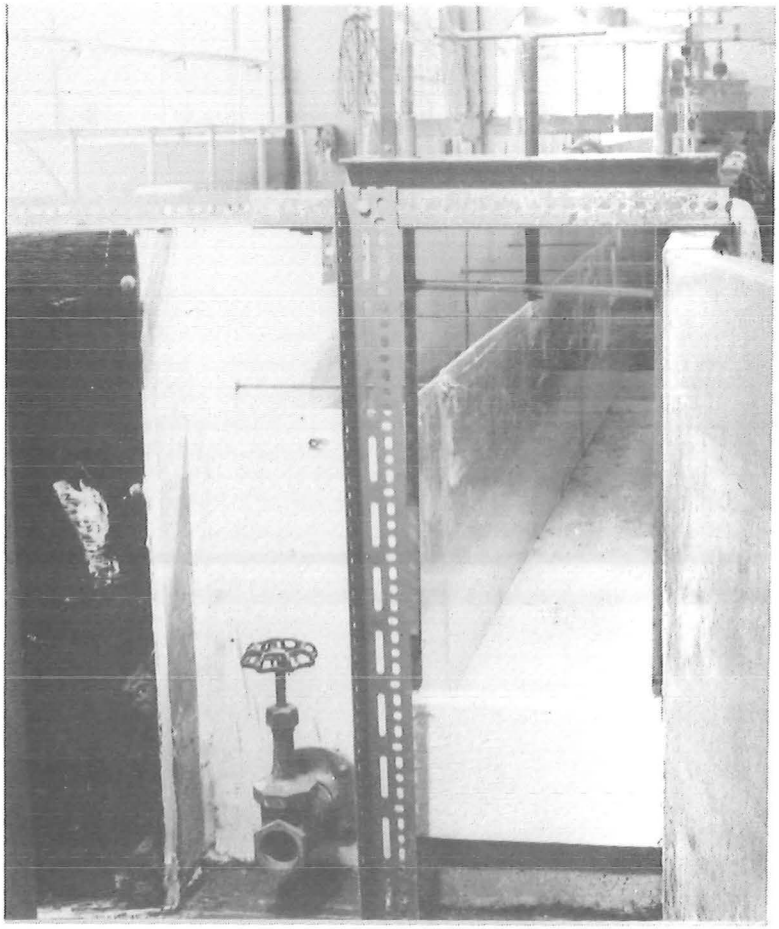

PLATE 4.3 : Outlet submerged weir

provided to control the outlet backwater curve (Figure 4.2). This was a knife-edged blade (304 mm x 180 mm x 20 mm) made from marine plywood, (Plate 4.3). A controlling screw mounting and the support rod guides were welded to a horizontal strut clamped on top of the flume walls. The weir height was read from a fixed scale marked by a pointer attached to a support rod. During non-steady runs with triangular waves, the weir was raised and lowered in small steps in delayed synchronisation with the opening and closing of the inlet flow valve. The delay or time lag was the time for the translation wave to reach the end of the test section. In a similar manner to the valve calibration, the weir settings were obtained by interpolation of the steady flow values. The height change for each adjustment step during a wave was 0.8 mm.

The water was returned to an underground sump through a calibrated pit which was used to measure steady discharge rates.

4.5.3 Sediment Injection

For sedimentation experiments in open-circuit flumes, gravel must sometimes be added to the flow. A vibrating hopper (Plate 4.4) was designed and constructed to feed air-dried gravel at various constant infeed rates. The hopper was suspended from the overhead laboratory crane just upstream of the movable bed. It was assembled in two sections made from galvanised steel plate; the main body was rectangular in section with vertical sides while the lower section was a truncated pyramid shape containing a slot in the base. The working components of the hopper were :

(1) A sliding gate with an attached scale providing a variable width aperture.

(2) Constant speed, three phase Sinex electric vibrator affixed to one of the sloping sides, which was suitably strengthened.

Problems were encountered with occasional clogging at the outlet. The performance was greatly improved by a steel rod inside the hopper attached to the vibrator anchorage plate and extending to the outlet region. Extensive calibration tests were conducted. The relationship between outflow mass rate (gm/s) and the aperture opening was linear for the low rates, departing slightly from this trend for the higher rates. An error spread about the mean flow rate was ±4%. The outflow mass rate was independent of the gravel head in the hopper until it was half empty, so the hopper was topped up at various stages of a run. The slowest infeed rates (below 2 gm/s) required the use of a small calibrated glass measuring cylinder from which a specified mass of gravel was manually dropped into the flow every 15 to 30 seconds.

4.5.4 Bedload Discharge Measurement Device

Two different devices were used during the experimental programme to measure the bedload transport rate, but they shared the same measurement system and electronic circuitry. The original device, which was fixed in position at the end of the erodible reach, was designed and used by Griffiths (1976). Another device was subsequently designed to follow the level of the gravel bed during degradation.

(1) Fixed Bedload Collector

The bedload recorder was capable of measuring the accumulated weight of submerged gravel continuously. A rectangular steel tank (845 mm x 250 mm x 490 mm) was bolted to the underside of the flume to cover a hole cut in the channel floor. A wire mesh basket was suspended in this box, (Plate 4.5), from a load cell by a thin high tensile rod to minimise the flow disturbance. Above the floor opening a steel frame was placed consisting of a grill of transverse steel plates spaced 65 mm apart. This frame was mounted on legs to

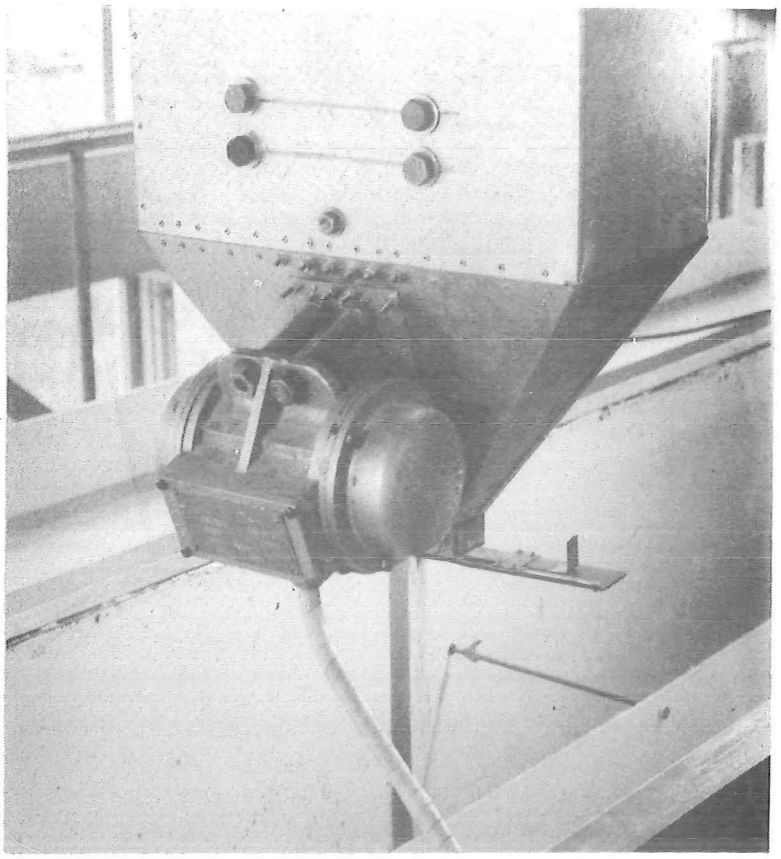

PLATE 4.4 : Sediment vibrating hopper

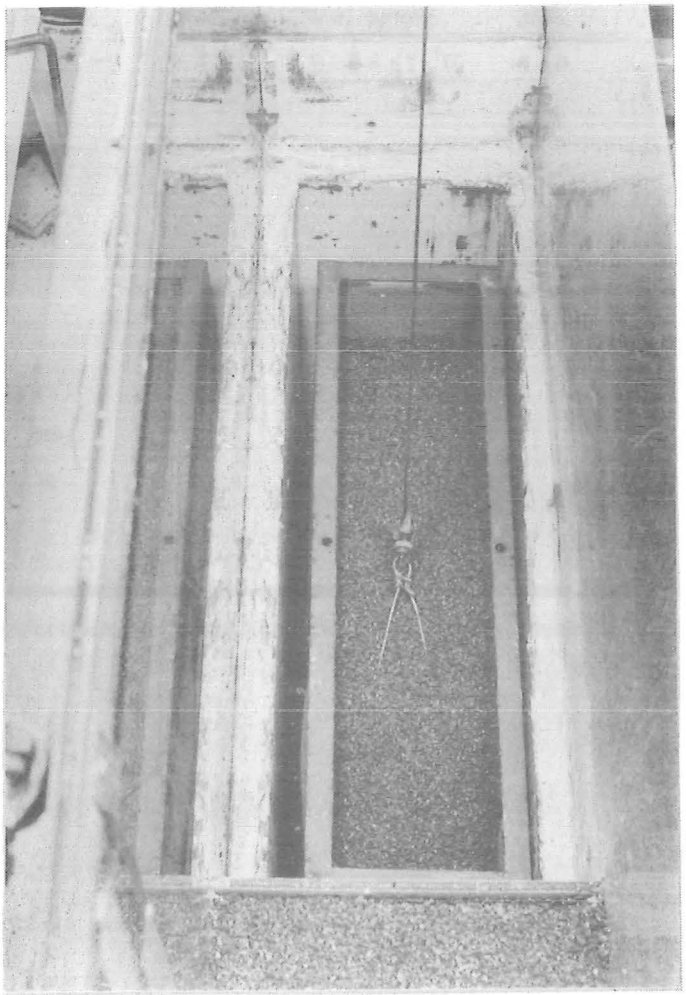

PLATE 4.5 : Bedload collector mesh basket

bring it to the initial level of the gravel bed; its function being to provide continuity of roughness and to develop vortices between the grill plates to assist the entrainment of sediment particles. A galvanised sheet was placed over the upstream half of the frame to direct the bedload into the central portion of the mesh basket to maintain it in an evenly balanced position. As the bulk of the bedload was entrained within one grid spacing, the length of galvanised steel was critical, being determined by trial and error. The load cell was mounted on the base plate of a small rectangular steel frame which was suspended by a threaded rod from a gantry, the legs of which were bolted to the flume deck either side of the main flume walls.

At the completion of each run, the basket was lowered to the floor of the trap, uncoupled from the load cell and the galvanised sheet and grill removed. The overhead laboratory crane was used to lift the basket, which after emptying was replaced and the collector unit reassembled in reverse order.

(2) Adjustable Bedload Collector (Plate 4.6)

Another bedload collector unit was constructed to facilitate the lowering of one or both ends of the grill in order to follow the degrading bed level during non-equilibrium experiments. The same grill pattern of transverse steel plates, spaced 60 mm apart, was incorporated in a hinged cradle frame, (Plate 4.7). The frame was suspended by threaded rods at each end from a rectangular hollow section beam perpendicular to the basket support gantry. By rotating a support rod, the frame could be raised or lowered at that end, with reference to a scale attached to the beam. At the upstream boundary, between the erodible bed and the bedload collector a joint was needed to provide flexibility in the vertical direction but also to prevent loss of gravel from the test reach underneath the grill

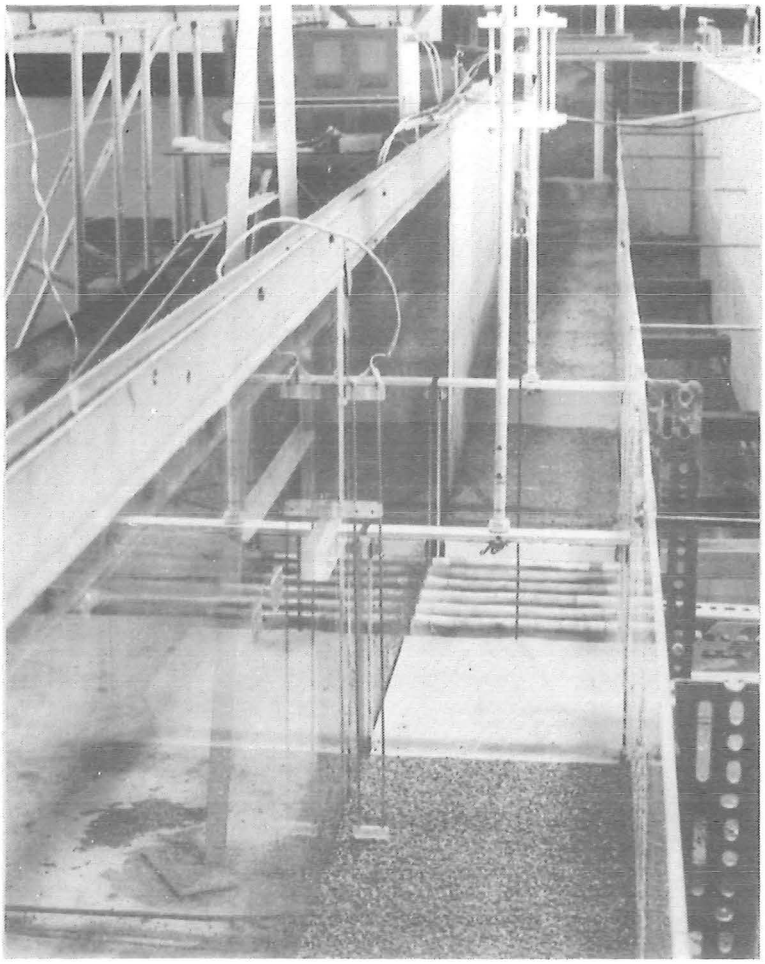

PLATE 4.6 : Adjustable bedload collector unit

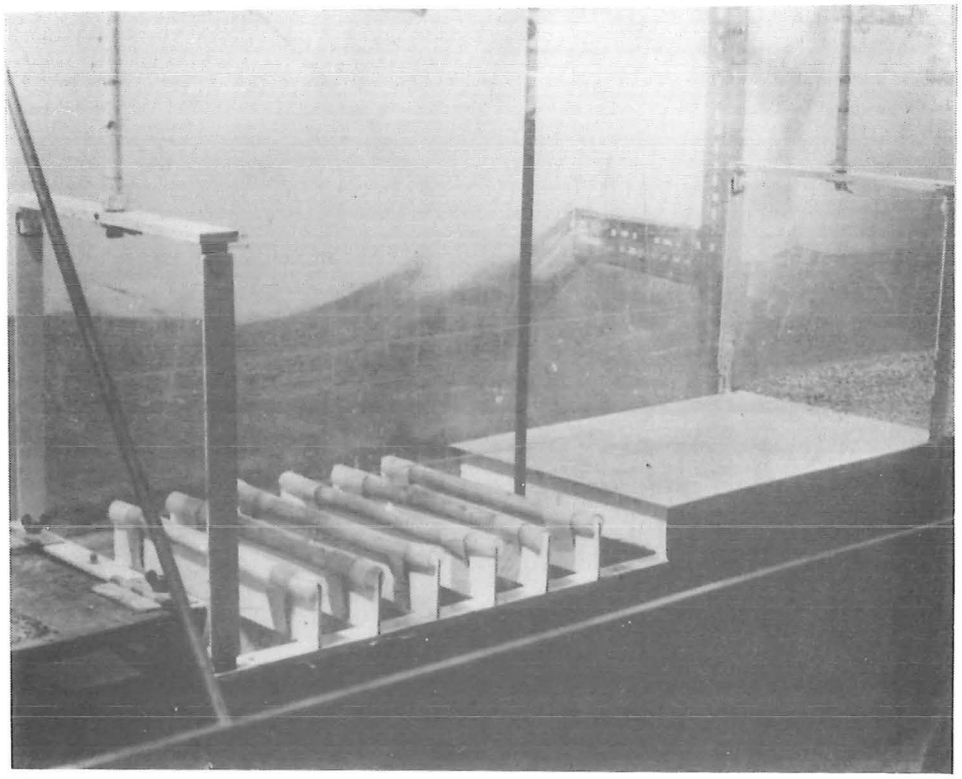

PLATE 4.7 : Hinged cradle frame

frame. This flexible joint was provided by a 2 mm thick insert rubber sheet (306 mm x 125 mm) connected between the frame and a 110 mm high partition board at the downstream end of the test reach. The downstream end of the bedload collector unit was also made adjustable to streamline the bed profile in the vicinity of the collector and thereby prevent steep adverse slopes for the bedload collector grill when significant bed degradation occurred (see Figure 5.4). This was achieved by removing an initial 0.8 m length of the fixed rough bed, and inserting a length of marine plywood, hinged at both ends, into the gap. This board was coated with a bitumen-based paint and while wet, covered with a layer of gravel particles to provide commensurate roughness, (Plate 4.6).

(3) Load Cell and Circuitry (for both bedload collectors)

The entire weight of the sediment laden mesh basket was supported by a thin-walled aluminium load cell on which four strain gauges were arranged, (Plate 4.8). The electronic apparatus, shown in Plate 4.9, amplified the output from the strain gauge bridge which was then displayed on a digital voltmeter and recorded by a Datel thermal printer at intervals of either 30 or 10 seconds. The electronic apparatus was allowed to warm up for 15 minutes prior to each run to prevent drift in the output voltage values. Before the commencement of the experiment the 1000X amplifier was shorted across its input terminals and adjusted to give an output of zero volts.

To calibrate the weighing system, pre-weighed samples of air dried gravel were added to the immersed basket and the resultant output voltage recorded. The relationship between a change in accumulated dry weight and a change in output voltage was found to be constant within the limits of accuracy of the device. This constant was checked several times during the experimental programme.

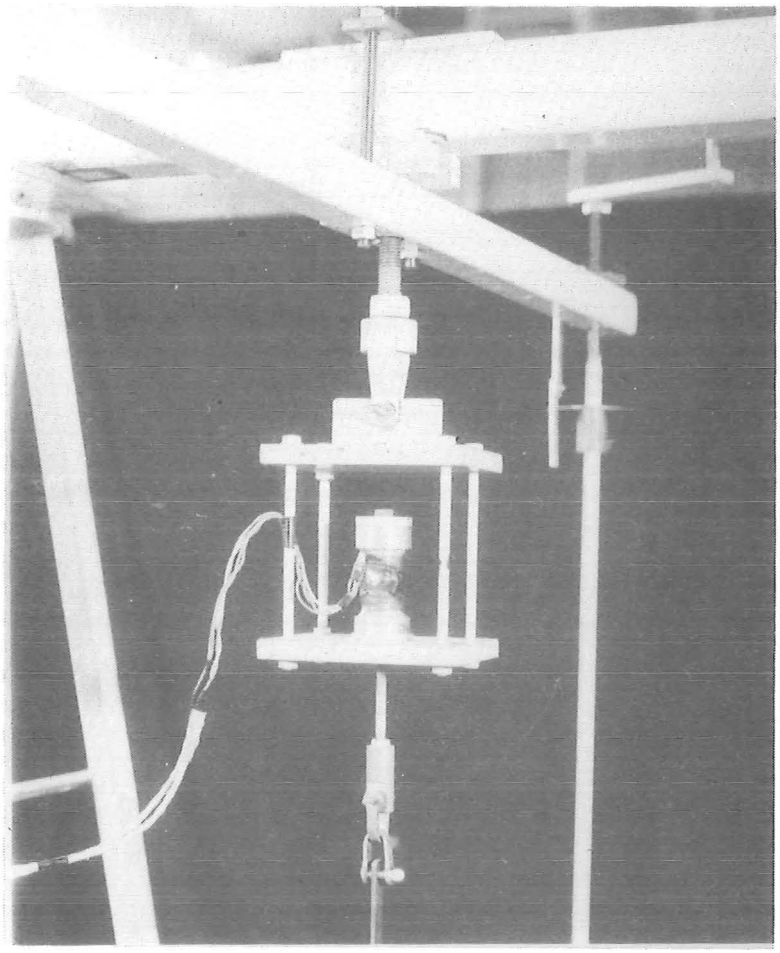

PLATE 4.8 : Aluminium load cell and support frame

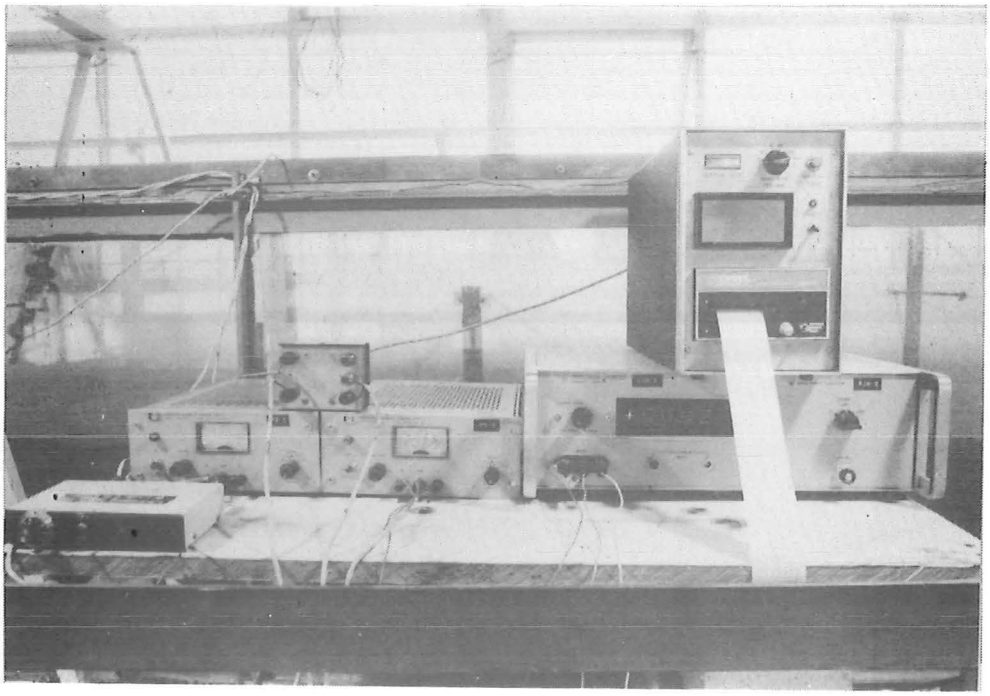

PLATE 4.9 : Electronic apparatus for bedload collector

4.5.5 Stage and Bed Level Measuring Devices

The devices used for the determination of stage and erodible bed levels were mounted on a four-wheeled carriage at a position corresponding to the centreline of the channel, (Plate 4.10). The elevation of the water surface, relative to the carriage rails, was measured by a point gauge during steady flow runs, to the nearest 0.1 mm using a vernier scale. To measure the stage level continuously during non-steady flow runs, two water level recorders were used at various fixed stations, (p and q). A profile of the bed surface could be obtained from an ultrasonic bed level recorder.

(1) Water Level Recorders

Resistance water level probes were used in conjunction with a Hewlett-Packard two channel pen recorder to measure the water level as a function of time at a specific location. The probe consists of two 3.18 mm stainless steel rods 450 mm long, at 26 mm spacing, which were anchored in perspex blocks, (see Plate 4.6). The lower perspex block of each probe was given a streamline shape to minimise the disturbance of the flow and the bed. The imbalance in a bridge circuit, caused by a change in resistance, from the balanced position (set for the base flow) was recorded as an output voltage on the chart recorder.

The output was non-linear so calibration curves were established between chart record displacement and the corresponding point gauge reading. There was a tendency for the calibration to shift slightly for different runs, therefore the calibration was checked at various times during each non-steady flow experiment by point gauge readings.

(2) Ultrasonic Depth Meter (Plate 4.11)

The ultrasonic depth meter was obtained on loan from the Central Laboratories, Ministry of Works and Development. Full details of

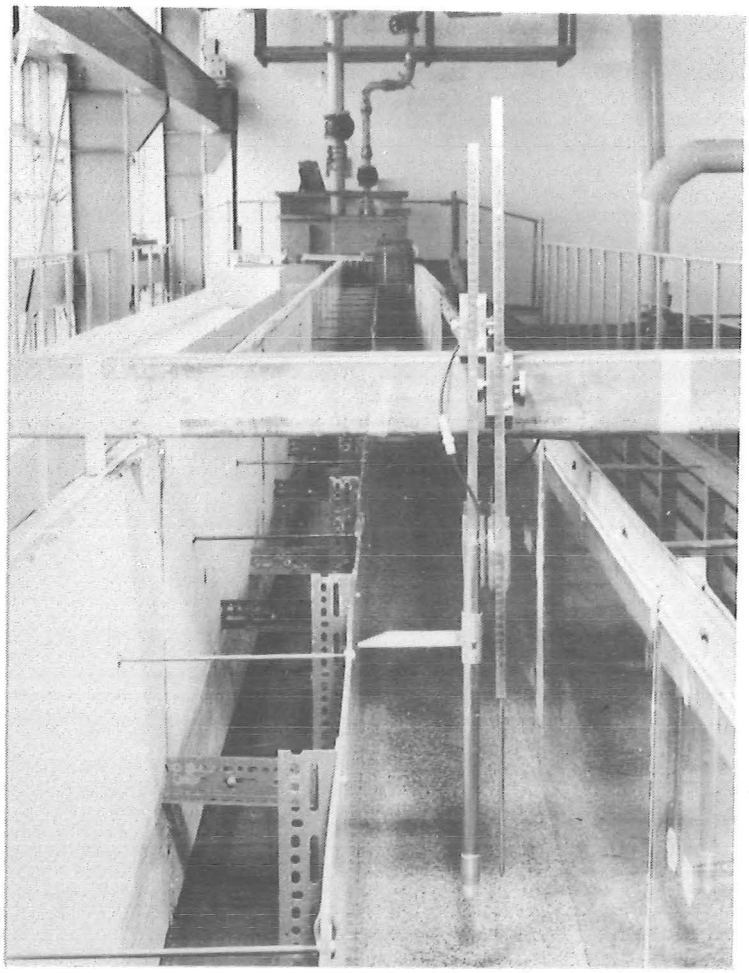

PLATE 4.10 : Carriage with mounted ultrasonic probe and point gauge

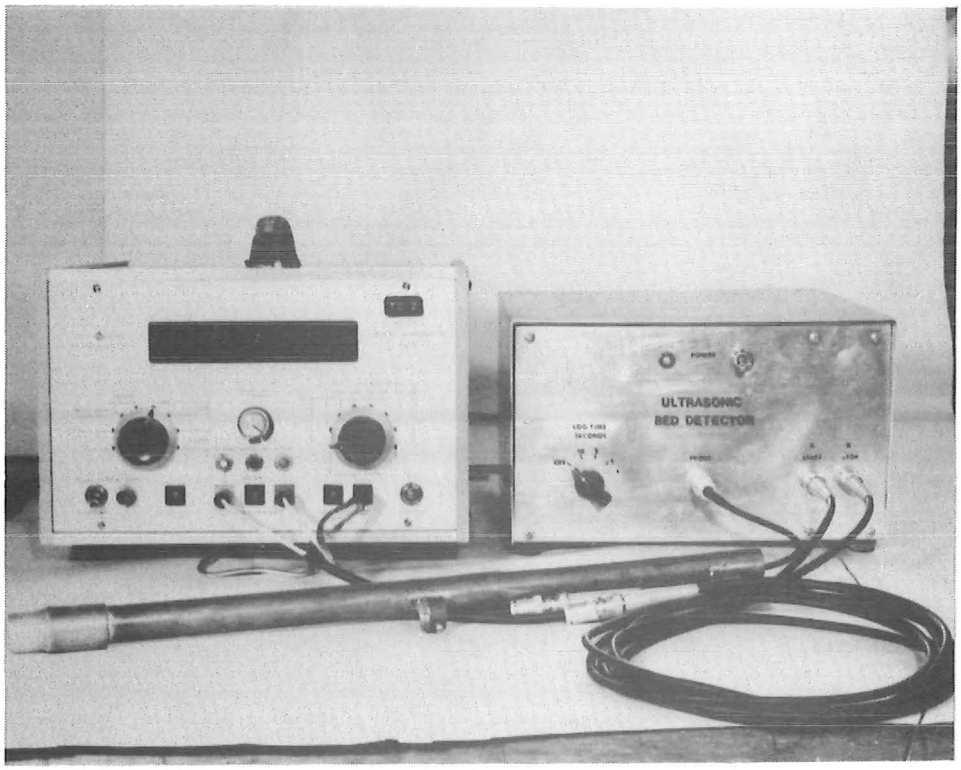

PLATE 4.11 : Ultrasonic depth meter and timer/counter

design and performance have been described in Spinks and Keller (1976).

The circuit of the main unit comprised an ultrasonic transmitter, an ultrasonic receiver and a gate circuit to separate the transmitted pulses from the received pulses and transmit them in the correct sequence to an electronic timer/counter, (Plate 4.11). The source of the ultrasonic beam is a 2 MHz piezo-electric crystal probe (20 mm diameter), of a type commonly used for non-destructive metal testing, and was connected to the main unit by a 50 m stereo cable.

The probe was mounted on the end of a 20 mm diameter tube, 440 mm long and sealed with silicone rubber to prevent entry of water. The tube was clamped onto another point gauge on the carriage, (Plate 4.10), and could thus be lowered or raised with water level. With the emitting surface of the probe below the water level, the time taken for a pulse to travel to the bed and back is equal to twice the water depth between the probe and the bed, divided by the celerity of sound waves in water. The time is measured with the timer/counter and displayed in micro-seconds. The only available timer/counter unit had no output facilities other than a digital display, therefore readings at different stations were recorded manually. Location of each station was determined with the aid of a pointer attached to the probe mounting and distances marked on the top of the perspex channel wall.

Calibration of the bed level meter was carried out in a large perspex tank, and the results plotted on a graph of depth, from the probe to the tank floor, versus pulse travel time. This resulted in a linear relationship, which was expected since the slope is the constant velocity magnitude of sound in water, provided the temperature range is not large e.g. Spinks and Keller (1976) found an error range of ∓2% for a temperature range of $\pm 12^0$C, which is well outside the range of $\pm 3^0$C achieved in the present study. The depth resolution

from the calibration tests was found to be ±0.73 mm which coincides with the wavelength of a pulse triggered at a frequency of 2 MHz at the average temperature of 15^0C.

4.5.6 Ultra-Violet Light Source

A device which generated an ultra-violet light beam from a portable shielded hand-lamp was used to trace the movement of single gravel particles coated with a fine layer of fluorescent paint. Observational experiments using the ultra-violet light were conducted to count tagged moving particles and also to trace the remaining particles within the bed after the completion of the experiemnt.

4.6 BED MATERIAL

The bed material used was derived from a deposit of Rangitata River sand obtained by British Pavements Canterbury Limited, with an initial D_{50} = 1.77 mm and σ_g = 1.56. It was sieved twice between mesh screens of 3.35 mm and 1.70 mm spacing. The resultant bed material was a fine gravel with a mean size of 2.11 mm with sub-rounded to rounded grains. The grain size distribution curve (Figure 4.3) was derived from the sieve analysis results performed for two random samples of approximately 1 kg. Relevant properties of the fine gravel material are given in Appendix A.

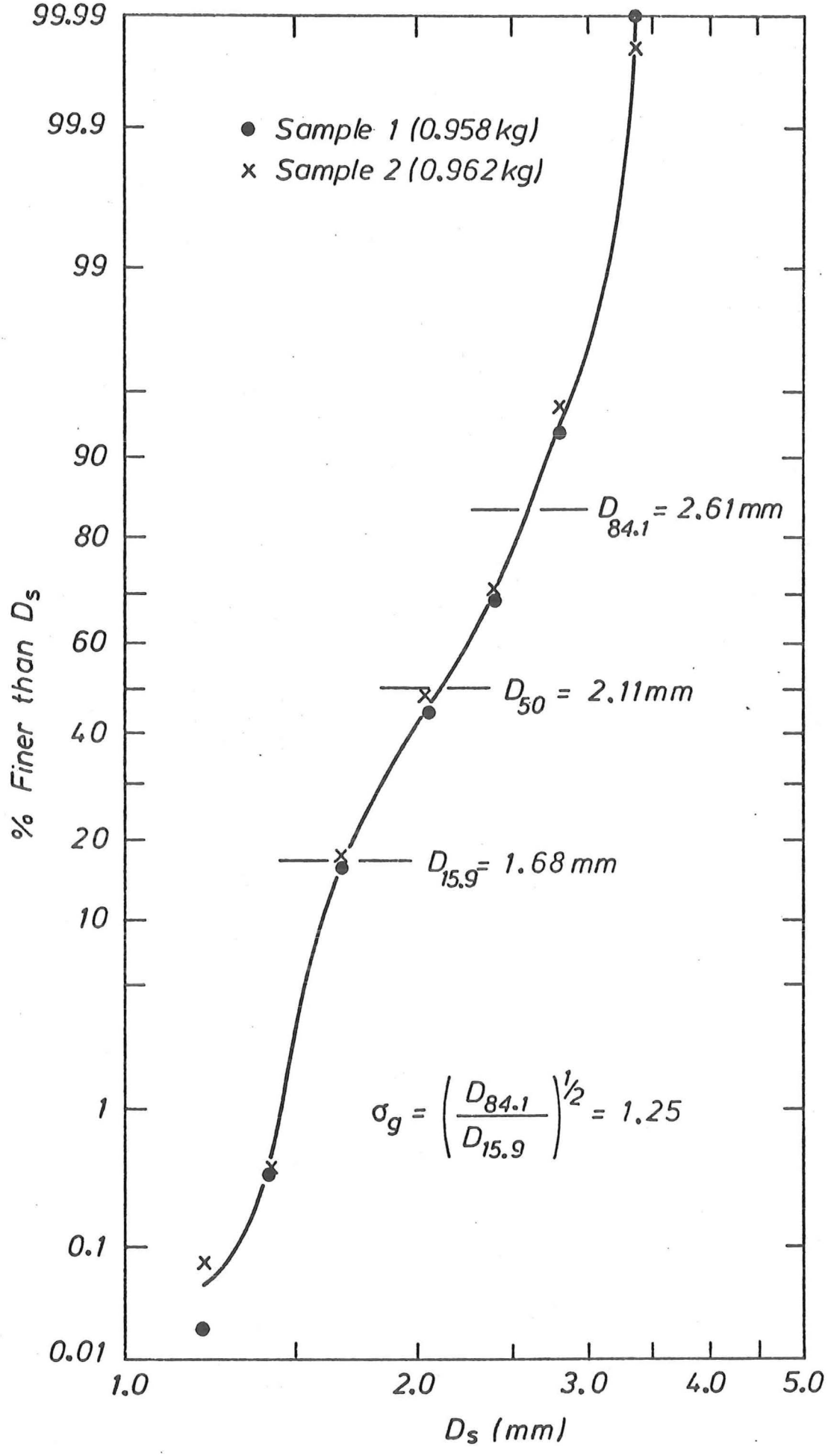

FIGURE 4.3 : Bed particle size distribution curve

CHAPTER V

LABORATORY EXPERIMENTS : PROCEDURE AND ANALYSIS

5.1 SYNOPSIS

This chapter describes typical experimental procedures for each series of experiments performed and the measurements that were recorded. The final section explains the methods of data analysis which were employed.

5.2 IDENTIFICATION CODE FOR EXPERIMENTS

The identification code for each particular run is a six letter-figure combination, the first two being letters identifying the particular series to which the experiment belonged. The next two figures indicate the wave or run number in that particular series, while the last two figures refer to the length of erodible bed in the test section e.g. NS0617 specifies a non-steady triangular wave No. 6 (Figure 5.2), for a reach length of 1.74 metres. A summary of the identification code components is given in Table 5.1 .

SERIES	CODE	WAVE OR RUN NO.	REACH LENGTH	CODE
Initial Motion	IM	01,02,03,...,10	0.74 m	07
Steady ~ Equilibrium	SE		1.74 m	17
Steady ~ Non-Equilibrium	ST	(except skew-triangular waves in series NS where 28 is used for a combination of wave No. 2 & No. 8)	3.53 m	35
Non-Steady ~ Triangular Wave	NS		5.29 m	53
Step Change in Discharge	SC		9.29 m	93
Linear Change in Discharge	LC			

TABLE 5.1 : Components of the Identification Code

5.3 MEASUREMENTS

Measurements were made during the course of each experiment, either automatically at small time intervals, or manually sampled over greater time periods, using the following methods.

5.3.1 Water Discharge

The calibrated pit (Section 4.5.2) was used to measure the steady flow rate twice during each run of series IM, SE, ST and SC. Possible errors in this collection method are ±0.5%. The steady flows measured in this way were used to check the calibration of the larger valve (152 mm) for operation during the NS and LC series.

5.3.2 Water and Bed Surface Elevations

Water surface elevations, with respect to the flume slope, for steady flow rates were measured by point gauge at several stations along the test reach (Figure 5.1). The water surface profile was obtained at least four times during a run. The water level for series NS was continuously monitored by the two water level recorders (Section 4.5.5 (1)) situated near the ends of the test reach (Figure 5.1). The outputs from the two gauges were traced on a chart record moving at 1 mm/sec, the time record being marked by a separate pen every second. The water surface elevation could be obtained as a corresponding point gauge reading from the calibration curves for the two probes.

The bed profile was measured indirectly with the ultrasonic probe (Section 4.5.5 (2)), for all series of experiments, by recording the pulse travel time when the probe was positioned at specified stations along the test section (Figure 5.1). Using the calibration curve the depth from the base of the probe to the bed surface could be determined to the nearest ±0.7 mm.

The datum level for each reach length was nominated as 0.10 m

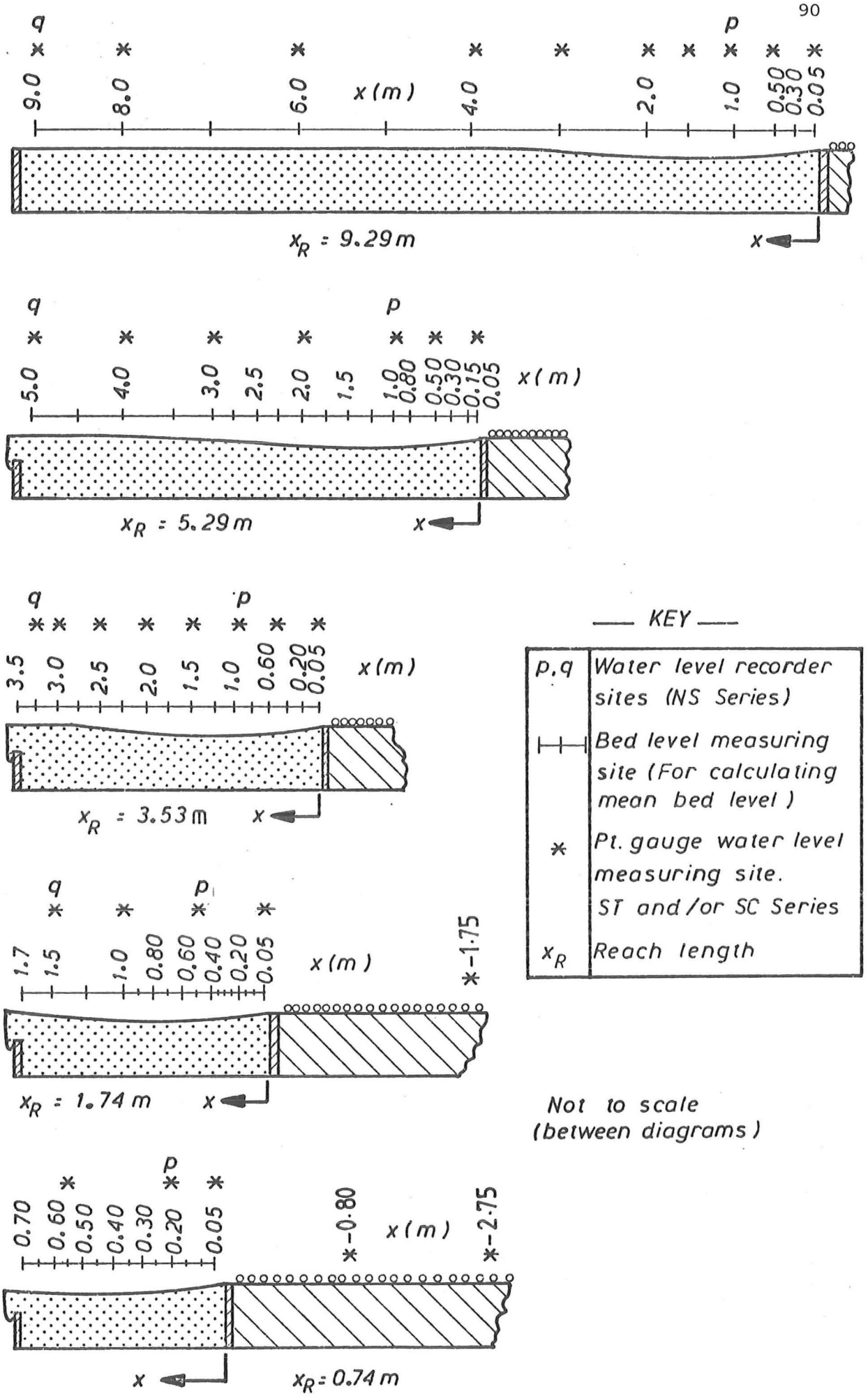

FIGURE 5.1 : Measurement stations for different reach lengths

below the level of the upstream partition board between the fixed and erodible sections. The top level of this partition board was measured by both the point gauge and ultrasonic depth meter to tie the water and bed levels to this common datum.

5.3.3 Bedload Transport Rate

The bedload transport rate was measured indirectly by the bedload collector (section 4.5.4) throughout the duration of all runs with the exception of the IM series. Instantaneous sediment transport rates were obtained by computation from the slope of the cumulative weight versus time plots, using the calibration coefficient to convert a voltage difference to a change in dry weight of gravel.

When the sediment hopper was used for the SE and ST series, the mass flow rate calibration curve for the hopper was checked prior to each run, in the vicinity of the estimated transport rate for that run.

5.3.4 Water Temperature

The temperature of the water was measured at the beginning and end of each run. The maximum variation during a run was 2^0C while the temperature range for the whole experimental programme was 14 - 19^0C. Variations were small because the water circulated throughout the whole laboratory system and was changed every week.

5.3.5 Bed Configuration

The bedform configurations were measured at convenient times using the following methods :

(1) Bedform Height

A difference in depth from the crest to the trough using either the point gauge or the ultrasonic probe.

(2) Bedform Wavelength

The horizontal distance between bedform crests on a fixed scale attached to the flume wall, or by direct measurement with a tape.

(3) Celerity

Calculated from the time required for a bedform to travel a certain distance marked by grid lines on the glass sidewall.

5.4 EXPERIMENTAL PROCEDURES - CONTROL REACH LENGTH (x_R = 9.29 m)

The procedure is outlined for a typical run in each series of experiments for the control test reach, x_R = 9.29m.

5.4.1 Initial Motion Studies (IM--93 Series)

This series of runs was performed to determine baseflows for which conditions on the bed were close to critical.

Conditions of movement were defined by the number of grains displaced downstream of a marked area of erodible bed in a certain time interval. Yalin (1977) suggests that for geometrical similarity between sets of experiments using different mean grain sizes (D_{50}), the area for observation of particle detachments should be proportional to D_{50}^2. Griffiths (1976) performed similar experiments in the same flume using a test area 610 mm x 305 mm, a sediment size of 4.02 mm and bed slope 0.0023. Hence the length of the test area for the present experiments was computed to be 168 mm from the ratio of the two different sediment sizes squared, keeping the width constant. This area was positioned at 5.8 m from the upstream concrete apron.

The bed was levelled throughout the reach length with a scraper attached to the movable carriage prior to each run. The bed was then brushed lightly, with particular attention being given to the

test area. Immediately upstream of this test area, a sheet metal plate 500 mm long coated with a layer of glued bed sediment particles, was placed in the bed flush with the graded bed surface. This plate prevented particles from moving into the test area, so that only detachments from the required area would be counted. The flume was filled slowly with a hose, after the erodible section was sprayed lightly with water to prevent the uplift of dry sediment grains due to surface tension effects. The smaller upstream valve was opened slowly to the designated flow rate and the downstream weir lowered so a uniform flow depth was obtained in the reach length. The time for 80 particles to detach from the test area was measured for each run. Nine runs were completed with a bedslope of 0.0030 for various discharges and two runs with a bedslope of 0.0020.

5.4.2 Steady Flow ~ Equilibrium Transport (SE--93 Series)

To achieve equilibrium conditions on the bed in an open circuit flume system, the sediment transport rate output from the erodible reach must be close to the sediment input rate from the vibrating hopper.

The sediment bed was graded parallel to the flume slope and sprayed with water to dampen the surface. The flume was slowly filled by a hose with the downstream weir elevated, while the smaller valve was opened to set the base flow. To begin each run, the required flow rate was quickly set on the larger valve and the downstream weir lowered to obtain the correct uniform flow depth. The sediment hopper was started when continuous bedload movement occurred. At the same time the starting point was marked on the chart output of the bedload collection device at the downstream end of the erodible reach. The sediment mass input rate from the hopper was adjusted continually, to match the sediment output measured as a bedload transport rate. With the onset of equilibrium conditions, the hopper sediment mass

flow was held at the required constant value. Periodic measurements of the bed level were made using the ultrasonic probe. The water surface level, using the point gauge, the flow rate and the water temperature were also measured.

The criteria used to determine whether equilibrium conditions were present after a run duration of between 2 - 2½ hours was :

(a) initial mean bed elevation equal to the final bed elevation, within 2.5 mm;

(b) input transport rate approximately equal to the output transport rate;

(c) friction slope approximately equal to the bed slope which should be constant.

Often these runs were unsuccessful, as the initial input rate to the system must be close to the output rate, otherwise non-equilibrium conditions (aggradation or degradation) develop, requiring a long period of time to reverse the trend and restore the system to equilibrium. Twelve runs were successfully completed in this series, in accordance with the above criteria. Three of the twelve runs had the same water discharge and were used to assess the reproducibility of the results.

5.4.3 Steady Flow ~ Non-Equilibrium Transport (ST--93 Series)

Non-equilibrium conditions for this series were created by having no sediment input at the upstream boundary of the test reach. To obtain a steady flow non-equilibrium system without introducing an initial transient phase in the output transport rate, the experiments were performed as steady equilibrium transport runs (Section 5.4.2) until the equilibrium transport rate was attained. The sediment mass input was then suddenly halted, the time reset to zero and measurements for the ST--93 series begun. The downstream bedload transport rate was sampled at 30 second intervals and the bed levels

were measured at five minute intervals for the first 15 minutes. Thereafter the bedlevels were measured at 15 minute intervals. The steady water discharge, water surface elevations and bedform configurations were measured throughout the run. The initial and final temperatures were also noted.

The transport rates from these runs were to serve as comparable rates for bedload transport rates obtained during non-steady water flow experiments, therefore the steady discharge values were chosen within the range of $q_c < q \leqslant q_{max}$ of the chosen triangular flood waves (5.4.5), where q_c = the ciritcal base flow. The duration of the runs in this series was two hours, except for the larger flow rates, which were terminated when the bedload collector was full. Nine runs were completed during this series.

5.4.4 Step Change in Discharge - Non-Equilibrium Transport (SC--93 Series)

Preparation for this series of runs followed the procedure outlined for the ST--93 series, (section 5.4.3). The baseflow, from the smaller valve, was established over the bed with the downstream weir set at the level corresponding to the desired final steady flow (q_o) and the water depth (y) obtained from the ST series. Hence before t = 0, the mean velocity was below the threshold value and the bed was initially plane for each run in this series. At t = 0, the extra flow required from the larger valve was quickly, (within 15 seconds), superimposed upon the baseflow, with no sediment input at the upstream end for all time. The final flow values (q_o) were set as closely as possible to the flow values used in the ST--93 series, so that the bed response due to different initial conditions could be compared.

The water and bed levels were recorded at various time intervals and the bedload accumulated weight was recorded at 30 second intervals. The discharge q_o was measured during the run and the ini-

tial and final temperatures recorded. Nine runs were completed in this series.

Most of the above experiments were re-run so that more fundamental observations, using tagged bed-material particles, could be made concerning the response of single grains to step changes in water discharge. Air dried grains were sprayed lightly with fluorescent paint and allowed to dry. Before each run the particles were soaked in water to prevent the attachment of air bubbles when placed in the main flow. After soaking for some time, 140 particles were counted and placed transversely across the bed at 0.05 m downstream of the fixed apron. The flume was filled slowly with the hose, care being taken not to disturb the tagged particles. The rest of the starting procedure was as outlined above. During the course of the run, the bedload collector plate was monitored by the ultra-violet light beam (section 4.5.6) to identify the number of fluorescent particles passing out of the test reach. After the run, the bed was allowed to drain and then divided into segments. The number of coloured particles found on and below the bed surface, with the aid of the ultra-violet light source, was tabulated for each segment along the reach length. A high recovery rate from the bed was obtained using this method, typically 95%.

5.4.5 Triangular Translation Wave ~ Non-Equilibrium Transport (NS--93 Series)

To investigate the bed response to fast rising flood waves, eight symmetric triangular waves of various wave periods and maximum flow rates were chosen. Each of the translation waves was superimposed on a base flow of 0.03 $m^3/s/m$, which was chosen, using a dimensionless threshold erosion rate (N) equal to 0.5×10^{-6}, (Figure 6.1). The chosen hydrographs are shown in Figure 5.2.

Prior to the commencement of each wave passage, the erodible bed was artificially levelled with the scraper and dampened. While

the flume was filled slowly with the hose, the water level probes were attached to the glass side wall at the chosen stations. The smaller

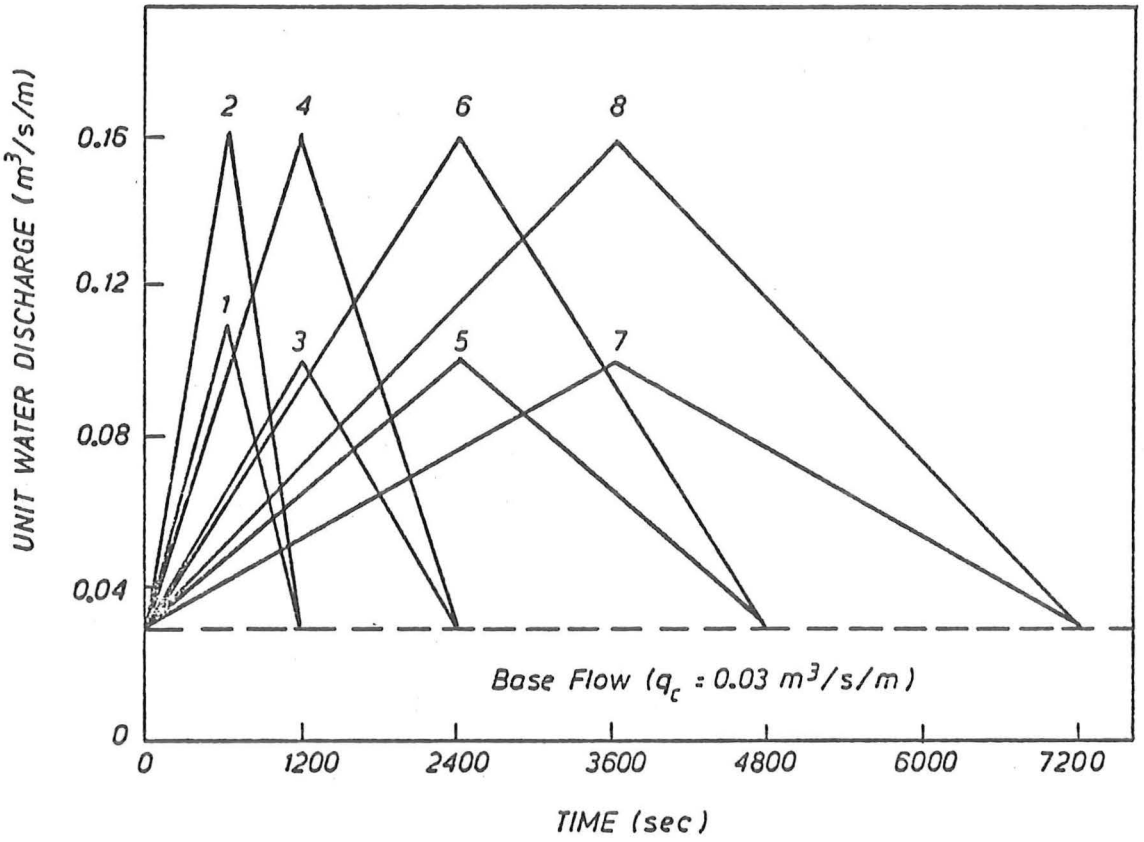

FIGURE 5.2 : Triangular translation wave hydrographs (NS series)

valve was opened slowly until the base flow was reached and the downstream weir lowered to give a uniform starting depth at critical conditions. The initial water and bed levels were measured as well as the temperature. The signal was then given to the operator of the larger valve to commence the predetermined programme of valve settings with corresponding time values. Measurements began when the leading edge of the flood wave reached the first water level gauge. The down-

stream submerged weir was raised and lowered at a predetermined rate derived from the flow rating curve for the steady flow experiments. The weir operation commenced when the leading edge of the wave reached the second water level gauge. No upstream sediment input was used in this series.

The bed levels were measured at selected time periods during the wave passage, with shorter intervals near the wave peak. Water level readings from the point gauge were obtained during the wave to check the calibration of the water level gauges. The bedload accumulated mass was recorded at 10 second intervals for wave Nos. 1,2,4 and at 30 second intervals for the remaining waves. At the end of each wave passage the final bed and water levels and temperature were measured.

Other variations of non-steady flow hydrographs that were run in a manner similar to that outlined above were:

(a) Skew-Triangular Translation wave, comprising the first half of Wave No. 2 and the second half of Wave No. 8 (Figure 5.3 (a)).

(b) Symmetric Triangular Wave of base period 4 hours (Wave No. 10) which was run for only the first 125 minutes (Figure 5.3(a)).

(c) Linear Change in flow discharge between two constant discharges of q_c and q_{max} = 0.16 $m^3/s/m$, the first half of Wave No. 2, thereafter maintaining the constant peak flow value with time (Figure 5.3(b)).

A separate study of bedform geometric properties (height and wavelength) was implemented by re-running four of the symmetrical triangular waves, Nos. 2,4,6,8. In these tests, bed levels were measured by the positioning of the ultrasonic probe at successive bedform crests and troughs, during a traverse of the erodible reach. The position of each measurement was noted from a fixed scale along the top of the flume wall with the aid of a pointer attached to the carriage. Bedform celerities were measured during another re-run of Wave No. 4.

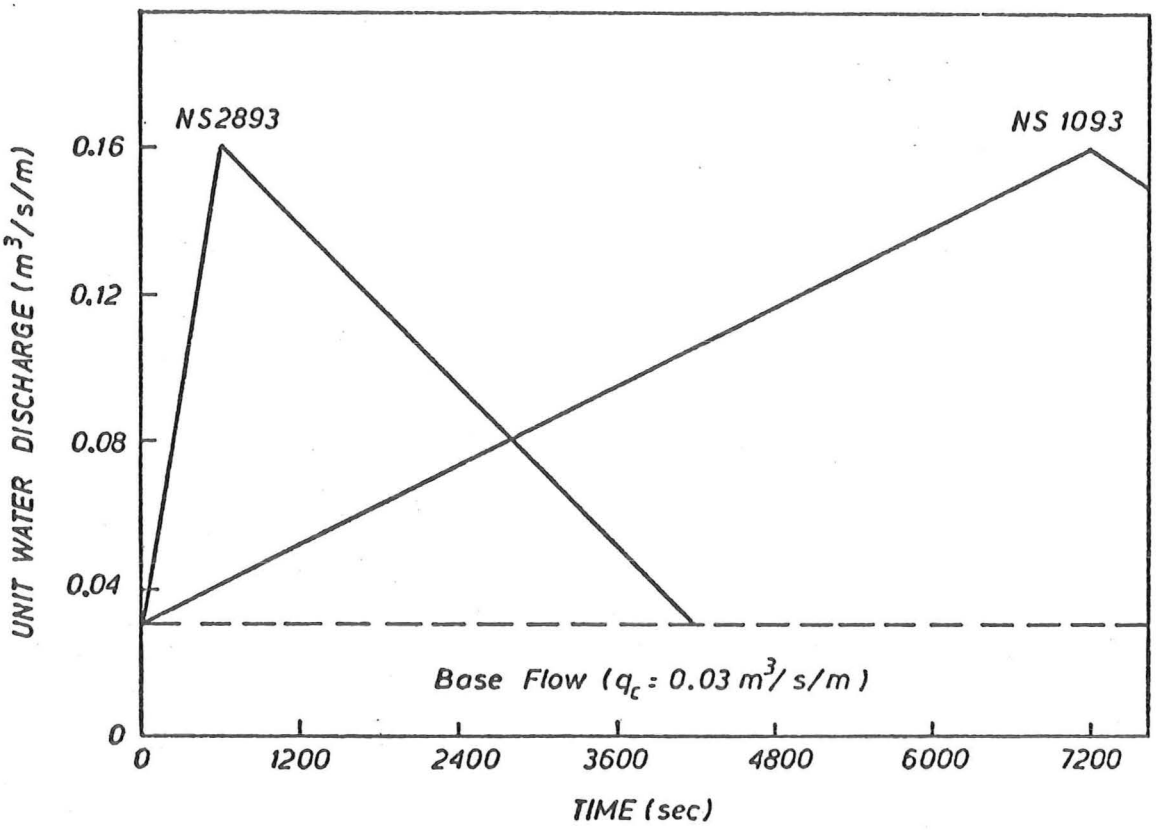

(a) Skew triangular wave and long period wave

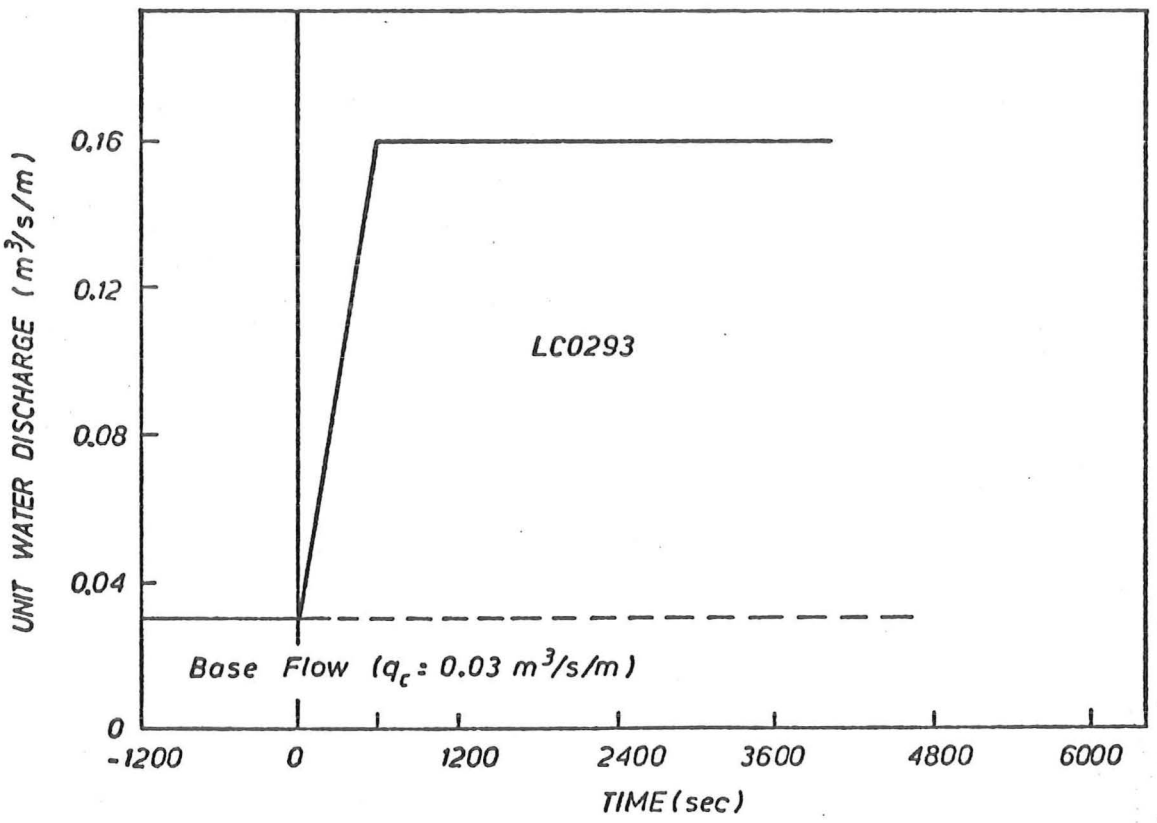

(b) Linear change in discharge

FIGURE 5.3 : Variations of non-steady flow hydrographs

5.5 EXPERIMENTAL PROCEDURES ~ SHORTER REACH LENGTHS

To investigate the spatial variation of the bed response to steady and non-steady flows under non-equilibrium conditions, five different reach lengths of erodible bed were used. The experimental programme for the longest reach length of 9.29 m, described in the previous section, served as a control series, where the fixed bedload collector (section 4.5.4(1)) acted as a downstream control for the sediment phase. At the completion of these experiments, the next selected reach length of 5.29 m was obtained by lengthening the upstream fixed roughened bed in the downstream direction. This was repeated for reach lengths of 3.53 m, 1.74 m and 0.74 m. The process of moving the fixed bed progressively downstream effectively moves the bedload sampling point further into the general scour hole. To simulate conditions within the general scour hole, as the test reach is reduced, that are similar to the control experiments, the grill of the adjustable bedload collector unit (section 4.5.4(2)) must be lowered as the bed degrades to prevent interference with the bedload movement.

The steady flow non-equilibrium (ST series) and the triangular flood wave (NS series) experiments were repeated for the four shorter reach lengths. The step-change in discharge experiments (SC series) were repeated for the 1.74 m reach length. The procedure for each of the repeated experiments was the same as for the control experiments, but included the additional task of lowering the upstream end of the adjustable bedload collector grill as the bed degraded according to predetermined scale settings. The settings were determined from bed profiles for the same run obtained during the control experiments by taking the mean degradation with time at the two measured stations in the vicinity of x = new reach length e.g. for the steady flow run ST0535, the required settings with time were obtained from

the mean degradation at the 3.0 m and 4.0 m stations of the ST0593 profiles. For the greater degradation at the end of the 1.74 m and 0.74 m reach lengths, the downstream end of the bedload collector grill was also lowered for each setting by approximately 25% of the upstream end value, so that the surface profile simulates more realistically the shape of the local scour hole (Figure 5.4).

5.6 ANALYSIS PROCEDURE

5.6.1 Computed Variables

Combinations of the various measured parameters can be used to compute relevant variables to evaluate flow and sediment transport

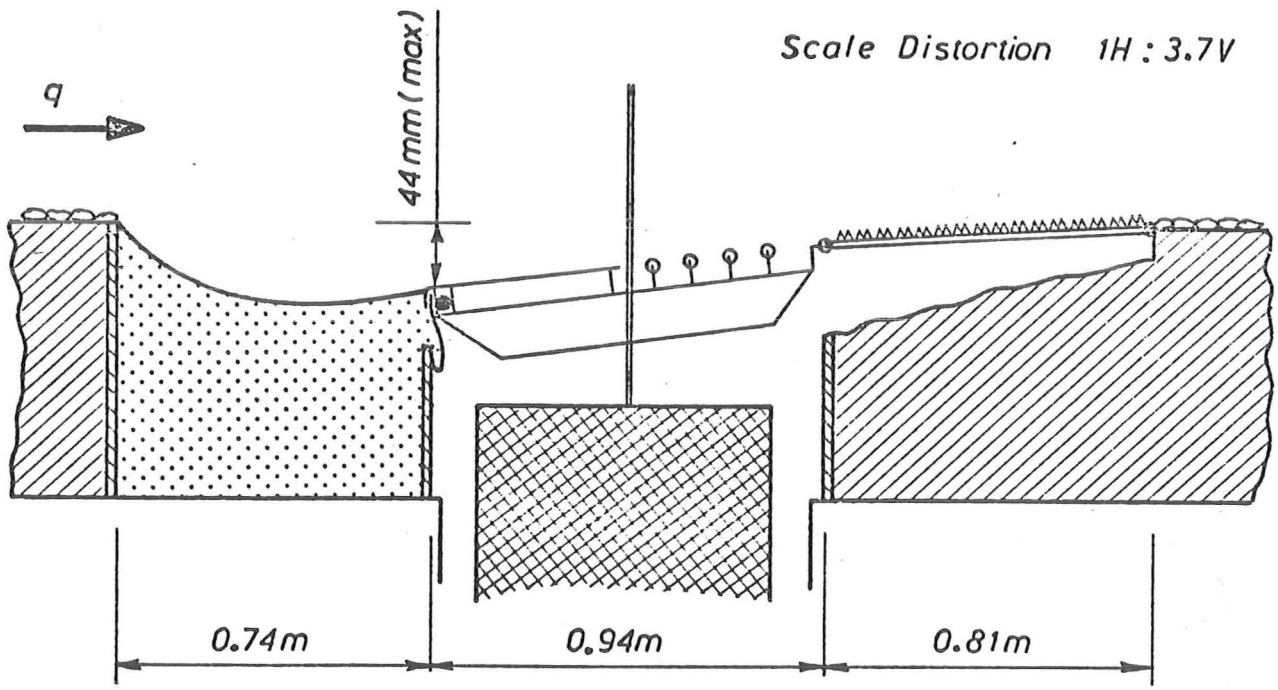

FIGURE 5.4 : Lowering of the bedload collector cradle for short reach lengths

relationships. The computed variables used in this study include:

(a) Unit Water Flow Rate, Sediment Transport Rate

(b) Mean Velocity, Depth, Bedlevel, Stage

(c) Water Surface Slope

(d) Shear Velocity and/or Bed Shear Stress

(e) Froude Number, Grain Reynolds Number, Entrainment Number

(f) Flood Wave Parameters; Strouhal Number, Steepness

(g) Kinematic Viscosity

5.6.2 Mean Stage and Bed Levels for the Comparison Procedure

The bed levels derived from ultrasonic probe measurements during steady and non-steady non-equilibrium experiments, at the various locations shown in Figure 5.1, were averaged over the reach length to give a mean bed level $\bar{z}$.

Stage levels at the stations shown in Figure 5.1 for the ST series were also averaged over the reach length for each time value to give a mean stage $\bar{h}^S$.

Continuous water level traces obtained during the NS series, in the form of voltage-time curves, were used to obtain stage levels at various times during the wave period, at the two selected water level gauge sites p, q, (Figure 5.1). The mean stage calculated from these two values was biased towards the higher water surface at the upstream end, which was caused by the out of phase response of the water surface profile to the local scour bed profile. To counteract this bias, (at the most 5 mm), a multiple regression analysis of all the water levels measured during the steady flow non-equilibrium transport runs was completed using the statistical computer package OMNITAB II (1971). The analysis related stages measured at sites p and q during each run of the ST series with the calculated mean stage $\bar{h}^S$ from all the measured stations of each run i.e.

$$\bar{h}^S = a\, h_p^S + b\, h_q^S + c \qquad \ldots (5.1)$$

where the subscripts p, q refer to the water level gauge sites. Therefore knowing the values of h_p^{NS} and h_q^{NS} for different times during a translation wave experiment, a corresponding mean stage, $\bar{h}^{NS}$, could be obtained from equation 5.1.

5.6.3 Bedload Transport Rate

The average bedload transport rate versus time curve for the ST series was obtained by drawing lines of best fit through the original data. This was achieved with the aid of mean transport rates which were calculated over sufficiently long time intervals to damp out the oscillations created by the bedforms, usually 10 to 20 minutes.

The bulk of the bedload yield, under the influence of a steep translation wave, arrived at the bedload collector in a series of spurts due to the presence of gravel bedforms on the bed. It was thus difficult to compute a representative instantaneous transport rate to compare with a steady flow non-equilibrium transport rate. The most satisfactory method of transforming the original transport rate time series to a smoother distribution, was the application of a linear centred moving average scheme. The computational procedure is a lead-lag process where the output is a function of (2m + 1) data points centred about the time value of interest, which can be shown in algebraic form as

$$g_s'(t) = b_o\, g_s(t) + b_1\, g_s(t-1) + \ldots + b_m g_s(t-m) + b_1^*\, g_s(t+1) + \ldots + b_m^* g_s(t+m) \qquad \ldots (5.2)$$

The smoothed transport rate for the next time value of interest is obtained by dropping the earliest transport rate $g_s(t-m)$ and picking up the transport rate, $g_s(t+m+1)$. Details of this procedure are con-

tained in Appendix B. The smoothed transport rate time series for the NS and SC series was plotted by computer in conjunction with the comparable average transport rate data fitted with a curve using a cubic spline piece-wise interpolation routine, (Appendix B).

CHAPTER VI

INITIAL MOTION AND STEADY FLOW EQUILIBRIUM TRANSPORT

6.1 SYNOPSIS

Observations and results are presented for the initial motion and equilibrium transport series of experiments, sections 5.4.1 and 5.4.2. These are discussed and compared with other sets of experimental data and formulae. The data, derived parameters, and formulae are listed in Appendices C and D.

6.2 INITIAL MOTION (IM SERIES)

6.2.1 Observations

In the process of counting the number of particle detachments from the test area, observations were made concerning the motion of single grains. Near critical conditions the motion of grains occurs in bursts when several grains detach from the bed. The frequency of these bursts increases as the mean bed shear stress increases. The bursts of movement appear to be random in time and position within the test area followed by relatively longer periods during which no motion occurs. It is generally accepted that these impulsive bursts of movement coincide with strong turbulent eddies impinging on the bed, {A.S.C.E. (1975)}.

Many of the grains exhibited an unstable oscillatory movement for a short period prior to detachment by the turbulent eddies. The majority of grains propagated with a rolling motion with a much smaller number moving by sliding and hopping. The step length for a single grain movement appeared to vary considerably, (from 1 up to 300 grain diameters), but the average step length generally increased with increasing flow rate ($.17 \leqslant q \leqslant .38 m^3/s/m$), from approximately 50 to 100

grain diameters. The penetration of a grain in motion into the flow was never more than approximately 2 grain diameters above the bed surface for hopping movements.

6.2.2 Results

The data from the initial motion series, for two different bed slopes, is presented in Figure 6.1 in terms of the dimensionless erosion rate N and the entrainment function Y. Sidewall effects have been eliminated using the formula derived by Williams (1970) using coarse sand bed material. The data of Griffiths (1976), obtained by the same method using a larger grain diameter, has been included in Figure 6.1. It is clear that the data define a relationship between N and Y, which was determined by regression analysis as

$$\frac{nD_{50}^3}{u_{*_b}} = 2.83 \times 10^6 \left(\frac{u_{*_b}^2}{(S_s-1)gD_{50}} \right)^{8.9} \quad \ldots (6.1)$$

where n is the number of grains detached/unit area/unit time. The average value of the grain Reynolds number, Re_*, for the initial motion series was 71 and for the experiments of Griffiths, approximately 200.

The erosion rate from the test area, n, can be expressed as a transport rate, g_s, given by the relationship :

$$g_s = n \cdot l \cdot \rho_s g V_g \quad (N/s/m) \quad \ldots (6.2)$$

where l = grain step length ($50 \leqslant l/D_{50} \leqslant 100$) and V_g = equivalent spherical grain volume = $\frac{\pi D_{50}^3}{6}$ (m^3). The relation between the sediment transport rate and the entrainment function for the experimental data was found to be

$$g_s = 3.3 \times 10^{11} Y^{11.2} \quad (N/s/m) \quad \ldots (6.3)$$

6.2.3 Discussion of Results

The relationship shown in Figure 6.1, is of the nature suggest-

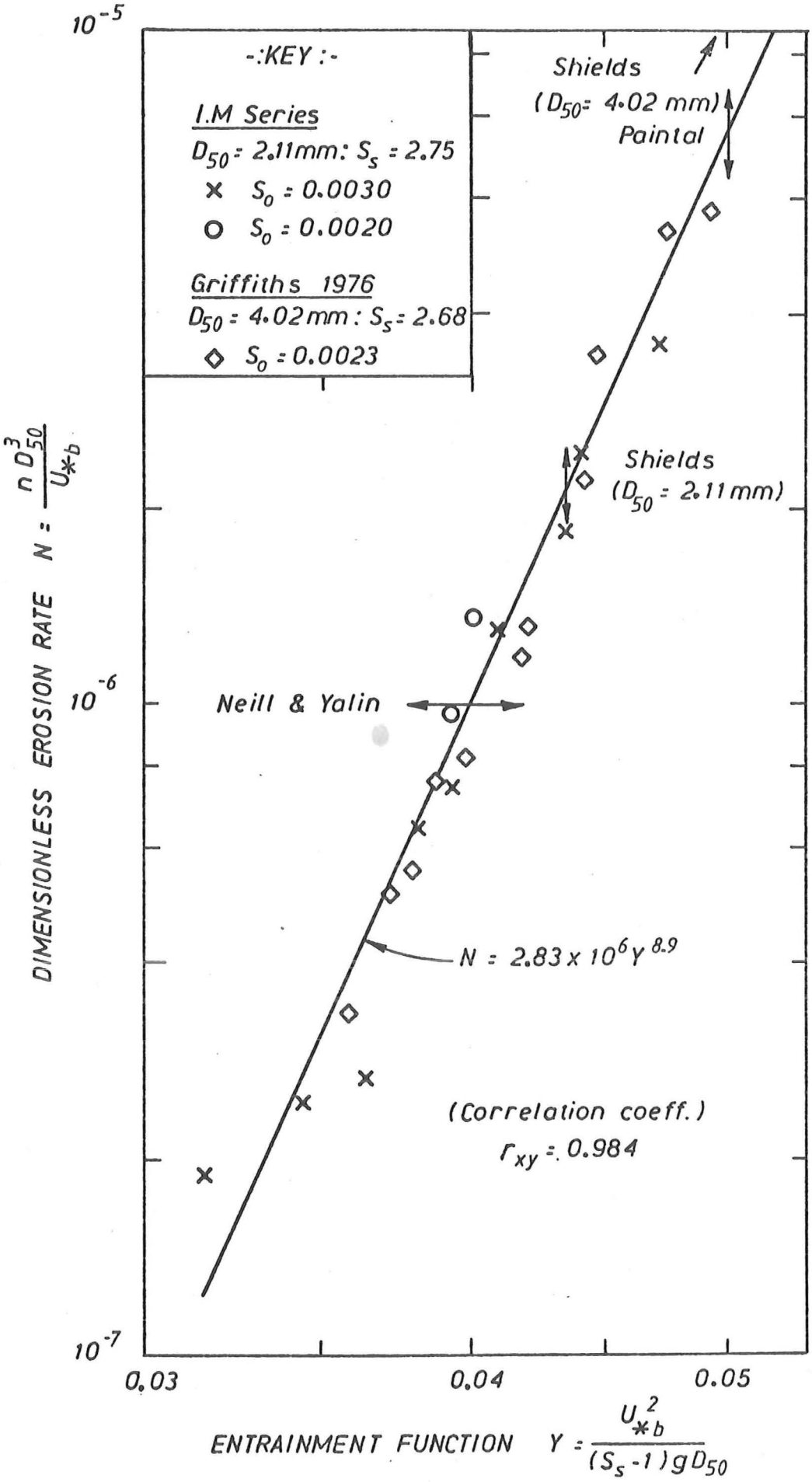

FIGURE 6.1 : Relationship between dimensionless erosion rate and Shields entrainment function

ed by Neill (1968) for flow conditions in the rough turbulent zone where the grain Reynolds Number effect is weak. The value of the grain Reynolds Number Re_* which defines the lower limit of the rough turbulent flow regime, varies among authors, but the minimum value of $Re_* = 70$ is commonly accepted. The experimental data for the initial motion series was obtained under conditions at this lower limit, but no differences were discernable when compared with the data of Griffiths (1976) for Re_* = 200. Together these experiments suggest that the erosion of particles under critical conditions is independent of the grain Reynolds Number in the rough turbulent zone extending down to $Re_* = 70$. Below this limit the grain Reynolds Number is expected to become a more significant parameter.

The critical point of motion for any one particular grain on the bed surface is strongly dependent on the relative protrusion into the flow above the surrounding bed surface, as found by Fenton and Abbott (1977). This could be one of the reasons for the scatter about the trend line in Figure 6.1, particularly for the low values of the entrainment function, even though the bed was brushed carefully prior to the commencement of each test.

The 11th power correlation of the transport rate and the entrainment function, and also the slope of the N versus Y relationship, is consistent with the observation that a small increase in applied bed shear stress coincides with a noticeable increase in the number of particles in transport. The exponent, shown in equation 6.3, lies between the values of 8.15, 16 and 17.5 obtained by Pazis *et al.* (1977), Paintal (1971a) and Taylor (1971) respectively. The trend lines obtained by the former two authors are shown plotted in Figure 6.2 along with the data from the IM series. Although the data plots above the mean line found by Paintal (1971a), all points lie within his band of scatter shown in Figure 6.2.

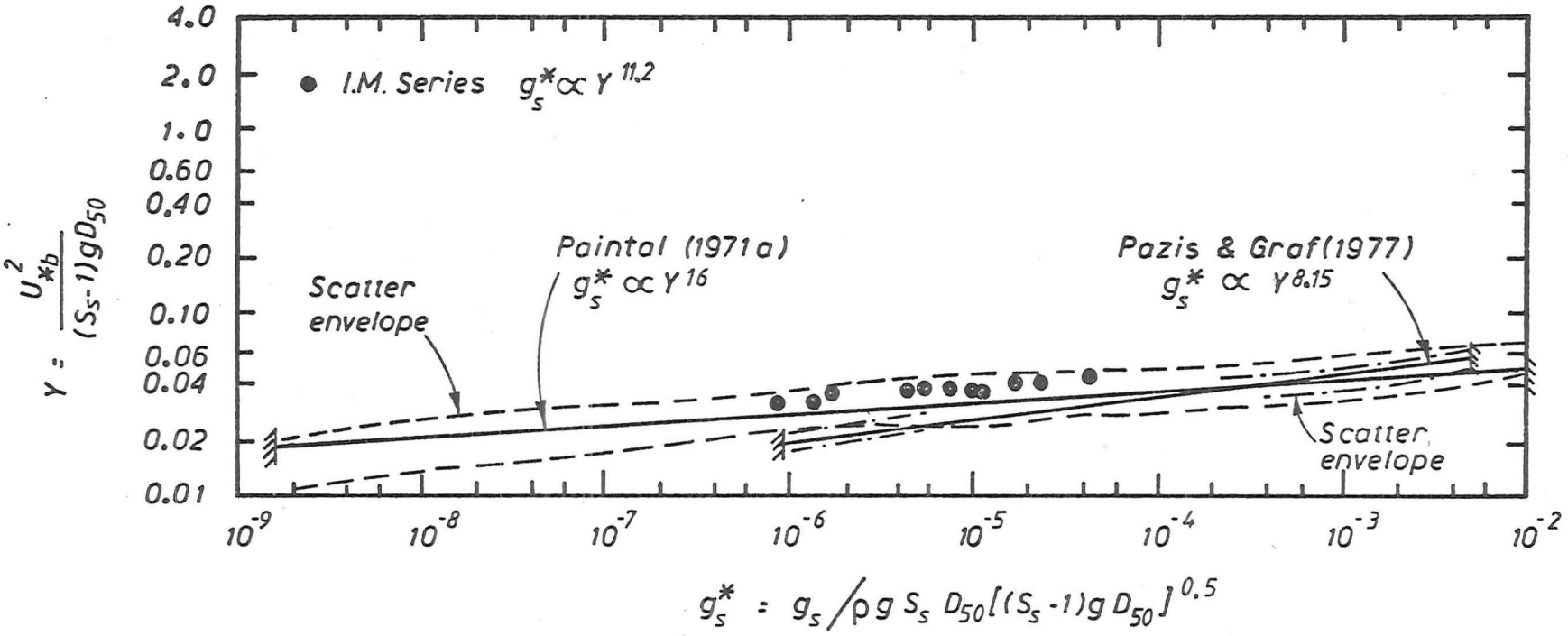

FIGURE 6.2 : Relationship between Shields entrainment function and dimensionless transport rate for weak sediment transport

For uniform grains, it is practical to use an arbitrary value of N as an initial motion criterion from which the actual erosion rate can be easily calculated, rather than to use a subjective critical point of motion. This approach could eliminate the confusion of whether to use an initial motion criterion of first displacement, $0.01 \leqslant Y \leqslant 0.03$, or for a "small" finite transport rate e.g. Y = .06. Alternatively, any of the established initial motion criteria could be used in conjunction with the N versus Y relationship, which would yield an estimate of the actual transport rate to be expected. The criteria put forward by three authors are plotted on Figure 6.1. The entrainment function values from the Shields curve for the two different grain sizes, (not shown is Y = .056 for the size D_{50} = 4.02 mm used by Griffiths (1976)), correspond to two values of the dimensionless erosion rate, N, which differ by more than an order of magnitude. This appears to confirm the suggestion that the Shields limit corresponds to a definite transport rate, which is a function of the grain size concerned, for the lower region of the rough turbulent regime, $70 \leqslant Re_* < 140$. The suggested criterion of Neill and Yalin (1969), $N = 1 \times 10^{-6}$, is reasonable (Y = .04) and is associated with a transport rate of approximately 4 grains/m^2/s (D_{50} = 2.11 mm) or $q_s = 7.8 \times 10^{-5}$ N/s/m, (using equation 6.2 with a step length $1/D_{50} = 70$), which is very small.

An arbitrary value of $N = 0.5 \times 10^{-6}$ was chosen as the criterion for the base flow (q_c) used in the non-steady flow non-equilibrium series, giving a value of $q_c = .03 m^3/s/m$.

6.3 STEADY FLOW - EQUILIBRIUM TRANSPORT (SE SERIES)

6.3.1 Observations

As the shear stress on the bed is increased more particles are set in motion over the whole bed resulting in an increased inci-

dence of inter-particle collisions. The modes of transport for bed material grains can be classified as rolling, sliding, hopping and saltating. The predominant mode of transport was rolling while the other modes occurred less often. Saltation was only observed when some grains were propelled from the upstream face of a bedform over the trough region, penetrating the flow more than the 1 - 2 grain diameters observed for hops. (Plate 6.1).

Step lengths for a single grain movement varied considerably more than for critical conditions ranging from 1 - 1000 grain diameters. Usually for plane bed conditions, which occurred before the development of bedforms, particle movement proceeded in several steps interspersed with short rest periods. When bedforms were present, most particles moved in one sweeping motion over the upstream slope, coming to rest in the trough region after sliding down the steep downstream face. For the high water discharges, it appeared that the majority of surface particles are in general movement, but calculation of the effective height, H_s, of the moving sediment layer spread over the flume width reveals that

$$H_s = \frac{q_s}{\bar{u}_p P_s} \doteq 0.1 \text{ mm}$$

(where $\bar{u}_p$ is the mean particle velocity), which is much smaller than a grain diameter.

The interaction between the flow and the sediment bed can deform the boundary into different shapes. For the range of water discharges tested ($.07 \text{ m}^2/\text{s} < q < .15 \text{ m}^2/\text{s}$), the only bedforms encountered were long gravel bars or two dimensional dunes {(Simons and Richardson (1961)}, distinguished by their steep faced, flat topped shape with a long gently sloping tail (Plate 6.1). As the dunes developed on the bed, the water surface profile became out of phase with the bed profile i.e. a drop in the water surface level occurred near the dune crest.

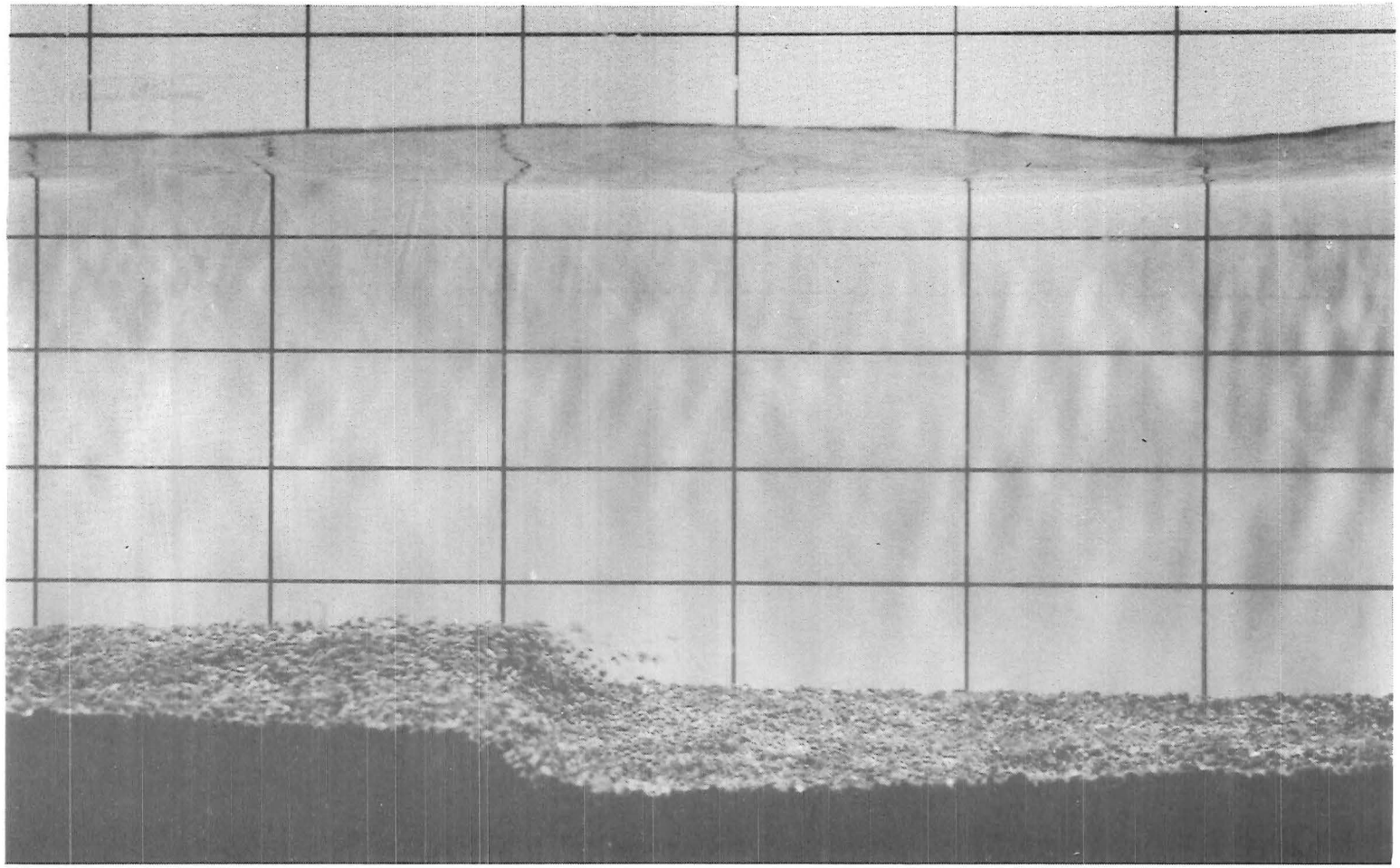

PLATE 6.1 : Typical dune bedform profile in motion,
q = 0.16 m^3/s/m, y = 0.20 m (grid 100 mmH x 50 mm
V) [Flow from left to right]

6.3.2 Results

Ten runs were completed for a range of water discharges, including three runs performed with the same flow rate to assess the reproducibility of the tests. A maximum difference in bedload transport rate of 0.008 N/s/m, corresponding to a 3% difference, was obtained for the three similar runs. This falls within the experimental error of ±4%, estimated for the operation of the sediment hopper.

The flume data is plotted in Figure 6.3 with curves of predicted values of equilibrium sediment transport rates, derived from various formulae, for comparison. Equations of the form

$$g_{se} = a\, q^{b} \quad , \quad g_{se} = a\bar{u}^{b}$$

(where g_{se} is the equilibrium capacity transport rate), can be used to approximate the flume data for $q > .08$ $m^3/s/m$. The result of the regression analyses was

$$g_{se} = 76.3\ q^{2.78} \quad N/s/m \quad (r_{xy} = .996) \qquad \ldots (6.4)$$

$$g_{se} = 2.63\ \bar{u}^{8.0} \quad N/s/m \quad (r_{xy} = .997) \qquad \ldots (6.5)$$

The typical features of the dune bedform profiles (Plate 6.1) were :

(1) Wavelength (λ_d)

There was no obvious trend with increasing discharge, the wavelength varying during runs in the range $0.6\ m \leq \lambda_d \leq 1.5\ m$. The ratio of dune wavelength to water depth was generally between 5 and 15, decreasing to the lower figure for the maximum discharge.

(2) Height (Δ_d)

The dune height increased with increasing water discharge, from a value of 6 mm up to a maximum height of 22 mm.

(3) Steepness ($S_d = \Delta_d/\lambda_d$)

The steepness of the dune profiles ranged from a minimum of

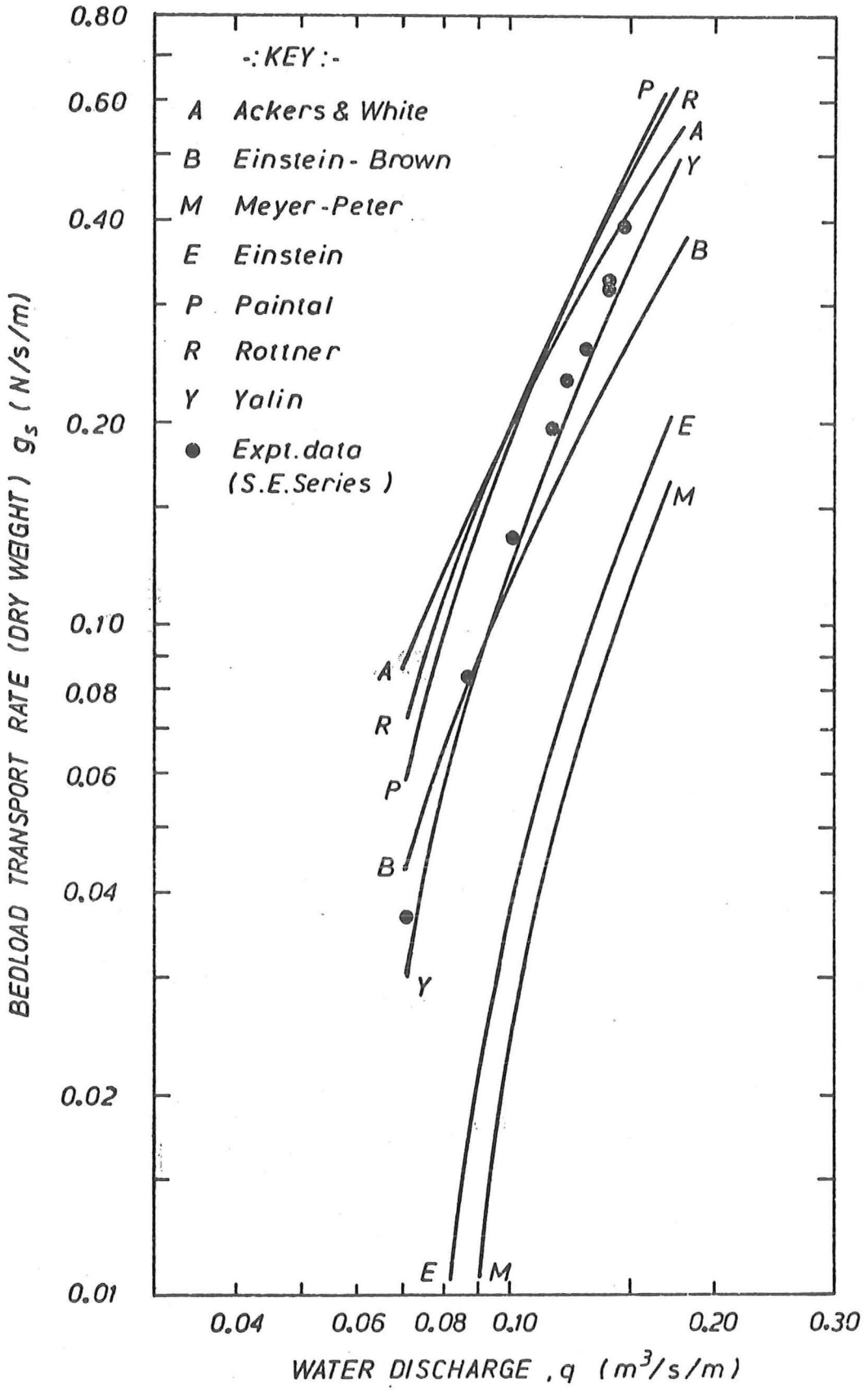

FIGURE 6.3 : Predicted and measured equilibrium transport rate rating curves

0.003 to a maximum of 0.025 for the largest flow. A more detailed analysis of bedforms is carried out in section 7.5.

6.3.3 Discussion of Results

The overall performance of the equilibrium formulae, shown in Figure 6.3, is generally poor, particularly for the lower water discharges, where differences up to an order of magnitude are evident. This is a direct consequence of the various subjective initial motion criteria used as a basis for the formulae. The bedload formula of Yalin (1963) fits the flume data with remarkably little error, despite an assumption used in the derivation of his formula which imposed a limitation to plane bed conditions. The formula is based on a detailed analysis of the saltation mechanism, which is more appropriate for coarse grains such as gravel. Yalin's bedload formula has been found to fit other well-known experimental data for coarse grains, {Henderson (1966)}, however, for finer grain sizes, considerable discrepancies occur between calculated and measured transport rates as shown by White, Milli and Crabbe (1973). Paintal's (1971b) formula approximates the slope of the trend line of the experimental data, and thus would only require a magnitude adjustment to match the data.

The equilibrium transport data, in the form of equation 6.5, will be used to compare with transport rates under steady flow non-equilibrium conditions and to serve as a check on the initial transport rates at t = 0 of these runs, to determine if equilibrium conditions are present.

6.4 SUMMARY

The transport rate is strongly dependent on the applied bed shear stress near threshold conditions on the bed, hence the best method of determining a critical flow is to nominate a suitable transport or dimensionless erosion rate. The transport rate is independent

of the grain Reynolds Number Re_* for values of $Re_* > 70$. Reasonable agreement was obtained with the initial motion transport rates measured by Paintal (1971a).

The equilibrium transport formula which best predicted the experimental transport rates, was that of Yalin (1963). The only bedform type encountered in the range of flows tested was two-dimensional dunes or gravel bars.

CHAPTER VII

STEADY FLOW - NON-EQUILIBRIUM TRANSPORT

7.1 SYNOPSIS

The results and relevant discussion of the steady flow experiments under non-equilibrium conditions, (g_s input = 0 and q(t) = constant), are presented firstly for temporal variations at a fixed point in space, and secondly for spatial variations. Typical results from the experimental series are identified by the identification code outlined in section 5.2 The last section is an analysis of the geometric properties of the bedforms including comparisons between experimental results and predictions of published formulae. Detailed results are listed in Appendix E.

7.2 EXPERIMENTAL OBSERVATIONS

Nine runs were executed, as outlined in section 5.4.3, for each of the five test section lengths with various steady flow rates ranging from 0.045 - 0.160 $m^3/s/m$. The corresponding flow rates for each reach length differed slightly (3%), which was attributed to the difficulty of setting a desired flow precisely. During the initial equilibrium transport phase, immediately prior to t = 0, essentially plane bed conditions existed for flow rates less than 0.067 $m^3/s/m$, although small bedforms ($\Delta_d^* = .2D_{50}$) were observed later in the non-equilibrium phase for q = .067 $m^3/s/m$. For flow rates higher than .067 $m^3/s/m$, bedforms were present on the bed at t = 0.

For each run, after the upstream equilibrium sediment supply was severed at t = 0 the flow began to locally scour the erodible bed in the vicinity of the edge of the fixed apron, the intensity of

scouring depending on the flow rate. During runs with low flow rates, $q \leqslant .056$ $m^3/s/m$, the scouring intensity was low, and a localised scour hole first became apparent at approximately $t = {}^3/_4 - 1$ hr.

For the higher flows, $q \geqslant .067$ $m^3/s/m$, the flow immediately began to scour bed material from the upstream end of the test reach. This material was transported up the back slope of the last bedform, which had previously formed at the upstream end immediately prior to the input sediment cut-off, and was subsequently deposited as it avalanched down the steep lee face of the bedform. As scouring of the bed continued, under the higher flow rates ($q \geqslant 0.082$ $m^3/s/m$), the flow field in the local scour hole became dominated by a fluid vortex, ACB, shown in Figure 7.1, with a reverse flow, observed with the aid of dye, close to the bed surface. The fluid vortex occupied the zone of separation between the main stream and the degraded local scour hole surface. The scour hole continued to deepen under the fluid vortex and reached a maximum depth at the downstream extremity of the vortex. In this region, from the edge of the fixed apron to the area of maximum scour depth, typically 0.2 - 0.5 metres, the grain motion was disordered with motion forwards and/or backwards along the slope and also in the transverse direction. However, the overall tendency was to move down the slope showing gravity to be the dominant influence. As the bed degraded, the motion of grains in the scour hole became more sporadic, occurring in bursts, as observed during the initial motion runs (section 6.2.1).

The bed at point A (Figure 7.1), at the transition boundary always remained in contact with the corner edge of the fixed apron. During a preliminary series of steady flow experiments, after an initial period of scouring, the flow was stopped and the wedge of sediment ABD, shown in Figure 7.1, was then carefully removed by hand. Some time after the resumption of the steady flow rate, the volume

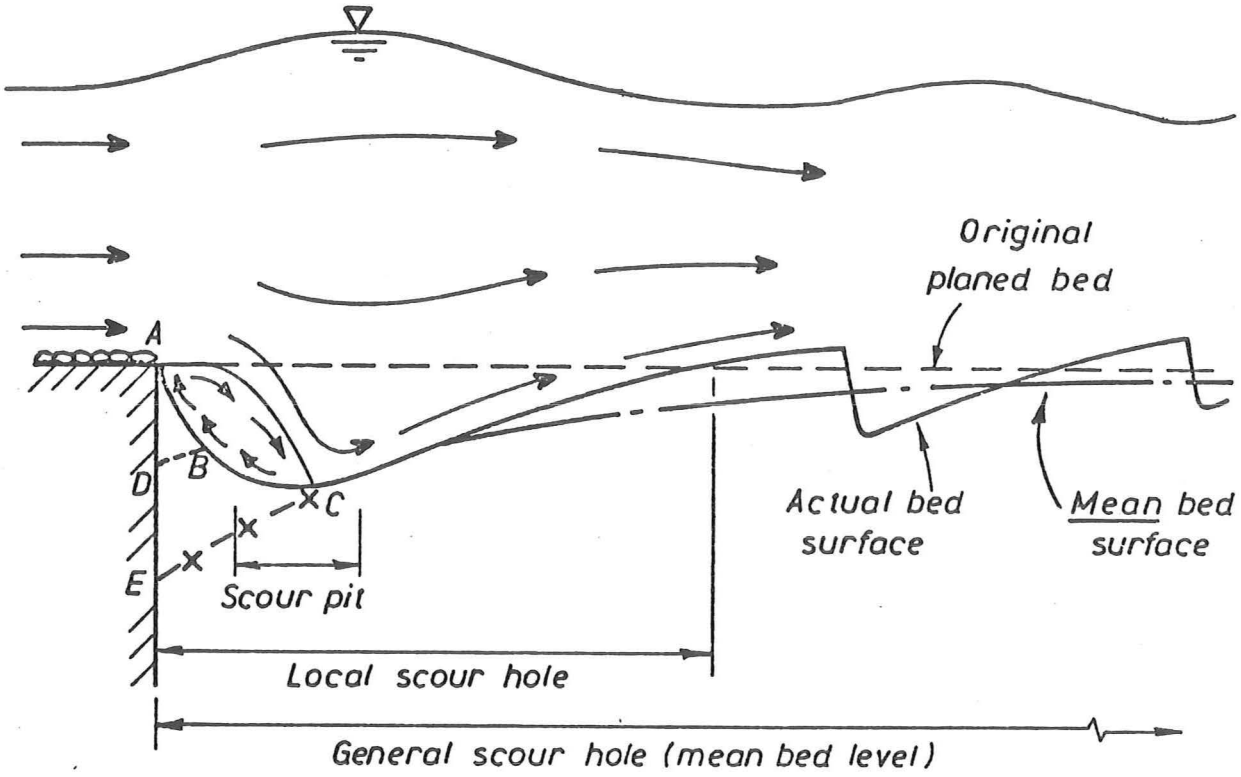

FIGURE 7.1 : Flow visualisation in local scour hole and definitions of scour hole regions

ABD was back-filled with sediment. Thus the fluid vortex had the ability to restore the local scour hole to its original shape, provided critical conditions had not already been reached at the base of the scour hole or scour pit, (Figure 7.1). This suggested that the characteristic shape of the upstream portion of the local scour hole was explained by the presence of the fluid vortex.

From the section of maximum depth, where the main flow stream re-established contact with the bed, the local scour profile rose to the point where it first reached the original bed level, Figure 7.1. This point moved at the dune celerity, as the back slope of the last bedform was continually eroded. Thus the downstream edge of the local scour hole propagates downstream with time.

The water surface above the scour hole was out of phase with the bed, as shown in Figure 7.1. The average level of the boil increased slowly with time, as the bed degraded, and was therefore higher than the boils associated with the trough regions of bedforms further downstream.

Several times during the higher discharge runs, small dunes developed on the back slope of the last parent dune bedform and propagated at a celerity faster than the original dune. As the smaller dunes approached the crest region, the parent dune slowed to a standstill until assimilation was completed. This phenomenon was also observed occasionally on dune bedforms downstream of the scour hole, especially if they were larger than the neighbouring dunes.

The motion of single grains, downstream of the scour pit, (area of maximum scour depth), was the same as that described in section 6.3.1 for plane bed and dune configurations, whichever was relevant to the particular run.

7.3 TEMPORAL VARIATIONS : RESULTS AND DISCUSSION

7.3.1 Bedload Transport Rates

(1) Results

The averaged* bedload transport rate-time curves for different flow rates are shown in Figure 7.2. They were measured at the sampling station at the end of the control test reach, 9.29 m from the start of the erodible bed. Plots of this form (one set for each reach length using data in Appendix E), were used to obtain comparable steady flow non-equilibrium transport rates for the non-steady flow series, by the comparison procedure shown in Figures 3.10, 11. By dividing the transport rate by the initial equilibrium capacity rate at $t = 0, g_{se_o}$, (obtained from equation 6.4), the variation with time

*section 5.6.3

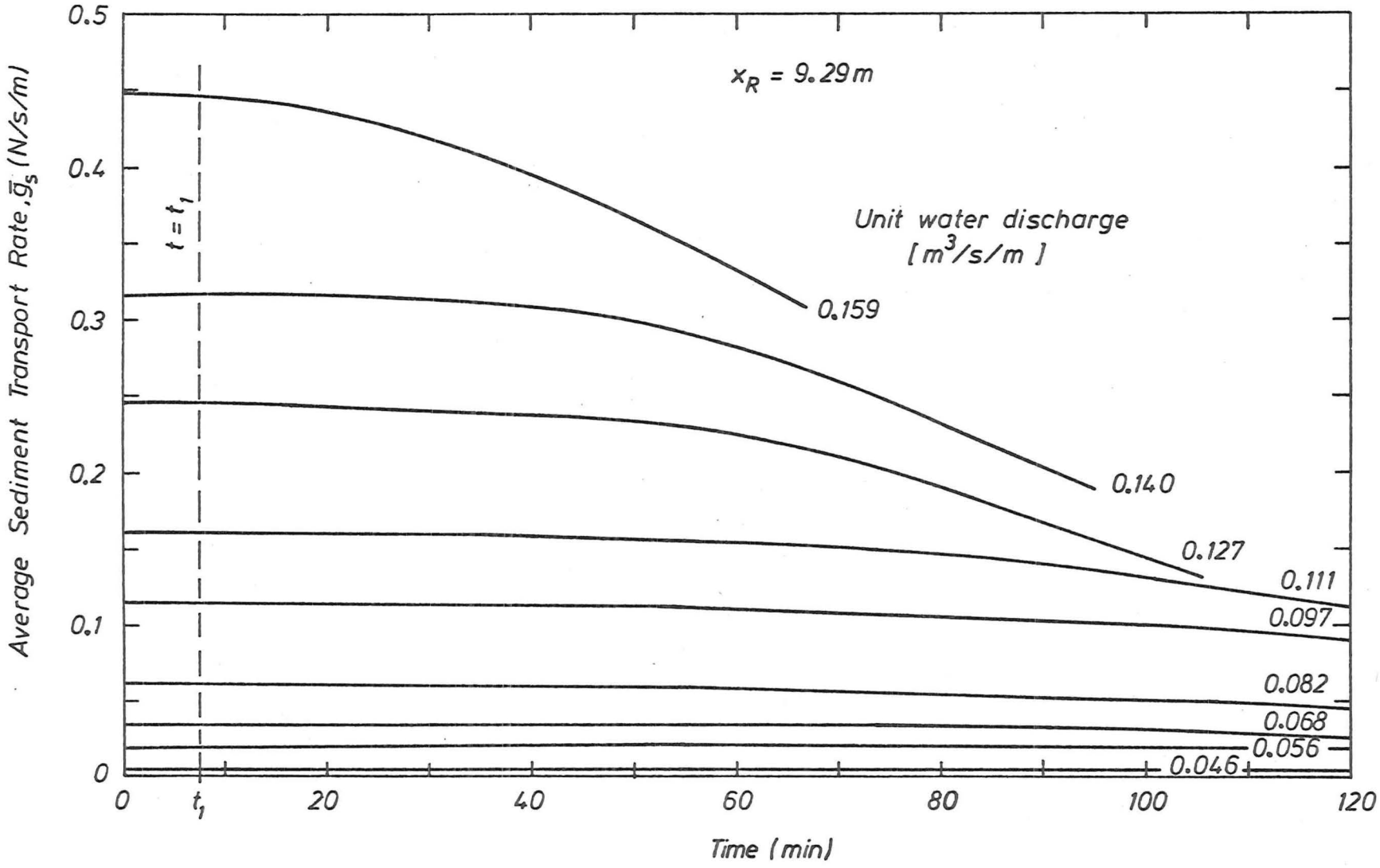

FIGURE 7.2 : Steady flow non-equilibrium transport rates (ST--93 series)

of the transport rate and the elapsed time for the reduction in the transport rate to begin, for different flow rates, could be more clearly seen as shown in Figure 7.3 for the test reach length x_R = 1.74 m.

(2) Discussion of Results

During the steady flow non-equilibrium runs, after t = 0, the downstream end of the general scour hole which forms on the erodible bed, progressively moves downstream with time. This migration of the scour hole explains the shapes of the bedload curves in Figures 7.2 and 7.3. As equilibrium transport conditions were established prior to t = 0, the bedload transport rate at the measuring station at e.g. $t = t_1$, is close to the equilibrium value initially (Figure 7.3). The reasons for the variation of $\bar{g}_s/g_{se_0}$ about the value 1.0 at t = 0 can be attributed to experimental variations, particularly variations in the initial mean bedlevel at t = 0, which will alter the mean flow velocity, relative to the flow rate q, for which g_{se_0} was calculated. The transport rate decreases once the downstream end of the scour hole has passed the sampling point. For the low flow rates, $q \leqslant .056$ $m^3/s/m$, shown in Figure 7.2, this effect was not noticeable because the duration of the runs (two hours) was not sufficient for the scour hole profile to affect the transport rate at the measuring station at x_R = 9.29 m. With increasing water discharge, transport rates during a run did reduce, with commencement time for the reduction being smaller for the higher discharges, (see Figure 7.2 and 7.3). Neither the time of arrival of the leading edge of the scour hole nor the time when the transport rate reduces, can be clearly defined and so they cannot be correlated definitively.

Thus under non-equilibrium conditions the transport of bedload is obviously a non-steady process. As the bed, at any section within the non-equilibrium region, degraded, the local bedload transport capacity also decreased. Whether or not the decrease of the actual bedload transport rate at that point is commensurate with the decrease

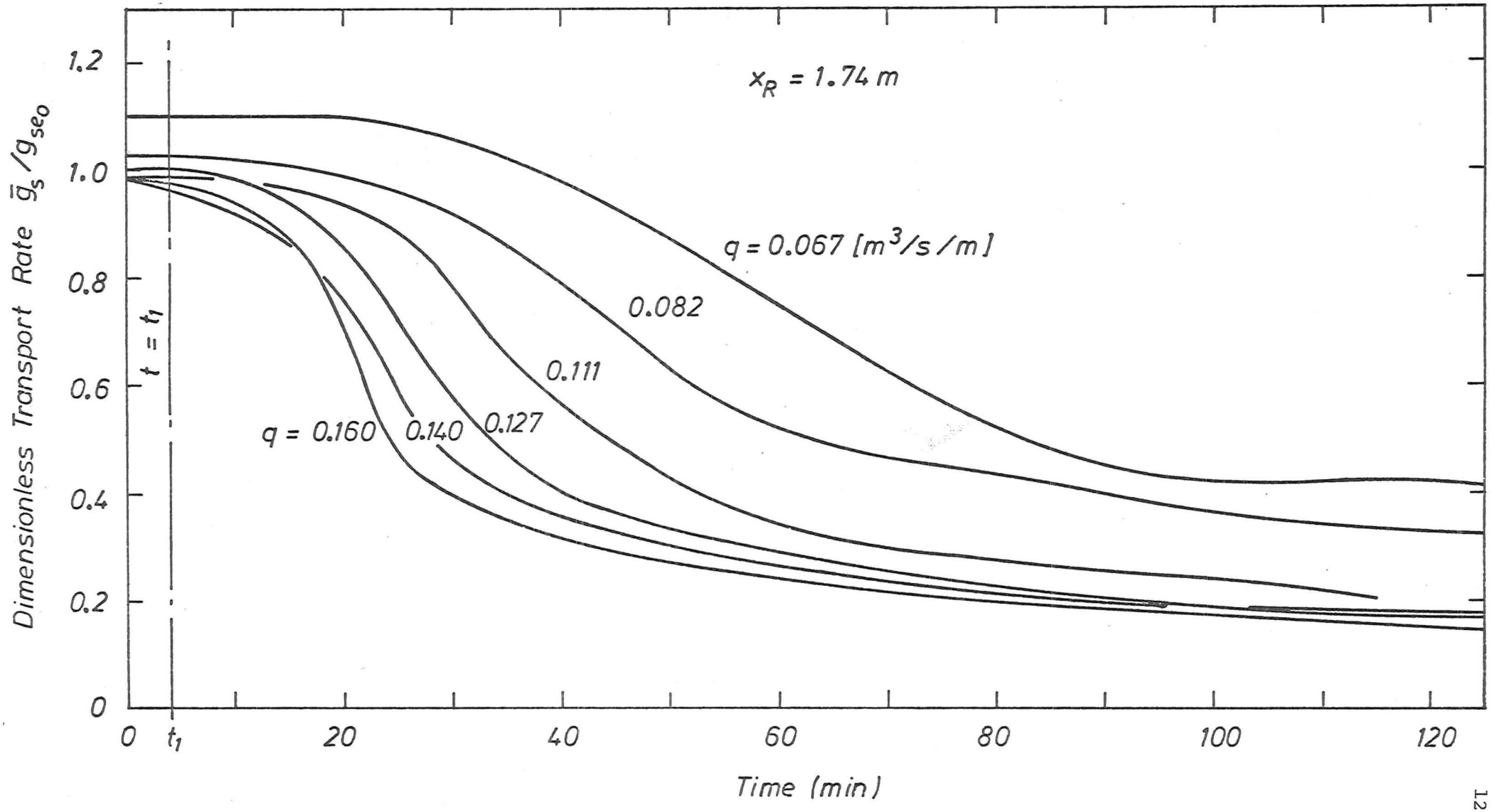

FIGURE 7.3 : Steady flow non-equilibrium dimensionless transport rates (ST--17 series)

in transport capacity, particularly in the local scour area, will be discussed later in section 7.4.3.

7.3.2 Maximum Scour Depth

(1) Results

From the bed elevation profiles measured at various stages during a run, the maximum scour depth, d_{max}, could be obtained. The point where the maximum scour depth occurred migrated downstream very slowly compared with the leading edge of the local scour hole and was generally located between 0.15 - 0.4 m from the edge of the fixed bed. The temporal variation of d_{max} for the different flow rates is shown on the logarithmic plot of Figure 7.4 for x_R = 5.29 m. The other four test reaches yielded approximately the same scour development.

After the initial transition period (approximately 10 minutes), the maximum scour depth followed a power relationship with time of of the form

$$d_{max}(q,t) = at^b \qquad \ldots (7.1)$$

where a, b are functions of the fluid and sediment properties. Apart from the data for the smallest discharge shown, where the final d_{max} value was only $4D_{50}$, the mean value of b was 0.31.

(2) Discussion of Results

Chuna (1975) has suggested that for any local scour phenomenon, the time history of scouring development consists of four distinct phases, (section 2.3.2). Only the first two phases were present in the ST series because of the short 2 hour run duration. These phases as shown on Figure 7.4 were the initial transition phase and the first principal phase, where according to Chuna (1975),

$$\frac{d_{max}}{y_o} = a' t^b \qquad \ldots (7.2)$$

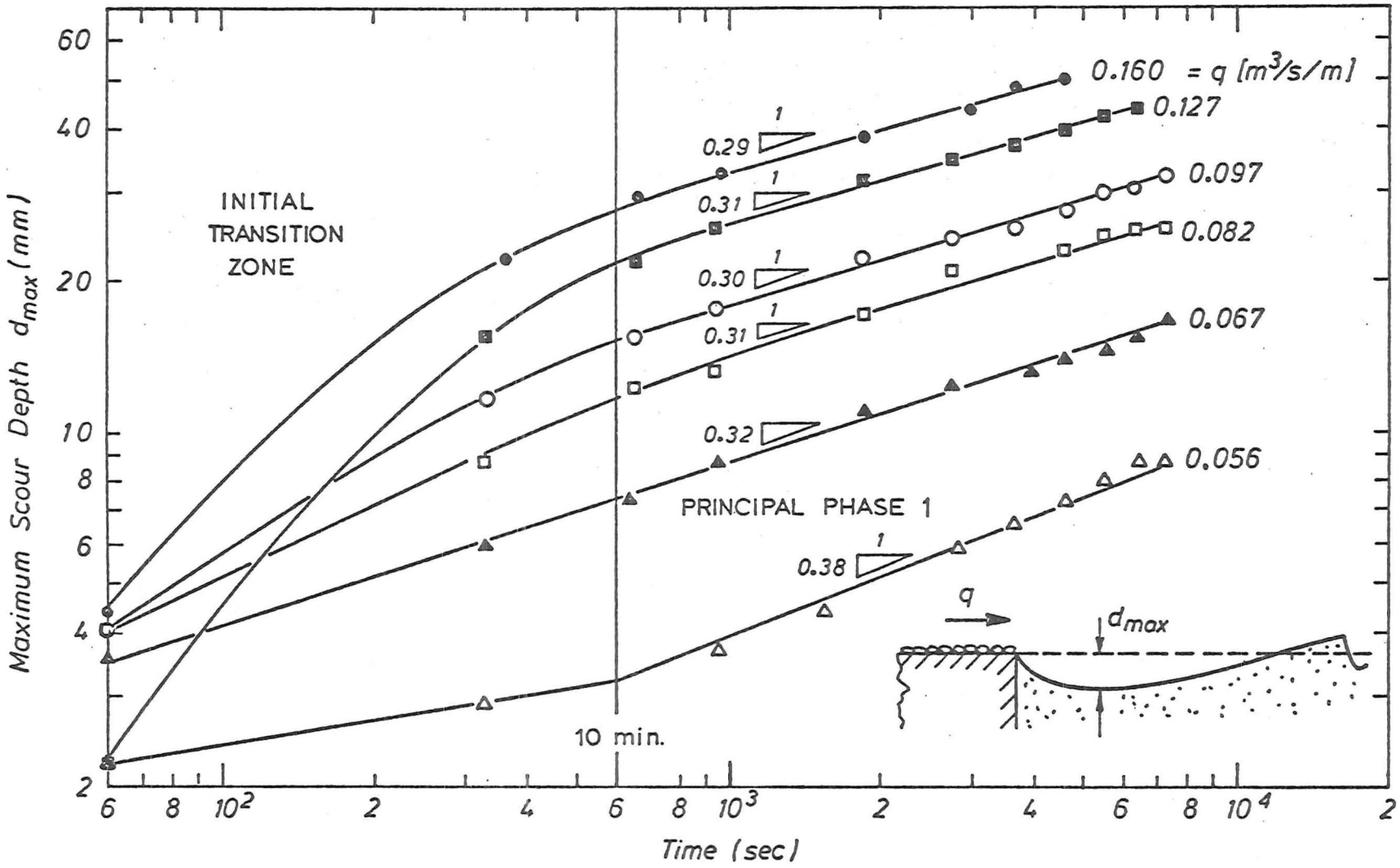

FIGURE 7.4 : Maximum scour hole depth with elapsed time (ST--53 series)

where y_o is the approach flow depth.

In the present study the transition period was present for the first 10 minutes, (Figure 7.4). The increase in the slope of the curves in this period with increasing discharge reflected the increasing mismatch or step change between the input equilibrium transport rate for the particular flow rate and the zero input transport rate at t = 0.

The slope of the experimental curves for all the runs with the onset of the principal phase approached a constant value, where equation 7.1 was applicable, and similarly equation 7.2 if y_o is incorporated in the constant a. By that stage the fluid vortex system, which occupied the separation zone at the upstream end, was developed and would account for the constant power correlation with time for all the runs shown in Figure 7.4. The exponent values, b, lie in the range between 0.38 found by Breusers (1966) and 0.20 from the results of Colaric, Pichon and Sananes (1967) for similar experiments. Run STO253 with the lowest flow rate yields a value of 0.38 for b which is the same as Breusers' value, however the results have a greater experimental uncertainty as the changes in d_{max}, for each time step, are of the order of a grain size.

With only a limited range of hydraulic conditions, using a single bed material and the two hour duration, it was not possible to ascertain generalised values of the constants a' and b in equation 7.2. Any theoretical approach to predict values of a' and b for a maximum scour depth-time formula will be strongly dependent on the initial motion criterion which is used in the formulation, as was the case for the various equilibrium transport formulae discussed previously (6.3.3).

7.4 SPATIAL VARIATIONS : RESULTS AND DISCUSSION

7.4.1 Scour Hole Profiles

(1) Results

Two sequences of typical scour hole profiles are shown in Figures 7.5, 7.6 for a low and a high steady discharge respectively. For comparison, the original graded bed levels, prior to the commencement of the runs, are also shown. These levels are not to be confused with the bed profiles at t = 0, when the equilibrium sediment input rate was suddenly reduced to zero. The oscillations in bed level, shown in Figure 7.6, downstream of the local scour hole, but within the general scour hole (Figure 7.1), are due to the presence of dunes. However, the profile as shown does not correspond to the actual continuous profile, since elevations were measured at discrete intervals one metre apart after x = 3 m.

Together with the maximum scour depth, the slope of the scoured bed at the edge of the solid apron is important in describing the local scour hole shape. Apart from the three lowest flow rates, $q \leqslant .067$ $m^3/s/m$, where the scour hole profile is much flatter, the maximum angle between the original bed level and the scoured bed surface α, (shown in Figure 7.6c) was reasonably constant, lying in the range $17^0 - 20^0$.

(2) Discussion of Results

The general scour hole profile for the low flow rates (Figure 7.5) assumed a much more slender profile than those obtained for the higher discharges. Erosion of the bed essentially occurred as a thin sheet of bed material in the absence of any visible bedforms. A shallow local scour hole has developed in Figure 7.5(a). The hole continues to deepen in (b) but with time the rate of change of the maximum scour depth slows e.g. compare (b) and (c) where d_{max} is essen-

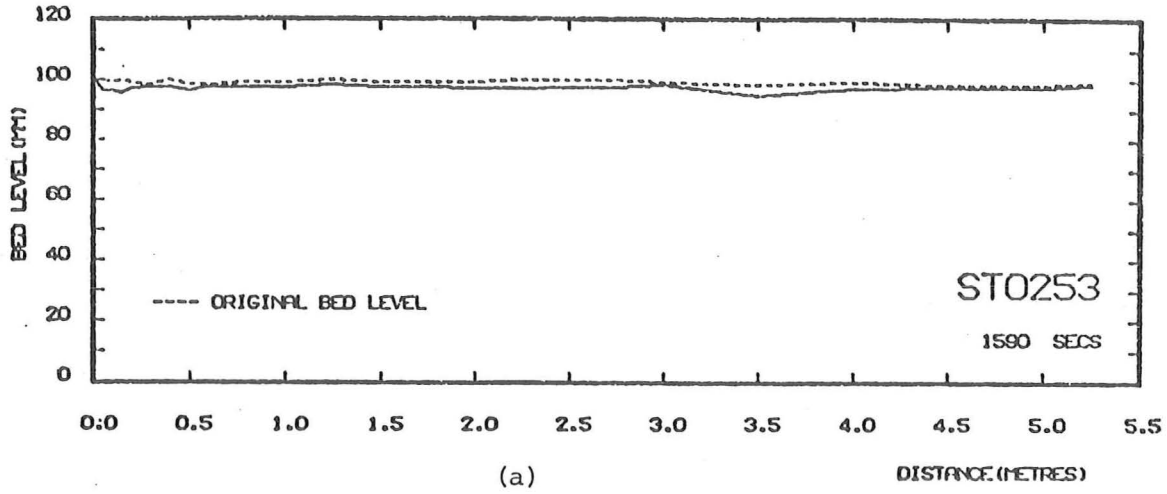

(a)

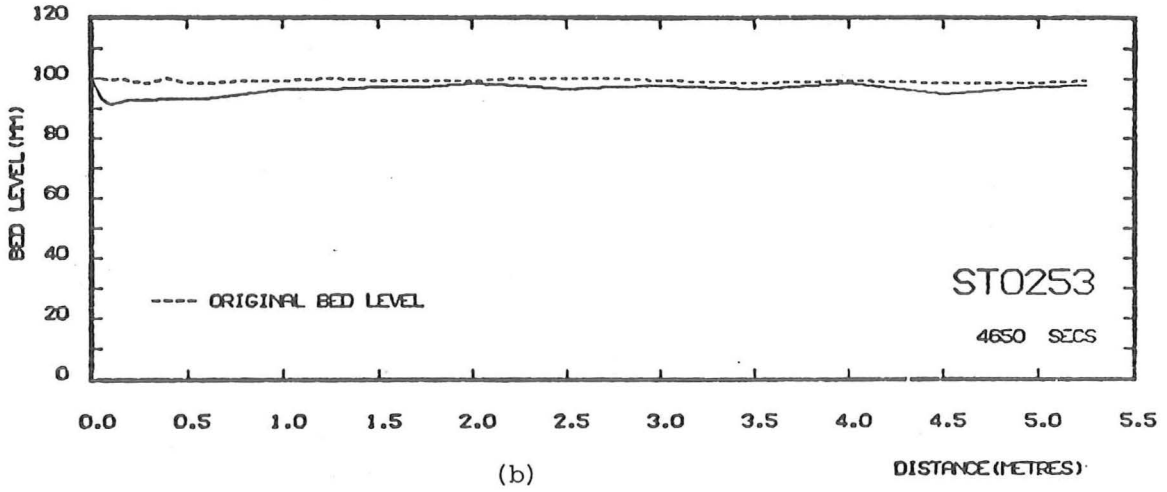

(b)

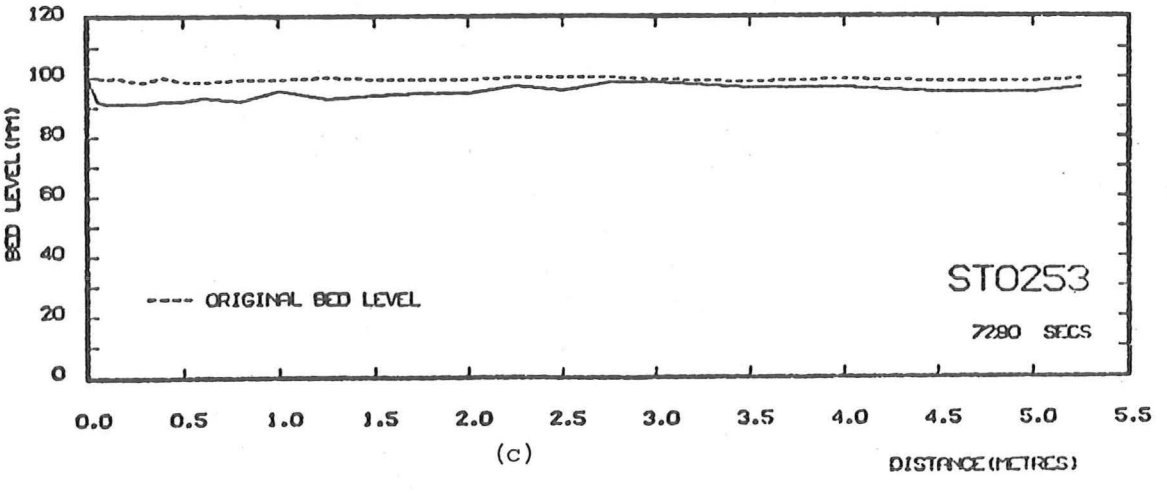

(c)

FIGURE 7.5 : Scour hole development with time

(q = .056 $m^3/s/m$, y_o = .099 m)

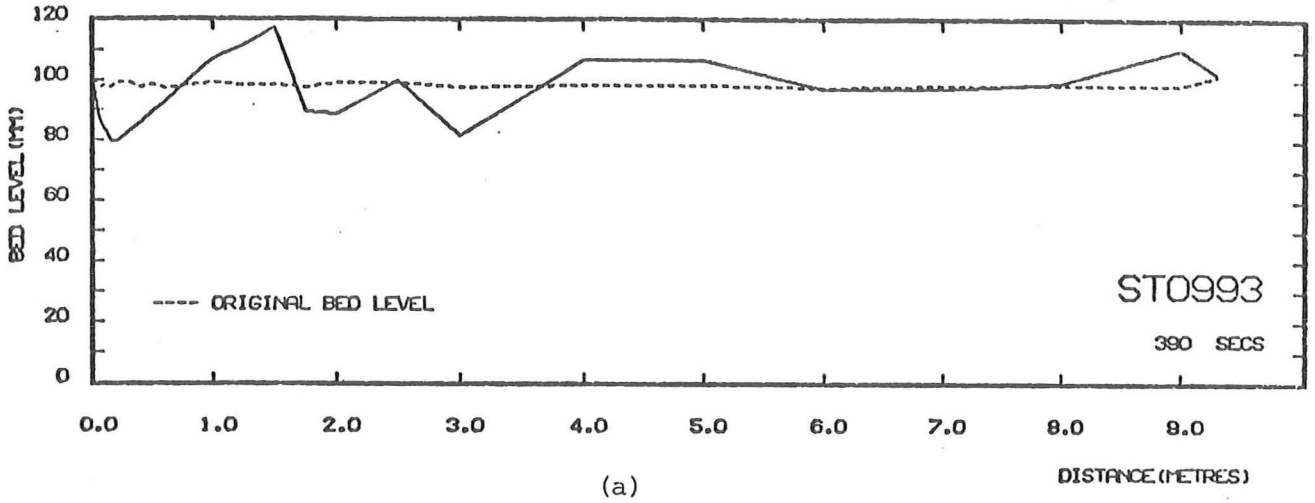

(a)

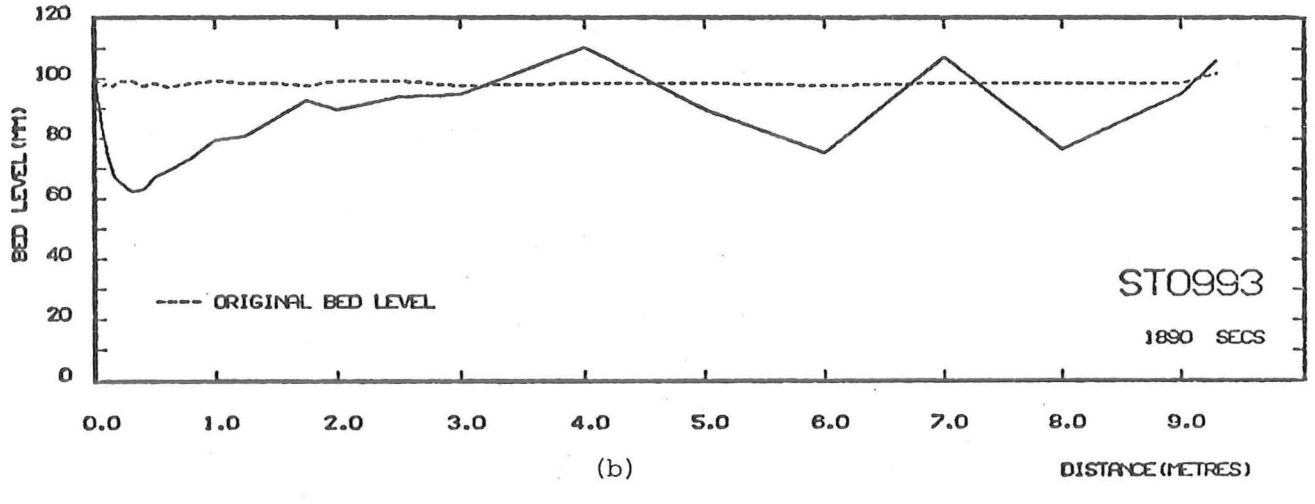

(b)

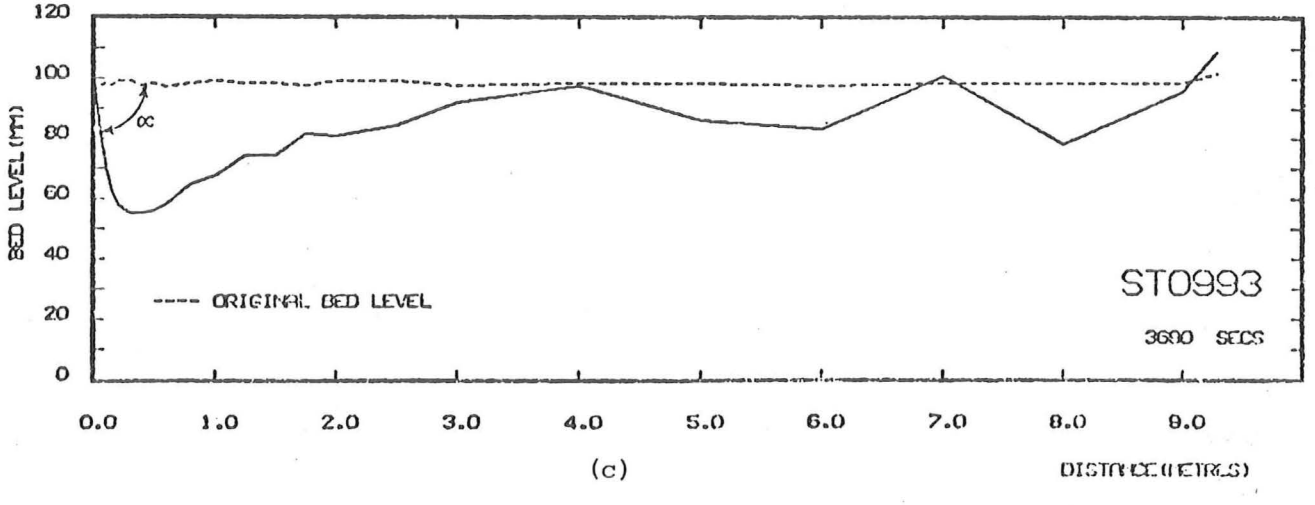

(c)

FIGURE 7.6 : Scour hole development with time
($q = .159\ m^3/s/m$, $y_o = .200\ m$)

tially unchanged over 2600 seconds, while the scour hole length continues to grow.

In contrast, the scour hole development for the maximum steady flow rate (Figure 7.6), occurred rapidly after the upstream sediment supply was severed. Figure 7.6(a) shows the profile measured after an average elapsed time of 6½ minutes. The increase in the maximum scour depth, d_{max}, which occurred in such a short span of time, emphasizes the mismatch condition which was present in the initial transition period. This rapid growth may be ascribed to the large difference between zero and equilibrium capacity bedload transport rates.

The scoured bed material became an integral part of the sediment transfer processes of the last dune bedform which had previously formed at the upstream end of the erodible reach, immediately prior to the input sediment cut-off. As the ability to transport the available bed-material diminished in the scour pit region, the deficit of material to satisfy the flow transport capacity at points further downstream, is eroded from the sloping back of the dune, thus elongating the scour hole profile (Figure 7.6(b)), while the point of maximum scour depth remains relatively fixed.

Figure 7.6 (c) exhibits a further advanced stage, where the general scour hole occupied the whole test reach, even though the bed profile locally crosses or touches the original bed level at x = 4 m, 7m. This makes the definitive estimation of the general scour hole length more complex than estimates of the maximum scour depth, as a continuous mean bed elevation trend line must be used.

A comparison of Figures 7.5 and 7.6 reveals that the bedform at the downstream extremity of the local scour hole, plane bed and dune bedform respectively, is indeed related to the bedform regime further downstream, (shown more clearly for dune bedforms in Figure 8.19). This relationship was postulated by Padmavally et al. (1980)

for dunes and shown in Figure 2.2, by Raudkivi (1965), for ripples, (see section 2.3.2).

The slope angle α, or the upstream slope of the local scour hole profile was always much less than both the angle of repose ($\phi = 35^0$) and the slope of the lee face of the dune bedforms. This is probably due to the more pronounced reverse flow of the fluid vortex, which maintains the shape as observed in section 7.2, compared to the fluid eddies which exist in the lee of the dune crest, where particles were not observed moving up the dune face. Also the bed particles in transport, which avalanche down the lee slope of a dune, create a steeper slope. Such avalanching does not exist at the upstream end of the scour hole where there is no sediment input to the reach. The constancy of the angle α appears to be the result of a delicate balance between the fluid forces exerted by the fluid vortex and the effects of gravitational forces on the surface particles.

Scour hole profiles typical of those computed from a mathematical model of the water and sediment phase interactions are shown in Figure 7.7, adapted from Chen (1973). They differ significantly from the experimentally obtained profiles (Figure 7.6), at both extremities of the scour hole. Just as physical processes e.g. the fluid vortex, determine the shape of the experimental scour hole profile, so also the numerical processes used in the mathematical model, determine the profile in Figure 7.7. Existing mathematical models for steady flow, non-equilibrium conditions incorporate two equations (section 2.3.3), one of which describes the sediment phase, a continuity equation, in conjunction with an equilibrium transport formula. Hence, only one boundary condition can be specified for the bedload i.e. the sediment hydrograph at the upstream end, e.g. $g_s(o,t) = 0$. The explanation of the shape of the scour hole at the upstream end of Figure 7.7, is that at x=0 there is a discontinuity, where the bedload transport rate at the boundary is, in this example, zero, but everywhere

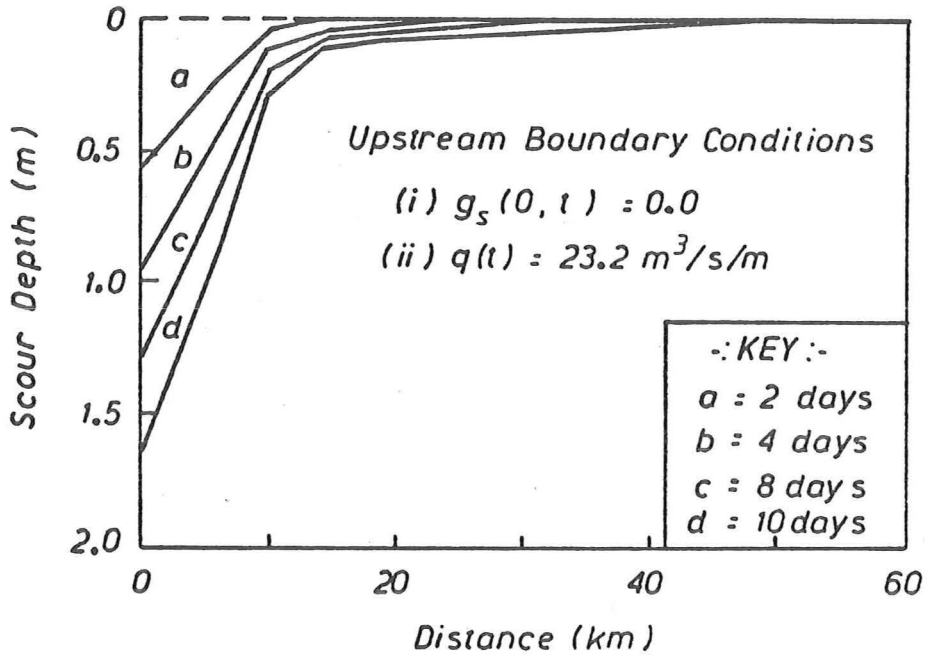

FIGURE 7.7 : Typical scour hole profiles predicted by a mathematical model (adapted from Chen (1973))

else in the reach attains its equilibrium value. Thus the maximum scour depth will occur at $x = 0^+$, and not further downstream as was the case under the fluid vortex. This will lead to a slightly greater maximum scour depth as the sediment wedge AEC (Figure 7.1) is neglected. The general mathematical model cannot fully model microscale features on the bed such as dunes, therefore the profile of Figure 7.7 approaches asymptotically to the x axis. However, this limitation is not serious with regard to the general scour hole shape for steady flows, as the experimental scour hole length is probably best determined using a mean bed elevation trend line.

7.4.2 Bedload Transport Rates

(1) Results

By collecting transport rate-time curves at several stations along the control test reach, the spatial variation of bedload transport rates can be determined. Bedload transport rate-time curves for two constant water discharges and seven different reach lengths are presented in Figures 7.8a,b. The data derived for the two shortest reach lengths shown, 0.2 m and 0.4 m, was obtained from a time series of scour hole profiles for that particular discharge, using the finite difference equation 3.6. The plots in Figures 7.8a,b can also be redrawn to show the bedload transport rate variation with x with time as the third parameter. These are shown in Figures 7.9 a,b for the same discharges of 0.127 $m^3/s/m$ and 0.159 $m^3/s/m$ respectively.

(2) Discussion of Results

With reference to Figure 7.8, the transport rate initially was close to the equilibrium transport capacity, for all points in the test reach. The rate soon decreased at the upstream section due to the effect of the non-equilibrium sediment boundary condition, $g_s(t) = 0$. The affected bed length increased with time, so at bedload sampling points downstream, the transport rate successively dropped from the equilibrium value. The decrease in transport rate was rapid in the scour pit area, (up to $x_R = 0.74$ m), but became less severe with distance downstream. Comparing Figure 7.8(a) and (b) shows that the drop in transport rate occurs much sooner and at a faster rate for the larger flow rates than for the smaller flow rates.

After the initial rapid decrease, the bedload transport rate decreases much more slowly with time, for small values of x_R, with critical transport conditions being approached asymptotically. The close proximity of the transport rate curves for the longer reach lengths reflects the small rate of change of g_s with x, $\frac{\partial g_s}{\partial x}$, where

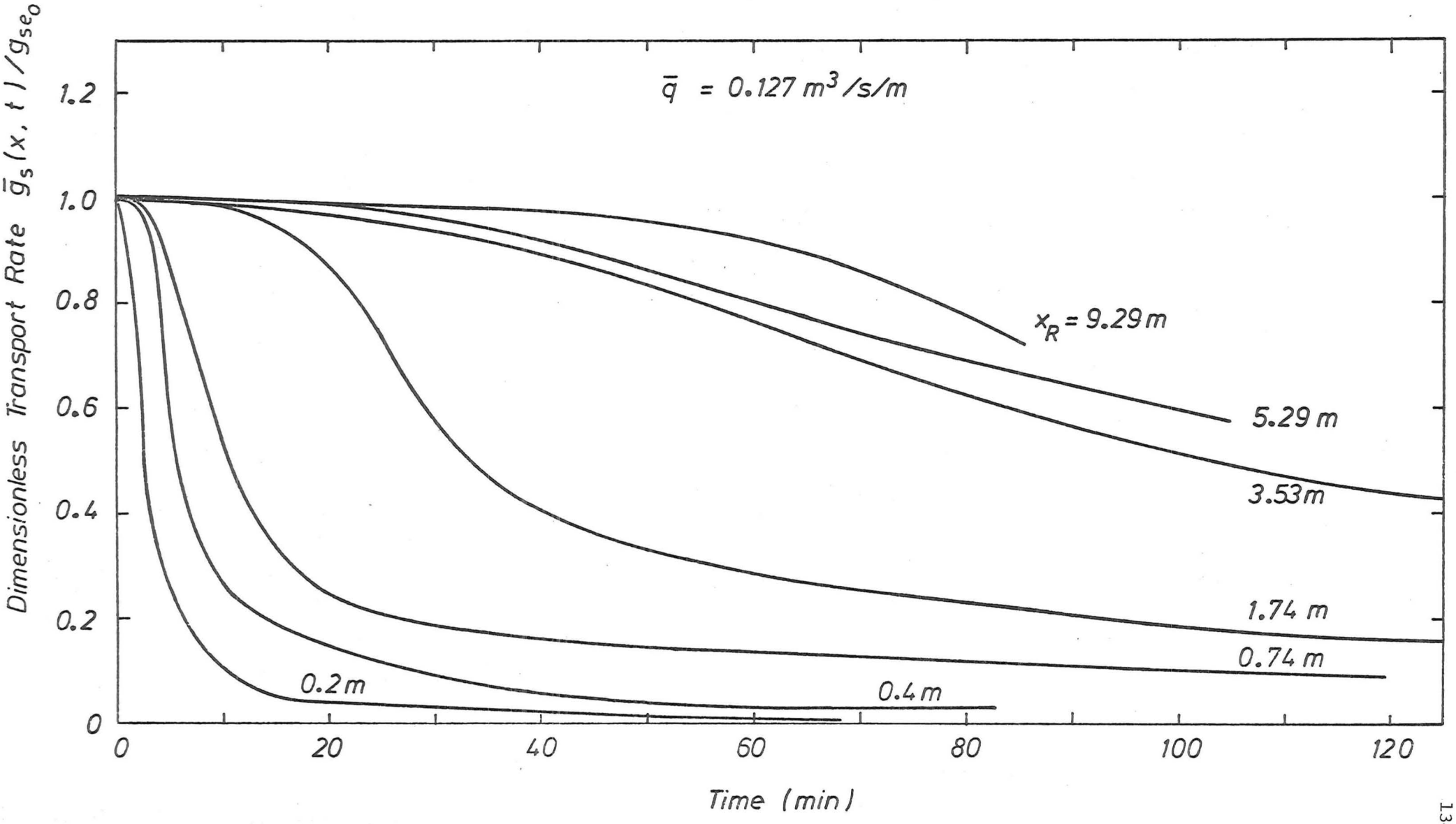

FIGURE 7.8 (a) : Dimensionless transport rates versus time and distance downstream

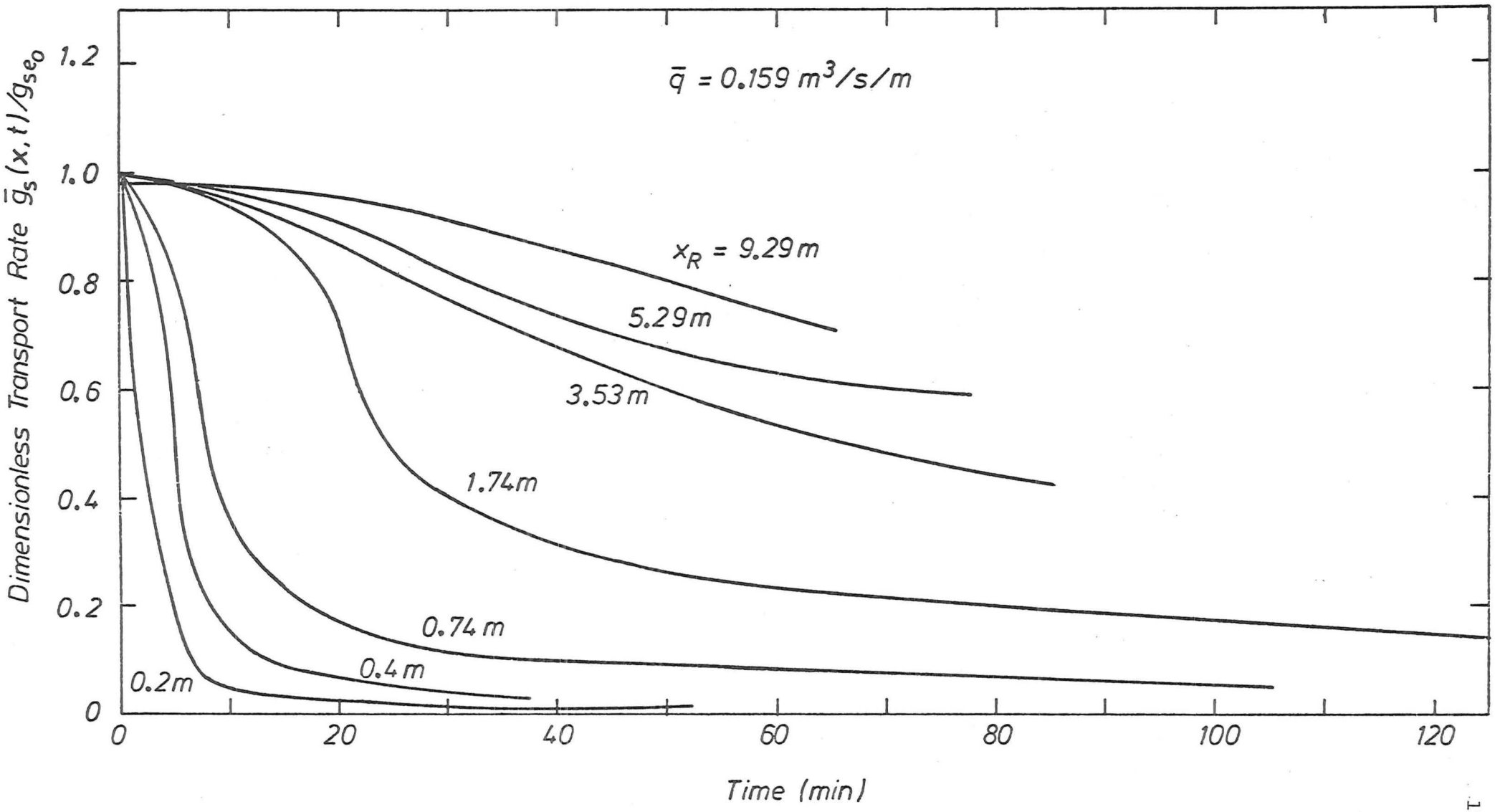

FIGURE 7.8 (b) : Dimensionless transport rates versus time and distance downstream

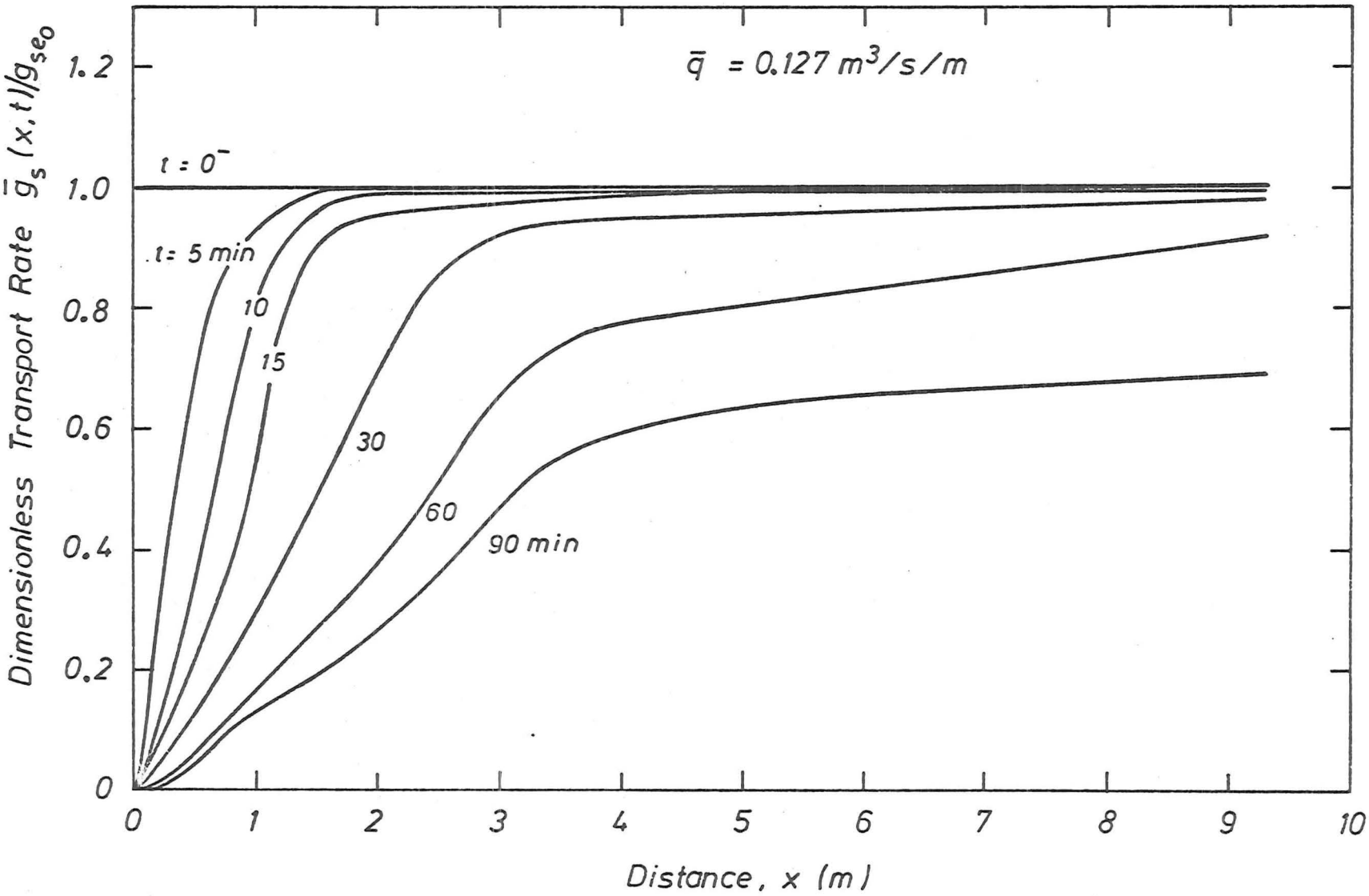

FIGURE 7.9 (a) : Dimensionless transport rates versus distance downstream and time

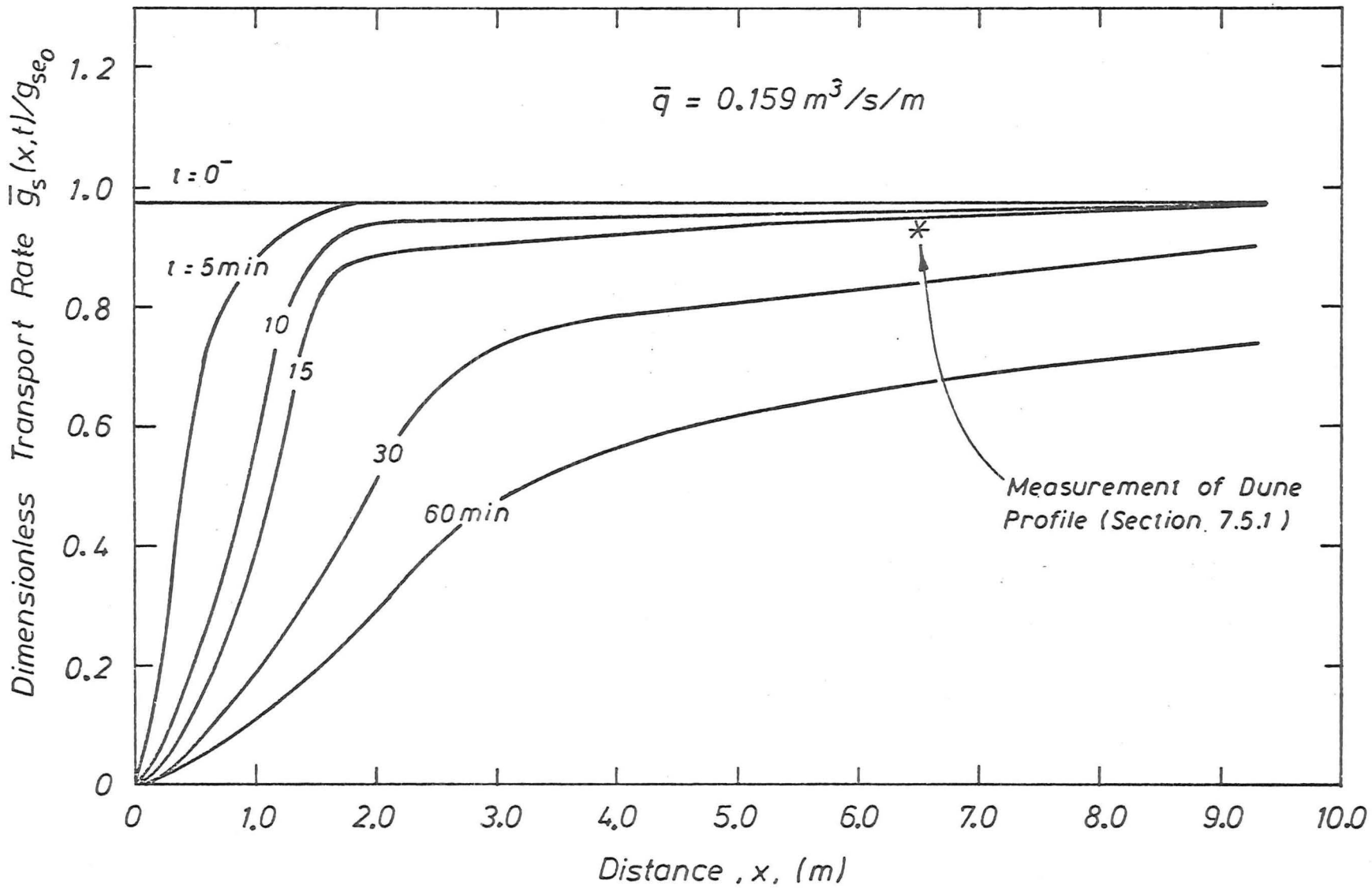

FIGURE 7.9 (b) : Dimensionless transport rates versus distance downstream and time

the general scour hole profile approached close to the original bed level (Figure 7.9). A similar plot to Figure 7.8 of the transport rate variation with x and t was obtained by Soni, Garde, and Ranga Raju (1977) for the non-equilibrium case of aggradation, but the asymptote in their case was the overload transport rate, $g_{se} + \Delta g_s$.

The plots shown in Figure 7.9 display more clearly, than Figure 7.8, the actual spatial distribution of the transport rate at any particular time. The transport rate increased rapidly from the value of zero at the upstream boundary with distance x. As the equilibrium transport capacity of the flow was approached, the rate of change, $\left(\frac{\partial g_s}{\partial x}\right)$, asymptotically approached zero, where the constant state region of Figure 3.5 exists. However the curves in Figure 7.9 do not display a simple function, where the variation in slope $\left(\frac{\partial g_s}{\partial x}\right)$, with distance x, is continuously decreasing from x = 0 as would be expected, (see Figure 8-5 in Gessler (1971)). Instead the slope $\left(\frac{\partial g_s}{\partial x}\right)$ at first increases and then subsequently decreases giving rise to the distorted S-curves shown in Figure 7.9. The main reason for the distorted S-shaped curve is thought to be the vigorous scouring action of the downstream end of the fluid vortex in the scour pit region where the inflexion point of $\left(\frac{\partial g_s}{\partial x}\right)$ occurs, giving a local maxima. Another effect which will be present is the rapid decrease in the local transport capacity in the scour pit because of the rapid degradation of the bedlevel, for the same flow rate. This effect will be investigated in the next section.

7.4.3 Transport Rate Comparison With Comparable Equilibrium Transport Rates

(1) Results

The previous results section 7.4.2 showed that the bedload transport rate decreases as the bedlevel drops at any point x. The

drop in bedlevel also in turn reduces the bedload transport capacity at that point. To determine the deficit, $\Delta g_s'$, between the actual transport rate $g_s(x,t)$ and the comparable local equilibrium transport capacity $g_{se}(x,t)$, if any, the comparison procedure, outlined in detail in section 3.3.2, was used. The time series of scour hole profiles used in the comparison procedure were measured at five minute intervals initially for 15-20 minutes when the scouring intensity and $\left(\frac{\partial g_s}{\partial x}\right)$ were high at the upstream end, and then at 15 minute intervals thereafter.

The results of the analyses for stations x_R = 0.3 m, and x_R = 0.4 m, where the maximum scouring action occurs, are shown in Figure 7.10 for increasing values of time t. The steady flow equilibrium transport relationship, equation 6.5, is also included. The comparable equilibrium capacity could be obtained by entering the equilibrium curve at the same local mean velocity as in the non-equilibrium run. An example is shown in Figure 7.10 for the ST0753 run at x_R = 0.4 m. At $\bar{t}$ = 12.5 minutes, the mean calculated transport rate is .049 N/s/m and the mean flow velocity is .653 m/s. The above transport rate can be compared with the comparable equilibrium transport capacity rate, $g_{se}(0.4,12.5)$ = .087 N/s/m at the same mean velocity. The equations for each of the straight line segments of the non-equilibrium curves in Figure 7.10 are summarised in Table 7.1. (where $g_s(x,t) = a_* \bar{u}^{b_*}$ N/s/m and r_{xy} = correlation coefficient.)

(2) Discussion of Results

The transport rate initially was close to the equilibrium rate, which can be seen in Figure 7.10 for the first five minutes, although with some scatter about the equilibrium transport curve, due to the short base time for averaging the bedload transport rate. However soon after the initial period of five minutes, the actual bedload transport rate, $g_s(x,t)$, decreased much more rapidly than the comparable local equilibrium capacity, $g_{se}(x,t)$, calculated using the mean

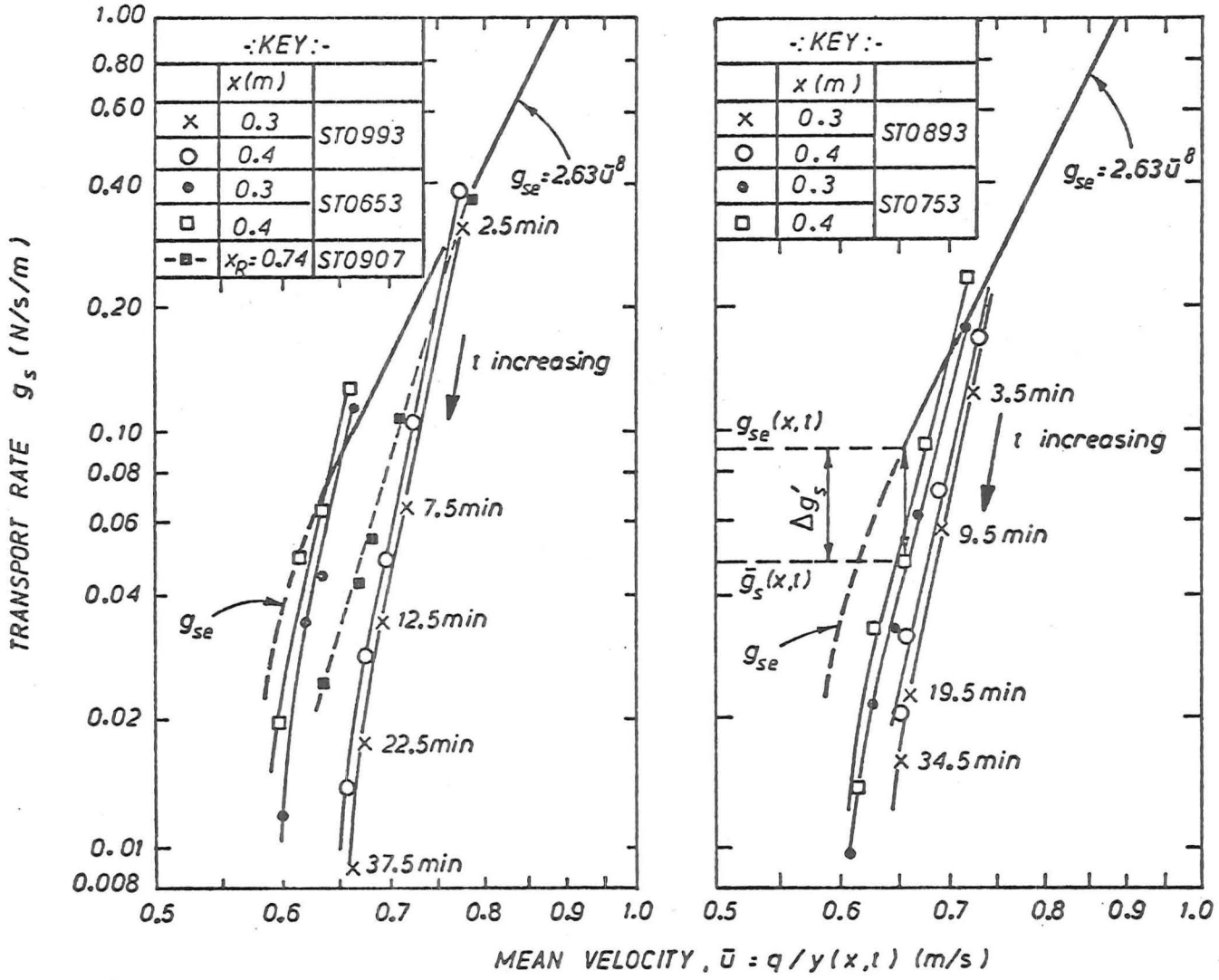

FIGURE 7.10 : Transport rate comparison with comparable equilibrium transport rates

TABLE 7.1 : Non-Equilibrium Transport Rate Equations.

Run	No. of Points	x (m)	a_*	b_*	r_{xy}
	Equilibrium		2.63	8.0	
ST0993	4	0.3	62.4	20.3	.999
	5	0.4	70.6	20.1	.997
ST0893	3	0.3	63.4	18.9	.999
	4	0.4	49.8	17.7	.989
ST0753	4	0.3	34.4	15.7	.992
	4	0.4	40.8	15.5	.994
ST0653	3	0.3	216	18.3	.988
	4	0.4	210	17.7	.984
ST0907	5	0.74	10.2	13.4	.999

flow velocity. This trend created a proportionately increasing deficit $\Delta g_s'$ between non-equilibrium and comparable equilibrium transport rates with time. Soni et al. (1977) also found that the actual non-equilibrium transport rate was generally lower than the equilibrium rate for aggrading channels.

The local bedload transport rates computed at x_R = 0.3 m and 0.4 m, using the finite difference continuity equation 3.6, followed the same trend as the g_{se} versus $\bar{u}$ curve in Figure 7.10 where a straight line segment, corresponding to high transport rates, gives way to a curve as the transport rate diminishes. The slopes of the straight line sections are much greater than that of the g_{se} versus $\bar{u}$ curve as shown by the high values of b_* in Table 7.1.

For the curves obtained from a particular run (q = constant), the straight line segments are approximately parallel for the two different stations within the scour pit region, but for the downstream

station, x_R = 0.4 m, the slope is always less (Table 7.1). The deficit $\Delta g_s'$ between the actual and equilibrium capacity transport rates is also less for the downstream station x_R = 0.4m, given the same mean velocity. This decrease in the deficit with distance downstream must necessarily be so, as further downstream of the general scour hole in the constant state region, the actual transport rate equalled the equilibrium capacity rate. Additional evidence is obtained from the actual transport rate curve measured at 0.74 m during run ST0907 (q = .160 $m^3/s/m$) and plotted in Figure 7.10 where the slope (or b_*) is much lower than for the curve at x_R = 0.4 m obtained during run ST0993 (q = .159 $m^3/s/m$).

The other main feature of the results, for a particular run, is the proportionately increasing transport rate deficit $\Delta g_s'$ with time (Figure 7.10 and also shown by the values of b_* larger than that of the equilibrium equation) e.g. at $\bar{t}$ = 7.5 minutes during run ST0993, for x_R = 0.3 m, $\Delta g_s'$ is 62% of $g_{se}(0.3,7.5)$, while at $\bar{t}$ = 37.5 minutes, $\Delta g_s'$ is 91% of $g_{se}(0.3,37.5)$.

However one of the reasons for this proportionately increasing deficit, is inherent in the definition of the local equilibrium capacity rate based on mean flow velocity. From measurements of turbulence and velocity profiles within the scour hole by Breusers (1966, 1975), where the local scour hole can be compared to a free mixing layer, the choice of the mean flow velocity $\bar{u}$ to determine the transport rate does not adequately represent the distorted velocity profiles near the scoured bed. A more pertinent approach would be to relate the local flow velocity near the bed surface to the local transport capacity. However it remains to be seen whether a transport rate deficit would still exist between the actual transport rate and a capacity transport rate based on the local mean bed velocity, which may well be negative for x < 0.3 m.

Figure 7.10 also shows a decrease in slope of the $g_s(x,t) - \bar{u}$ line segments, and thus the transport rate deficit, with decreasing flow rate, (see exponent b_* in Table 7.1), with the exception of run ST0653 which had the lowest flow rate shown. This is the same effect as was present in the transition zone of the d_{max} versus t curve (Figure 7.4), where the mis-match between the zero input bedload transport rate at x = 0, and the equilibrium transport capacity for x > 0, decreases with decreasing water discharge. The reason for the increase in the exponent b_* for run ST0653 was the close proximity of the bedload transport curve to the steeper curved segment of the equilibrium transport relationship for weak sediment transport.

The relationship between the dimensionless sediment transport rate $\frac{g_s(x,t)}{g_{se_o}}$ and distance x shown in Figure 7.9(b) can be replotted using the ratio of the actual transport rate to the local transport capacity viz. $g_s(x,t)/g_{se}(x,t)$ where calculation of $g_{se}(x,t)$ is based on the mean flow velocity. This ratio is shown in Figure 7.11, which shows the spatial variation of the dimensionless transport rate deficit, $\Delta g_s'/g_{se}(x,t)$ for one particular flow rate $\bar{q}$ = .159 $m^3/s/m$, at different stages during the development of the general scour hole. The spatial variation of the dimensionless deficit occurs because the flow requires a finite length of bed to erode sufficient bed material to satisfy the equilibrium capacity g_{se_o} of the flow downstream of the scour hole. As expected, the deficit is greatest at $x = 0^+$, where the local transport capacity is g_{se_o} but the actual transport rate is approximately zero. Because of the large difference between the capacity and actual transport rates near the upstream end, and the scouring action of the downstream end of the fluid vortex, the gradient $\left(\frac{\partial g_s}{\partial x}\right)$ attained its maximum value in the scour pit region, 0.1m - 0.4 m depending on the time.

A relationship was assumed by Foster and Meyer (1972) for ero-

sion of soil in rills, where the rate of erosion is proportional to the difference between the actual transport rate and the transport capacity for the flow conditions. This is equivalent to

$$e_s = \frac{\partial g_s}{\partial x} = C(g_{se} - g_s) \qquad \ldots (7.4)$$

where the parameters are all expressed at a common point and a particular time and e_s = local erosion rate and C is a constant, with dimensions $\{m^{-1}\}$. The behaviour of the curves drawn in Figure 7.11, is in close agreement with the integrated form of equation 7.4, if the small distance x_o from the upstream end of the fixed bed is ignored e.g. x_o = .28 m in Figure 7.11 for t = 60 minutes. The integrated form of equation 7.4 is

$$\frac{g_s(x,t)}{g_{se}(x,t)} = 1 - e^{-C(x-x_o)} \qquad \ldots (7.5)$$

After choosing a value of x_o for each time, the value of C, which yielded the best fit of the data in Figure 7.11, was chosen by trial and error. They are listed in Figure 7.11.

Dividing by the local transport capacity, equation 7.4 becomes

$$\frac{e_s}{Cg_{se}} + \frac{g_s}{g_{se}} = 1 \qquad \ldots (7.6)$$

where Cg_{se} can be associated with the erosion capacity. This equation describes simply the interaction between the sediment transfer processes of erosion and transport under non-equilibrium conditions, as outlined in the conceptual model, section 3.2.3. Thus when the local transport rate g_s is small, the local erosion rate e_s will be close to the erosion capacity of the flow, but as the local transport rate approaches the local equilibrium capacity, the erosion rate becomes small.

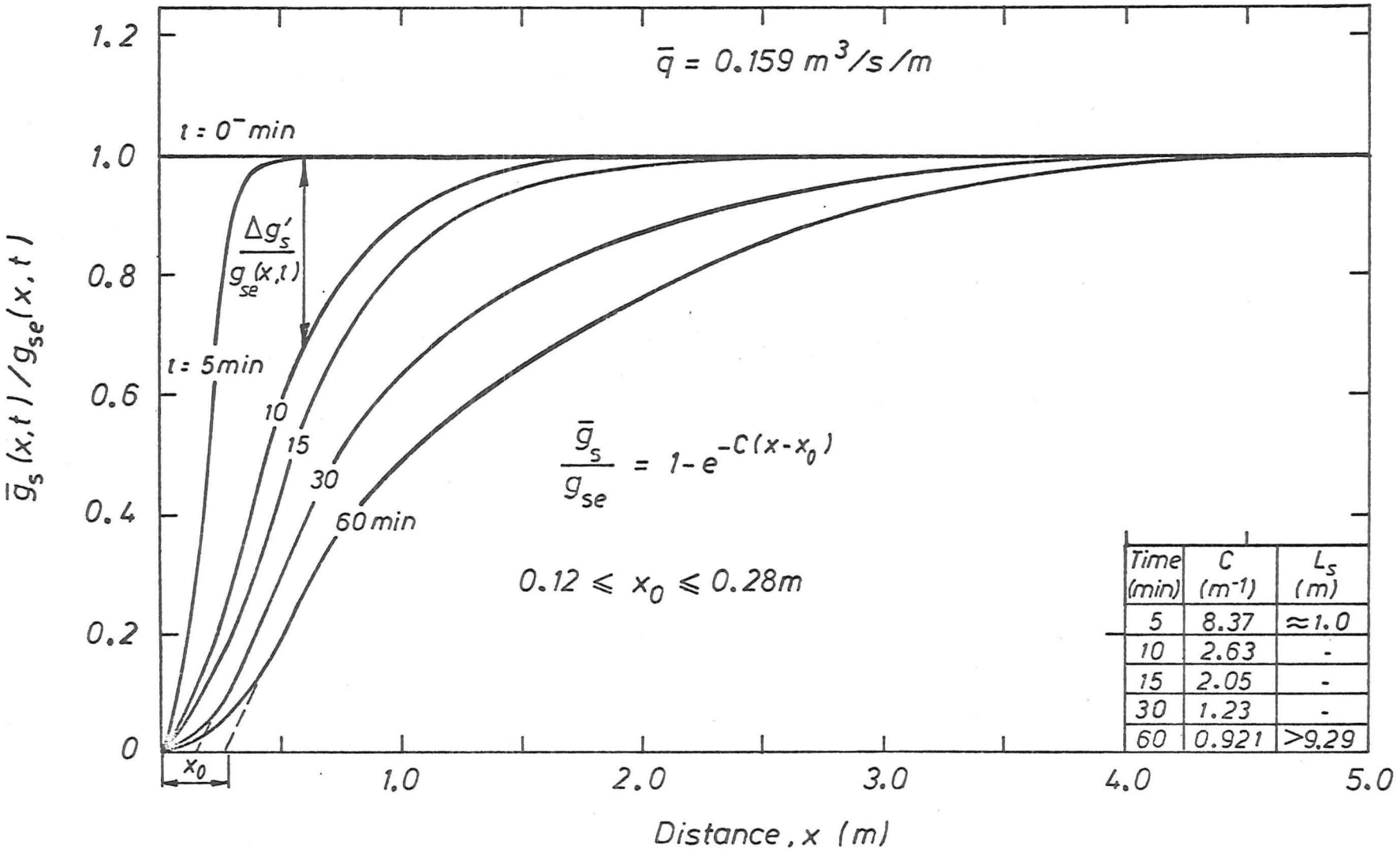

Time (min)	C (m^{-1})	L_s (m)
5	8.37	≈1.0
10	2.63	-
15	2.05	-
30	1.23	-
60	0.921	>9.29

FIGURE 7.11 : Dimensionless transport rate $\bar{g}_s(x,t)/g_{se}(x,t)$ versus distance downstream and the associated transport rate deficit $\Delta g_s'/g_{se}(x,t)$

The curves of Figure 7.11 also reveal that the dimensionless deficit, $\Delta g_s' / g_{se}(x,t)$, is not present over the whole length (L_s) of the general scour hole e.g. for q = .159 $m^3/s/m$ (ST0993) the general scour hole occupied the entire reach, Figure 7.6(c), yet the dimensionless deficit is present for only the first 4.0 m when t = 60 minutes. Four metres is approximately the length of the local scour hole, defined between the edge of the fixed apron and the first dune bedform, as shown in Figure 7.6(c) for that run.

As a consequence of the transport rate deficit $\Delta g_s'$ between the actual non-equilibrium transport rate and local capacity transport rate (computed from $\bar{u}$), the performance of steady-flow non-equilibrium mathematical models will be affected in the upstream section of the scour hole. An equilibrium transport formula of the form

$$g_s = g_{se} = a\bar{u}^b \qquad \ldots (7.7)$$

where a,b are arbitrary constants, is widely used to close the solution set for the model formulation and is applied everywhere in the spatial domain except at x = 0. Thus any computation of the time dependent local scour hole development e.g. d_{max}, using the formula 7.7, will underestimate the time scale, because in this region the actual transport rate is lower than the local capacity transport rate of the flow, defined by equation 7.7.

7.5 BEDFORMS

7.5.1 Dune Profiles (see also Plate 6.1)

A detailed analysis of bedform geometric properties for steady flow, non-equilibrium conditions was performed. The results were compared with the prediction methods for bedforms under equilibrium conditions by Yalin (1964) and Gill (1971), to provide a reasonable data base for comparison with bedforms under non-steady flows. The

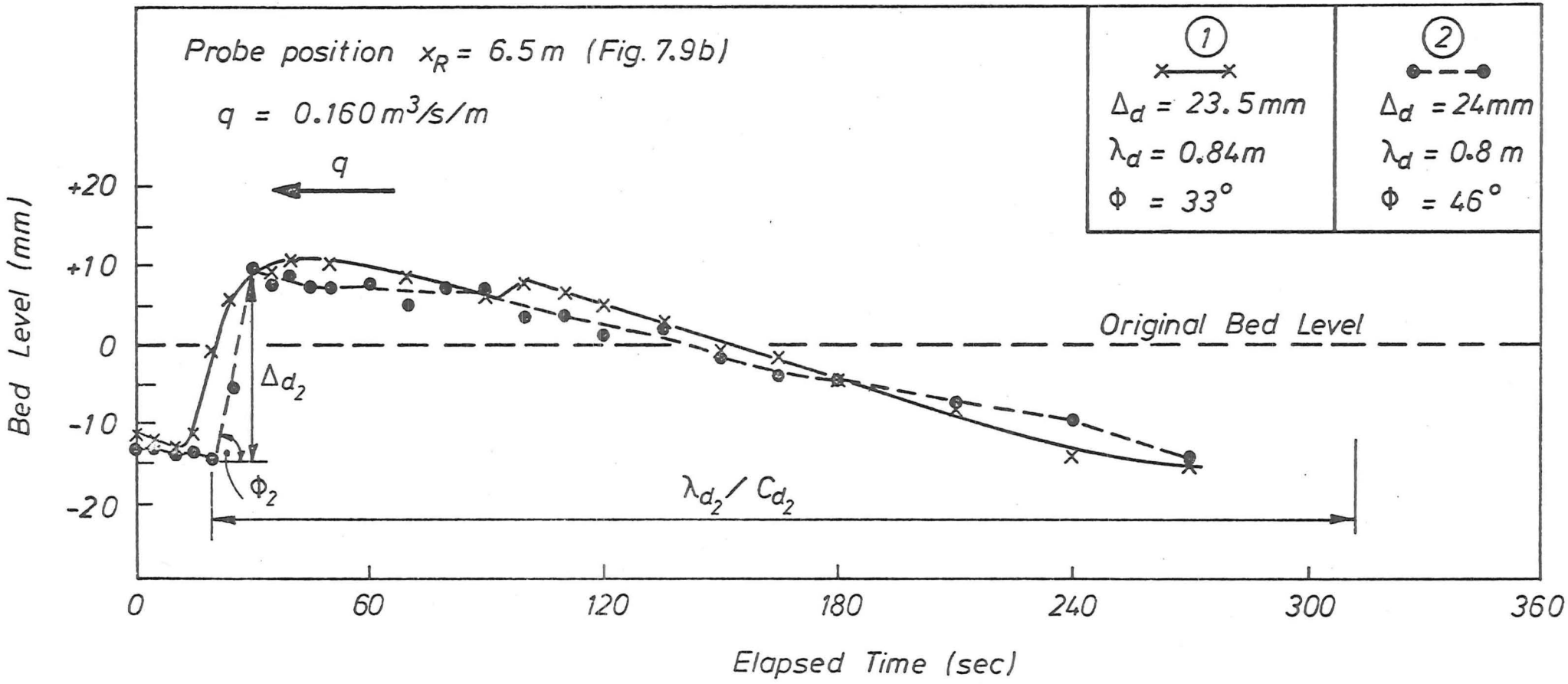

FIGURE 7.12 : Dune bedform profiles obtained by the ultrasonic probe during run ST0993

dune height (Δ_d), celerity (C_d) and particularly the wavelength (λ_d), varied considerably about an average value in both the spatial and temporal domains.

Two typical triangular shaped dune profiles were obtained in the temporal domain with the ultrasonic probe positioned at a fixed station as the bedform propagated past the probe, and are shown in Figure 7.12. An interesting feature of profile No. 1, is the small dune which formed on the back slope of the parent dune. This phenomenon was observed a number of times as noted previously in section 7.2. The angle between the original bed level and the steep downstream face of the dunes continuously varied between 32^0 and 46^0, but was generally greater than the measured angle of repose for the bed material in still water of $\phi = 35^0$.

7.5.2 Dune Wavelength

The wavelength correlation with water depth(similarly with q), is presented in Figure 7.13. For large values of $Z(= y/D_{50})$, $Z \geq 100$, Yalin (1977) predicted a theoretical value of wavelength to depth ratio of

$$\frac{\lambda_d}{y} = 2\pi \qquad \ldots (7.8)$$

However, despite the scatter of the data in Figure 7.13, the mean wavelength $\bar{\lambda}_d$, appears to be independent of the water depth for the larger values of Z. For smaller values of Z, $Z<70$, the mean wavelength actually increases with decreasing depth. These dunes can be likened more to long gravel bars present in coarse grain rivers with low values of Z. The maximum value of the ratio λ_d /y obtained from the data was 15 and the lowest was 3.5, while the mean value ranged from 13 to 6, with increasing Z. The larger values of λ_d/y above Yalin's (1977) value of 2π were also confirmed by Yalin and Karahan (1979) for values of $Z < 100$.

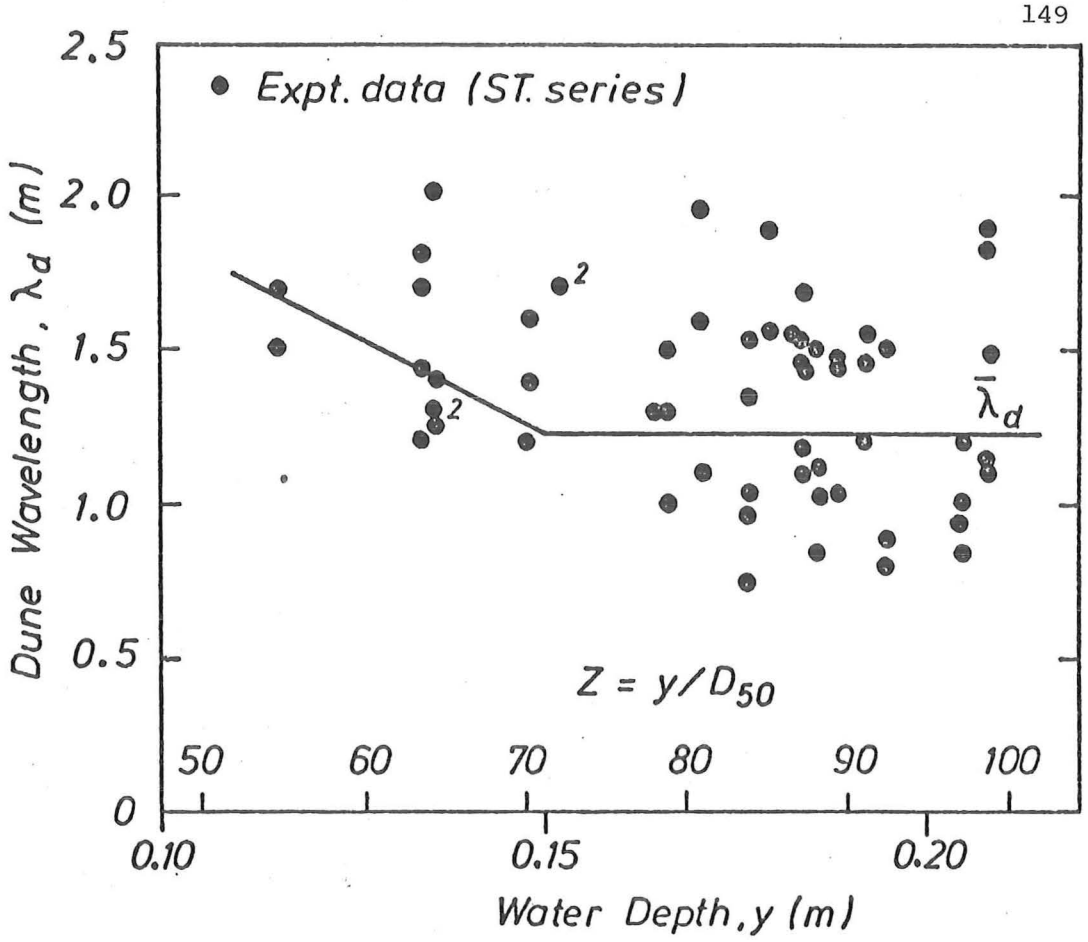

FIGURE 7.13 : Dune wavelength correlation with water depth

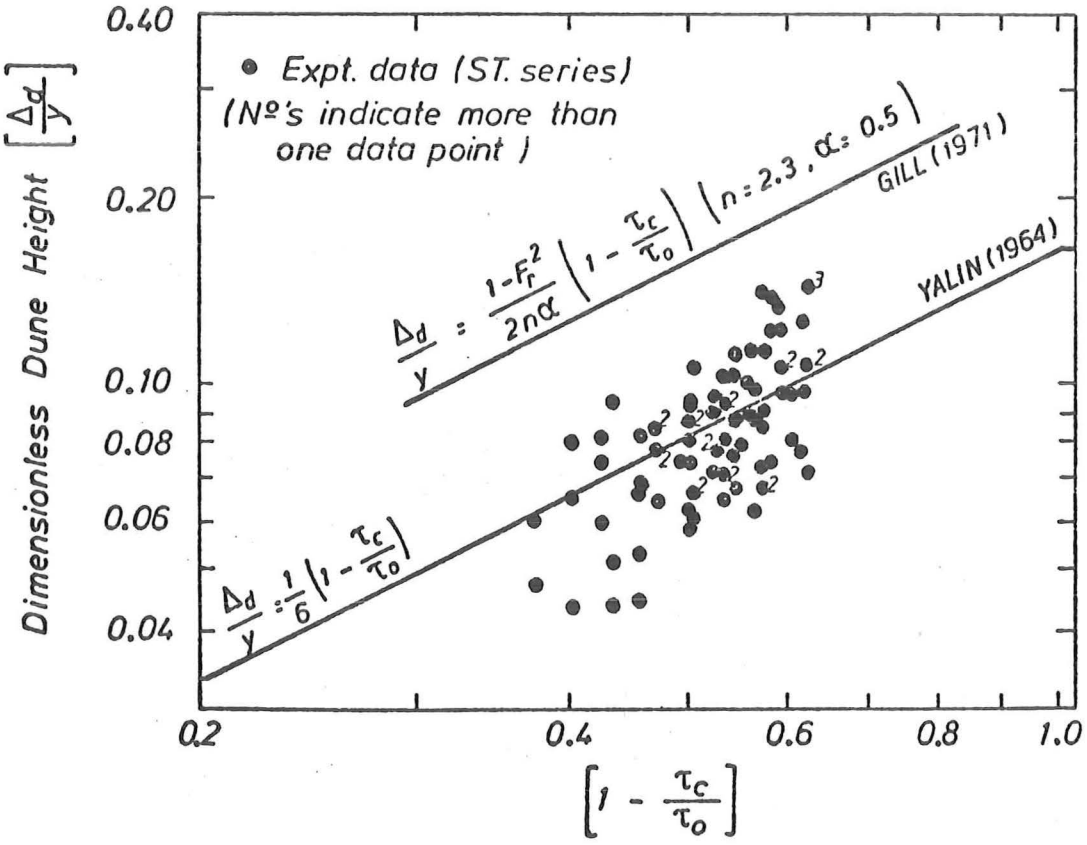

FIGURE 7.14 : Dimensionless dune height correlation with a dimensionless shear stress parameter

No real trend was discerned between the dune wavelength and the spatial position in the test reach.

7.5.3 Dune Height

The dune wave height, Δ_d, measured between the maximum crest level and the minimum trough level, is shown in Figure 7.14. A plot of the form

$$\frac{\Delta_d}{y} \quad \text{versus} \quad \left(1 - \frac{\tau_c}{\tau_o}\right)$$

where τ_c = critical shear stress and τ_o = bed shear stress, is convenient to compare the experimental data with the formulae of Yalin (1964) and Gill (1971). Once again, there is considerable scatter of the data points, yet the trend of the data is more obvious than was the case for the dune wavelength. The formula proposed by Yalin (1964) passes through the data, which actually follows a line of slightly greater slope. The modification to Yalin's formula, as proposed by Gill (1971), appears to overestimate the height of dune bedforms for the present experimental series.

7.5.4 Dune Steepness

The ratio of dune height to wavelength, defined as the dune steepness S_d where

$$S_d = \frac{\Delta_d}{\lambda_d} \qquad \ldots (7.9)$$

is an important parameter which can be used to relate the dune geometric properties to a resistance coefficient such as the friction factor, Fredsøe (1975). The dune steepness is plotted in Figure 7.15 against a dimensionless shear stress

$$\eta = \frac{\tau_o}{\tau_c} \qquad \ldots (7.10)$$

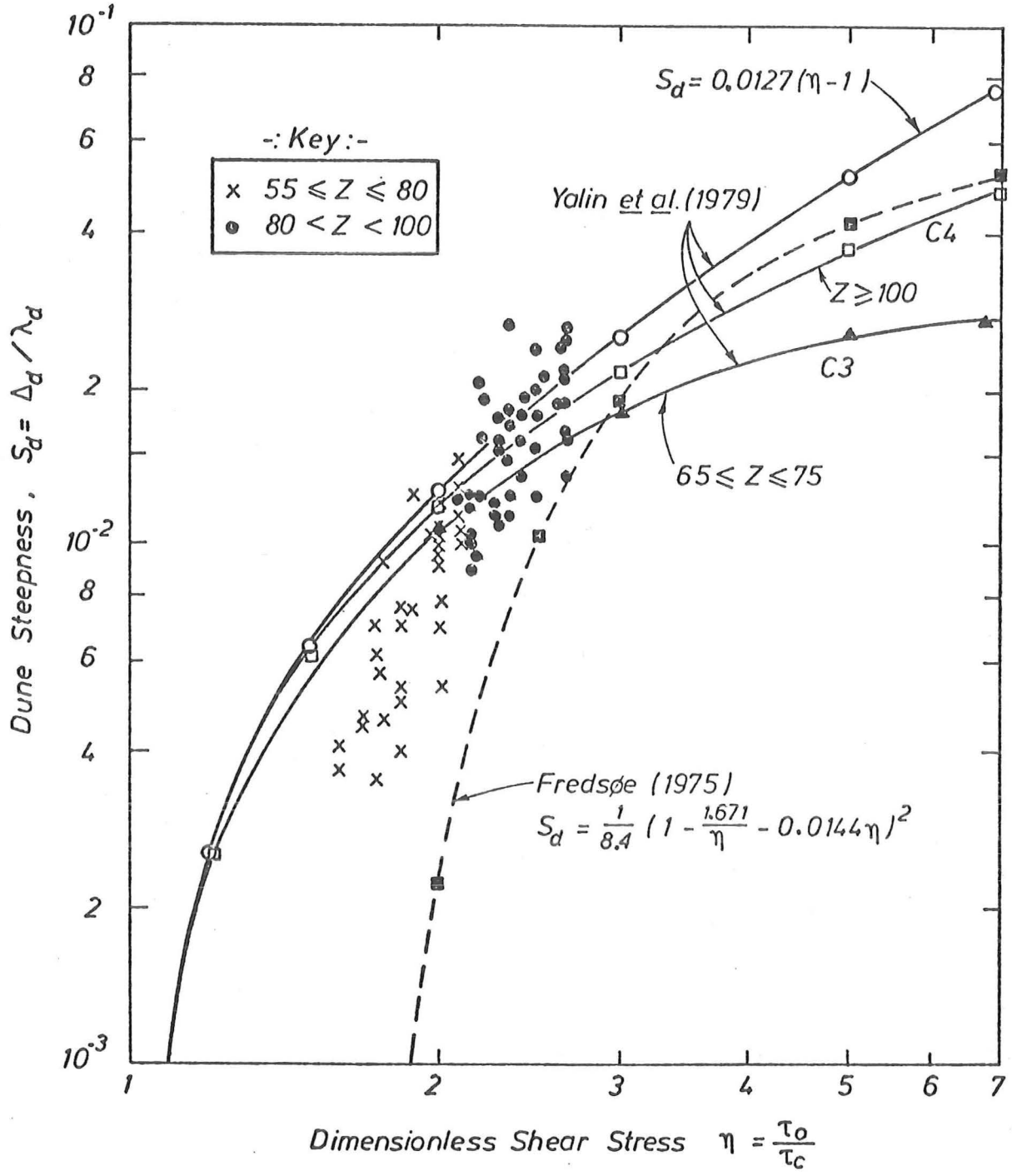

FIGURE 7.15 : Dune steepness versus dimensionless shear stress η

so that the curves obtained by Yalin and Karahan (1979) could be included for comparison. The curve represented by

$$S_d = .0127\ (\eta - 1) \qquad \ldots (7.11)$$

in Figure 7.15, is the limiting dune steepness for all values of Z, proposed by Yalin et al. (1979). An expression derived by Fredsøe (1975)

$$S_d = \frac{1}{8.4}\ \left(1 - \frac{.06}{Y} - 0.4Y\right)^2 \qquad \ldots (7.12)$$

was adapted to include the dimensionless shear stress by introducing the value of $Y_c = 0.036$ derived from the choice of an arbitrary N value in section 6.2.3. This gave

$$S_d = \frac{1}{8.4}\left(1 - \frac{1.671}{\eta} - .0144\eta\right)^2 \qquad \ldots (7.13)$$

and is shown in Figure 7.15. It drops more sharply for lower η values, than the curves of Yalin et al. (1979), because the original expression, 7.12, of Fredsøe (1975) gave a zero value of S_d at $Y = Y_c = 0.0615$.

Because of the influence exerted by the dimensionless depth (Z) effects, the experimental data was split into two groups :

$$55 \leqslant Z \leqslant 80$$

$$80 < Z < 100$$

The data of the latter group spread across and beyond the relevant region between the curves C3 and C4 of Yalin et al. (1979) on Figure 7.15, but the former data group falls below the relevant curve C3. Thus the overall trend of all the data points has a greater slope than these curves, but follows more closely the slope of the curve derived by Fredsøe (1975).

7.5.5 Dune Celerity

A limited data set of dune celerities, C_d, was measured during the ST series when dunes were present on the bed (14 measurements). The data, which is plotted in Figure 8.18, is described deterministically by the equation

$$C_d = 5.9 \times 10^{-3} \bar{u}^{3.1} \quad \text{(m/s)} \qquad \ldots (7.14)$$

This is very similar to the third power correlation, obtained by Guy, Simons and Richardson (1966), between the bedform celerity and the mean flow velocity.

7.5.6 Bedform Data Base

From the variability of the data, describing the geometric properties of bedforms, it is obvious that individual dune forms are the result of random processes, nevertheless mean properties can be related deterministically to the flow conditions. These mean steady flow geometric properties can be used as a reasonable basis of comparison for non-steady flows, under similar non-equilibrium conditions, provided mean geometric properties during the latter experiments are also used. Because the two sets of non-equilibrium experiments, steady and non-steady flow, compare transport rates by equating stage and bed levels, then the effects of a slight decrease in e.g. dune height, as the bed level degrades, will be minimised if the dune properties are likewise compared.

7.6 SUMMARY

The particular non-equilibrium system in which water flows from a fixed rough bed onto an erodible bed, with no sediment input at the upstream end, was investigated. Two types of degradation were observed :

(1) Localised degradation, which was dominated by a vortex roller which formed between the fixed-to-erodible bed boundary and the point of maximum scour depth (or scour pit region). In this region two temporal phases were present:

(a) Initial transition phase which was a relatively short period of rapid scouring

(b) Principal phase where the maximum scour depth was related to the elapsed time by a constant power relation.

(2) General degradation downstream of the local scour hole, where the mean bed level asymptotically approached the original bed level. In this region dune bedforms were the distinguishing feature for all but the lowest flow rates.

At any point, the transport rate decreases with time after the general scour hole reaches the vicinity of that point. Non-equilibrium transport is thus a non-steady process.

At any time, the transport rate varies spatially, increasing rapidly from zero, at the upstream boundary, and through the region of the scour pit, but increasing more slowly as equilibrium transport conditions were approached at the downstream end of the general scour hole.

The non-equilibrium transport rate results have been compared to comparable local equilibrium transport capacity rates in the general scour hole. The differences found between these two transport rates are those between the actual transport rate and the local capacity of the flow (computed in terms of mean flow velocity) for steady flows. The difference or deficit in the transport rates exhibits a spatial variation. It decreases rapidly in the scour pit region from a maximum at $x = 0^{+}$, decreasing more slowly as the end of the local scour hole was approached. Further downstream, in the general scour hole, the differences were insignificant. The spatial variation ex-

ists because the flow requires a finite length of bed to erode sufficient bed material to satisfy the transport capacity of the flow segments, as shown by the conceptual model in Chapter 3.

Although the geometric properties of individual dune bedforms, downstream of the local scour hole, varied considerably (particularly wavelength), mean properties could be related deterministically to the flow properties. The various properties were also compared with formulae proposed by other researchers. The data forms a reasonable base for comparison with similar non-equilibrium situations with non-steady flows, (Chapter 8).

CHAPTER VIII

NON-STEADY FLOW NON-EQUILIBRIUM TRANSPORT

8.1 SYNOPSIS

The response of a coarse alluvial bed is investigated, using the results of experimental measurements, for two different non-steady flow conditions; a step change between two steady flow states (SC series) and a triangular translation wave (NS series). The procedures adopted in carrying out these experiments are detailed in section 5.4. Specific aspects of the bedload and bedform response are discussed in detail while resistance and stage-discharge relationships are dealt with briefly.

Using the comparison procedure (section 3.3), to relate steady and non-steady flow values of bedload transport rates and bedform properties, any differences in magnitude will be in addition to the non-equilibrium magnitude differences shown in the previous chapter. Details of the results are relegated to Appendix F.

8.2 OBSERVATIONS

As sediment was not added to the flow, a local scour hole developed at the upstream end of the movable bed, after $t = 0$ in a similar fashion to that of the steady flow experiments. However the scour hole was of a finite length after the passage of a triangular translation wave as critical base flow conditions were once again present at the end of the wave period. The fluid vortex system and the characteristic grain motion in the local scour pit were similar to that described in section 7.2.

Similarity of the nature of individual particle motions downstream of the scour pit between steady and non-steady flows was also

observed. The introduction of coloured grains at the upstream end of the test reach showed that grain motion varied from short bursts to a series of long steps with short intermediate rest periods. Rolling was also observed as the prevalent type of grain motion.

For the experimental series with step changes, from one steady flow (approximately threshold conditions), to a higher one, where at t = 0 plane bed conditions were present, a transitional growth of bedforms was observed initially. This observation contrasted with the situation at t = 0 for the steady flow non-equilibrium experiments, where the bedform configuration was fully developed at t = 0. The initial growth of the dune bedforms during the SC series occurred rapidly, soon after the step change in discharge. Dune heights increased more rapidly than dune lengths. The growth rate slowed considerably as the dune configuration presumably approached equilibrium with the imposed flow. The first noticeable stage in the development of the dunes was the local congregation of groups of particles at various positions along the test reach downstream of the scour pit. These local concentrations of particles appeared to have a positive feedback response, thus promoting the continued growth of the mound of particles. These mounds quickly developed into dunes with a characteristic triangular shape. This is in line with Raudkivi's (1963) and Williams and Kemp's (1971) suggestions for mechanisms of bedform formation. The bedforms were two-dimensional extending across the flume width in the direction tranverse to the flow. A similar development of dunes was observed under a triangular translation wave, but at a slower rate, depending on the wave period and steepness.

8.3 STEP CHANGE IN DISCHARGE (SC SERIES)

8.3.1 Introduction

Nine runs with varying values of Δq, the step change in water

discharge, were completed for two test reach lengths of 9.29 m and 1.74 m. The final discharge for each run, q_o (= q_c + Δq), was kept within experimental error, to the value of the discharge used during each of the corresponding steady flow runs. (q_c is the threshold base flow).

The system parameters monitored at various times during the whole run were; water level, water discharge, bedform dimensions, the mean bed profile including the maximum scour depth and the bedload transport rate. The maximum scour depth versus time relation was essentially the same as for the corresponding steady flow runs, even though the initial conditions, with regard to the water flow and sediment phases, were different.

8.3.2 Bedload Transport Rates

(1) Results

The results of the smoothed bedload transport rate time series, (section 5.6.3), and the comparable steady flow transport rate-time curves (section 3.3.3) are presented in Figures 8.1 and 8.2 for three typical runs, representing the overall range at both reach lengths tested, 9.29 m and 1.74 m respectively.

The different statistical techniques used to obtain the two curves in Figures 8.1 and 8.2 will now be reiterated. The monotonically decreasing curve, representing the comparable steady flow non-equilibrium transport rate, has been obtained at the points marked, from the output of the comparison procedure. The input transport rate data for this comparison procedure was obtained from averaged bedload transport rates (section 5.6.3) of the raw data for the steady flow non-equilibrium experiments. Thus the oscillations due to the bedforms have been damped out, as is usually the case for equilibrium transport experiments.

The other oscillating curve represents the smoothed transport

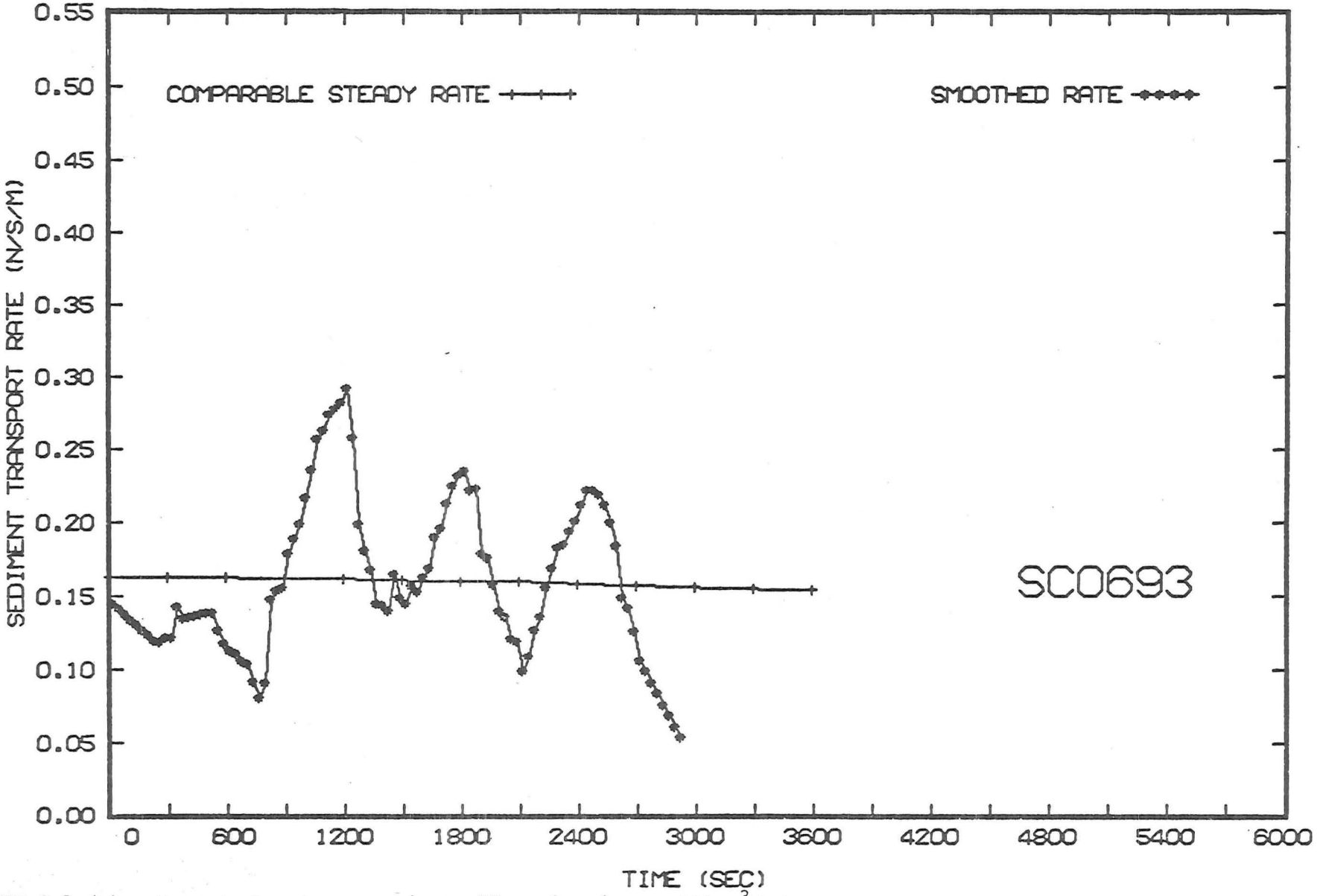

FIGURE 8.1 (a) : Transport rate comparison, SC series (q_o = .111 $m^3/s/m$, x_R = 9.29 m)

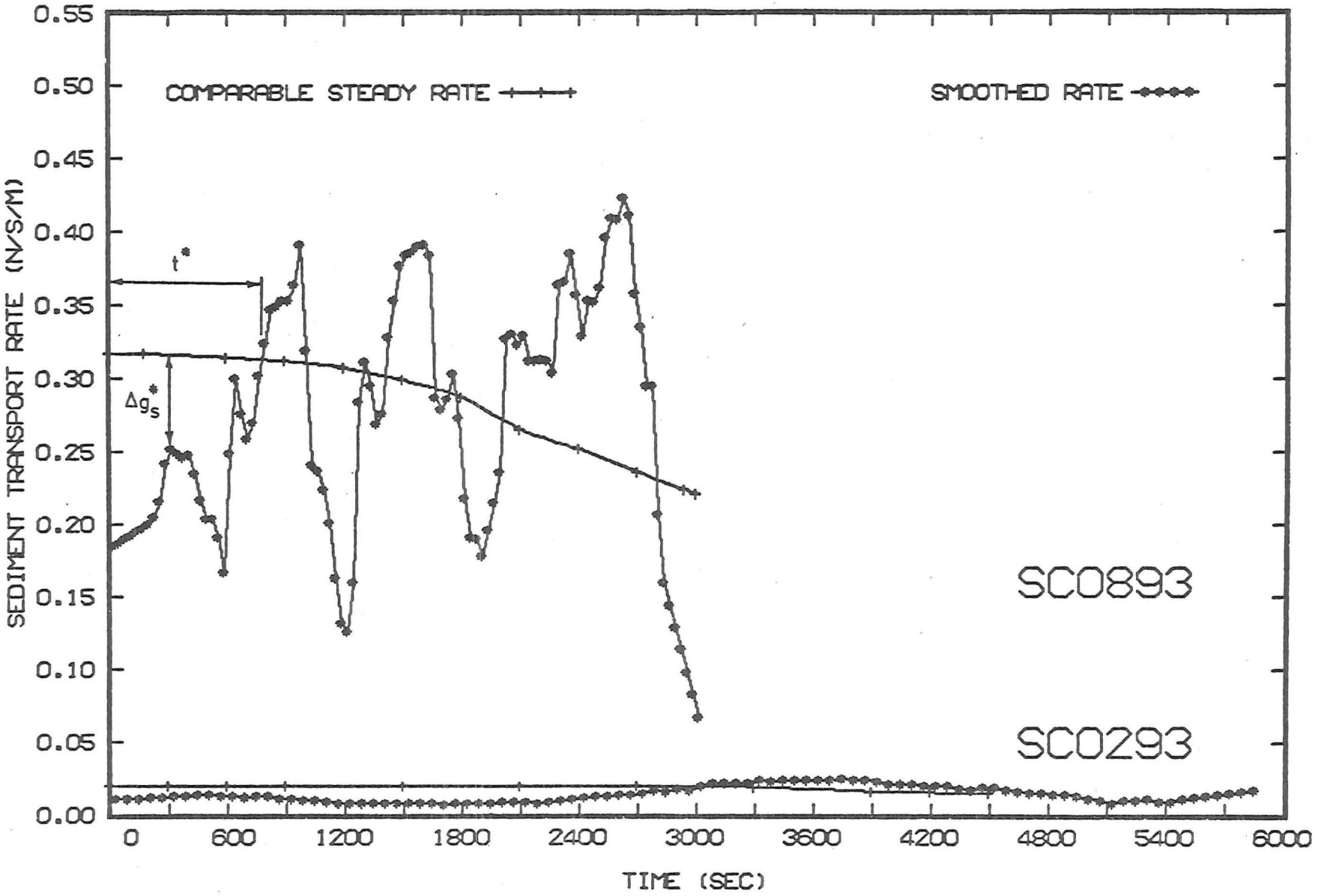

FIGURE 8.1 (b) : Transport rate comparison, SC series (q_o = .140, .056 $m^3/s/m$, x_R = 9.29 m)

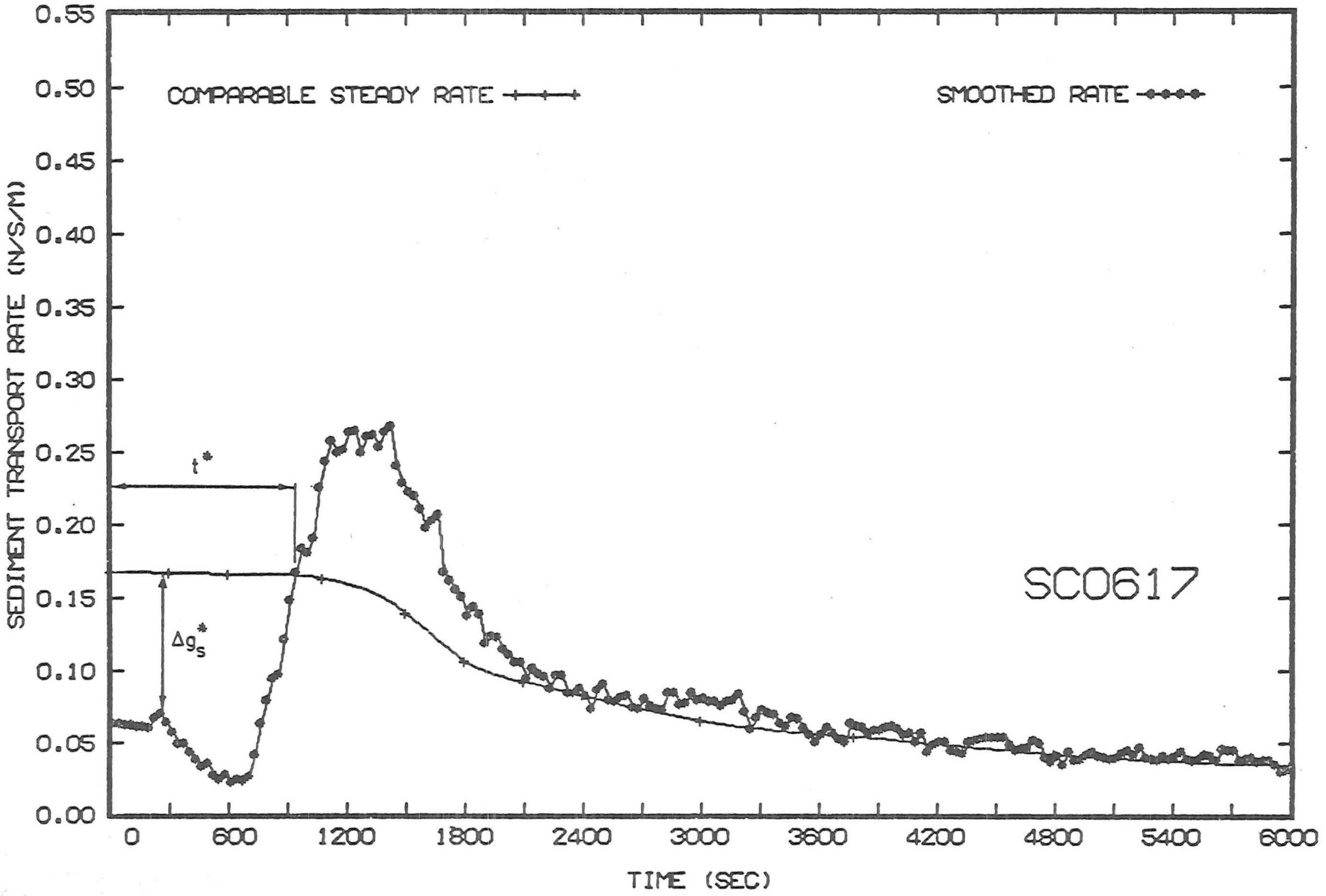

FIGURE 8.2 (a) : Transport rate comparison, SC series (q_o = .111 $m^3/s/m$, x_R = 1.74 m)

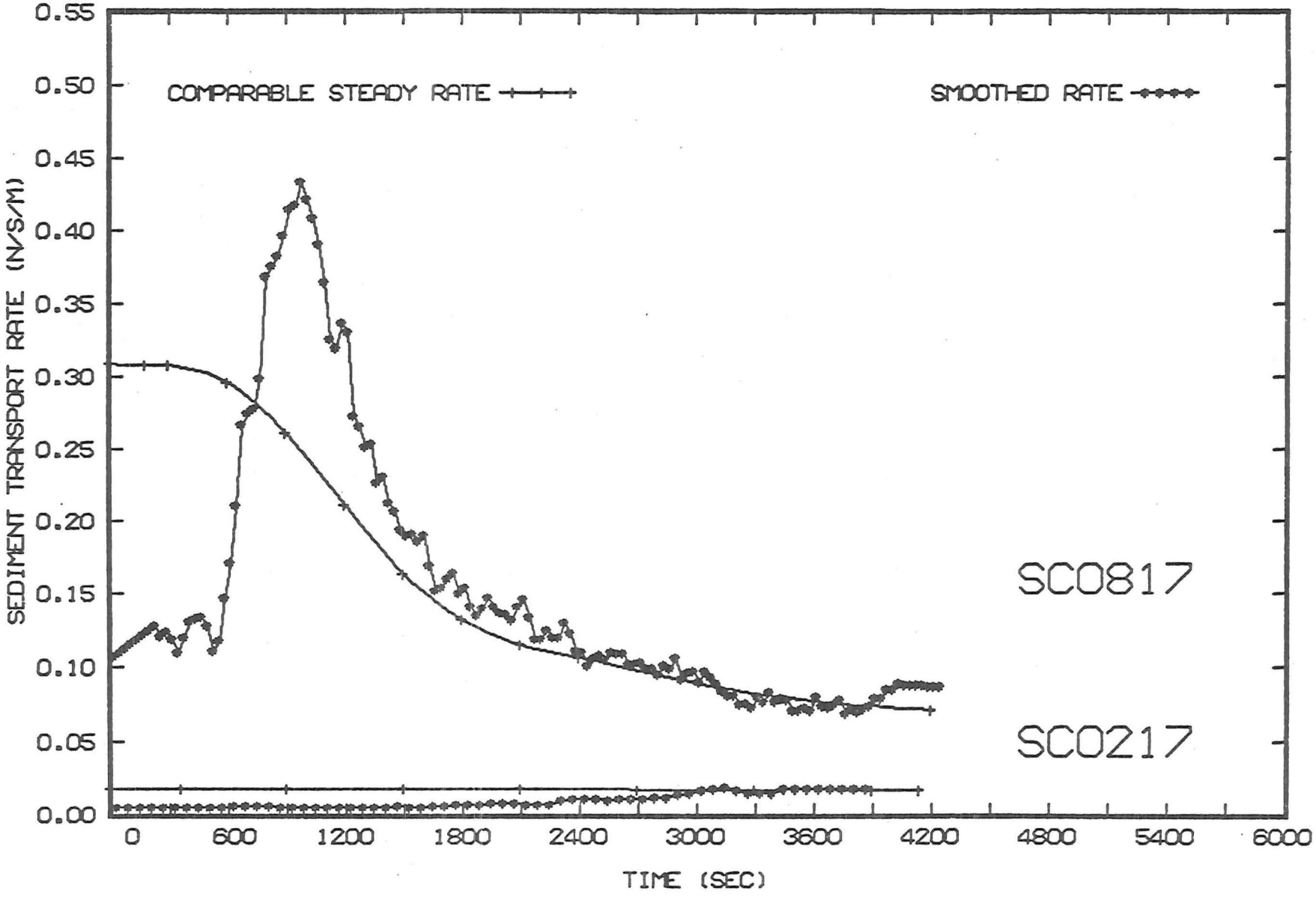

FIGURE 8.2 (b) : Transport rate comparison, SC series (q_o = .140, .055 $m^3/s/m$, x_R = 1.74 m)

rate for the step change in water discharge runs. The smoothed transport rates were the output data from a centred moving average routine or digital filter, (see Appendix B), where the phase length was (2m + 1) raw data points. The value of (2m + 1) was chosen arbitrarily for each run, {Kendall (1973)}, to smooth the minor oscillations sufficiently, but without loss of detail e.g. (2m+1) was usually 11,13 or 15 data points for higher values of Δq and 15,17 or 19 for small values of Δq. The transport rate data was monitored at 30 second intervals during the experiments, therefore the phase length (2m+1) chosen was always less than a dune wavelength. For smoothing the measured data at either end of the record, lines through the initial (m) and final (m) points have been approximated by straight lines, (Appendix B), in Figures 8.1 and 8.2, because strictly, a moving average is not defined in these regions. Therefore the error of fit will be greater than for the central core of the data. The linear approximation is the reason why the smoothed transport rate does not begin at the origin at t = 0, and a further reason why a large phase length was not chosen.

The sudden step change in discharge resulted in a transient in the bedload response, which was defined by a temporal lag, t^*, and a resulting magnitude deficit, Δg_s^* , shown in Figure 8.1(b) and 8.2(a). The temporal lag, t^*, was the time delay between the change in discharge and the time when the actual bedload transport rate attained the comparable steady flow value. The temporal lag is plotted against Δq in Figure 8.3 for all the runs at both test reach lengths.

The magnitude deficit, Δg_s^* , was defined as the difference between the comparable transport rate and the non-steady flow <u>smoothed</u> transport rate at the first local maximum. This corresponded to the first dune bedform to enter the bedload collection zone and was indicative of the response of the bedforms resulting from a step change in discharge. The magnitude deficit for each run is shown in Figure

8.4 for both reach lengths. The trends exhibited by both curves in Figure 8.4 were repeated if the magnitude deficit was replaced by the bedload yield magnitude difference ($G_{ST} - G_{SC}$), over the time interval t^*, where G_{ST} is the steady flow comparable yield and G_{SC} the non-steady flow measured bedload yield. Thus the effect of the smoothing technique on the trend of the Δg_s^* versus Δq curve was small.

The ratio $(G_{ST} - G_{SC})/G_{ST}$ was approximately constant for each of the runs in a series, (constant reach length). The mean value of the ratio was 0.38 for the reach length of 9.29 m and 0.58 for the reach length of 1.74 m.

(2) Discussion of Results

An understanding of the response of the bedload, under the influence of a step change in discharge, is realised by comparing the actual transport rates with comparable steady flow non-equilibrium transport rates. (Figures 8.1 and 8.2.)

(a) Transient Phase ($t \leq t^*$)

The transient phase is characterised by large differences between the actual smoothed transport rate and the average comparable transport rate, with the latter always being larger. Since the matching procedure (section 3.3.3) accounts for non-equilibrium effects, the differences in transport rate during the transient phase must be due to an inertial bed response effect and to changes in the friction slope, S_f, due to the difference between the underdeveloped bedforms and the established bedforms of the ST series.

Generally the temporal lag t^*, (the period of the transient phase), was the elapsed time for two bedforms to reach the bedload collector. The values of t^* plotted against Δq in Figure 8.3, indicate an inverse relationship, whereby the temporal lag decreases as the discharge step increases. For larger values of Δq, the curve may well approach an asymptote at a small finite time value. This suggests that a saturation level could be reached, say five minutes

for the SC series described, where larger values of Δq would result in only minor changes in the temporal lag of the bedload, provided a different bedform regime was not entered, viz. transitional plane bed conditions. The temporal lag increases sharply for small values of Δq, because the change in applied bed shear stress is small, and therefore the pressure to conform to the new flow condition is much less. Moreover, the bedload transport, which is the mechanism by which the bed roughness is changed, is low for conditions just above the threshold level, therefore small perturbations in flow conditions will result in much longer response times.

From the results of a theoretical model for dune modification under weakly periodically varying discharge, Fredsøe(1979), similarly found that the time scale was increased significantly as the shear velocity approached the critical or threshold value.

The magnitude deficit Δg_s^* , increases as Δq increases, see Figure 8.4. Δg_s^* is a measure of the difference between the transport rates shown when the first non-steady flow dune reaches the bedload collector. For all runs, except those with small Δq steps, this occurred approximately 300 seconds after the imposed change in discharge. The dominant factor determining Δg_s^* is thus the mismatch between the zero transport before the change and the transport rate corresponding to the new imposed flow q_o. This mismatch increases much more rapidly than Δq, perhaps as $(\Delta q)^2$, and thus Δg_s^* will increase rapidly with Δq as shown in Figure 8.4.

For small values of Δq, dunes do not form so readily and thus the time at which Δg_s^* occurs is much larger, in the limit, approaching t^*. Under these conditions Δg_s^* is almost independent of Δq. This effect is more noticeable at the reach length of 9.29 m than at 1.74 m. The differences which occur in Δg_s^* between the two reach lengths is further discussed under (c) below.

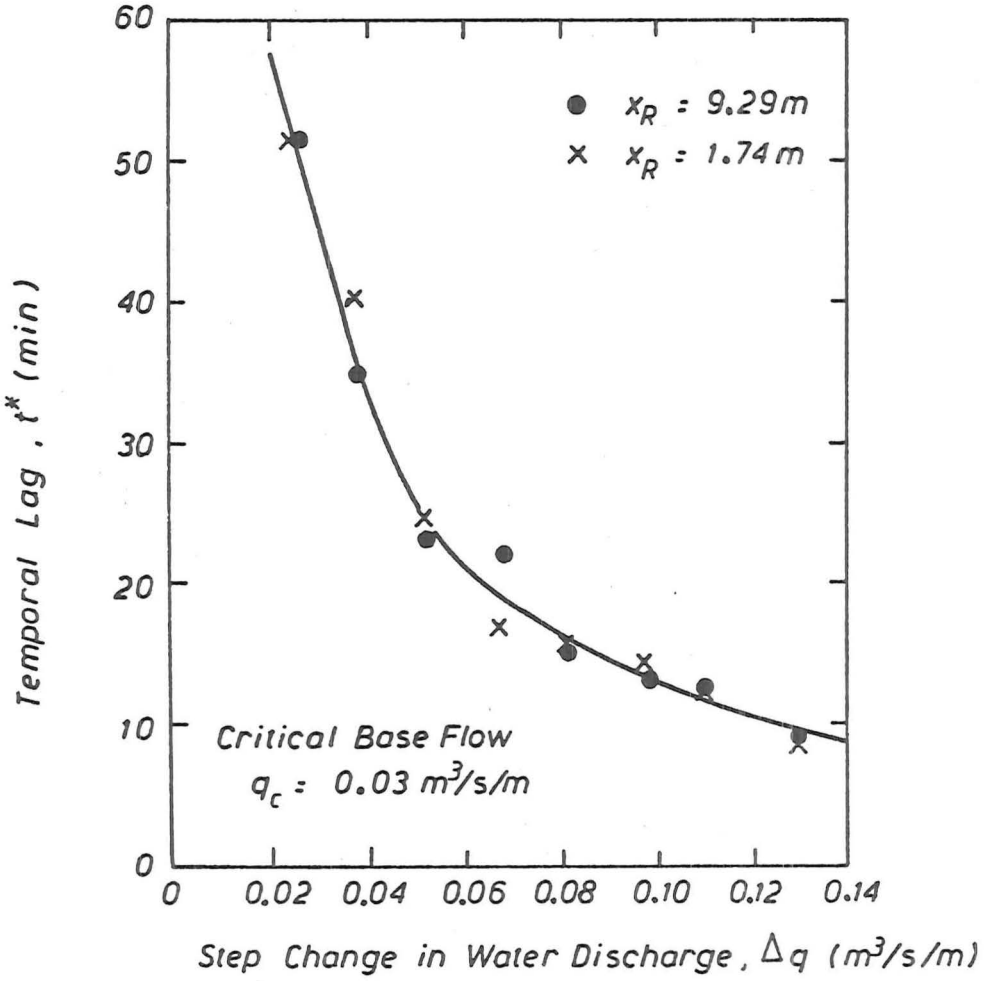

FIGURE 8.3 : Temporal lag of the transient phase versus Δq

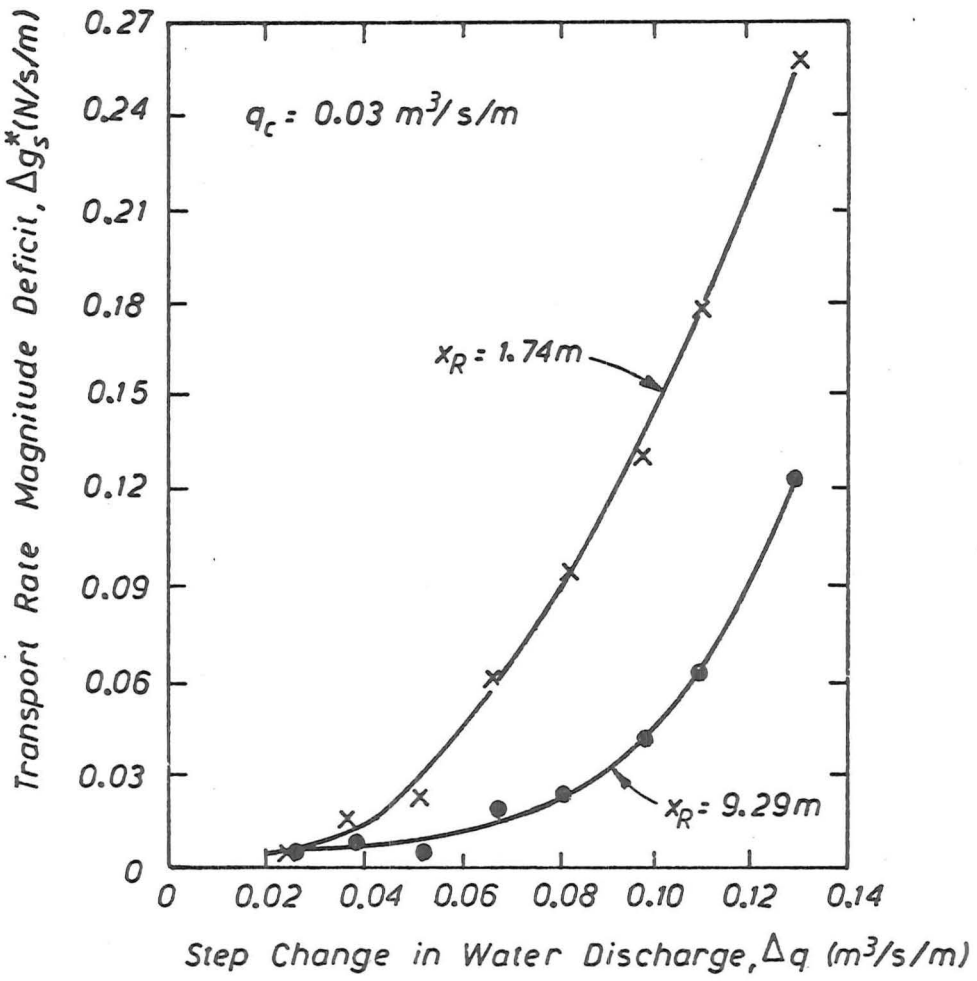

FIGURE 8.4 : Transport rate magnitude deficit versus Δq

(b) Later Phase ($t>t^*$)

Once the bedload transport rate and the bedforms have attained comparable steady flow values (not necessarily at the same time), conditions on the bed will be similar to the steady flow non-equilibrium experiments. This is shown in Figures 8.1(a) and (b), where the actual bedload transport rate oscillates about the average steady flow comparable curve. The oscillations were due to the presence of bedforms, where the local maxima coincided approximately with the arrival of dune crests at the end of the test reach.

The behaviour of the transport rate after the transient phase for the 1.74 m reach length (Figure 8.2) was of a different nature to that of the 9.29 m reach length, because of the effect of the local scour hole. The transport rate at 1.74 m reached a peak value, having previously attained the comparable transport rate. This peak coincided with the last dune to reach the sampling point. No further dunes were generated, as the local scour hole profile dominated the test reach. The transport rate thus decreased until the comparable transport rate was reached, from which time it oscillated weakly about the comparable transport rate curve.

(c) Spatial Variations

In the local scour hole, during the transient phase, for $x < \simeq$ 1m, the maximum scour depth at any time was approximately the same as that recorded during comparable steady flow non-equilibrium experiments (Figure 7.4). Thus a bed response effect, due to the non-steady step change in flow, does not appear to be present in the local scour hole, where the non-equilibrium bedload response is dominant.

Allowing for experimental scatter, the temporal lag t^* does not appear (Figure 8.3) to have a spatial variation along the test reach downstream of the local scour hole, $x > \simeq$ 1m . Thus the dev-

elopment time required for the bedload transport to obtain the steady flow comparable rate, for any given step discharge, Δq, is independent of the distance downstream.

The magnitude deficit Δg_s^* however, exhibits a marked spatial variation (Figure 8.4), for the higher values of Δq, for the two test reach lengths which were tested during the SC series. This magnitude deficit, between the comparable steady flow non-equilibrium transport rate and the measured non-equilibrium rate at the first local maximum, is additional to any deficit present due to the steady flow non-equilibrium effect. To gain an appreciation of the existence of Δg_s^*, and possibly of its spatial variation, the conditions on the bed during the initial stages of the steady flow and step change in discharge experiments must be contrasted.

Initially, at $t = 0^-$, for the SC series, critical base flow conditions were present on a plane bed with little or no movement of particles over the entire reach. When the flow rate was quickly changed by Δq to a new value q_o, the flow immediately acquired a much higher transport capacity. Therefore the situation at $t = 0^+$ was one in which the flow segments immediately began to entrain particles from the bed at all points, which were under the higher discharge, to begin to satisfy their transport capacity while further downstream critical conditions were still present. Thus the flow segments during the initial stages of the transient period have a high erosive capacity, because they receive only a small portion of their transport capacity from preceding flow segments. This is in a similar fashion to the conceptual model for the translation wave (section 3.2.4), where changes in entrainment rate occur more slowly than imposed changes in discharge.

This situation, at $t = 0^+$, must be constrasted with the corresponding steady flow non-equilibrium case, where the dune bedforms are fully developed and the mean transport rate is close to the equ-

ilibrium rate, g_{se_o}. The sediment transfer mechanisms are shown in the steady flow non-equilibrium conceptual model in Figure 3.7.

The two contrasting states point to the reason for the existence of a magnitude deficit, Δg_s^*, but the reasons for the spatial variation of this deficit are not clear from the two reach lengths tested. What does emerge is the existence of two distinct regions : the local scour hole which developed immediately downstream of the fixed apron at a rate similar to the steady flow local scour hole; and the reach downstream of the local scour hole where the developing bedforms are expected to play a dominant role in the delayed response of bedload, and possibly the spatial variation of Δg_s^*. The assumed spatial variation of the transport rate, and thus the magnitude deficit, is shown in Figure 8.5 for these two regions for the largest Δq value tested, where Δg_s^* occurred at approximately five minutes. The local scour hole profile ($x \leqslant 1.0m$) was approximately the same for both steady flow and step change in discharge experiments, at that time, therefore the transport rates are assumed to be similar by the sediment continuity equation. Hence the only deficit present is due to non-equilibrium effects Δg_s. Immediately after the local scour hole, the maximum non-steady flow deficit, Δg_s^*, occurs in the vicinity of $x_R = 1.74$ m, which is additional to the small deficit, Δg_s, but is assumed to slowly decrease with distance downstream. It is expected that further downstream, Δg_s^*, will approach a non-zero constant for any given Δq value, because of the mismatch between the zero transport initial condition and the transport capacity associated with q_o. Whether or not this has been achieved at $x_R = 9.29$ m is unknown.

8.3.3 Bedforms

It would appear, from the previous section, that for coarser bed material, viz. gravel, an inertial effect is present on the bed-

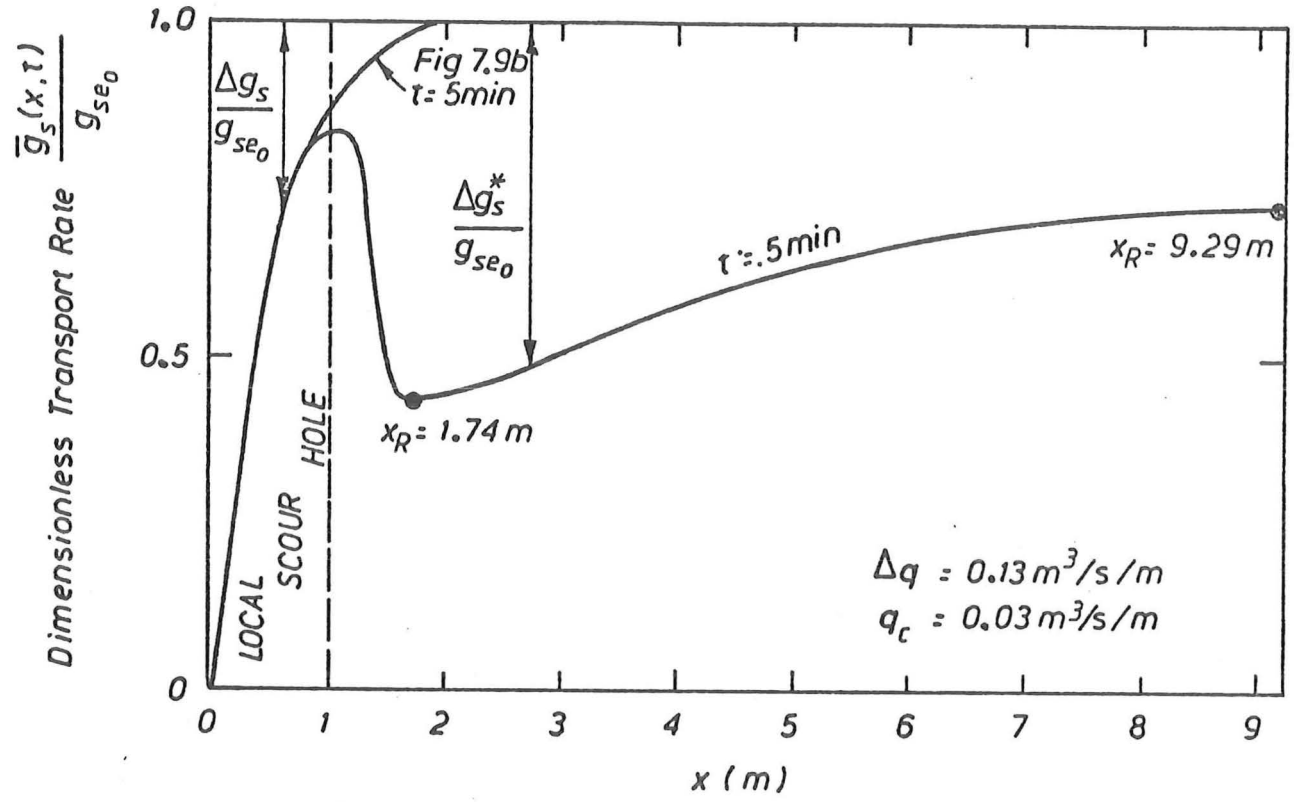

FIGURE 8.5 : Assumed spatial variation of the transport rate deficits due to non-equilibrium and non-steady flow effects

load transport rate. The inertia of the bed-material particles which prevents the bedload reacting instantaneously to the bed shear stress was suggested by Parker (1975) as one of the causes of antidunes. Obviously then, the behaviour of bedforms is intimately connected with the bedload transport (Figure 3.2) and so bedforms will play an important role in the overall response of the bed to non-steady flows.

(1) Results

The mean dune height at the end of the transient phase, was found to be close to the mean height obtained during the steady flow non-equilibrium runs. However, the mean dune wavelength, for each run at $t = t^*$, was consistently below the comparable mean wavelength

in Figure 7.13 e.g. for SC0693, $\bar{\lambda}_d^{SC}(t=t^*)$ = 0.95 m compared with $\bar{\lambda}_d^{ST}$ = 1.23 m.

Knowledge of the geometric properties (Δ_d,λ_d) of dune bedforms before and after the transient phase, made it possible to calculate the minimum change in dune volume following the method of Gee (1975). Consider the idealised triangular representation of a two dimensional dune bed shown in Figure 8.6, which is different from Gee's sinusoidal representation. To transform the plane bed (t=0) into the dune profile at $t = t^*$, the minimum volume of gravel which can have passed through section |2| per unit width in this time must be

$$\int_{x_o}^{x_o + \lambda_d/2} f(x)dx = \tfrac{1}{2}\left(\frac{\Delta_d}{2}\right)\left(\frac{\lambda_d}{2}\right) \qquad \ldots (8.1)$$

The minimum volume per unit width passing section |1| in the same time must be zero. Thus the average bulk volume of gravel passing through any section is ($\Delta_d\lambda_d/16$), which is dependent in reality on the mean size of the dune configuration. As the bedload transport is a necessary condition for the alteration of the bed profile, Gee (1975) related the change in dune volume over a transition, resulting from a step change in discharge, to the actual bulk transport volume (V_s) during the transition. The results for a reach length of 9.29 m are presented in Figure 8.7.

(2) Discussion of Results

The initial rapid growth of dunes from a plane bed profile, following a step change in discharge, has already been mentioned in section 8.2. The results of the measured geometric properties at the end of the bedload transient phase ($t=t^*$) suggest that changes in dune height occur more readily than changes in wavelength when a sediment bed is subjected to a sudden change in flow. This observation has also been noted by Fredsøe (1979) and Allen (1976b). The initial rapid growth in dune height, followed by a period of slower

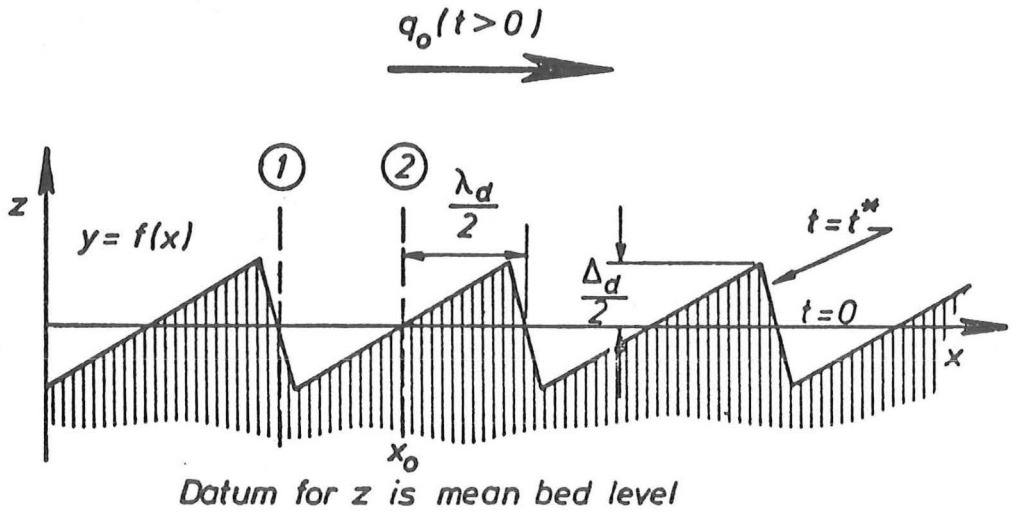

FIGURE 8.6 : Idealised triangular representation of a dune bed configuration

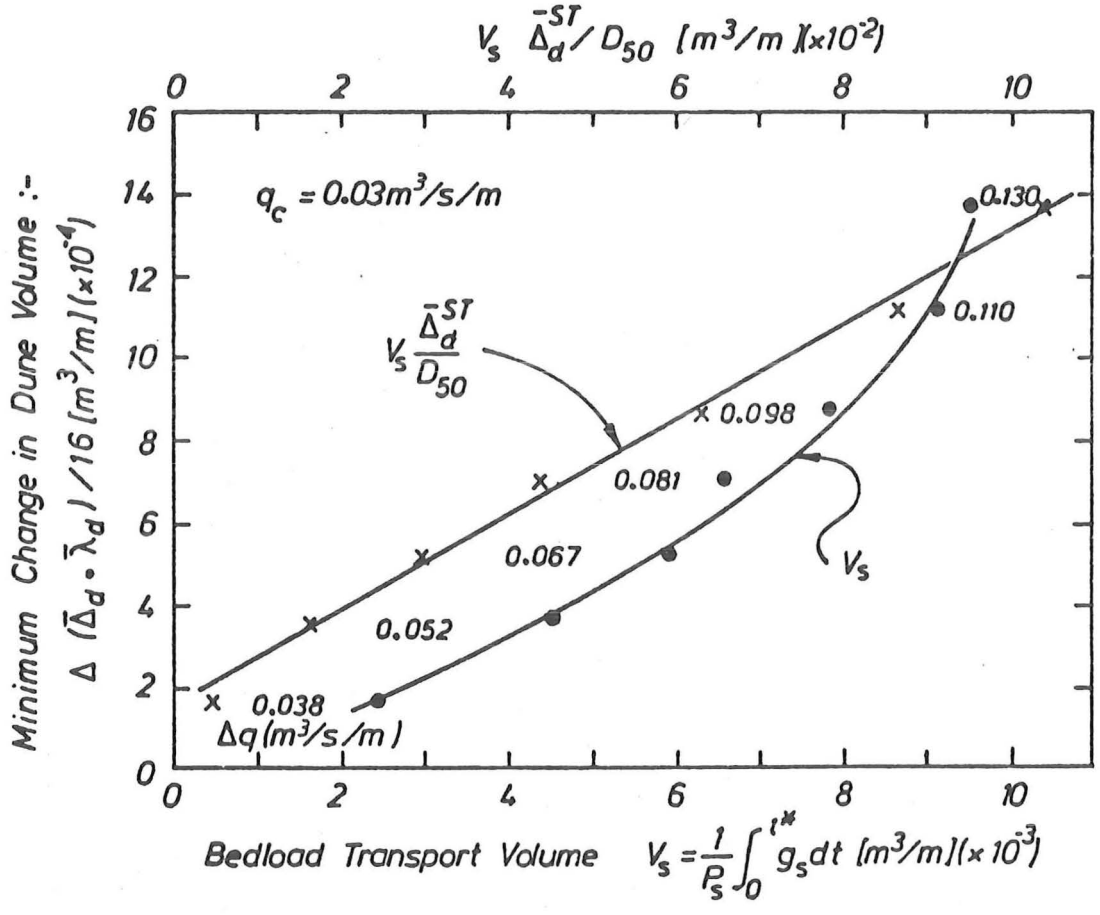

FIGURE 8.7 : Minimum change in dune volume versus bedload yield volume during the transient phase

growth seems to be indicative of an exponential relationship, similar to the erosion of sediment under steady flow non-equilibrium conditions with distance x downstream (section 7.4.3). Thus the relationship is likely to be of the form suggested by Allen (1976b)

$$\frac{d\Delta_d}{dt} \propto \left(\frac{\Delta_d^{ST} - \Delta_d}{\Delta_d}\right) . C_d \qquad \ldots (8.2)$$

where $\Delta_{d_o} \leqslant \Delta_d \leqslant \Delta_d^{ST}$ and Δ_d^{ST} is the steady flow comparable value of dune height, Δ_{d_o} is the initial dune height and Δ_d, C_d the instantaneous dune height and bedform celerity respectively.

The plot of the minimum change in dune volume versus bedload transport volume V_s, Figure 8.7, yields a definite relationship between the two quantities. The experimental data plot along a curve, where for larger step changes in discharge, the change in dune volume becomes less dependent on the transport rate. This is evident by the steeper slope of the curve as V_s increases and is contrary to the linear relationship found by Gee (1975) for sand bed materials. Allen (1976b) criticised Gee's correlation between the change in dune volume and the transport volume. Although he agreed with the necessary condition that change is dependent on the presence of sediment transport, Allen suggested that Gee's analysis needed an extra parameter to represent the net tendency for the system to move in a certain direction, similar to the proportionality 8.2. This net tendency towards change in the system can be represented approximately by the ratio of dune heights before and after the transient phase, assuming the wavelength is constant. The modified proportionality given by

$$\frac{1}{16}\Delta(\bar{\Delta}_d \cdot \bar{\lambda}_d) \propto \frac{V_s \Delta_d(t^*)}{D_{50}} \qquad \ldots (8.3)$$

was investigated as shown plotted in Figure 8.7, where D_{50} is representative of the bed profile undulations at t = 0. This relationship

proved to be linear except for small changes in dune volume where the dune height was of the order of 2 D_{50}. This data suggests that the correlation between the two parameters in (8.3) more adequately describes the change in bedform profile in a linear form, than does the correlation of Gee (1975).

The ratio of transported bedload volume V_s to minimum change in dune volume ranges from 6.9 to 14.1 as the step change in discharge decreases. Thus for the largest values of Δq, where the net tendency towards change in dune volume is greatest, a higher proportion of the bedload transport yield is used to increase the storage capacity of the dunes during the period of growth. This is also another reason why the magnitude deficit Δg_s^* (Figure 8.4), at any one point, increases with increasing Δq. The range of the ratio of transported volume to change in dune volume is below the value of 20 obtained by Gee (1975) for his Type 2 transitions (i.e. plane bed to dune bed). However, the bedload transition time for the SC series is shorter than the bedform transition time, with regard to dune wavelength, and would thus effect the comparison of the ratios.

8.3.4 Coloured Grain Experiments

(1) Results

The procedure for these experiments, where a number (140) of fluorescent sediment grains were placed near the upstream end of the erodible reach, was discussed in section 5.4.5. The spatial distribution of coloured grains at the end of some of the reruns of the SC--93 series (reach length 9.29 m) are shown in Figure 8.8.

(2) Discussion of Results

The spatial distribution of fluorescent particles (Figure 8.8) leads to a confirmation in the understanding of the response of individual grains and hence the bedload to sudden changes in discharge.

The results for the smaller step changes in discharge shown,

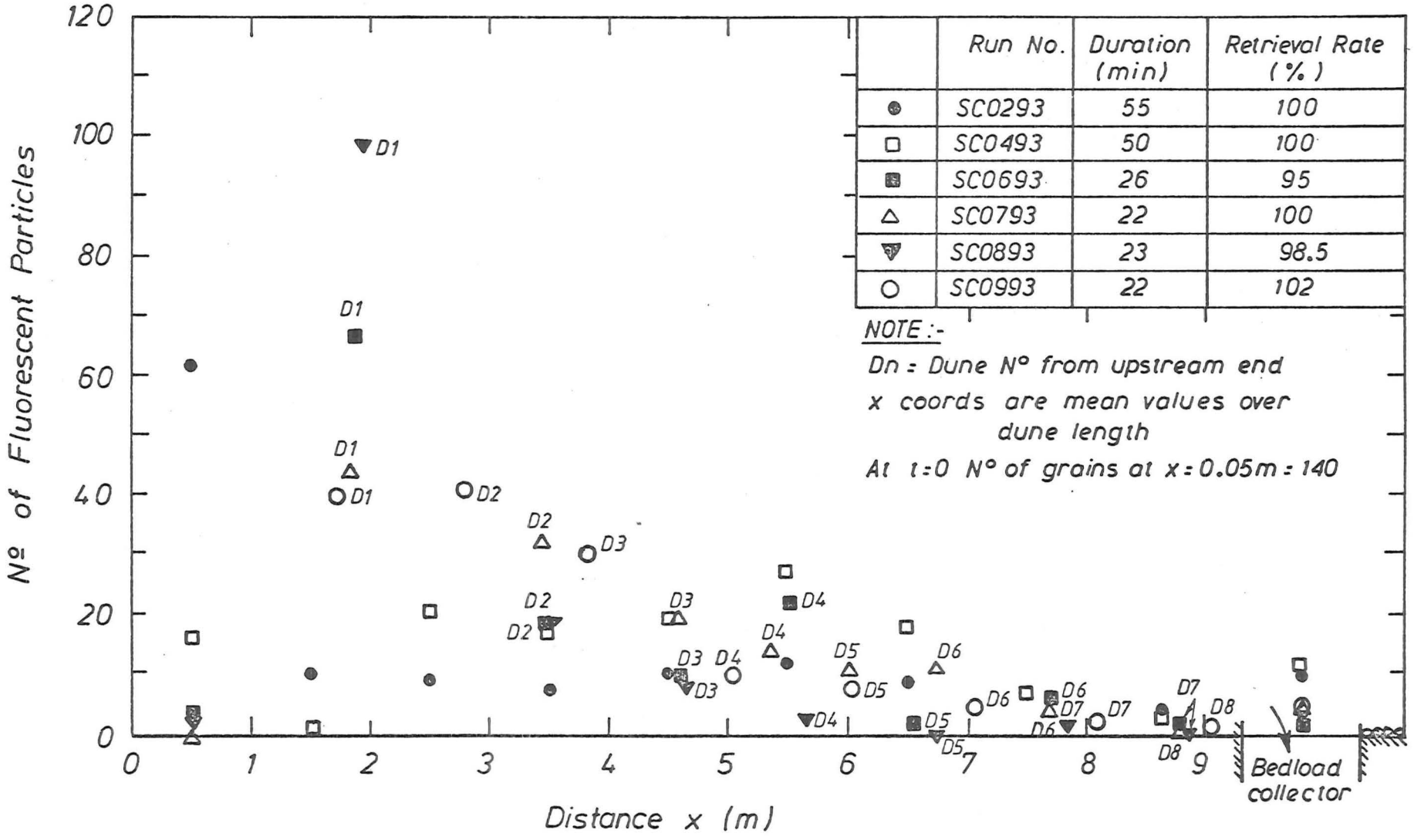

FIGURE 8.8 : Spatial distribution of fluorescent particles for the SC series

SC0293 and SC0493, possess a more uniform spread of gravel particles throughout the test reach than for the runs with higher values of Δq, however, for Run SC0293, 43% of the coloured grains remained at the section where they were placed initially. For these two runs, particularly SC0293, the dunes on the bed were small or non-existent, so essentially plane bed conditions existed. Therefore individual particle movements, which occurred as a series of steps and rest periods, could proceed downstream unhindered by bedforms.

For the higher discharge changes, when dunes became a more dominant feature of the bed profile downstream of the local scour hole, the spatial distribution was weighted towards the upstream end. Few of the coloured particles reached the end of the test reach, usually during the first few minutes, and the remainder were found trapped in the first few dunes after the local scour hole. Thus the bulk of the bedload particles received at the downstream end of the reach must have been entrained from the bed in the vicinity of the downstream end of the test reach, rather than supplied from the upstream local scour hole. This result confirms the importance of the bedform behaviour on the bedload response to non-steady flows, in both the spatial and temporal domains, particularly for the higher values of Δq where the mismatch between threshold conditions and the new transport capacity is greater.

8.4 TRIANGULAR TRANSLATION WAVES (NS SERIES)

8.4.1 Introduction

Symmetrical triangular translation waves were used so as to simplify the interpretation of the non-steady effects. Eight hydrographs, (Figure 5.2), were routed through the flume for five different reach lengths. The results of these runs are presented below with the exception of runs NS0753, NS0553 and NS0535, where the accumu-

lated bedload weight-time records were influenced by drift produced by the electronic circuit of the bedload collector. Additional wave forms (Figure 5.3a) and a half wave followed by an extended period of the peak flow rate were also studied (Figure 5.3b).

8.4.2 Maximum Local Scour Depth

(1) Results

A steady water discharge q_d^S which produces the same maximum scour depth in the same time as the wave period can be defined. These values of q_d^S were obtained from a graph of d_{max} versus q_d^S using the data from the ST--53 series (Figure 7.4), with time as the third variable. It is irrelevant as to which ST series is used for the maximum scour depth-time relation, as approximately equal maximum scour depths were obtained for the same flow rate, over each of the reach lengths. The value of the mean wave water discharge $\bar{q}_d^{NS}$ was computed using

$$\bar{q}_d^{NS} = \frac{1}{T}\int_0^T q(t)dt \qquad \ldots (8.4)$$

where q(t) is the relevant hydrograph function and T is the wave period. The results are presented in Table 8.1.

TABLE 8.1 : Steady Discharges Required to Give the Same Maximum Scour Depth

Run No.	T (min)	$d_{max}(T)$ (mm)	$\bar{q}_d^{NS}$ ($m^3/s/m$)	q_d^S ($m^3/s/m$)	$\bar{q}_d^{NS}/q_d^S$
NS2893(skew)	70	30.0	.095	.1045	.91
NS0893	120	36.7	.095	.105	.90
06	80	33.8	.095	.1075	.88
04	40	27.9	.095	.1065	.89
02	20	22.0	.095	.1045	.91
07	120	21.3	.065	.075	.87
05	80	16.1	.065	.070	.93
03	40	12.5	.065	.069	.94
NS0193	20	11.7	.070	.072	.97

The mean value of the discharge ratio ($\bar{q}_d^{NS}/q_d^S$) was 0.91. Although the maximum scour depth for the translation wave was taken at the end of the wave period, scouring of the bed in the scour pit effectively ceased, on average, at t = 0.65T on the falling limb of the symmetrical waves. This was the result of an oversized local scour pit, for the discharges occurring for t greater than .65T, such that conditions below the threshold level existed at the base of the scour hole. However, the ratios of $(\bar{q}_d^{NS}/q_d^S)_t$, where the base time was changed to 0.65T for both water discharges, were found to have the same magnitudes ±.02 as those shown in the final column of Table 8.1.

(2) Discussion of Results

The maximum local scour hole depth is a function of the time history of flow for a translation wave and therefore it cannot be calculated by a steady flow relationship similar to equation 7.1. This is because the constants a',b' of a similar relation for a translation wave would be functions of the wave parameters. However, the maximum scour depth obtained at the end of the wave period could be related to a steady flow discharge q_d^S which produced the same scour depth in the same time as the wave. The results of Table 8.1 show that a trend towards a slightly higher discharge ratio is apparent for the waves with the smaller peak discharge, q_{max}. Despite this, an estimate of the maximum scour depth for each wave could be calculated by virtue of the approximately constant mean value.

$$\frac{\bar{q}_d^{NS}}{q_d^S} = 0.91 \qquad \ldots (8.5)$$

Knowing the wave period, t = T, and $\bar{q}_d^{NS}$, the value of q_d^S is obtained from equation (8.5). Substitution of $q = q_d^S$ and t = T into the relation $d_{max} = fn(q,t)$ shown in Figure 7.4, yields the approximate maximum scour depth for the wave.

The small differences in the discharge ratio (shown in Table 8.1) for different wave steepnesses, given a particular peak discharge, particularly the highest q_{max} value (even numbered waves), suggest that a non-steady flow bed response effect is not significant in the local scour pit region, taken over the total wave period. This result is consistent with the observations noted for the maximum scour depth during the SC series, where the maximum scour depth-time development was approximately the same as for the steady flow non-equilibrium experiments.

8.4.3 Bedload Transport Rates and Yields - Temporal Variations

(1) Results

The variations in transport rate with time are illustrated in Figure 8.9, which is a series of plots for each of the eight triangular waves of the control series at a reach length of 9.29 m. Results for other reach lengths are discussed below in 8.4.4. It exhibits the relationship between the measured bedload transport rates smoothed by a centred moving average routine (section 5.6.3) and the comparable steady flow non-equilibrium rates obtained for several points on the wave hydrograph using the comparison procedure, which was developed in section 3.3.4.

Similar plots for the rising limb of NS1093 (T = 4 hours) and the skew-triangular wave NS2893 (T = 70 min.) are shown in Figure 8.10. Figure 8.11 shows the bedload transport results from LC0293 where the change in water discharge, from the base flow, q_c to the peak wave discharge q_{max}, was linear (i.e. same as the rising limb of NS0293), followed by a sustained period at the constant peak discharge.

The actual measured transport rate, before the moving average smoothing technique was applied, was highly oscillatory in nature, particularly for the waves with the maximum peak discharge

(q_{max} = 0.16 $m^3/s/m$). See Figure B.1 in Appendix B. The reason, as cited previously, was due to the presence of bedforms, whose shape and celerity varied considerably with the rise and fall of the flow.

The use of a gravel size bed material, proved to be a slight disadvantage, when the bedload yield under the wave, particularly for the short period waves, consisted of only a few bedforms. This resulted in a greater chance of variability when investigating trends between various translation wave runs. Repeatibility tests for the bedload yield under waves NS0493, NS0693 and NS0893 furnished differences of 6%, 15% and 2% respectively.

If the partial differential equations governing the continuity of water and sediment are normalised with respect to appropriate reference parameters, then the resulting coefficients are dimensionless parameters. The continuity equations are

$$\text{Water phase} \quad \frac{\partial y}{\partial t} + u \frac{\partial y}{\partial x} + y \frac{\partial u}{\partial x} = 0 \qquad \ldots (8.6)$$

$$\text{Sediment phase} \quad \frac{\partial g_s}{\partial x} + P_s \frac{\partial z}{\partial t} = 0 \qquad \ldots (8.7)$$

The variables can be non-dimensionalised in the following manner :

$$u' = \frac{u}{U_o}, \quad t' = \frac{t}{T_o}, \quad y' = \frac{y}{Y_o}, \quad x' = \frac{x}{L_o}, \quad z' = \frac{z}{D_o}, \text{ and}$$

$$g_s' = \frac{g_s}{G_o/T_o}$$ where the subscript ($_o$) represents a constant reference parameter. Substituting these quantities into equations 8.6 and 8.7 yields

$$\frac{\partial y'}{\partial t'} + \left(\frac{U_o T_o}{L_o}\right) u' \frac{\partial u'}{\partial x'} + \left(\frac{U_o T_o}{L_o}\right) y' \frac{\partial u'}{\partial x'} = 0 \qquad \ldots (8.8)$$

$$\frac{\partial z'}{\partial t'} + \left(\frac{P_s D_o L_o}{T_o G_o/T_o}\right) \frac{\partial g_s'}{\partial x'} = 0 \qquad \ldots (8.9)$$

The above equations yield two dimensionless parameters

$$\frac{U_o T_o}{L_o} = \text{Strouhal Number}$$

$$\frac{P_s D_{50} L_o}{G_o} = \text{Bedload Yield Number}$$

Suitable forms of these parameters for the triangular translation waves were chosen as

$$S_t = \frac{u_{*b}(\max).T}{y_{max}} \quad , \quad G_Y = \frac{G_{NS}}{D_{50} y_{max} P_s} \qquad \ldots (8.10)$$

where $u_{*b}(\max)$ and y_{max} are the wave peak values of the bed shear velocity and the water depth respectively and G_{NS} is the total wave bedload yield.

The Strouhal Number is plotted against the bedload yield number in Figure 8.12a for the eight symmetrical waves and the skew triangular wave NS2893. The data of Griffiths (1976), from the bedload yields of six triangular waves routed over a test reach of 8.9 m, are also presented in Figure 8.12a. However the data plotted in Figure 8.12a revealed that a third dimensionless variable, $\left(\frac{q_{max}}{q_c}\right)$ was needed, where q_{max} and q_c are the wave peak and threshold base flows respectively. The threshold base flow rate (q_c) of Griffith's experiments was altered to correspond with the same dimensionless erosion rate, N, (Figure 6.1), as for the present series.

By assuming straight line fits to the data for each $\left(\frac{q_{max}}{q_c}\right)$ value, the following relation results

$$S_t \propto G_Y^b \qquad \ldots (8.11)$$

where b = 0.89. The introduction of the third variable, $\left(\frac{q_{max}}{q_c}\right)$, into equation 8.11 leads to

$$S_t = a.\left(\frac{q_{max}}{q_c}\right)^{b'} G_Y^{0.89} \qquad \ldots (8.12)$$

The values of b' and a were found to be -2.60 and 2.0×10^3 respectively. The relation

$$S_t \left(\frac{q_{max}}{q_c}\right)^{2.60} = 2x10^3 \, G_Y^{0.89} \qquad \ldots (8.13)$$

is plotted in Figure 8.12b.

From the areas under each of the triangular waves in Figure 8.9 and their corresponding comparable steady flow non-equilibrium transport rate curves, a ratio of bedload yields can be determined as

$$\frac{G^*_{ST}}{G_{NS}} = \frac{\int_0^T g_s(\text{comparable steady flow})\, dt}{\int_0^T g_s\,(\text{measured non-steady flow})\, dt} \qquad \ldots (8.14)$$

The parameter G^*_{ST} is a pseudo "bedload yield", which would have been the bedload yield of the translation wave if the bedload could respond perfectly to the changing flow conditions.

The best correlation of the ratio (G^*_{ST}/G_{NS}) with the wave characteristics was obtained using a modified Strouhal Number, $(y_c^2/q_{max}T)$ where y_c is the threshold base flow water depth. The results are presented in Figure 8.13.

(2) Discussion of Results

General observations can be made concerning non-steady flow non-equilibrium transport, for the specific case of a triangular translation wave, by referring to Figures 8.9, 8.10 and 8.11.

(a) The measured bedload transport hydrographs all have the same general shape of an upward curved triangle, similar to the com-

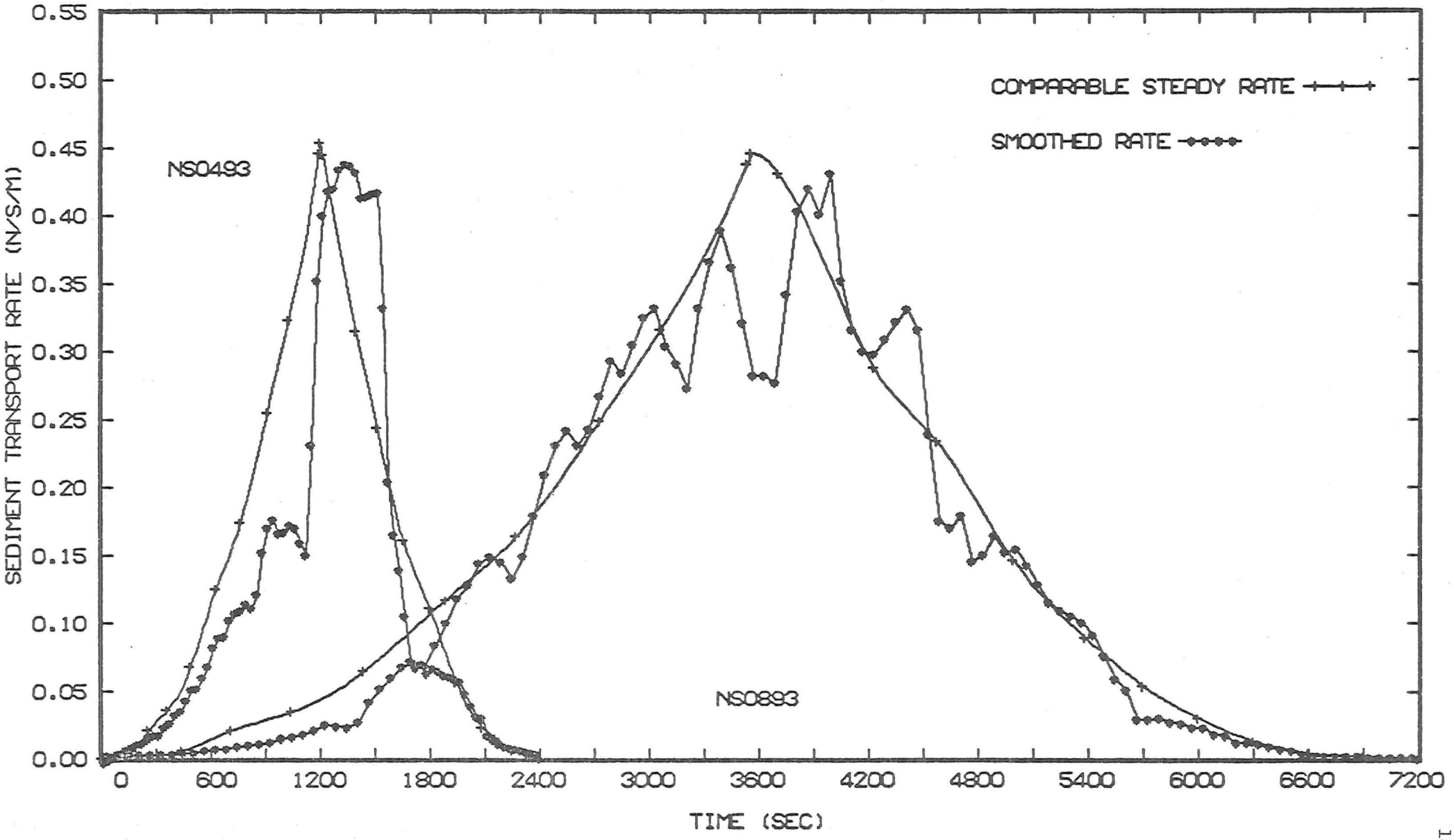

FIGURE 8.9 (a) : Transport rate comparison, NS series (q_{max} = 0.16 $m^3/s/m$, T = 40, 120 min)

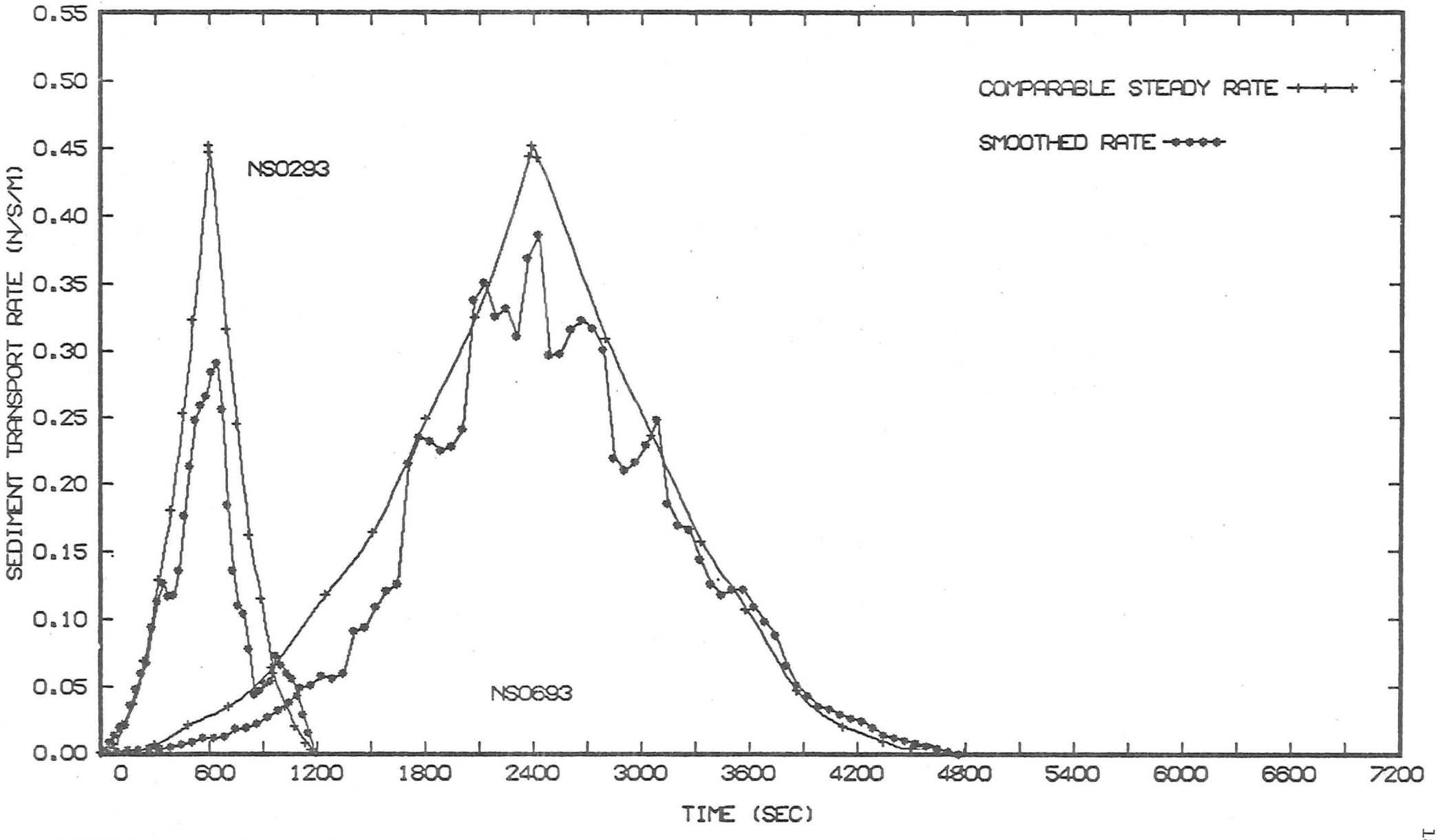

FIGURE 8.9 (b) : Transport rate comparison, NS series (q_{max} = 0.16 $m^3/s/m$, T = 20, 80 min)

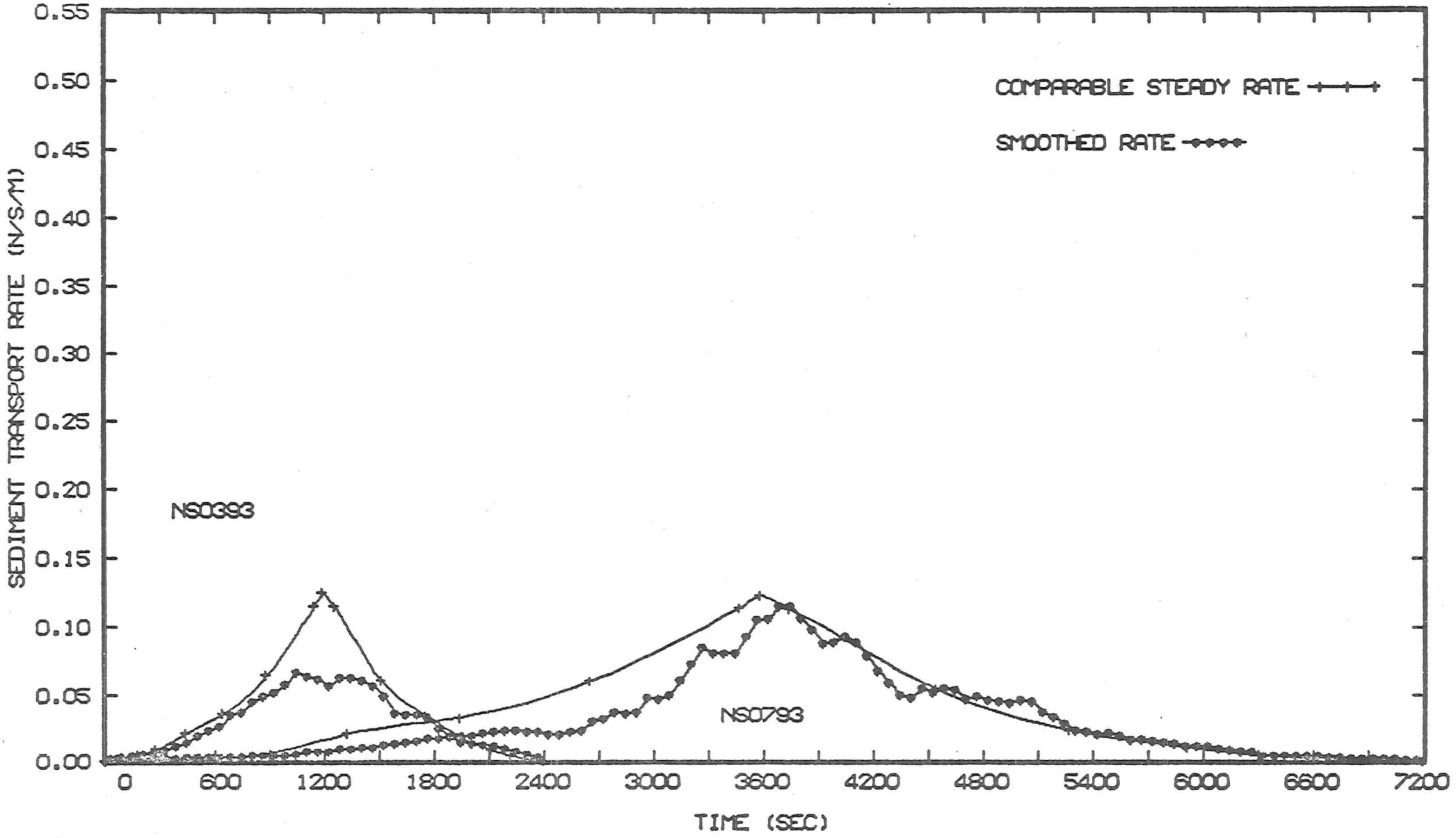

FIGURE 8.9 (c) : Transport rate comparison, NS series (q_{max} = 0.10 $m^3/s/m$, T = 40, 120 min)

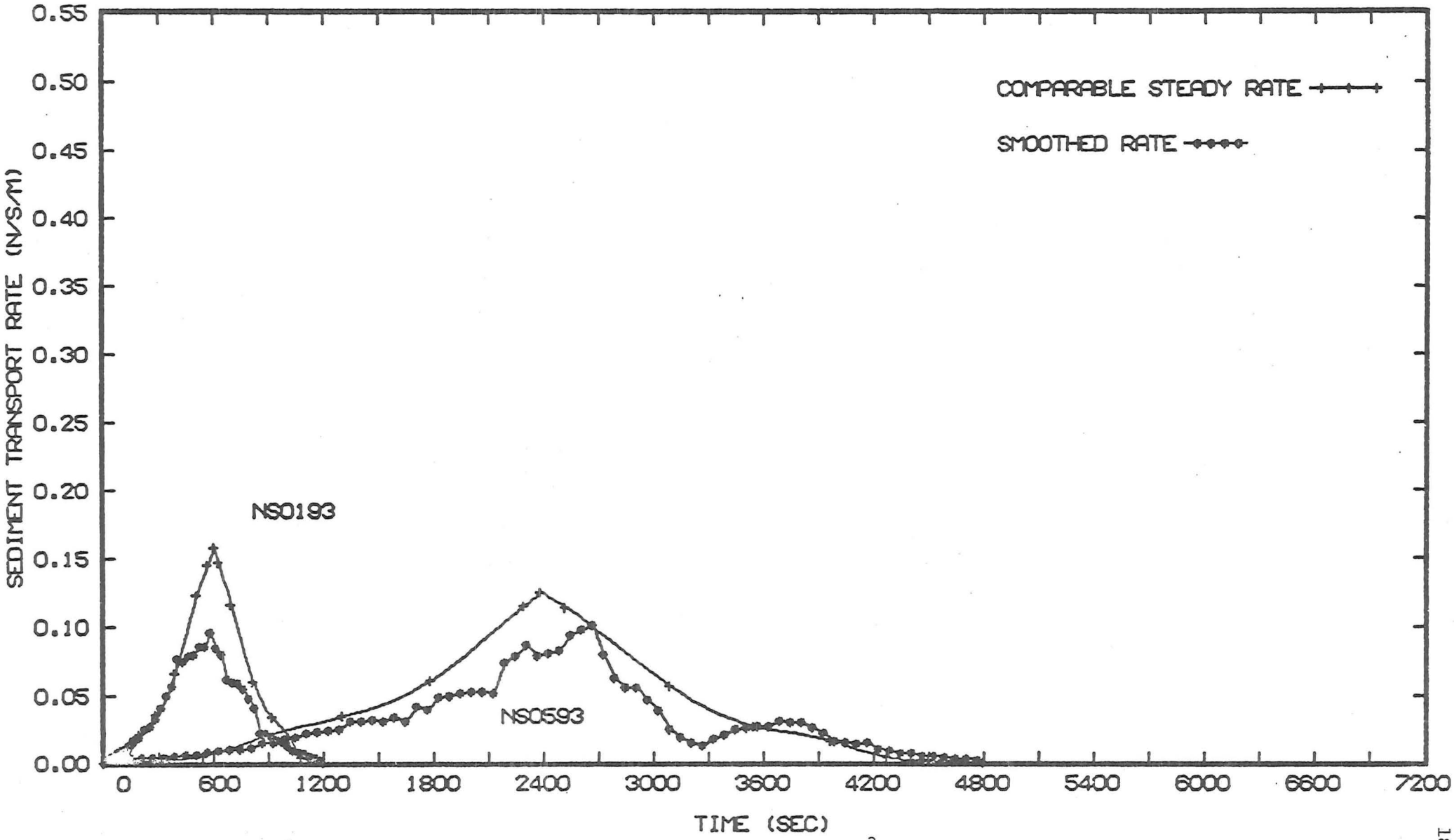

FIGURE 8.9 (d) : Transport rate comparison, NS series (q_{max} = 0.11, 0.10 $m^3/s/m$, T = 20, 80 min)

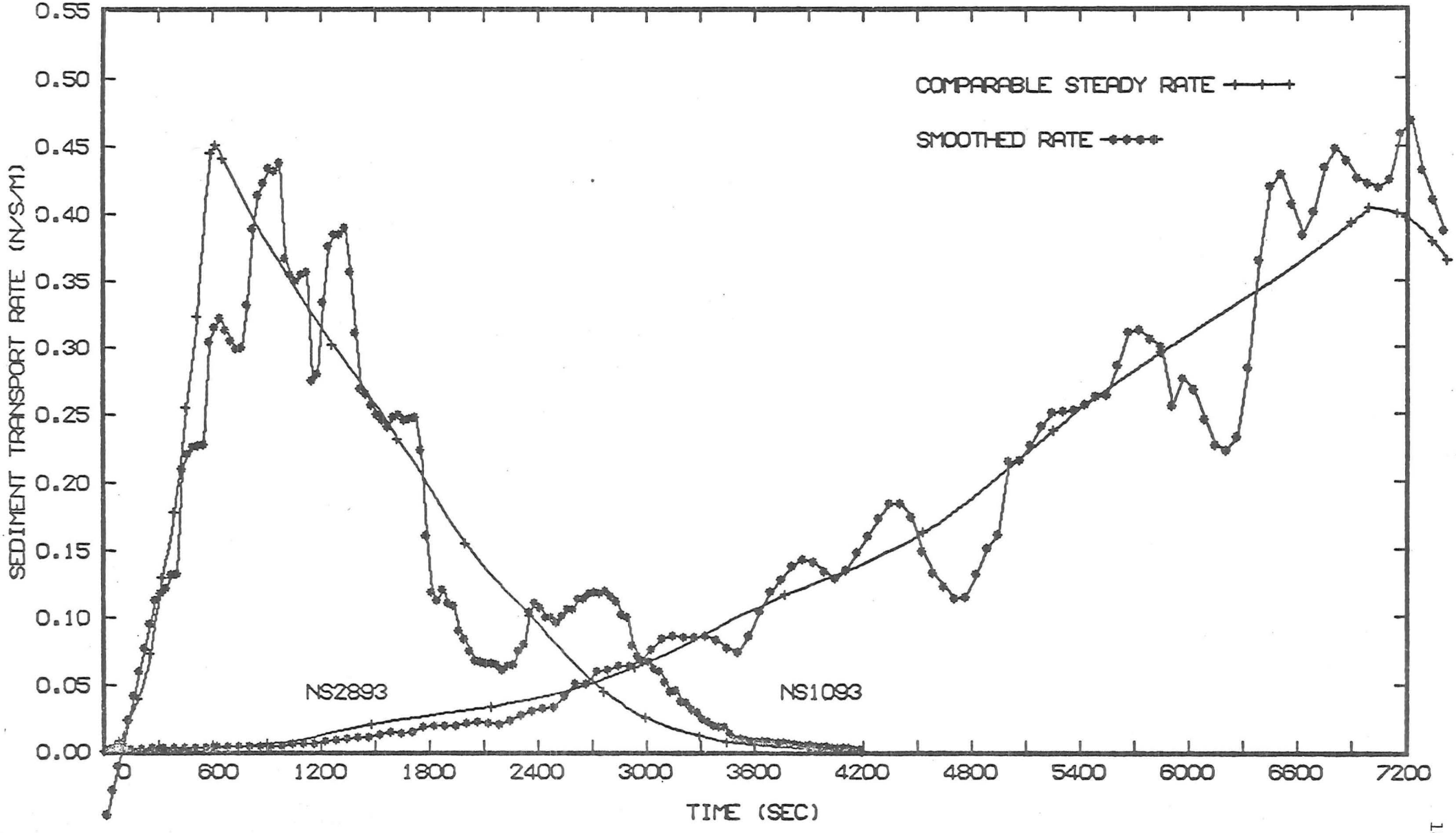

FIGURE 8.10 : Transport rate comparison, NS series, skew triangular wave NS2893 and NS1093.

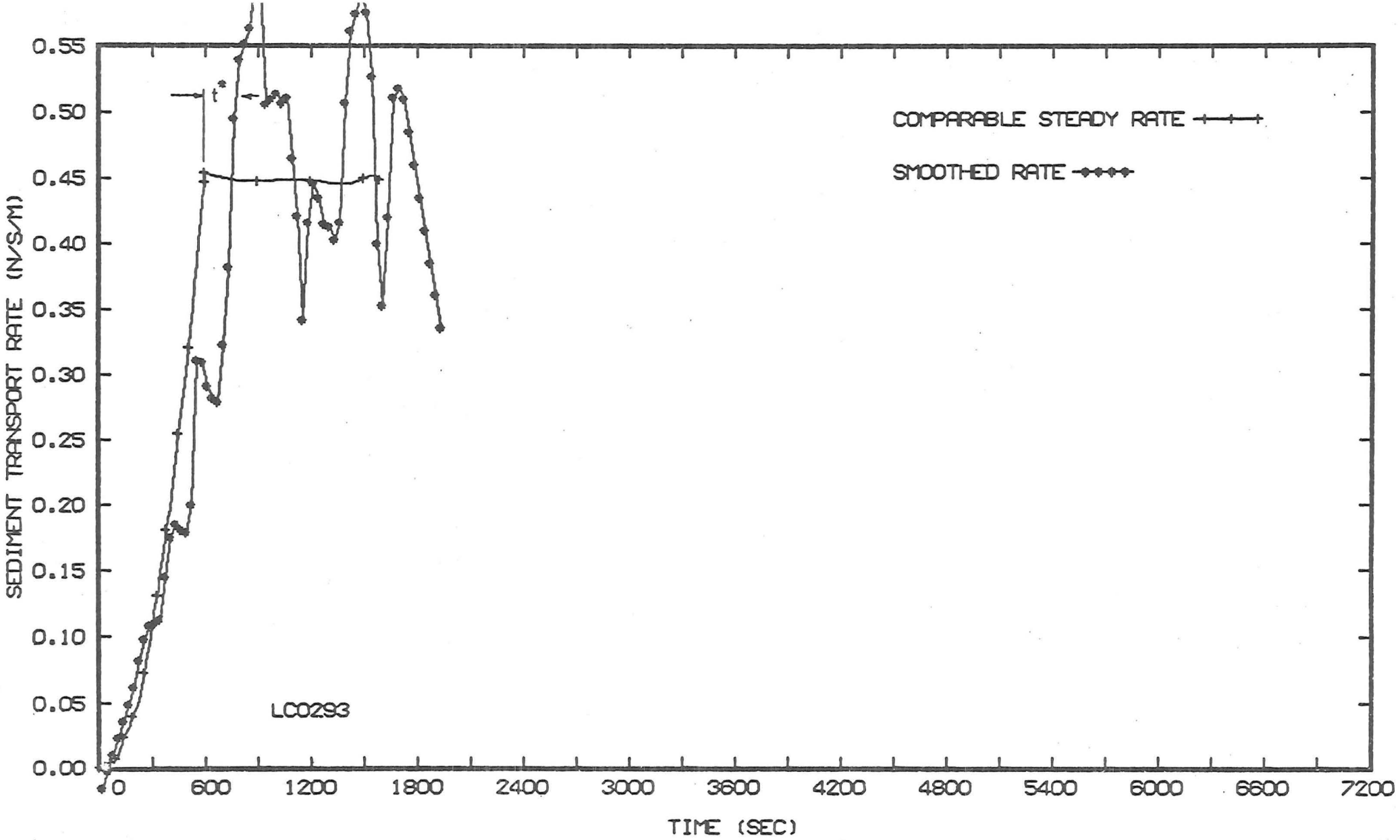

FIGURE 8.11 : Transport rate comparison, linear change in discharge, LC0293

parable transport rate curve. This curved shape is the result of the power correlation between the flow rate, which varied linearly, and the bedload transport rate.

(b) Figure 8.9 reveals that differences occur between the steady flow comparable transport rates and the measured non-steady flow transport rates for the rising limb of each wave. The faster rising waves are associated with greater proportionate differences than the longer period waves for the same peak discharge. This deficit in magnitude is additional to the deficit arising from the non-equilibrium effect. That this must be so is by virtue of the non-equilibrium comparison procedure. Thus a bed response (or inertial) effect* is apparent from the results where the rate of change with time of the water discharge, and hence the transport capacity, exceeds the rate at which the bedload can respond. The response effect is more severe when the discharge is changing more rapidly, given the same peak discharge. These observations confirm those of Griffiths (1976) and Sutherland and Griffiths (1975) for triangular waves under non-equilibrium conditions where the sediment input to the test reach was zero.

The results for the rising limb of wave NS1093 in Figure 8.10, show that the bed response effect was small for slowly rising waves, (T = 4 hours).

The magnitude difference meant there was necessarily a finite time (or temporal lag) between a change in water discharge (transport capacity) and the attainment of the bedload transport rate appropriate to the new instantaneous discharge at a particular location. The cumulative effect of this temporal lag is shown in Figure 8.11, where the peak discharge was maintained after the rising limb of the wave. The temporal ** lag t^* , for this example was 3 minutes, which

*(includes differences in comparable friction slope values, S_f)

**defined as the elapsed time between the last change in discharge and the attainment of the steady flow comparable transport rate.

is understandably less than the temporal lag associated with a step change in discharge up to the same peak flow rate q_{max}.

(c) The peak value of the measured non-steady flow transport rate occurred in the vicinity of the peak water discharge. The peak transport rates for waves NS0193 and NS0393 preceded the peak wave discharge, for waves NS0293 and NS0693 it coincided and for the remaining waves it occurred after the wave peak. The bedload transport under each wave near the peak discharge was comprised of moving bedforms, which required a finite time to travel a distance equal to their wavelength. Thus, a bedform could conceivably arrive at the bedload collector slightly before or after the wave peak.

However another effect is also discernable, by comparing waves NS0293 (Figure 8.9b), NS2893 (Figure 8.10) and LC0293 (Figure 8.11), which all have the same rising limb steepness and peak discharge, but have differing falling limb characteristics. The peak transport rate values occurred at ½, 6, 4½ minutes after the peak discharge respectively. The shortest elapsed time between the peak discharge and the maximum transport rate occurs for wave NS0293, because the bedforms and thus the bedload transport rate have not had sufficient time to develop fully, during the period in the vicinity of the wave peak, before the imposition of a rapidly falling stage. For the other extreme case, wave LC0293, there is no restraint on the time available for the bedload transport rate to respond fully to the peak flow rate. For wave NS2893 (Figure 8.10), the maximum transport rate occurred after the longest elapsed time, because firstly : a longer period near the peak discharge is available for the transport rate to build up than for wave NS0293, and secondly : the discharge is slowly decreasing on the falling limb as distinct from the constant peak discharge for LC0293. Therefore the transport rate near the wave peak of the skew triangular wave NS2893, is less than that of wave LC0293, because of the decreasing discharge, and thus perturb-

ations on the bed will travel more slowly as evident by the longer elapsed time value.

(d) Wave NS2893 is composed of the rising limb of NS0293 and the falling limb of NS0893. As the local mean transport rate at the wave peak of NS0293 and NS0893 separately is different because of the bed response effect, the principle of superposition will not apply when combining the halves of any two different waves to form a skew triangular wave, provided a bed response effect is present for at least one half. The greatest mismatch, in respect of the principle of superposition, will be wave LC0293 for the waves tested, where a fast rising wave during the first period is followed by a sustained steady flow.

(e) The differences in magnitude between the measured and comparable transport rates for the falling limb are generally less than those obtained for the rising limb of the same wave. This is shown by inference in Table 8.2 by comparing the bedload yields for each half of each of the waves. Larger bedload yields in the latter half imply smaller transport rate differences on the falling limb, the more so, if the area under the comparable transport rate curve is smaller on the falling limb than the rising limb. The slightly asymmetrical shape of the comparable steady flow transport rate curve is due to the reducing effect on the transport rate of the general scour hole, when it occupies the entire test reach.

This comparison between the bedload yields on the rising and falling limbs is however, influenced by the time at which the peak transport rate occurred, whether before or after the wave peak.

Comparing the magnitude deficit between the comparable and non-steady flow transport rates of the various waves, solely on the falling limb (Figure 8.9), once again the differences are generally more severe for the faster falling waves of the same peak discharge.

(f) The total measured bedload yield, G_{NS}, under each trans-

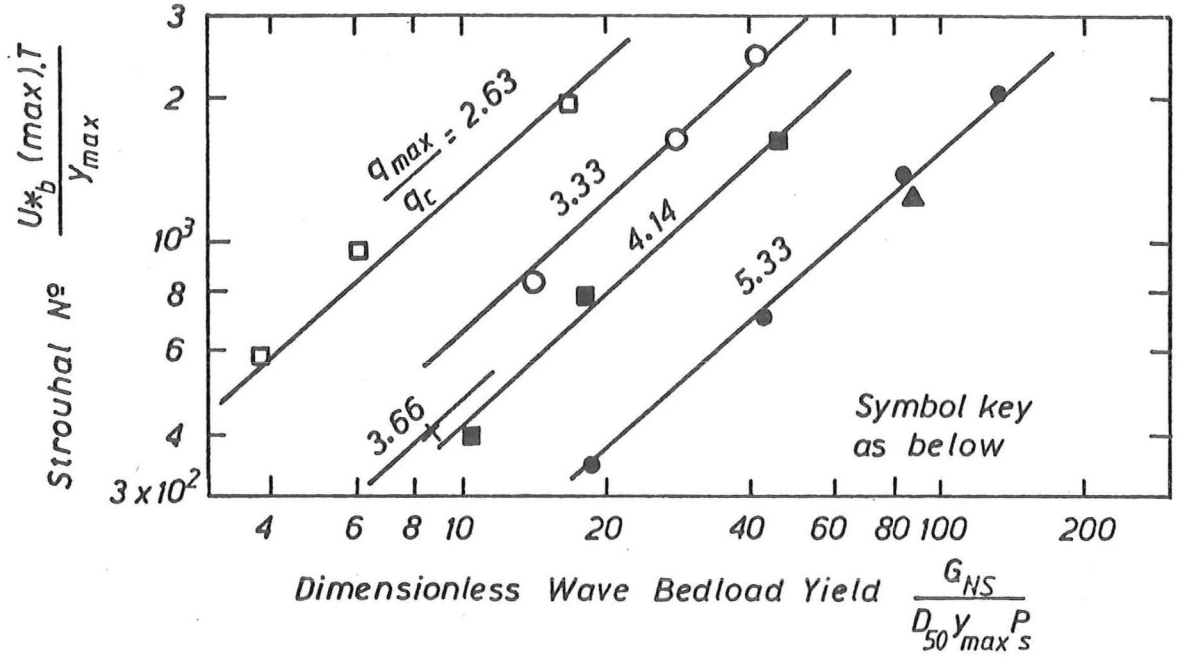

FIGURE 8.12 (a) : Strouhal No. versus dimensionless bedload yield

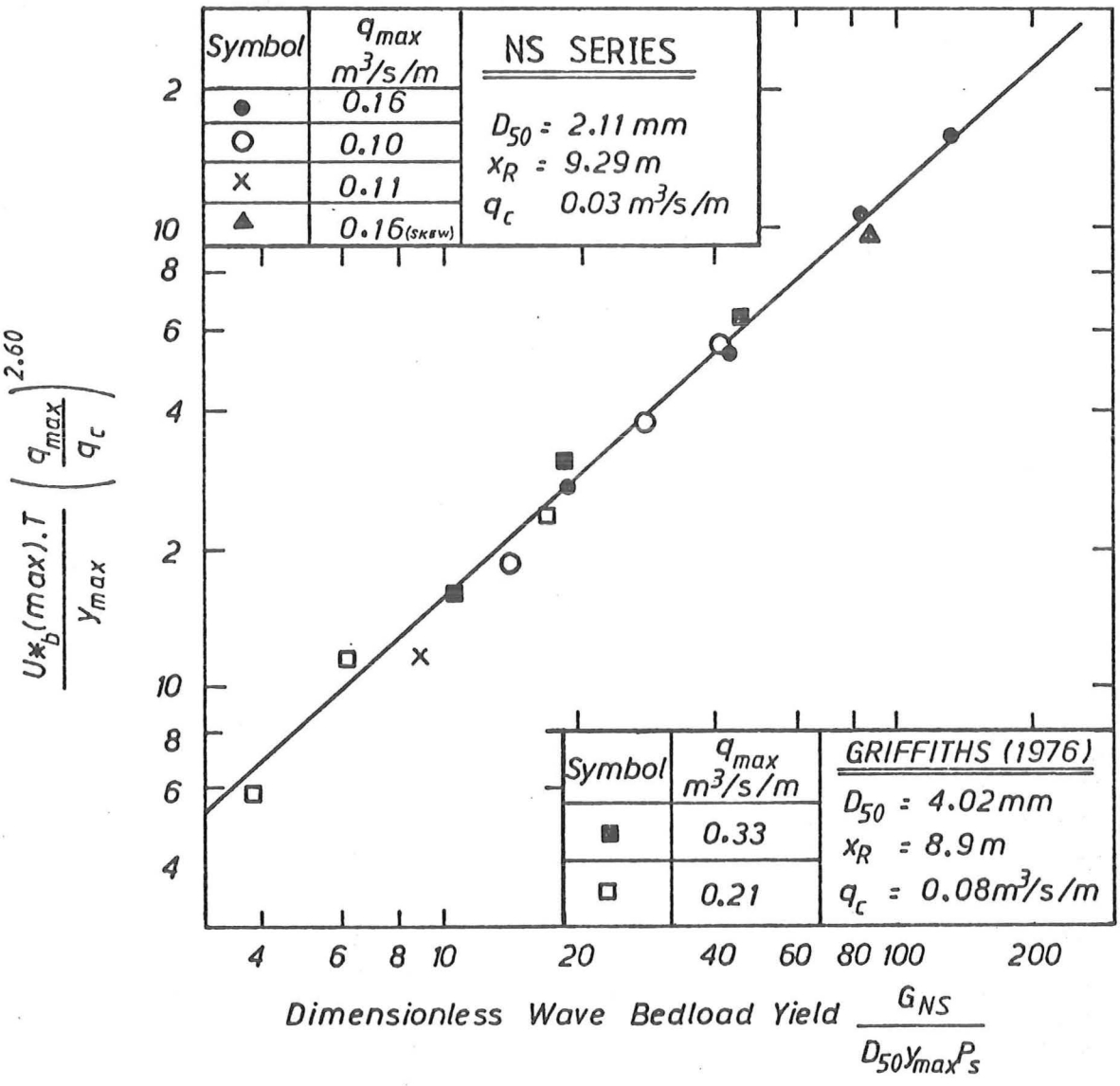

FIGURE 8.12 (b) : Strouhal No. - discharge ratio parameter versus dimensionless bedload yield

TABLE 8.2 : Wave Bedload Yields for the Rising and Falling Limbs

WAVE NO.	$0 \leq t \leq T/2$		$T/2 < t \leq T$	
	G^*_{ST} (N/m)	G_{NS} (N/m)	G^*_{ST} (N/m)	G_{NS} (N/m)
NS0893	520	470	494	474
NS0693	346	266	345	313
NS0493	175	104	174	196
NS0293	88	65	88	61
NS0793	141	87	126	119
NS0593	96	69	94	76
NS0393	50	36	48	44
NS0193	33	27	32	20

lation wave is represented in Figure 8.12b, along with the data of Griffiths (1976). This plot is not intended to represent a sediment yield formula, but to show the difficulties associated with the additional complexity of a non-steady flow, where an additional dimensionless parameter $\left(\frac{q_{max}}{q_c}\right)$ (Figure 8.12a) was needed to define the bedload yield besides the Strouhal Number. Variations about the lines of constant $\left(\frac{q_{max}}{q_c}\right)$ and the single line in Figure 8.12b were influenced mainly by the stochastic nature of the few bedforms which made up the bedload yield.

(g) The ratio of the comparable steady flow and non-steady flow bedload yield, shown in Figure 8.13, was plotted against a form of the Strouhal Number, $y_c^2/q_{max}T$. Various forms of the Strouhal Number were used to find the best fit with the bedload yield ratio. Griffiths (1976) found good agreement with a percentage difference between the measured and comparable yields using the form of Strouhal Number, $y_c/u_{*b}(max)T$. However the results of the NS series revealed a tendency for the waves with the smaller peak discharge (q_{max} = 0.10 $m^3/s/m$) to have greater proportionate differences in bedload yield than the larger waves (q_{max} = 0.16 $m^3/s/m$), given the same Strouhal Number in

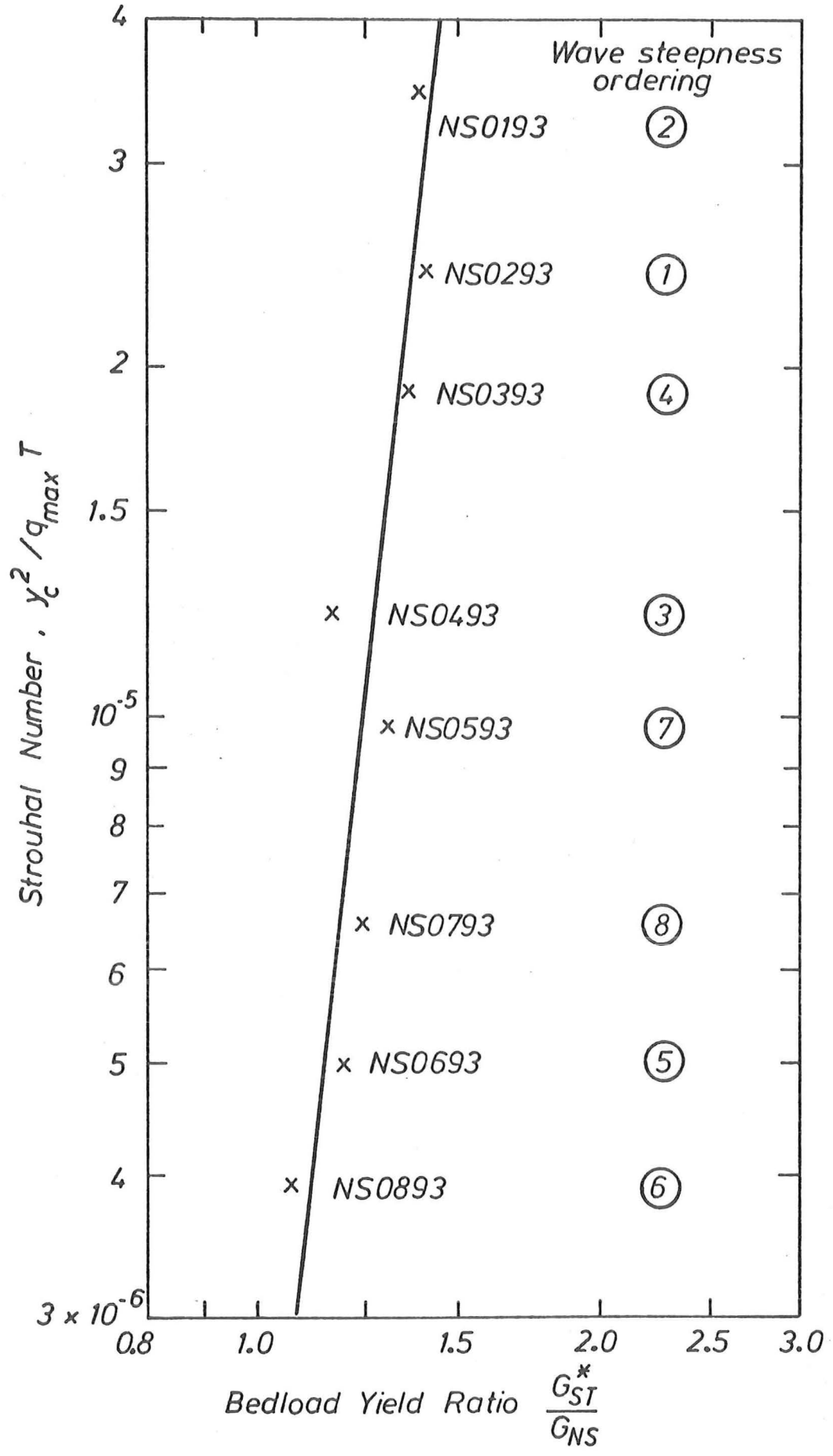

FIGURE 8.13 : Bedload yield ratios between steady comparable and translation wave experiments (x_R = 9.29 m)

the form used by Griffiths. Thus the form used in Figure 8.13 appeared to compensate more for the stronger effect of the wave characteristic $\left(\frac{q_{max}}{q_c}\right)$. The plot shows a reasonable trend through the data, where the faster rising waves, given the same peak discharge, q_{max}, are associated with greater ratios of bedload yield between measured non-steady flow and comparable steady flow conditions.

8.4.4 Bedload Transport Rates and Yields - Spatial Variations

(1) Results

The translation wave series described in the previous section for a test reach length of 9.29 m was repeated for four shorter test reach lengths. Thus the sampling point was effectively moved upstream, further into the scour hole which forms. The results for one of these waves, No. 2, are shown in Figure 8.14 for four different positions within the control test reach.

The bedload yield data could be presented in a similar manner to the results for the maximum scour hole depth at the end of the wave period. For any time $t \leq T$, an equivalent steady flow discharge, q^{ST}, which yielded the same bedload in the same time t as did the wave could be defined. A graph of the actual steady flow bedload yield, G_{ST}, versus q^{ST} with time as the third variable was plotted, for a particular reach length from the results of the steady flow non-equilibrium experiments. Each value of t and thus a non-steady flow bedload yield

$$G_{NS} = \int_{o}^{t} g_s^{NS}(t)dt$$

implied a value of q^{ST} by virtue of the equivalence of G_{NS} and G_{ST}. A ratio was formed between $\bar{q}^{NS}$ and q^{ST} where the former was the mean water discharge of the wave up until time t defined by

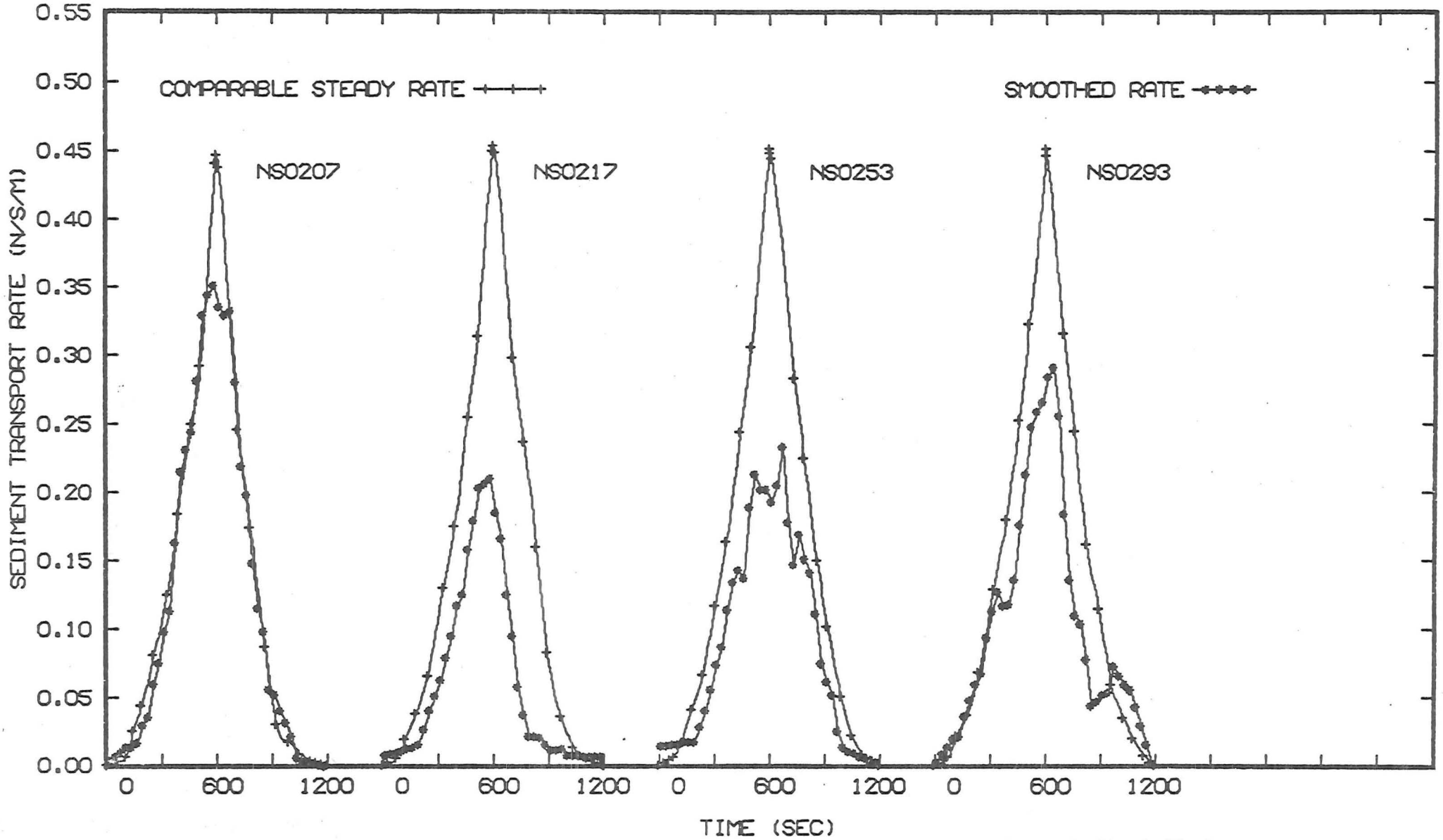

FIGURE 8.14 : Spatial variation of transport rates under wave No.2 (x_R = .74, 1.74, 5.29, 9.29 m)

$$\bar{q}^{NS} = \frac{1}{t}\int_{o}^{t} q(t)dt \ .$$

The results of this analysis are shown in Table 8.3 for two contrasting reach lengths, 9.29 m and 1.74 m.

The relationship between the Strouhal Number $y_c^2/q_{max}T$ and the ratio of the psuedo comparable bedload yield to the measured non-steady flow bedload yield (G^*_{ST}/G_{NS}) was extended from Figure 8.13 to the other four reach lengths in Figure 8.15.

(2) Discussion of Results

(a) Clearly a spatial variation exists (Figure 8.14) for the magnitude differences between comparable steady flow and measured non-steady flow transport rates, given the same wave characteristics. As the bedload sampling point is effectively moved further downstream of the local scour hole, the magnitude differences decrease, being a maximum for the reach lengths shown, at x_R = 1.74 m, which is immediately downstream of the local scour hole. This suggests that the translation wave is continually filling with sediment as it progresses downstream, until it is assumed to reach a stage where the deficit between the comparable steady flow and wave bedload yields is constant, where the bedload response continues to lag changes in discharge. This spatial variation was similarly noted for the series of runs where the system was subject to step changes in discharge (Figures 8.4 and 8.5). It is important to realise that the deficit is not due to non-equilibrium effects but to non-steady flow effects, as the steady flow comparable transport hydrograph, was derived from steady flow non-equilibrium experiments at the same section.

The reasons for the existence of a magnitude deficit, due to the non-steady flow component can be explained in a diagrammatic form by reference to the non-steady flow conceptual model (Figure 3.8). Although the model was limited to understanding the particle motion

on a plane bed, the net effect on the bedload movement over one bedform length will be similar as shown for steady flow equilibrium transport (section 3.2.2). In other words, as the entrainment of sediment particles will fall behind the change in transport capacity for plane bed conditions, so also will the entrainment of particles in a bedform system and therefore the size of the bedform will lag behind correspondingly. From the conceptual model, a flow segment receives fewer particles in transport from the preceding flow segment than it would if the flow was steady. However, the reasons for the spatial variation are not obvious and can only be tentatively proposed.

From the significant transport rate deficit exhibited by Wave NS0217, shown in Figure 8.14, it would appear that downstream of the local scour hole, the entrainment rate of particles by a flow segment starts well behind the steady flow non-equilibrium entrainment rate, for steep waves. With step changes in discharge from threshold conditions (Section 8.3.2), it was the region immediately downstream of the local scour hole from which the flow must re-derive its bedload from the bed. This occurs since the bed material eroded from the initial section of the test reach, travels much slower than the propagation celerity of the flow segment.

With distance downstream, the entrainment rate increases relative to the steady flow non-equilibrium comparable entrainment rate. This can be seen in Table 8.3 by comparing corresponding discharge ratios, $(\bar{q}^{NS}/q^{ST})$ for the reach lengths tabulated. The equivalent steady flow discharge q^{ST}, which yields the same bedload quantity, is generally lower, shown by a higher value of the ratio, at the wave period fractions shown for $x_R = 1.74$ m than for $x_R = 9.29$ m. For $x_R = 9.29$ m, $q^{ST} > \bar{q}^{NS}$ and for $x_R = 1.74$ m, $q^{ST} < \bar{q}^{NS}$. The difference in ratio between the two reach lengths is again more noticeable for the steep translation waves. The mean value of the discharge ratio at $x_R = 9.29$ m for the last three columns in Table 8.3 was 0.96, which

TABLE 8.3 : Ratio of Average Wave Discharge to a Steady Discharge which Produces the same Bedload Yield as the Wave.

RUN NO.	$\bar{q}_{NS}/q_{ST}$			
	0 - .25T	0 - .5T	0 - .75T	0 - 1.0T
		Reach Length = 9.29 m		
NS1093	.98	.85	-	-
NS0893	1.11	.88	.91	.88
NS0693	1.11	.91	.94	.91
NS0493	1.09	1.00	.92	.90
NS0293	.95	.94	.98	.95
NS0793	1.02	1.08	1.02	.99
NS0593	.97	1.03	1.03	.99
NS0393	1.00	1.01	1.02	1.01
NS0193	.96	.95	1.01	.99
		← mean value = 0.96 →		
NS2893 (skew)	-	.90 (t=10min =.14T)	-	.89
		Reach Length = 1.74 m		
NS0817	1.23	.94	.99	.88
NS0617	1.21	.99	1.01	.93
NS0417	1.14	1.13	1.05	.97
NS0217	1.12	1.10	1.22	1.18
NS0717	1.06	1.11	1.03	.99
NS0517	-	1.18	1.09	1.05
NS0317	-	1.13	1.20	1.16
NS0117	-	1.15	1.22	1.19
		← mean value = 1.08 →		
NS2817 (skew)	-	1.09 (t=10 min =.14T)	-	.89

was close to the value of 0.95 obtained by Griffiths and Sutherland (1977) for x_R = 8.9 m. The mean value for x_R = 1.74 m was 1.08. Thus there is clear evidence that a spatial variation of the non-steady flow transport rate deficit does exist, downstream of the local scour hole, for the steep translation waves tested.

As clear water moves from a fixed bed to an alluvial bed, the actual transport rate, at any time during a translation wave, increases from zero with distance downstream, due to the non-equilibrium effect. Further downstream the transport rate will reach a maximum value and then decrease with distance as the leading edge of the wave is approached. Also at any location within the general scour hole, the transport rate will decrease for corresponding points on the rising and falling limb, as the scour hole deepens. Therefore the shapes of the non-steady flow bedload transport rate hydrographs will deviate increasingly from a symmetrical curved triangular shape, as the sampling point is moved upstream towards the local scour pit, and the wave period is increased. (see Appendix F.)

(b) As the bedload sampling point was effectively moved upstream into the local scour pit region, viz. x_R = 0.74 m, the differences in magnitude between comparable and measured transport rates became less than those obtained for the four longer test reaches. In this local scour region, a different flow phenomenon is encountered viz. the fluid vortex system, than that which exists further downstream where the bedforms appear to govern the response of the bedload transport rate. The contrast between the two flow phenomena was also evident in the original bedload transport rate time series before smoothing, where the trace at x_R = 0.74 m possessed much smaller oscillation amplitudes than the traces for the sampling points further downstream, see Appendix B.

(c) The ratio of the psuedo bedload yield under the steady flow comparable curve and the bedload yield under the translation

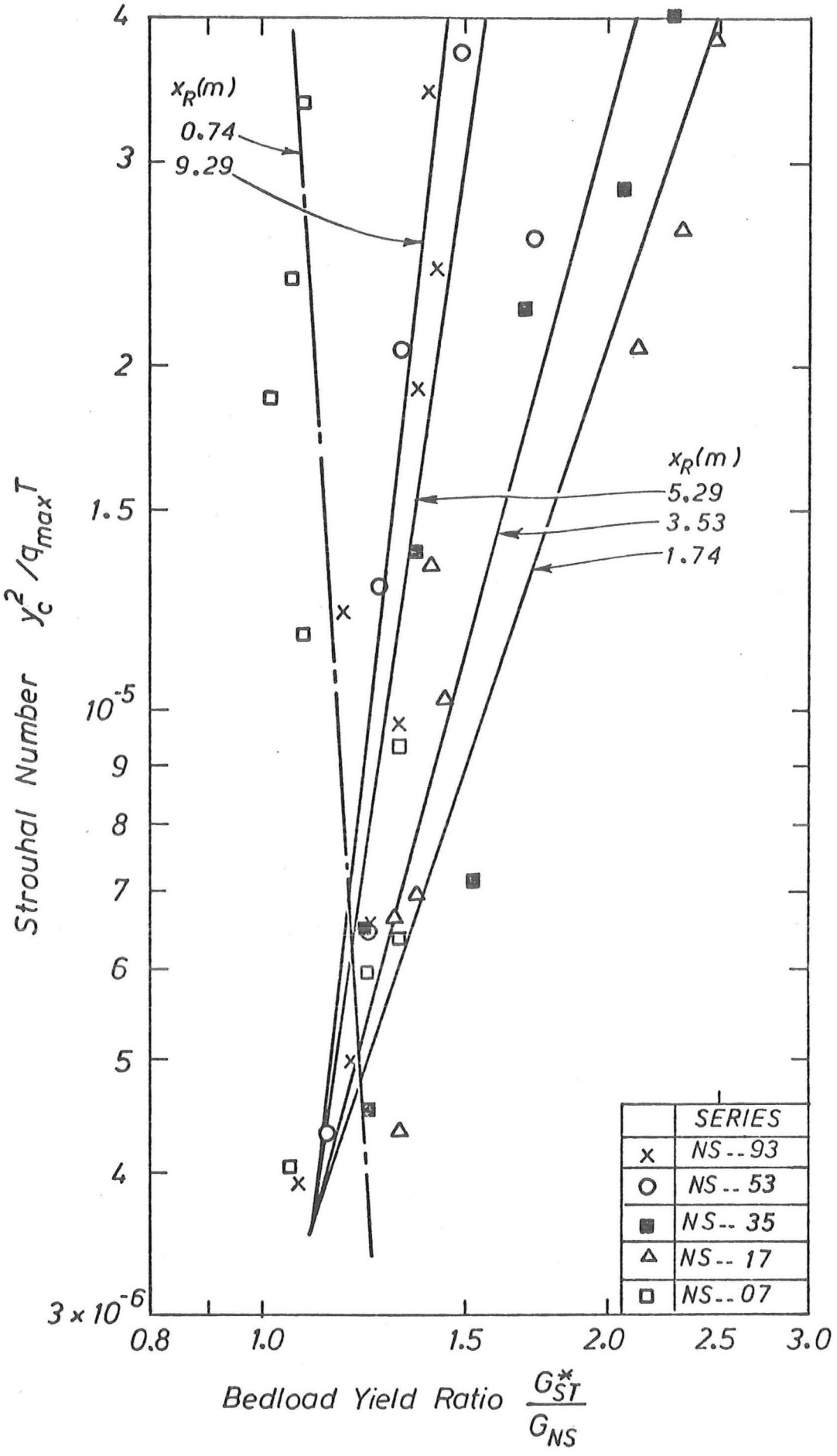

FIGURE 8.15 : Bedload yield ratios between steady comparable and translation wave experiments (all reach lengths)

wave, shown in Figure 8.15, quantifies the spatial variation of the overall deficit in the transport rates between the two flow conditions. The ratio G^*_{ST}/G_{NS} is a function of the Strouhal Number, $(y_c^2/q_{max}T)$, which represents the translation wave characteristics, with the third parameter being the test reach length. Although the data scatter is considerable about the regression* lines shown in Figure 8.15, nevertheless, a trend with the Strouhal Number is evident. For low values of the Strouhal Number, say $(y_c^2/q_{max}T)<10^{-5}$, the spatial variation of the bedload yield ratio is small. As the Strouhal Number increases, the spatial variation of the bedload yield ratio also increases as the regression lines diverge. This trend confirms the result that the spatial variation of the bed response effect becomes more severe for short period, fast rising waves under non-equilibrium conditions, provided the point of interest is located downstream of the local scour hole. This is analogous to the case for step changes in discharge where the spatial variation of the bed response effect is more severe for large values of Δq, when the mismatch between sediment transport and flow conditions was greatest. Similarly, the small spatial variation of the bed response for small values of Δq is analogous to the case for translation waves with small values of the Strouhal Number.

The different characteristic flow phenomenon in the local scour hole is clearly demonstrated in Figure 8.15, by the negative sloping line for $x_R = 0.74$ m.

(d) Downstream of the general scour hole profile, $x_R >> 9.29$ m, the bed is expected to behave in a state of "dynamic" equilibrium during the passage of a translation wave, with respect to conditions before and after the wave. The behaviour of the bed during a wave passage is expect to be a lowering of the mean bed elevation by de-

*the mean correlation coefficient for the four positive sloping regression lines was 0.88

gradation during the rising limb, followed by a return to approximately the initial mean bed elevation by deposition on the falling limb. The term "dynamic" equilibrium does not necessarily imply that the instantaneous transport rate, under a particular point on the wave, is equal to the equilibrium capacity for that flow segment. Indeed, it is expected that for particularly steep waves, there will be a continual temporal lag between changes in flow rate and corresponding changes in bedload transportation. Corroboration for this argument can be gained from the experiments of step changes in discharge for the SC--93 series, where a magnitude deficit in transport rate was evident initially, before the general scour hole had occupied the 9.29 m test reach. This deficit in instantaneous transport rates under a steep wave, if present approximately symmetrically for both rising and falling limbs, will still lead to a net equilibrium condition over the entire period of the wave, such that the bed returns to approximately the same mean bed level, provided the general scour hole has not reached that point.

8.4.5 Bedforms - Temporal Variations

(1) Results

Because the bedload response is intimately connected with the bedforms present on the bed downstream of the local scour hole, the development of the dunes was investigated by repeating runs with the four translation waves where q_{max} = .16 $m^3/s/m$. The bed profile was measured, using the ultrasonic probe, at the dune trough and crest regions, rather than at pre-selected stations as done previously; compare Figure 8.19 with Figure 7.6. The mean dune heights and wavelengths along the test reach* (x_R = 9.29 m) at various stages of the triangular translation waves are shown in Figure 8.16. The non-steady flow mean dune heights are matched with the corresponding steady flow

* the mean was taken over at least 5 bedforms along the test reach

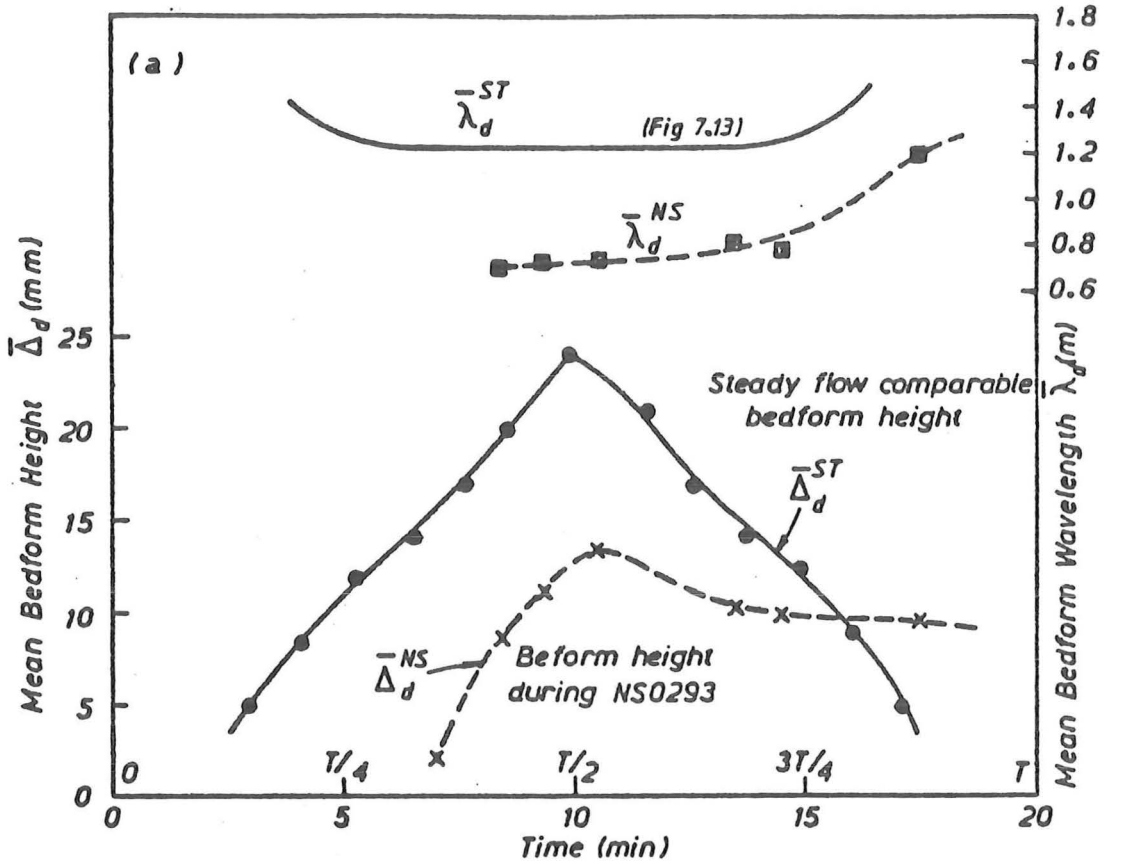

FIGURE 8.16 (a) : Dune bedform properties during wave NS0293

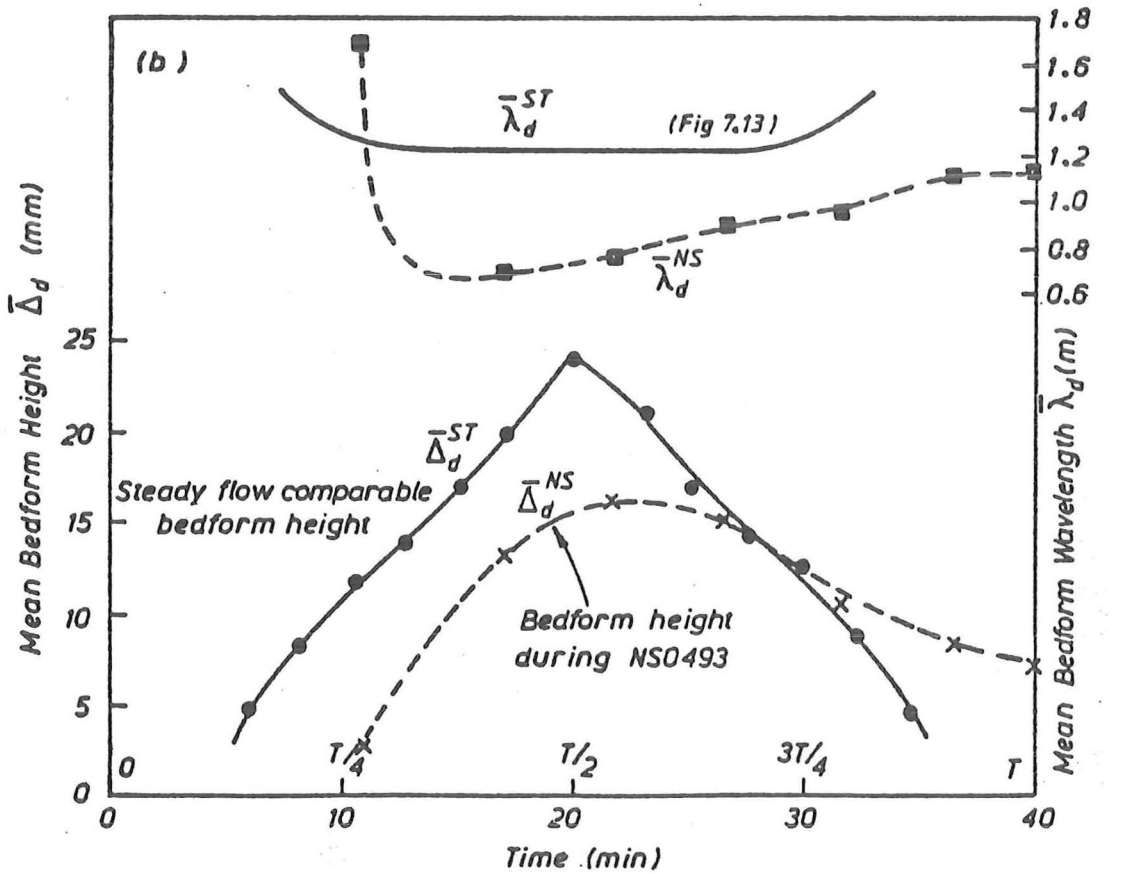

FIGURE 8.16 (b): Dune bedform properties during wave NS0493

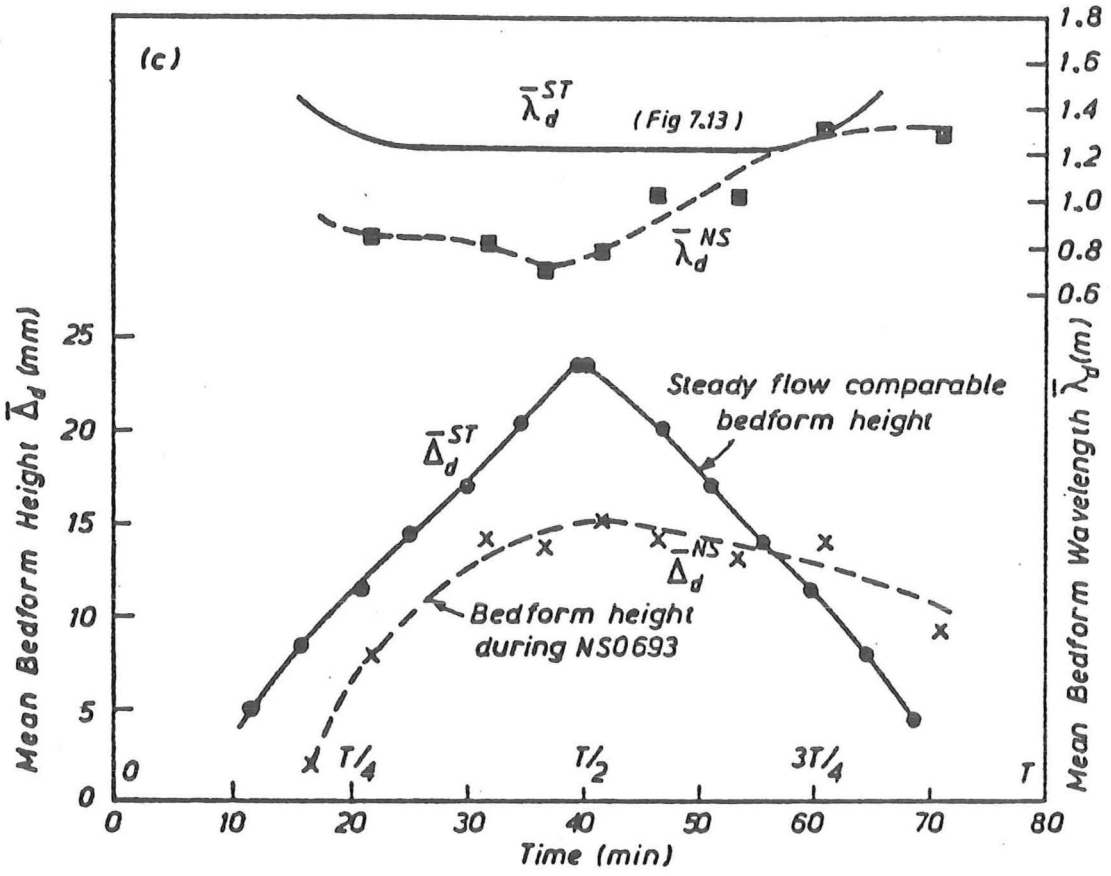

FIGURE 8.16 (c) : Dune bedform properties during wave NS0693

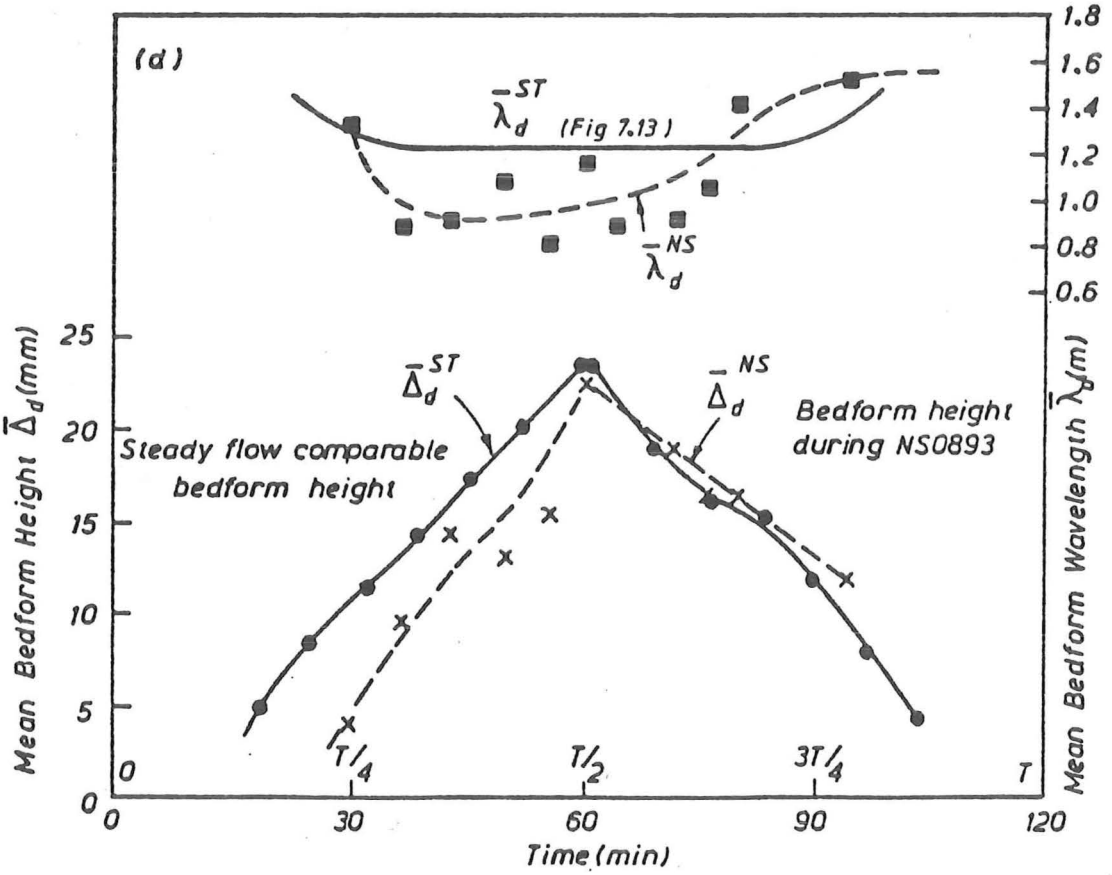

FIGURE 8.16 (d) : Dune bedform properties during wave NS0893

comparable bedform heights obtained in a similar manner to the transport rate comparison procedure used to derive comparable steady flow transport rates. The steady flow comparable dune height is the mean height that the dune configuration would possess, if at all times, the individual bedforms could respond perfectly to the changing flow conditions. The mean wavelength for the dune configuration is matched with the mean wavelength obtained from the steady flow experiments shown in Figure 7.13.

If time is eliminated between the variation of water discharge (independent variable) and the dune height (dependent variable) with time, a rating loop curve or phase diagram can be formed {Allen (1976 a)}. Phase diagrams for three of the translation waves are shown in Figure 8.17. The phase diagram for wave NS0693 was omitted for clarity. The relative ratio of the area within each loop to the area of an escribed rectangle around the loop, defined by $q = q_c$ and q_{max} and $\bar{\Delta}_d = \bar{\Delta}_{d_{max}}$ and D_{50} was calculated. Allen (1976a), using a doubly simple-harmonic theoretical model, (elliptical loop), related mathematically the relative area ratio to an equivalent phase difference or lag, δ. The approximate phase lag has been determined for each of the dune height-discharge loops and is shown in Table 8.4.

TABLE 8.4 : Phase Lags for Non-Steady Flow Dune Response

Wave	Relative Area Ratio	Phase Lag δ (rad.)
		($\leqslant 0.5\pi$)
NS0893	.26	0.10π
NS0693	.35	0.14π
NS0493	.44	0.19π
NS0293	.58	0.27π

The celerity of a few chosen dune bedforms was monitored at several stages during the passage of wave NS0493. The results are

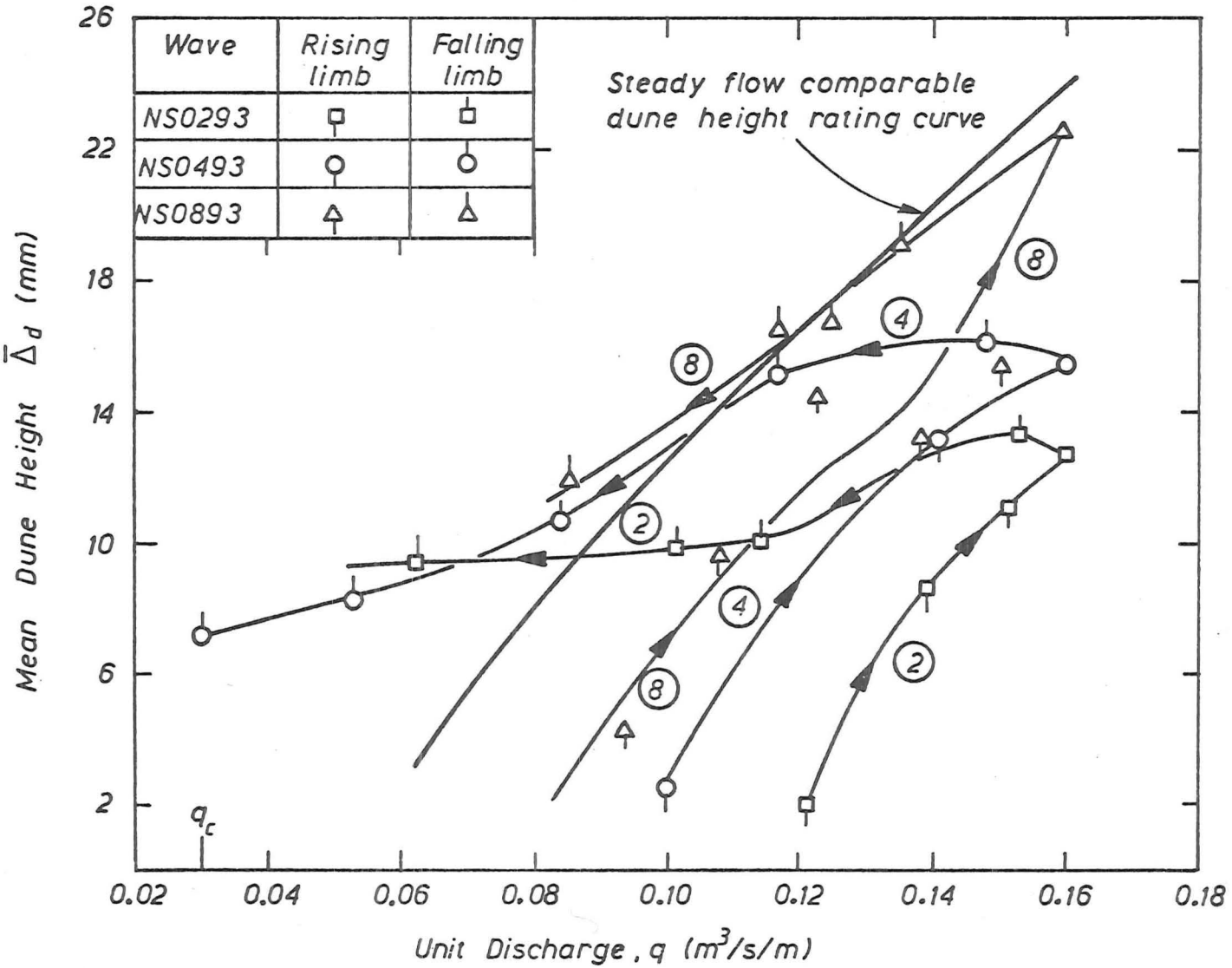

FIGURE 8.17 : Phase diagram of the dune height - discharge relationship for waves No. 2, 4 and 8

plotted with data from the steady flow non-equilibrium experiments in Figure 8.18.

(2) Discussion of Results

(a) Dune Height ($\bar{\Delta}_d$)

Figure 8.16 shows that the initial appearance of the dune bedforms during the rising limb of the wave occurred at a later time than the comparable steady flow bedforms. From that time onwards to the wave peak, the bedform height was always less in magnitude than the corresponding steady flow comparable dune height at any particular time. These differences were more severe for the faster rising waves. This effect describes an imperfect adjustment with the changing flow conditions, where the dune configuration carries foward in time the height dimensions of its past history. This effect is entirely in accord with those noted in regard to transport rates in section 8.4.3. Because the bedload transport is the means whereby transfer of bed material is accomplished, and hence the moulding of bedforms, a reduction in magnitude of the transport rate from the comparable transport rate will lead to a slower rate of change of the bedform volume. Thus the dune height will also be less than the comparable steady flow dune height.

The peak dune height occurred at or just after the peak wave discharge (Figure 8.16). This observation was also made, concerning triangular translation waves, by Griffiths (1976) and Jensen (1973).

On the falling limb a deficit between measured and comparable dune heights persisted after the wave peak for all the waves, except NS0893, until the point where the actual and comparable curves crossed. A comparison of the magnitude of the slopes for the non-steady flow mean dune height curves on the rising and falling limb of each wave (Figure 8.16 a,b,c), indicates a greater resistance to change (flatter slope) in the destruction process than for dune development. This difference between these two processes was reported by Gee

(1975) in a similar situation. He found that the dune destruction process, associated with a step increase in discharge to a new flow rate, pertaining to transitional plane bed conditions (Froude No. $\simeq$ 1.0), was less efficient than dune augmentation from a plane bed.

At the end of the wave passage, where critical conditions for the original plane bed were assumed once again ($q = q_c$), dunes were still present on the bed, their final height being greater for the steeper waves.

Table 8.4 shows an approximate measure of the phase lag associated with the dune height phase diagrams in Figure 8.17. As the rate of change of dune height with discharge, $\frac{d\Delta_d}{dq}$, is positive and the path taken along the loop curve is anticlockwise, the phase lag δ, must be less than or equal to $\pi/2$ radians*. Where no phase lag exists in the system e.g. following perfectly the steady flow dune height rating curve, the phase lag is zero. The results of Table 8.4 indicate that the phase lag increases as the wave steepness increases, given the same maximum discharge.

(b) Dune Wavelength ($\bar{\lambda}_d$)

The change in mean dune wavelength is also shown in Figure 8.16 during the wave passage. The mean dune wavelength along the test reach is less responsive to changes in discharge, particularly during the rising stage, where after an initial decrease, it remains essentially constant at a lower value than the mean steady flow constant value. This observation was also noted during the transition after a step change in discharge. Allen (1976a) suggested that dunes are less constrained in height than they seem to be in wavelength, primarily because a change in height does not involve the formation and disappearance of individual dunes.

*corresponds in the limit to a circular loop.

Although a greater variability existed for wavelengths in both steady and non-steady flows than for dune heights, differences in the magnitude of the mean values do exist between the two cases (Figure 8.16). These differences in magnitude also increase with wave steepness.

As the peak flow of the wave approached, the dune wavelength began to increase toward the steady flow magnitude and continued to increase until the end of the wave period. This behaviour during the falling stage was also observed by Jensen (1973) for dune wavelengths.

(c) Dune Celerity (C_d)

Limited data on the celerity of a few chosen dunes during one translation wave, NS0493, is shown in Figure 8.18. During the rising stage, beginning at t/T = 0.31, the celerities of the dunes appear to be greater than the steady flow celerity pertaining to the same mean velocity. During the falling stage, the dune celerity is less than the value at the corresponding point on the rising limb e.g. the mean celerity at t/T = 0.31 is approximately twice the celerity at t/T = 0.69. Znamenskaya (1963) observed that the celerity of dunes during the rise of a flood exceeded the celerity during the falling stage by 2 - 10 times.

A possible explanation of the greater celerity on the rising limb of a wave is the lower inertia or resistance to change of the dunes during the rising stage, where they are much smaller than the comparable dune height and the dune height at the corresponding point on the falling limb. It must be noted however that a higher dune celerity on the rising limb does not necessarily imply that the transport rate is higher, but it is the combination of $\Delta_d \times C_d$ which governs the bedload transport rate.

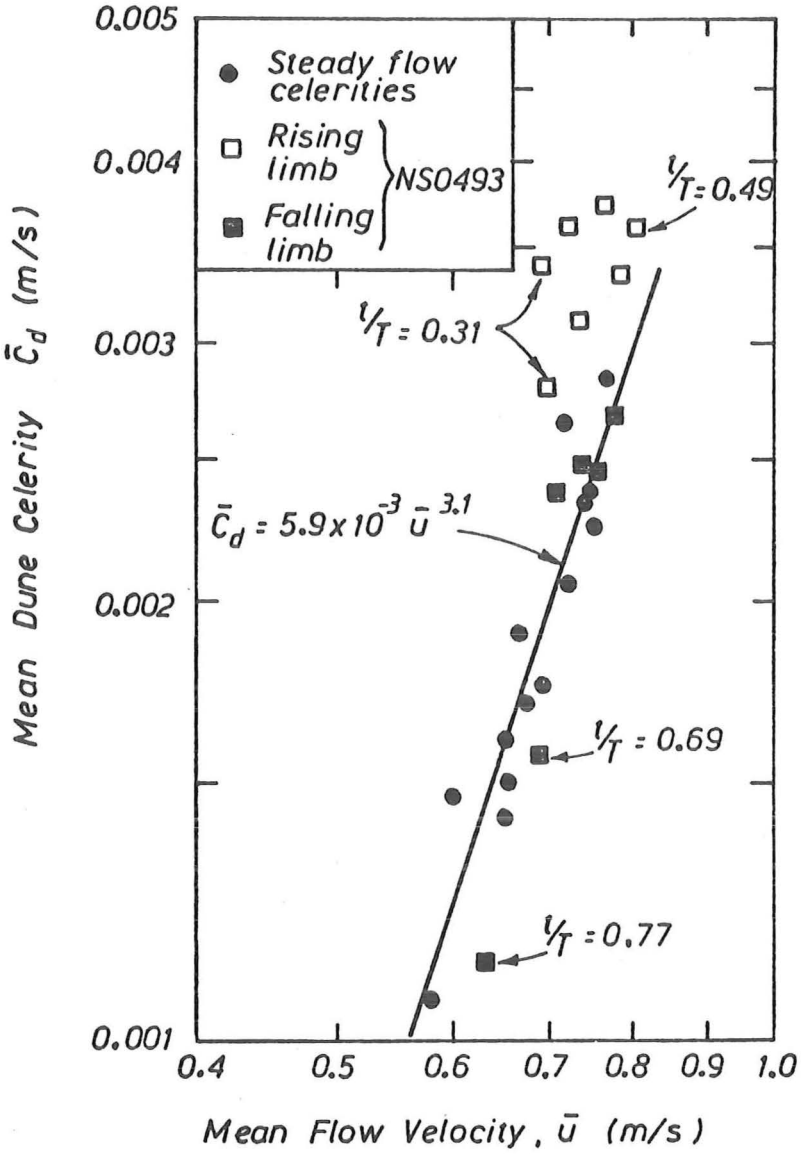

FIGURE 8.18 : Mean dune celerity relationship with mean flow velocity (Wave No. NS0493)

8.4.6 Bedforms - Spatial Variations

The bed profiles, measured at various discrete stations along the test reach where dune crests and troughs were present, are shown in Figure 8.19 for three different times during wave NS0893. The difficulty in determination of the general scour hole length is once again evident, particularly in Figure 8.19c, where the mean bed level of the bedform configuration is below the original bed level. This effect of the lowering of the mean bed elevation downstream, where bedforms were present, was much more noticeable here than during steady flow non-equilibrium experiments. This is because at a corresponding point near the end of the general scour hole, where a steady flow segment receives from the preceding segment almost its full transport capacity, a non-steady flow segment does not and must therefore erode more material from the bed.

The spatial variation of the magnitude differences in bedload transport rates, downstream of the local scour hole must be connected with the response of the bedforms. From Figure 8.19, a spatial variation, where the dune height increases downstream, can be distinguished in the bedform height distribution. The spatial distributions of bedform heights near the peak of the four waves used for bedform analysis, are examined quantitatively in Figure 8.20. The dimensionless bedform height $\Delta_d^{NS}(x,t)/\bar{\Delta}_d^{ST}(t)$, is the ratio of the instantaneous individual bedform height at time t during the translation wave, to the steady flow comparable mean (over the test reach) dune height at that time t. The spatial distribution of dune heights, shown only for $t/T \doteq 0.5$, predominantly in the range $1.5\ m < x < 4\ m$, was a general trend observed throughout the rising limb of each wave and a portion of the falling limb after the wave peak. Thus differences in mean dune height (taken over the 9.29 m test reach) between comparable steady and non-steady flows, shown in Figure 8.16, will be slightly over-emphasised for the dune response at the downstream end

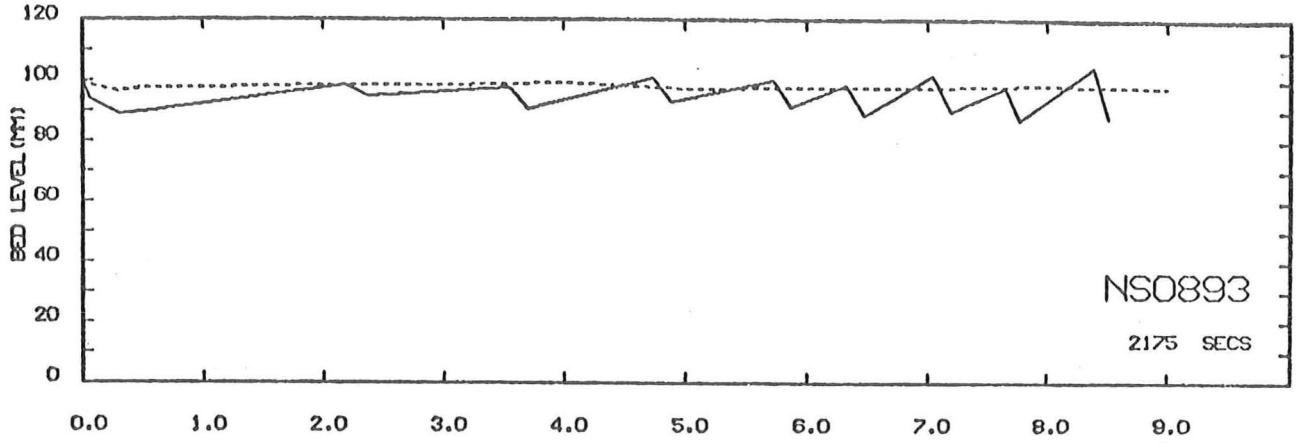

(a) t/T = 0.30

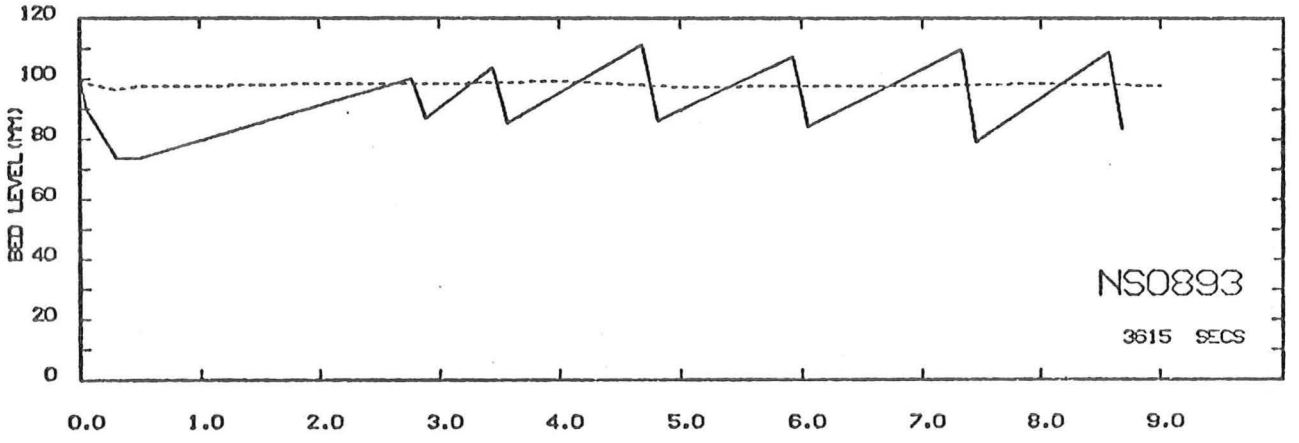

(b) t/T = 0.50

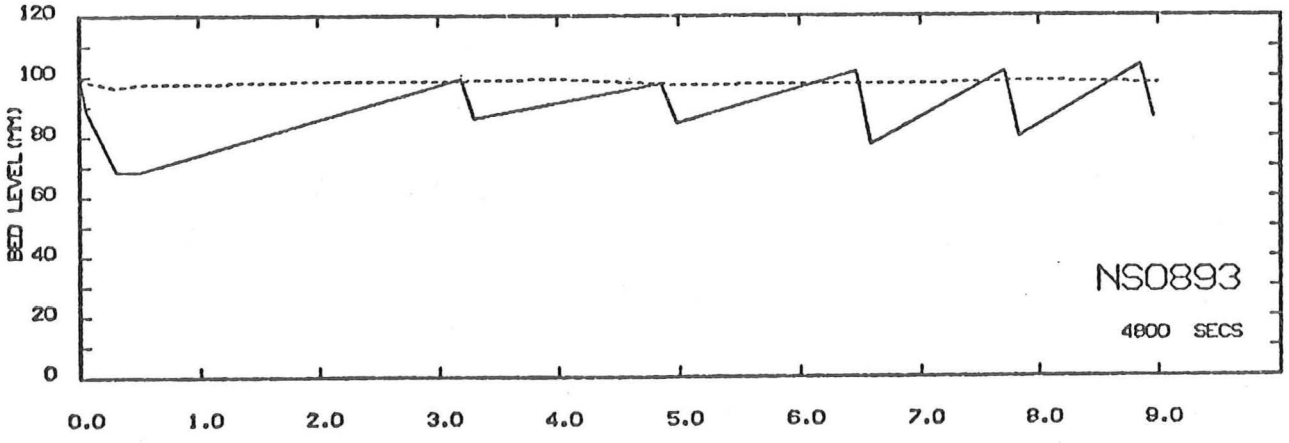

(c) t/T = 0.67

FIGURE 8.19 : Bed profiles for wave NS0893 (T = 7200 sec)

of the test reach (9.29 m), because of the smaller dunes present upstream. The lower values of the dune heights in the range 1.5 m < x < 4 m, is likely to be a significant factor in the spatial response of the bedload which occurs in this region particularly, downstream

TABLE 8.5 : Distribution of Dune Heights with Distance near the end of the Wave Period

WAVE	t/T	DUNE HEIGHT Δ_d (mm) DISTANCE x (m)					
NS0293	.88	15.4	8.1	6.6	6.6	6.6	13.9
		1.78	2.82	3.83	5.08	6.52	7.80
NS0493	.90	8.8	12.5	10.3	5.1	4.4	9.5
		2.55	3.90	5.05	6.09	6.82	8.16
NS0693	.89	7.3	10.3	5.1	11.7	11.7	
		3.53	4.59	5.99	7.23	8.69	
NS0893	.79	5.9	22.0	11.7	8.1		
		3.93	5.49	7.16	8.52		

of the local scour hole.

Further downstream, 4 m < x < 9.29 m, the spatial distribution of dune heights, (Figure 8.20), is more random, with no obvious trend, although often asmaller dune was present adjacent to a large dune, relative to the mean dune height.

During the latter portion of the falling limb of the waves, no general spatial variation was resolved; see Table 8.5. For the steepest wave NS0293 (Table 8.5), the spatial variation reversed as the end of the wave period approached, the bedform height being larger at the upstream section than at the end of the test reach.

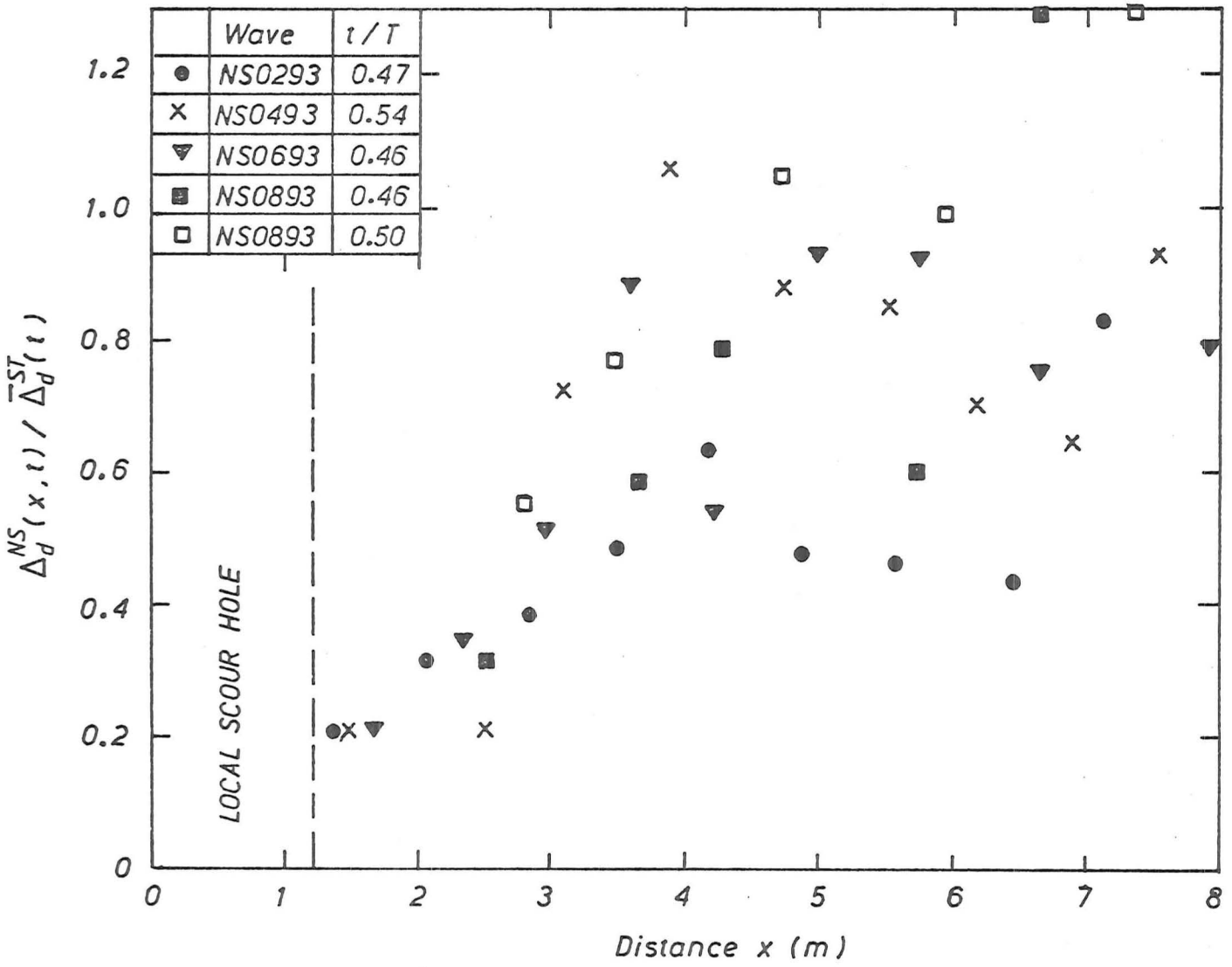

FIGURE 8.20 : Spatial distribution of dune heights near the wave peaks

8.4.7 Resistance

Resistance to flow and the bedload transport rate are related to the roughness of the bed profile. As the bed roughness changes, there is a corresponding change in resistance to flow, thus affecting the flow properties such as depth and mean velocity. During the rising limb of a translation wave, changes in dune geometry lag the changes in water discharge, and hence the bed roughness will similarly lag behind, particularly with regard to the form roughness. The total friction factor f can be split into two components, f', the grain resistance friction factor and f" the form roughness friction factor. From the form friction factor relation obtained by Engelund (1977) for dune beds,

$$f'' = 2.5 \exp\left(-2.5 \frac{\Delta_d}{y}\right) \frac{\Delta_d^2}{y\lambda_d} \qquad \ldots (8.15)$$

it can be shown that the form drag is more sensitive to dune height than wavelength, provided that

$$\frac{\Delta_d}{y} < 0.8 - \frac{S_d}{2.5}$$

which is approximately 0.8 as the dune steepness S_d is small. The above condition is certainly true in almost all flow cases. Therefore the initial increase in the roughness of the bed under non-steady flows, is best achieved by a proportionate increase in dune height rather than wavelength. This observation was noted for both step changes in discharge and triangular translation waves on the rising limb.

Fredsøe (1979) modelled theoretically the response of bedforms and resistance to a periodic weakly varying water discharge and found that the effective shear stress Y' (due to grain friction), was greater on the rising stage than for a decreasing discharge. He then con-

cluded that the sediment transport rate likewise was larger for an increasing discharge, assuming the inertia of the bed particles to be negligible. However the results of the NS series, for a fine gravel bed-material, indicate that the bedload transport rate is generally smaller on the rising limb than on the falling for steep translation waves, emphasising the role of the bed response effect on the bedload transport.

The magnitude deficit between comparable steady flow transport rates and non-steady flow transport rates, under non-equilibrium conditions, is due to both a bed response effect and changes in the friction slope S_f from under-developed dune bedforms. What is unknown, is the relative proportion of these two effects which lead to the magnitude deficit.

8.4.8 Stage - Discharge Relations

When the total resistance to flow (or bed roughness) lags the changes in discharge, the lower resistance to flow will cause the water depth to be lower than for steady flow conditions. {Simons et al. (1961)}. The opposite situation will occur on the falling limb of a flood wave. This effect creates a hysteresis loop in the stage-discharge curve. The stage-discharge curves for the two contrasting waves, NS0235 and NS0835 (q_{max} = 0.16 $m^3/s/m$), are shown in Figure 8.21. The stage was measured at x = 3.26 m, in the region where the dune height exhibited a spatial variation (Figure 8.20). Also shown in Figure 8.21 is the steady flow non-equilibrium rating curve obtained from the ST--35 series. The downstream weir, controlling the tail-water level, was carefully adjusted in small steps during the translation waves, using steady flow settings. Therefore the deviations from the steady rating curve reflect the dune and resistance behaviour. For wave NS0835, the loop in the stage-discharge curve, which is a maximum near the wave peak, is generally small,

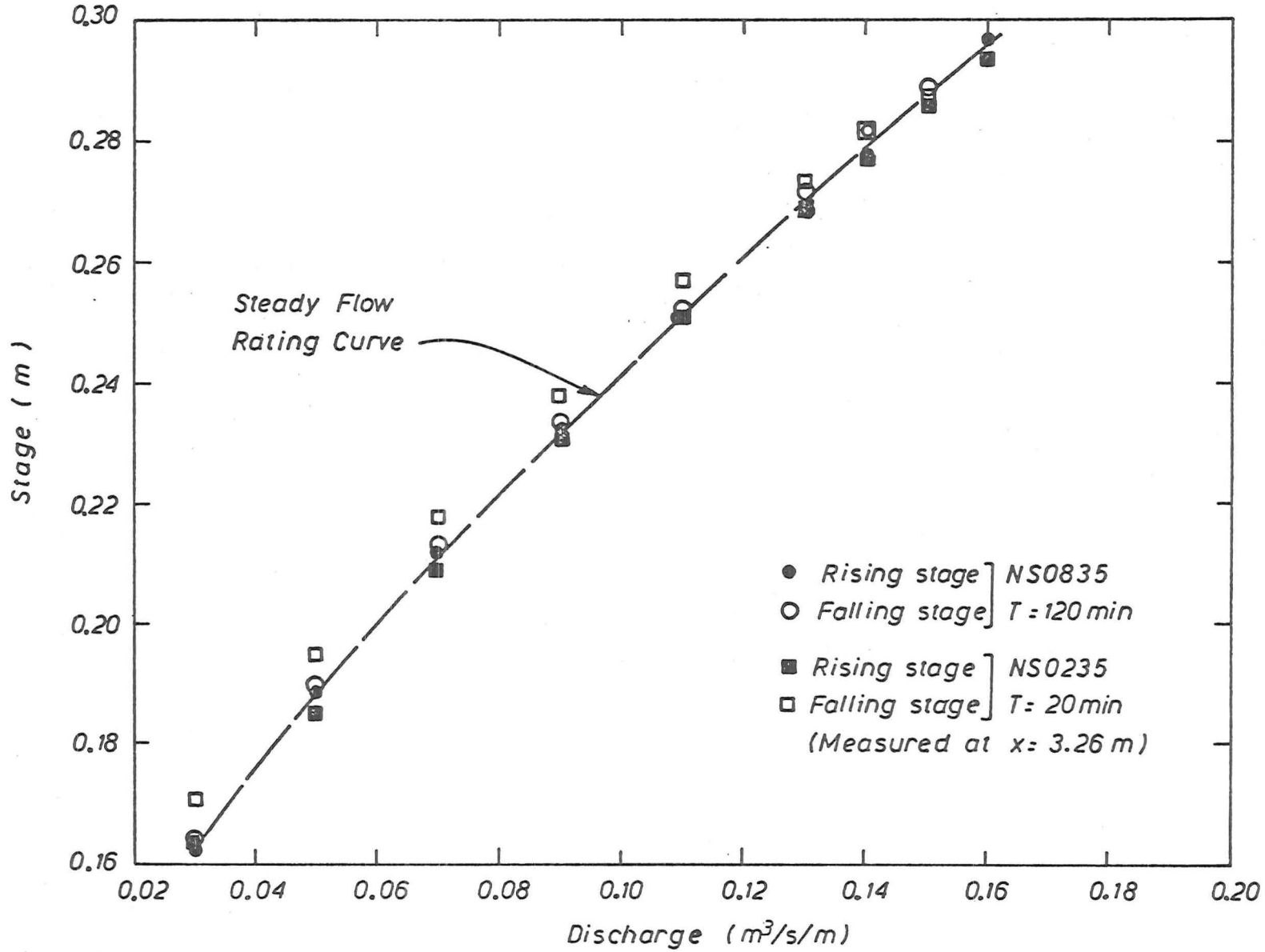

FIGURE 8.21 : Stage - discharge rating curves for waves NS0235 and NS0835

reflecting the smaller phase lag for dune development (Table 8.4). However for wave NS0235, the differences between stages on the rising and falling limbs, for a constant discharge, are larger. Near the end of the wave period, the stage remains above the steady flow rating curve, as relatively large dunes persist until the finish, compared with plane bed conditions which were present under the small steady flows.

8.5 SUMMARY

The particular non-equilibrium situation investigated, a change from a fixed bed to an erodible alluvial bed with no input of sediment, exhibited two contrasting regions :

(1) the local scour hole, particularly in the scour pit region, in which the flow and sediment behaviour is dominated by the non-equilibrium boundary conditions.

(2) the remainder of the control test reach in which the flow and sediment behaviour is dominated by the non-steady flow conditions and the resulting delayed response of the bedforms.

The results presented in this chapter have been compared to comparable steady flow non-equilibrium results. The differences observed are thus those between steady and non-steady flows and are in addition to those incurred by the non-equilibrium situation described in Chapter 7.

For step changes in discharge from initial threshold conditions, there was initially a transient phase, during which the measured transport rates were significantly less than the average comparable steady flow rates. The duration of this phase, defined as the elapsed time until the two transport rates first became equal, was inde-

pendent of reach length and decreased rapidly towards an asymptotic value, with increasing size of step change. The deficit, between the transport rates, chosen to characterise the transient phase; increased with an increase in step change because of the greater mismatch between zero transport and the newly acquired transport capacity; and decreased with increasing reach length.

After the transient phase, the non-steady transport rates tended monotonically towards the average steady flow transport rates for short reach lengths, reflecting conditions in the local scour hole, and oscillated about the steady flow rates at longer reaches reflecting the influence of bedforms.

Measurements of bedform properties showed that the dune height responds much more rapidly than the wavelength, the former almost reaching the steady flow comparable value at the end of the transient phase.

During the passage of triangular translation waves, the measured transport rates, at points downstream of the local scour hole, increased more slowly than the comparable steady flow transport rates, peaked at approximately the same time and then decreased with a smaller deficit. At times on the falling limb, the measured transport rates equalled and even exceeded the <u>average</u> comparable rates. Measured transport rates at equal times on the rising limb and at the wave peak, increased with reach length suggesting that the wave filled with sediment relative to the steady flow comparable transport rates as it progressed downstream. On the falling limb this effect, if present, was masked by the variations in the transport rate that characterised this portion of the wave.

Within the local scour hole, there were minimal differences, apart from the peak values, between steady and non-steady flow transport rates under non-equilibrium conditions.

Sediment yields from each wave could be correlated for the control test reach using a wave yield number, a Strouhal Number and the ratio of maximum to threshold water discharge. The steady discharge required to produce the same sediment yield in the same time as the wave was some 5% more for the longer reach length, and up to 20% less for the shorter reach lengths, than the mean water discharge of the wave up to that time.

Dune heights under the rising limb of a translation wave increased more rapidly than dune wavelengths, but lagged the steady flow comparable dune heights. On the falling limb wavelengths increased while heights decreased slowly. This suggests that dune augmentation is more efficient than the destruction process. It is this effect which gives rise to differing resistance to flow on the rising and falling limbs for the same discharge, thus producing a loop in the stage-discharge rating curve which is observed on some alluvial rivers.

CHAPTER IX

CONCLUSIONS AND RECOMMENDATIONS

9.1 CONCLUSIONS

The results of this study, which may be related to the aims set down in section 4.2, are summarised at the ends of Chapters 6,7 and 8. From these summaries the following points can be emphasised.

(1) Initial Motion

The transport rate or dimensionless erosion rate is strongly dependent on the applied bed shear stress near threshold conditions. From this relationship which applies for turbulent flow and uniform particles, the best method of determining threshold flow conditions is to nominate a suitable transport rate or dimensionless erosion rate. A quantitative estimate of the dimensionless erosion rate for other initial motion criteria can also be determined.

(2) Steady Flow, Non-Equilibrium Transport

At any point in the test reach, the transport rate decreases with time after the general scour hole reaches the vicinity of that particular point.

At any time, the transport rate varies spatially, increasing rapidly from zero at the upstream boundary, and through the region of the scour pit. With distance downstream in the general scour hole, the transport rate increased more slowly, tending asymptotically to the initial equilibrium transport rate.

Differences were apparent between the actual non-equilibrium transport rate and the comparable local equilibrium capacity rate in the local scour hole. These differences were a maximum at the upstream end of the reach, and decreased with distance downstream in the local scour hole. Further downstream in the general scour

hole, the deficit was insignificant. Hence the predictive power of steady flow non-equilibrium mathematical models will be poor in the local scour hole region if an equilibrium transport formula, based on mean flow velocity, is used in the formulation of the model.

(3) Non-Steady Flow, Non-Equilibrium Transport

Two contrasting regions are evident within the test reach, when the alluvial system is subject to non-steady flows :

(a) the local scour hole which is dominated by the non-equilibrium effect while the non-steady flow effect is small

(b) the remainder of the reach which is dominated by the effect of the non-steady flow on the bedload transport and bedform development

A comparison was made between actual non-steady flow transport rates and comparable steady flow transport rates. Significant differences between these two transport rates were observed downstream of the local scour hole and are in addition to those incurred by the non-equilibrium situation at the same point.

For step changes in discharge from threshold conditions, at any point downstream of the local scour hole, there was initially a transient phase during which the actual transport rates were significantly less than the comparable steady flow transport rates. The transport rate deficit increased with increasing size of the step change due to the greater mis-match between threshold conditions and the newly acquired transport capacity.

Measurements of bedform dimensions showed the dune height responds more rapidly than the wavelength during the transient phase.

For steep translation waves, significant differences in transport rate magnitude occurred, at any point downstream of the local scour hole, between the measured non-steady flow transport rate hydrograph and the comparable steady flow transport rate hydrograph.

This was particularly noticeable on the rising limb. Faster rising waves, given the same peak water discharge, were associated with greater differences. This suggests a bed response effect is present.

Dune heights under the rising limb of a translation wave increased more rapidly than dune wavelengths. On the falling limb wavelengths continued to increase while dune heights decreased, although at a slower absolute rate than for the increase on the rising limb. This suggests that dune augmentation is more efficient than the destruction process.

At any time, the transport rate deficit, for both step changes in discharge and translation waves, exhibited a spatial variation, being a maximum immediately downstream of the local scour hole. The deficit decreases in the downstream direction, suggesting the flow segments are filled as they progress. The deficit is assumed to approach a constant non-zero magnitude further downstream, for rapid changes in discharge. For slow changes in discharge the magnitude deficit in this region will be small. The reasons for the spatial variation of the deficit remain tentative.

Hence the performance of the non-steady flow non-equilibrium mathematical models, which use an equilibrium transport formula, can be expected to be poor if a non-steady flow bed response effect or changes in friction slope occur. The performance becomes more critical as the bedload sampling point is moved further upstream into the general scour hole. Consequently the bedload transport rate will be over-estimated for all reach lengths, downstream of the local scour hole, under rapid changes in discharge.

The essential contribution of this thesis, is a set of indications of the general physical behaviour of an alluvial system, under non-equilibrium conditions. This was achieved by the development of conceptual models and the results of laboratory experiments. To

study the physical behaviour under non-steady flows, conditions treated herein are severe, especially with regard to wave steepness and sudden step changes in flow. Therefore for smaller rates of change of discharge with time, the above conclusions will hold, but the transport rate deficit will be reduced.

9.2 RECOMMENDATIONS FOR FURTHER RESEARCH

This study has highlighted several areas of need in the field of initial motion studies and bedload transport transients. The scope for further research is wide, not only in the laboratory, but also in field data collection. The following recommendations are considered as the more important areas in experimental research.

(1) Initial Motion

More work is required to develop the quantitative definition of threshold conditions, particularly the measurement of small transport rates for different slopes and sediment sizes.

The initial motion results have been obtained for unifrom material. Further work with graded mixtures, where the sheltering effects of larger grains are significant, is required to generalise the relationship between the dimensionless erosion rate, N, and the Entrainment function Y.

(2) Steady Flow Non-Equilibrium Transport

There is a need to extend the data base by the measurement of actual transport rates for comparison with the local transport capacity within the local scour hole. This can be achieved using different bed slopes, sediment sizes and upstream sediment boundary conditions.

Theoretical work is also required to derive a bedload equation or computational scheme, possibly as a function of the flow velocity near the bed, which is applicable to the non-equilibrium

local scour hole situation. Hence the power of the mathematical models, to predict scour hole development and the final equilibrium depth will be improved.

(3) Non-Steady Flow, Non-Equilibrium Transport

The deficit, between comparable steady flow and non-steady flow transport rates, needs further attention. In particular, a limiting wave steepness needs to be defined, for both laboratory and field situations, above which the quasi-steady mathematical model is not applicable. Also the relative proportion of the transport rate deficit due to firstly bed response effects and secondly, to changes in the friction slope, remains unknown for various wave characteristics. Moreover, the deficit must be related to lags in the response of bedforms (height, wavelength, and celerity), if they are present.

Conclusive reasons for the presence of the spatial variation of the transport rate deficit to any steep non-steady flow form, need to be found.

Other non-equilibrium boundary conditions need to be tested under non-steady flows e.g. sediment overload of the system.

The response of the system under non-steady "equilibrium" conditions needs to be clarified.

(4) Resistance and Stage-Discharge Relations

At a more fundamental level, the relationship between changing bedforms, resistance and flow depths, for non-steady "equilibrium" and non-equilibrium conditions, is known only in outline, particularly for gravel bed-material. The estimation of the friction factor f for the prediction of stage-discharge relations, during steep flood waves, needs further attention.

(5) Mathematical Models

The mathematical models for any alluvial system remain to be

tested thoroughly against actual data covering a wide range of sediment and flow conditions. Further applicable data can be expected to contribute to the refinement of the mathematical model.

Clearly, much further work in the field of bedload transients is needed before the response of the bedload to non-steady influences, in both sediment and/or flow phases, can be fully comprehended.

REFERENCES

AKSOY, S. (1971) "River-Bed Degradation Downstream of Dams", Proc. of 14th Congress, I.A.H.R., Paris, Vol. 3, Paper C33, p 275-282.

ALLEN, J.R.L. (1976a) "Computational Models for Dune Time-Lag : General Ideas, Difficulties and Early Results", Sedimentary Geology, Vol. 15, p 1-53.

ALLEN, J.R.L. (1976b) "Bed Forms and Unsteady Processes : Some Concepts of Classification and Response Illustrated by Common One-Way Types", Earth Surface Processes, Vol. 1, p 361-374.

A.S.C.E. (1975) "Sedimentation Engineering", Prepared by the A.S.C.E. Task Committee for the Preparation of the Manual on Sedimentation of the Sedimentation Committee of the Hydr. Div., V.A. Vanoni, Ed., A.S.C.E. Manuals and Reports on Eng. Practice, No. 54, 745 p.

ASHIDA, K. and M. MICHIUE. (1971) "An Investigation of River-Bed Degradation Downstream of a Dam", Proc. of 14th Congress, I.A.H.R., Paris, Vol. 3, Paper C30, p 247-255.

BAGNOLD, R.A. (1966) "An Approach to the Sediment Transport Problem from General Physics", U.S. Geol. Surv. Prof. Paper 422-I p I3.

BAYAZIT, M. (1969) "Resistance to Reversing Flow over Moveable Beds", Jnl. of Hydr. Div., A.S.C.E., Vol. 95, No. HY4, p 1109-1127.

BENNETT, J.P. and C.F. NORDIN. (1977) "Simulation of Sediment Transport and Amouring", Hydrological Sciences - Bulletin, Vol. 22, No. 4, p 555-569.

BOGARDI, J.L. (1965) "European Concepts of Sediment Transportation", Jnl. of Hydr. Div., A.S.C.E., Vol. 91, No. HY 1, p 29-54.

BOUVARD, M., J.P. CHOLLET and J.A. CUNGE. (1977) "Progrès Récents et Difficultés de Simulation Mathématiques des Rivières Alluvionnaries", Proc. of 17th Congress, I.A.H.R., Baden-Baden, Vol. 1, Paper A22, p 165-172.

BREUSERS, H.N.C. (1966) "Conformity and Time Scale in Two-Dimensional Local Scour", Golden Jubilee Symposia, Poona, India, Vol. 1, p 1-8.

BREUSERS, H.N.C. (1975) "Computation of Velocity Profiles in Scour Holes", Proc. of 16th Congress, I.A.H.R., Sao Paulo, Vol. 2, Paper B37, p 300-306. (Also Delft Hydr. Lab. Publ. No. 152).

CAREY, W.C. and M.D. KELLER. (1957) "Systematic Changes in the Beds of Alluvial Rivers", Jnl. of Hydr. Div., A.S.C.E., Vol. 83, No. HY4, 24 p.

CHANG, F.F.M. (1969) "Computer Simulation of Riverbed Degradation and Aggradation by the Method of Characteristics", Proc. of 13th Congress, I.A.H.R., Kyoto, Vol. 1, Paper A37, p 337-344.

CHANG, H.H. and J.C. HILL. (1977) "Minimum Stream Power for Rivers and Deltas", Jnl. of Hydr. Div., A.S.C.E., Vol. 103, No. HY12, p 1375-1389.

CHEN, Y.H. (1973) "Mathematical Modeling of Water and Sediment Routing in Natural Channels", Ph.D. Dissertation, Colorado State Univ., Fort Collins, 253 p.

CHEN, Y.H. and D.B. SIMONS. (1975) "Mathematical Modeling of Alluvial Channels", Symp. on Modeling Techniques, Waterways, Harbours and Coastal Engineering Div., A.S.C.E., San Francisco, Vol. 1, p 466-483.

CHIEN, N. (1954) "The Present Status of Research on Sediment Transport", Proc. A.S.C.E., Hydr. Div., Vol. 80, Separate No. 565, 33 p.

CHUNA, L.V. (1975) "Time Evolution of Local Scour", Proc. of 16th Congress, I.A.H.R., Sao Paulo, Vol. 2, Paper B36, p 285-299.

COLARIC, PICHON and SANANES. (1967) "Etude Des Affouillements A L'aval D'un Seuil Deversant", Proc. of 12th Congress, I.A.H.R., Fort Collins, Vol. 3, Paper C37, p 322-329.

CUNGE, J.A. and N. PERDREAU (1973) "Mobile Bed Fluvial Mathematical Models" La Houille Blanche, No. 7, p 561-580.

CUNGE, J.A. and D.B. SIMONS. (1975) "Mathematical Model of Unsteady Flow in Movable Bed Rivers with Alluvial Channel Resistance", Proc. of 16th Congress, I.A.H.R., Sao Paulo, Vol. 2, Paper B7, p 48-56.

DODDIAH, D. (1967) "Scour Below Submerged Solid Bucket-Type Energy Dissipators", Proc. of 12th Congress, I.A.H.R., Fort Collins, Vol. 3, Paper C13, p 105-116.

EINSTEIN, H.A. (1950) "The Bed-load Function for Sediment Transportation in Open Channel Flows", Tech. Bull. No. 1026, U.S. Dept. of Agriculture, Soil Conservation Service, Washington, D.C., 71 p.

EINSTEIN, H.A. and N.L. BARBAROSSA. (1952) "River Channel Roughness", Transactions of A.S.C.E., Vol 117, Paper No. 2528, p 1121-1146.

ENGELUND, F. (1977) "Hydraulic Resistance for Flow Over Dunes", Inst. of Hydrodynamics and Hydraulic Eng., Tech. Univ. of Denmark, Prog. Rept. No. 44, p 19-20.

ENGELUND, F. and E. HANSEN. (1967) "A Monograph on Sediment Transport in Alluvial Streams", Teknisk Forlag, Copenhagen, Denmark.

ETTEMA, R. (1980) "Scour at Bridge Piers", School of Engineering, Univ. of Auckland, Auckland, N.Z., Report No. 216.

FENTON, J.D. and J.E. ABBOTT (1977) "Initial Movement of Grains on a Stream Bed : the Effect of Relative Protrusion", Proc. of Roy. Soc. of London, Series A, Vol. 352, p 523-537.

FOLEY, M.G. (1975) "Scour and Fill in Ephemeral Streams", W.M. Keck Laboratory of Hydraulics and Water Resources, Cal. Inst. Tech., Report No. KH-R-33, 189 p.

FOSTER, G.R. and L.D. MEYER. (1972) "A Closed-Form Soil Erosion Equation for Upland Areas", Sedimentation, Symposium to Honour Prof. H.A. Einstein; H.W. Shen (Ed.), Colorado State Univ., Fort Collins, Chap. 12, 19 p.

FREDSØE, J. (1975) "The Friction Factor and Height-Length Relations in Flow Over a Dune-Covered Bed", Inst. of Hydrodynamics and Hydraulic Eng., Tech. Univ. of Denmark, Prog. Rept. No. 37, p 31-36.

FREDSØE, J. (1979) "Unsteady Flow in Straight Alluvial Streams : Modification of Individual Dunes", Jnl. of Fluid Mech., Vol. 91, Part 3, p 497-512.

GEE, D.M. (1975) "Bed Form Response to Nonsteady Flows", Jnl. of Hydr. Div., A.S.C.E., Vol. 101, No. HY3, p 437-449.

GESSLER, J. (1971) "Aggradation and Degradation", Chap. 8, River Mechanics, Vol. 1, (Ed. H.W. Shen), Colorado State Univ., Fort Collins, p 8.1-8.24.

GILL, M.A. (1971) "Height of Sand Dunes in Open Channel Flows", Jnl. of Hydr. Div., A.S.C.E., Vol. 97, No. HY12, p 2067-2074.

GRAF, W.H. (1971) "Hydraulics of Sediment Transport", McGraw-Hill, New York, 513 p.

GRIFFITHS, G.A. (1976) "Transport of Bedload by Translation Waves in an Alluvial Channel", University of Canterbury, Christchurch, N.Z., Research Report 76-1, 152 p.

GRIFFITHS, G.A. (1979) "Recent Sedimentation History of Waimakariri River, N.Z." Jnl. of Hydrology, N.Z., Vol 18, No. 1, p 6-28.

GRIFFITHS, G.A. and A.J. SUTHERLAND. (1977) "Bedload Transport by Translation Waves", Jnl. of Hydr. Div., A.S.C.E., Vol. 103, No. HY11, p 1279-1291.

GRUAT, J. and J. PICHON. (1971) "Influence de la Turbulence sur le Transport Solide a L'aval D'un Seuil Deversant", Proc. of 14th Congress, I.A.H.R., Paris, Vol. 3, Paper C44, p 363-370.

GUNARATNAM, D.J. and F.E. PERKINS. (1970) "Numerical Solution of Unsteady Flows in Open Channels", Hydrodynamics Lab. Report No. 127, Dept. Civil Eng. M.I.T., Cambridge, Massachusetts, 260 p.

GUY, H.P., D.B. SIMONS and E.V. RICHARDSON. (1966) "Summary of Alluvial Channel Data from Flume Experiments, 1956-61", U.S. Geol. Surv. Prof. Paper No. 462-I, 96 p.

HALES, Z.L., A. SHINDALA, and K.H. DENSON. (1970) "River-Bed Degradation Prediction", Water Resources Research, A.G.U., Vol. 6, No. 2, p 549-556.

HENDERSON, F.M. (1966) "Open Channel Flow", Macmillan Co., N.Y., 522 p.

HENRIQUES, A.G. (1977) "Mathematical Modelling of Unsteady Flow in Alluvial Channels", Proc. of 17th Congress, I.A.H.R., Baden-Baden, Vol. 1, Paper A19, p 145-150.

HILL, I.K. (1967) "Fluvial Sediment Transport at a Large Bed Shear Stress", Ph.D. Thesis, Univ. of Canterbury, N.Z., 236 p.

HUBBELL, D.W. and W.W. SAYRE. (1964). "Sand Transport Studies with Radioactive Tracers", Jnl. of Hydr. Div., A.S.C.E., Vol. 90, No. HY3, p 39-68.

HWANG, J.C. (1975) "Degradation of Sand-Bed Channel", Proc. of 16th Congress, I.A.H.R., Sao Paulo, Vol. 2, Paper B23, p 181-188.

I.A.H.R. (1967) "Erosion and Local Scour Downstream from Hydraulic Structures", Proc. of 12th Congress, Fort Collins, Vol. 3, Papers C1, 2, 7, 8, 10, 11, 24, 26 and 39.

IVANOVA, A.A. (1967) "Analysis of Relationships Between Water Discharges and Levels During the Propagation of Release Waves in a Prismatic Channel (Numerical Experiments)", Soviet Hydrology : Selected Papers, A.G.U., No. 2, p 121-135.

JENSEN, P.D. (1973) "Dune Formation Under Non Steady Conditions", Proc. of 15th Congress, I.A.H.R., Istanbul, Vol. 1, Paper A23, p 173-179.

KENDALL, M.G. (1973) "Time-Series", Charles Griffin & Co. Ltd., London, 197 p.

KENNEDY, J.F. and N.H. BROOKS. (1963), in A.S.C.E. (1975), "Sedimentation Engineering", Table 2.3, p 126.

KOMURA, S. (1971) "Prediction of River-Bed Degradation Below Dams", Proc. of 14th Congress, I.A.H.R., Paris, Vol. 3, Paper C31, p 257-264.

LANE, E.W. (1934) "Retrogression of Levels in River Beds Below Dams", Eng. News Record, June 28th, p 836-38.

LANE, E.W. (1955) "The Importance of Fluvial Morphology in Hydraulic Engineering", Proc. of A.S.C.E., Hydr. Div., Vol. 81, Paper No. 745, 17 p.

LAURSEN, E.M. (1952) "Observations on the Nature of Scour", Proc. 5th Hydr. Conf., State University of Iowa, June 9-11, Iowa City, Iowa, p 179-97.

LI, W.H. (1955) "Criteria for Similitude of Scour Below Hydraulic Structures", Proc. of 6th Congress, I.A.H.R., The Hague, Vol. 3, Paper C4, 6 p.

LUQUE, R.F. and R. van BEEK. (1976) "Erosion and Transport of Bed-Load Sediment", Jnl. of Hydr. Research, I.A.H.R. Vol. 14, No. 2, p 127-144.

MAHMOOD, K. (1975) "Mathematical Modeling of Morphological Transients in Sandbed Canals", Proc. of 16th Congress, I.A.H.R., Sao Paulo, Vol. 2, Paper B8, p 57-64.

MAHMOOD, K. and V.M. PONCE. (1976) "Mathematical Modeling of Sedimentation Transients in Sandbed Channels", Eng. Research Center, Colorado State Univ., Fort Collins, Report No. CER75-76KM-VMP28, 125 p.

MAHMOOD, K. and V. YEVJEVICH, (Eds.) (1975) "Unsteady Flow in Open Channels", 3 Vols., Water Resources Publ., Fort Collins, Colorado.

MILORADOV, M. and D. MUSKATIROVIC. (1971) "Calculation of River Bed Deformation in Unsteady Flow", Proc. of 14th Congress, I.A.H.R., Paris, Vol. 3, Paper C22, p 175-185.

NASNER, H. (1973) "On the Behaviour of Tidal Dunes in Estuaries", Proc. of 15th Congress, I.A.H.R., Istanbul, Vol. 1, Paper A24, p 181-188.

NEILL, C.R. (1968) "A Re-Examination of the Beginning of Movement for Coarse Granular Bed Materials", Report No. INT 68, Hydr. Research Station, Wallingford.

NEILL, C.R. (1969) "Bed Forms of the Lower Red Deer River, Alberta", Jnl. of Hydrology, Vol. 7, No. 1, p 58-85.

NEILL, C.R. and M.S. YALIN. (1969) "Quantitative Definition of the Beginning of Bed Movement", Jnl. of Hydr. Div., A.S.C.E., Vol. 95, No. HY1, p 585-587.

NEWTON, C.T. (1951) "An Experimental Investigation of Bed Degradation in an Open Channel", Trans. of Boston Soc. of Civil Engrs., 1951, p 28-60.

NOVAK, P. (1961) "Influence of Bed Load Passage on Scour and Turbulence Downstream of a Stilling Basin", Proc. of 9th Congress, I.A.H.R., Belgrade, Vol. 1, Paper 15, 10 p.

OMNITAB II (1971) Statistical Computer Package, National Bureau of Standards, Washington, D.C. 20234, Version 5.0, May 15th.

PADMAVALLY, K. (1977) "Speed of Inertial Bed Load Disturbances", Jnl. of Hydr. Div., A.S.C.E., Vol. 103, No. HY7, p 777-795.

PADMAVALLY, K., M.J. RAJMANE and D.B. SHIRKE. (1980) Discussion on "Modeling Alluvial Channel Bed Transients" by V.M. Ponce, J.L. Garcia and D.B. Simons; Jnl. of Hydr. Div., A.S.C.E., Vol. 106, No. HY1, p 227-8.

PAINTAL, A.S. (1971a) "Concept of Critical Shear Stress in Loose Boundary Open Channels", Jnl. of Hydr. Res., I.A.H.R., Vol. 9, No. 1, p 91-113.

PAINTAL, A.S. (1971b) "A Stochastic Model of Bed Load Transport", Jnl. of Hydr. Res., I.A.H.R., Vol. 9, No. 4, p 527-554.

PARKER, G. (1975) "Sediment Inertia as a Cause of River Antidunes", Jnl. of Hydr. Div., A.S.C.E., Vol. 101, No. HY2, p 211-221.

PAZIS, G.C. and W.H. GRAF. (1977) "Weak Sediment Transport", Jnl. of Hydr. Div., A.S.C.E., Vol. 103, No. HY7, p 799-801.

PEMBERTON, D.G. (1979) "Shingle Management on the Wairoa-Waimea Rivers, Nelson", N.Z. Eng., Jnl. of N.Z.I.E., Vol. 34, No. 5, p 98-101.

PENNINGTON, R.H. (1970) "Introductory Computer Methods and Numerical Analysis", 2nd Ed., Macmillan, London, 497 p.

PONCE, V.M., J.L. GARCIA and D.B. SIMONS. (1979) "Modeling Alluvial Channel Bed Transients", Jnl. of Hydr. Div., A.S.C.E., Vol. 105, No. HY3, p 245-256.

PRIEST, M.S. and A. SHINDALA. (1974) "Channel Changes Downstream from Dams", Water Resources Research Inst., Mississippi State Univ., Mississippi, 4 Composite Papers.

PULS, W., J. SUNDERMANN and H. VOLLMERS. (1977) "A Numerical Approach to Solid Matter Transport Computation", Proc. of 17th Congress, I.A.H.R., Baden-Baden, Vol. 1, Paper A17, p 130-135.

RAICHLEN, F. and J.F. KENNEDY. (1965) "The Growth of Sediment Bedforms from an Initially Flattened Bed", Proc. 11th Congress, I.A.H.R., Leningrad, Vol 3, Paper 3.7, p 1-8.

RAJARATNAM, N. and B. BERRY. (1977) "Erosion by Circular Turbulent Wall Jets", Jnl. of Hydr. Res., I.A.H.R., Vol. 15, No. 3, p 277-289.

RAUDKIVI, A.J. (1963) "Study of Sediment Ripple Formation", Jnl. of Hydr. Div., A.S.C.E., Vol. 89, No HY6, p 15-33.

RAUDKIVI, A.J. (1965) "Turbulence and Vorticity in Loose Boundary Hydraulics", Proc. of 2nd Australasian Conf. on Hydraulics and Fluid Mech., Univ. of Auckland, 6th-11th Dec., p A135-A142.

RAUDKIVI, A.J. (1976) "Loose Boundary Hydraulics", Pergamon Press, 2nd Edition, 397 p.

RICHARDSON, E.V. and D.B. SIMONS. (1973) "Stage Discharge Relations in Sand Channels", Proc. of 15th Congress, I.A.H.R., Istanbul, Vol. 1, Paper A17, p 123-130.

SAKHAN, K.S., J.P. RILEY and K.G. RENARD. (1972) "Hybrid Computer Simulation of Sediment Transport with Stochastic Transfer at the Stream Bed", Sedimentation, Symposium to Honour Prof. H.A. Einstein; H.W. Shen (Ed.), Colorado State Univ., Fort Collins, Chap. 21, 44 p.

SCHLICHTING, H. (1968) "Boundary Layer Theory", 6th Edition, McGraw-Hill, N.Y. 748 p.

SCHOPPMANN, B. (1975) "The Mechanics of Flow and Transport of a Progressive Scour", Proc. of 16th Congress, I.A.H.R., Sao Paulo, Vol. 2, Paper B24, p 189-195.

SHEN, H.W. (Ed.) (1971) "River Mechanics", 2 Vols., Colorado State Univ., Fort Collins.

SHEN, H.W. and H.F. CHEONG. (1977) "Statistical Properties of Sediment Bed Profiles", Jnl. of Hydr. Div., A.S.C.E., Vol. 103, No. HY 11, p 1303-1321.

SHIELDS, A. (1936) "Application of Similarity Principles and Turbulence Research to Bed-Load Movement", Berlin; English Trans. by W.P. Ott and J.C. van Uchelen, Soil Conservation Service, Cal. Inst. Tech. Publ. No. 167.

SIMONS, D.B. and E.V. RICHARDSON. (1961) "Forms of Bed Roughness in Alluvial Channels", Jnl. of Hydr. Div., A.S.C.E., Vol. 87, No. HY3, p 87-105.

SIMONS, D.B., E.V. RICHARDSON and W.L. HAUSHILD. (1962) "Depth Discharge Relations in Alluvial Channels", Jnl. of Hydr. Div., A.S.C.E., Vol. 88, No. HY5, p 57-72.

SIMONS, D.B., E.V. RICHARDSON and C.F. NORDIN, JR. (1965) "Unsteady Movement of Ripples and Dunes Related to Bed-Load Transport", Proc. of 11th Congress, I.A.H.R., Leningrad, Vol. 3, Paper 3.29, 9 p.

SIMONS, D.B. and F. SENTÜRK. (1977) "Sediment Transport Technology", Water Resources Publications, Fort Collins, Colorado, 807 p.

SONI, J.P., R.J. GARDE, and K.G. RANGA RAJU. (1977) "Nonuniform Flow in Aggrading Channels", Jnl. of Waterway, Port, Coastal and Ocean Div., A.S.C.E., Vol. 103, No. WW3, p 321-333.

SPINKS, A.H. and R.J. KELLER. (1976) "An Ultrasonic Depth Meter for Hydraulic Models", Report No. 8-76/1, Central Laboratories, Ministry of Works & Development, N.Z., 22 p.

SUGA, K. (1969) "On the Simulation of River-Bed Variation by Characteristics", Proc. of 13th Congress, I.A.H.R., Kyoto, Vol. 1, Paper A32, p 289-296.

SUTHERLAND, A.J. and G.A. GRIFFITHS. (1975) "Non-steady Bed Load Transport by Translation Waves", Proc. of 16th Congress, I.A.H.R., Sao Paulo, Vol. 2, Paper B25, p 196-203.

TAYLOR, B.D. (1971) "Temperature Effects in Alluvial Streams", W.M. Keck Laboratory of Hydr. and Water Resources, Cal. Inst. Tech., Report No. KH-R-27, 204 p.

THOMAS, W.A. and A.L. PRASUHN. (1977) "Mathematical Modeling of Scour and Deposition", Jnl. of Hydr. Div., A.S.C.E., Vol. 103, No. HY8, p 851-863.

TINNEY, E.R. (1962) "The Process of Channel Degradation", Jnl. of Geophysical Research, Vol. 67, No. 4, p 1475-1480.

de VRIES, M. (1965) "Considerations about Non-Steady Bed-Load Transport in Open Channels", Proc. of 11th Congress, I.A.H.R., Leningrad, Vol. 3, Paper 3.8.

de VRIES, M. (1973) "River-Bed Variations - Aggradation and Degradation", Publ. No. 107, Delft Hydraulics Lab. 20 p.

de VRIES, M. (1975) "A Morphological Time-Scale for Rivers", Proc. of 16th Congress, I.A.H.R., Sao Paulo, Paper B3, p 17-23.

WATKINS, R.D. (1969) "Local Scour in Beds of Sand and Gravel Downstream from a Solid Apron", Civil Eng. Trans., Aust. Inst. of Engrs., Vol. CE 11, No. 1, p 97-106.

WHITE, W.R., H. MILLI and A.D. CRABBE. (1973) "Sediment Transport : An Appraisal of Available Methods", Hydraulics Research Station, Wallingford, 2 Vols., Report No. INT 119.

WILLIAMS, G.P. (1970) "Flume Width and Water Depth Effects in Sediment-Transport Experiments", U.S. Geol. Surv. Prof. Paper No. 562-H, 37 p.

WILLIAMS, P.B. and P.H. KEMP. (1971) "Initiation of Ripples on Flat Sediment Beds", Jnl. of Hydr. Div., A.S.C.E., Vol. 97, No. HY4, p 505-522.

WOLMAN, M.G. (1977) "Changing Needs and Opportunities in the Sediment Field" Water Resources Research, A.G.U., Vol. 13, No. 1, p 50-54.

WU, C.M. (1973) "Unsteady Flow in Open Channel with Movable Bed", Proc. of I.A.H.R. International Symposium on River Mechanics, A.I.T., Bangkok, Vol. 3, Paper C-40.

WU, C.M. (1976) "Movable-Bed Flow Routing in Open Channels and its Calibration", Proc. A.S.C.E. Symposium on Inland Waterways for Navigation, Flood Control and Water Diversions, Rivers '76, Vol. 1, Colorado State Univ., Fort Collins.

YALIN, M.S. (1963) "An Expression for Bed-Load Transportation", Jnl. of Hydr. Div., A.S.C.E., Vol. 89, No. HY3, p 221-250.

YALIN, M.S. (1964) "Geometrical Properties of Sand Waves", Jnl. of Hydr. Div., A.S.C.E., Vol. 90, No. HY5, P 105-119.

YALIN, M.S., (1971) "Theory of Hydraulic Models", Macmillan Co., London, 266 p.

YALIN, M.S. (1975) "On the Development of Sand Waves in Time", Proc. of 16th Congress, I.A.H.R., Sao Paulo, Vol. 2, Paper B27, p 212-219.

YALIN, M.S. (1977) "Mechanics of Sediment Transport", Pergamon Press, 2nd. Edition, 298 p.

YALIN, M.S. and E. KARAHAN. (1979) "Steepness of Sedimentary Dunes", Jnl. of Hydr. Div., A.S.C.E., Vol. 105, No. HY4, p 381-392.

ZNAMENSKAYA, N.S. (1963) "Changes in Forms of River-Bed Sand Dunes with the Passage of a Flood", Soviet Hydrology : Selected Papers, A.G.U., No. 5, p 524-529.

APPENDIX A

EXPERIMENTAL CONSIDERATIONS

A.1 FIXED BED LENGTHS

A fixed bed, whose surface was composed of rounded gravel particles (D_{50} = 4.02 mm), was placed in the upper reach of the working section of the flume (Figure 4.2) to allow the development of the turbulent boundary layer. A similar fixed section was provided at the downstream end to shift backwater effects, associated with the outflow weir, away from the erodible test reach. The gravel particles in these two regions were sprayed with a fluid mixture of cement and water and allowed to harden. These two fixed bed regions were separated from the erodible section by partition boards which were sealed to prevent seepage of water between the fixed and erodible beds.

The minimum fixed bed length upstream was determined using the analogy of the boundary layer growth on a rough plate. For a given maximum flow depth (y) and an equivalent grain roughness ($k_s \simeq 2\ D_{50}$) on the fixed bed, the minimum length of bed could be determined such that the boundary layer thickness (δ) was equal to the flow depth. Combining the coefficient of total skin-friction drag on a rough plate, {Schlichting (1968)}, and the universal velocity distribution for a completely rough region, knowing $y = \delta$ and k_s leads to a minimum distance required for the boundary layer to fully develop, {Griffiths (1976)}.

The vertical velocity profile near the end of the upstream fixed bed was checked with a Pitot tube at the centre line of the

flume channel. It revealed that the boundary layer was indeed fully developed and thus the 6.5 m length of fixed bed downstream of the flow straightening device was deemed to be sufficient for x_R = 9.29 m.

The length of fixed bed in the downstream section was dictated by the position of the bedload collection device, but was sufficient to contain the backwater curve from the submerged outlet weir.

The roughness variation, which may be estimated by Manning's n, from the fixed bed to the erodible bed was small. Using the Manning-Strickler formula

$$n = .013\ D_{65}^{1/6} \qquad \ldots (A.1)$$

where D_{65} is in mm, yields n = .017 for the fixed bed and n = .015 for the stationary plane erodible bed. Owing to the presence of bedforms at the higher flow rates, the roughness of the loose bed will increase to more closely match the roughness of the upstream fixed bed.

A.2 SEDIMENT PROPERTIES

The bed sediment was obtained from a deposit in the Rangitata River. It was sieved to within 1.70-3.35 mm limits. The grain size distribution curve is shown in Figure 4.3. Relevant properties of the sediment include:

(1) Size

D_{50} = 2.11 mm (Fine gravel size)

$D_{84.1}$ = 2.61 mm

$D_{15.9}$ = 1.68 mm

σ_g = 1.25

(2) Specific Gravity

Five samples of the bed sediment were oven dried, placed in a flask, filled with distilled water and boiled in a vacuum desiccator. The results were:

Sample No.	S_s
1	2.76
2	2.75
3	2.74
4	2.75
5	2.74
Mean	2.75

(3) Porosity of the Sediment Bed

Using the formula

$$\gamma_d = (1 - p)\ \rho_s g \qquad \ldots (A.2)$$

and knowing the values of γ_d and ρ_s, the value of the porosity p can be determined. Two determinations produced porosity values of 0.421 and 0.418 to give a mean value of $\bar{p} = 0.42$. Thus the value of the bulk specific dry weight in the bed, $P_s = (1 - p)\ S_s\ \gamma_w$, takes the value $1.565 \times 10^4\ N/m^3$.

(4) Fall Velocity

The mean fall velocity (w) of 50 particles dropped in a tall measuring cylinder was 0.180 m/s, at 15.7 ^oC.

(5) Angle of Repose

The angle of repose of the bed sediment (ϕ) in still water was 35^o.

(6) Particle Shape

The particle shape of the grains is shown in Plate A.1.

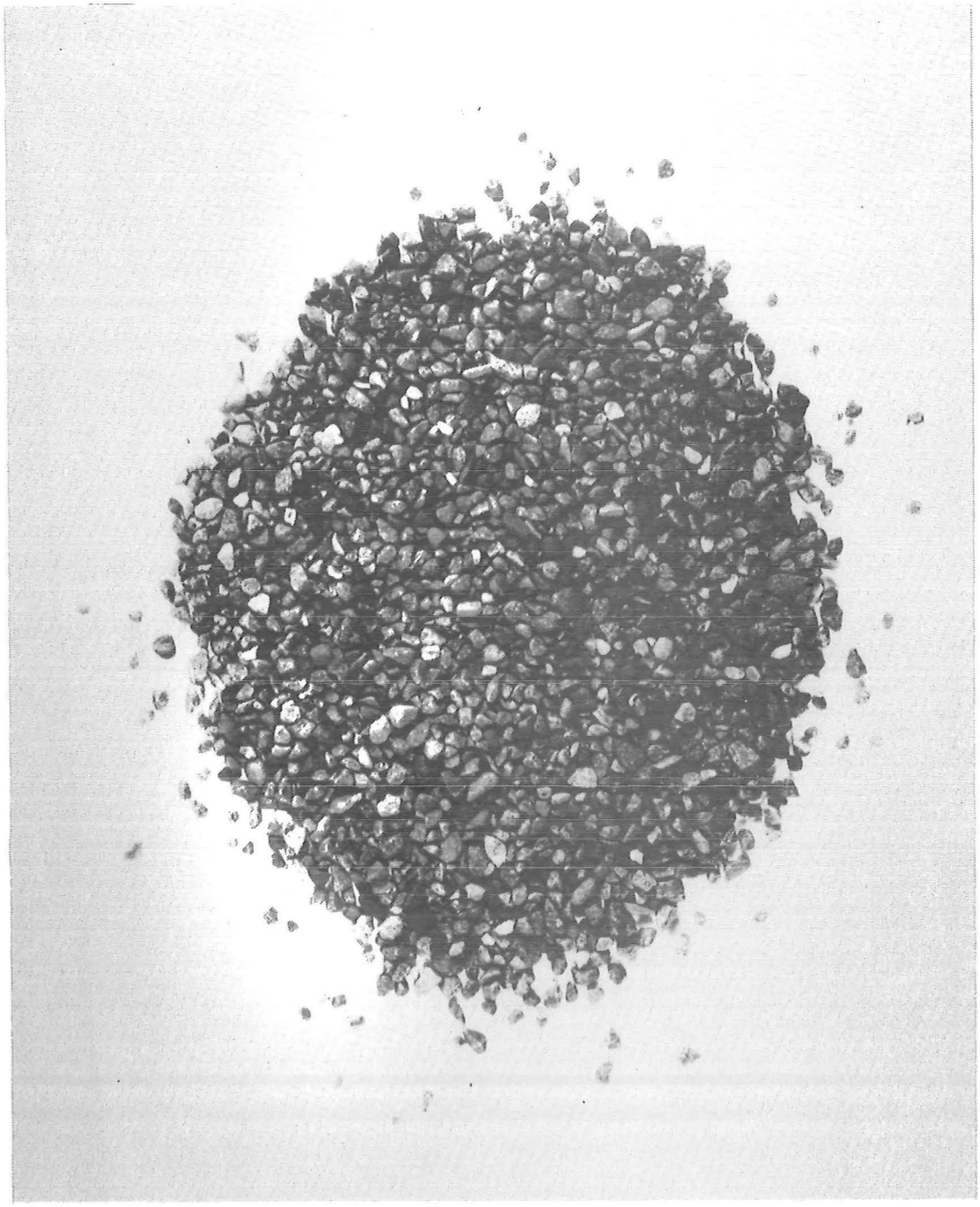

PLATE A.1 : Sediment Grain Shape (D_{50} = 2.11 mm)

APPENDIX B

TIME-SERIES ANALYSIS

B.1 NON-STEADY FLOW BEDLOAD TRANSPORT RATES

The bedload transport rate was sampled during the non-steady flows in a constant temporal order, therefore time series analysis is readily applicable to smooth the original raw data record. To isolate the trend component from the seasonal component, the preferable procedure is to use a centred moving average filter.

The mechanics of this procedure are as follows. A polynomial is fitted to the first 2m+1 measurements, which is termed the phase length, and is used to calculate the trend value at the central (m+1)th data point. The same order polynomial is then fitted to the data points i = 2, 3, ..., 2m+2 to determine the trend value for the (m+2)th data point and so on for the length of the data record. The coefficients for polynomials up to the quintic order have been worked out once and for all and were obtained from tables given by Kendall (1973). The linear polynomial, order one, proved to be the most satisfactory smoothing polynomial, reducing the coefficients to

$$\frac{1}{(2m+1)} \{1_1, 1_2, 1_3, \ldots, 1_{2m+1}\}$$

which sum to unity.

However the algorithm as it stands will not yield trend values for the first and last in values of the time series. Coefficients for the polynomials centred on each of the first and last m points can be obtained by an extension of the method, shown in Kendall (1973),

which effectively fits a straight line through the first and last m points. However the reliability of the trend values in these two end regions decreases, with respect to the central core of the data, as the two extreme end values are approached.

One disadvantage of the centred moving average scheme is the distortion and phase shift of the cyclic oscillations due to bedforms, see Figure B.1. However the bedload yield under the smoothed transport rate curve (Figure B.1) was approximately the same as the actual bedload yield. Figure B.2 shows the moving average scheme applied to a transport rate time series which was measured near the scour pit at x_R = 0.74 m, being much smoother initially because no bedforms were present.

The most suitable phase length for each data record was chosen by trial and error to give the smoothest trend distribution, while at the same time keeping $2m+1 \ll$ record length and $\leqslant$ a bedform wavelength.

B.2 COMPARABLE STEADY FLOW TRANSPORT RATES

So that a smooth curve could be drawn through the comparable steady flow transport rates, a cubic spline piece-wise interpolation algorithm was applied between the points. The algorithm fits a cubic polynomial to small segments between the data points. A necessary constraint is that the first derivative be the same at the end of one segment and at the beginning of an adjacent segment. Details of the procedure including the solution of the simultaneous equations by the Gauss Elimination method are given in Pennington (1970).

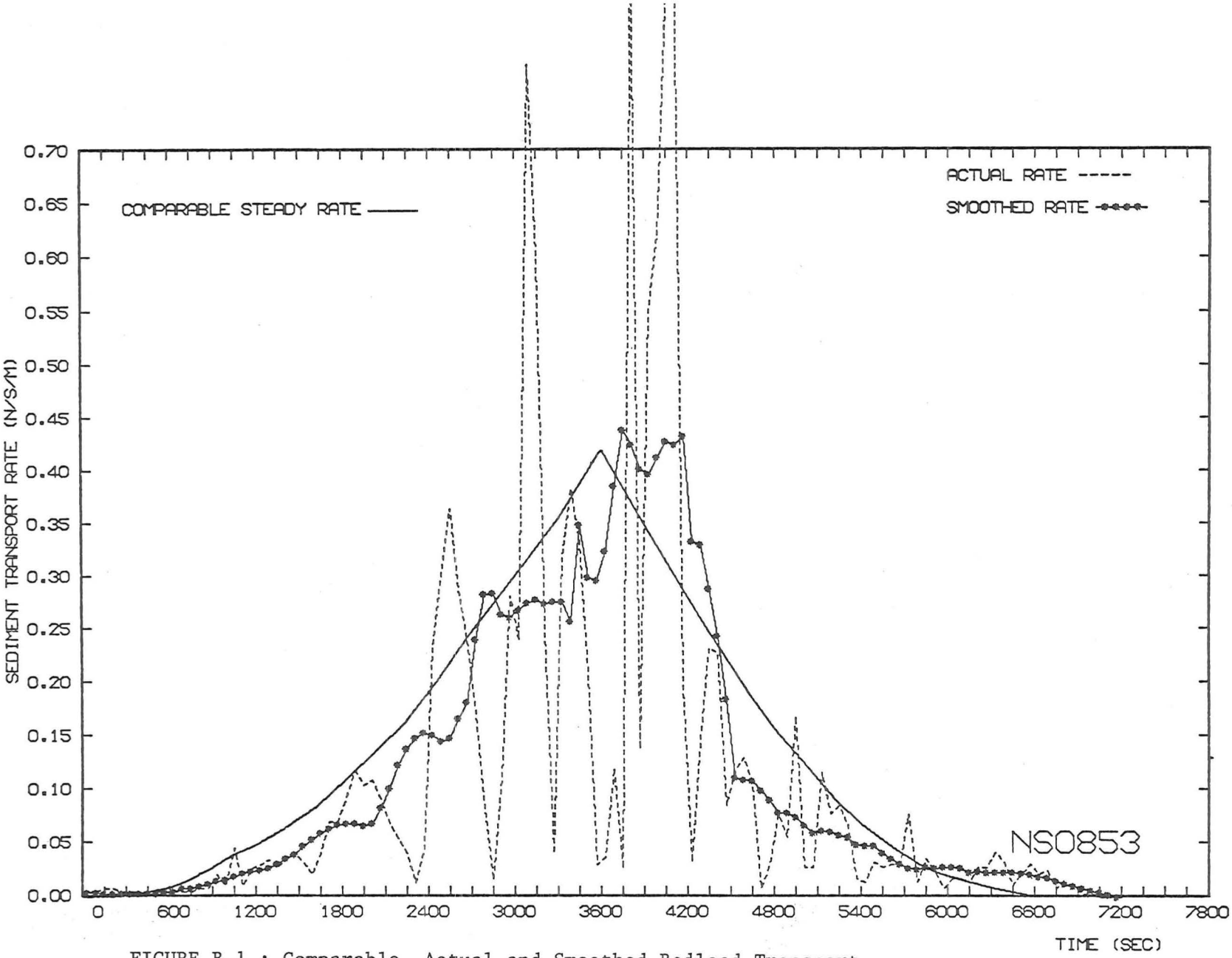

FIGURE B.1 : Comparable, Actual and Smoothed Bedload Transport Rates (NS0853)

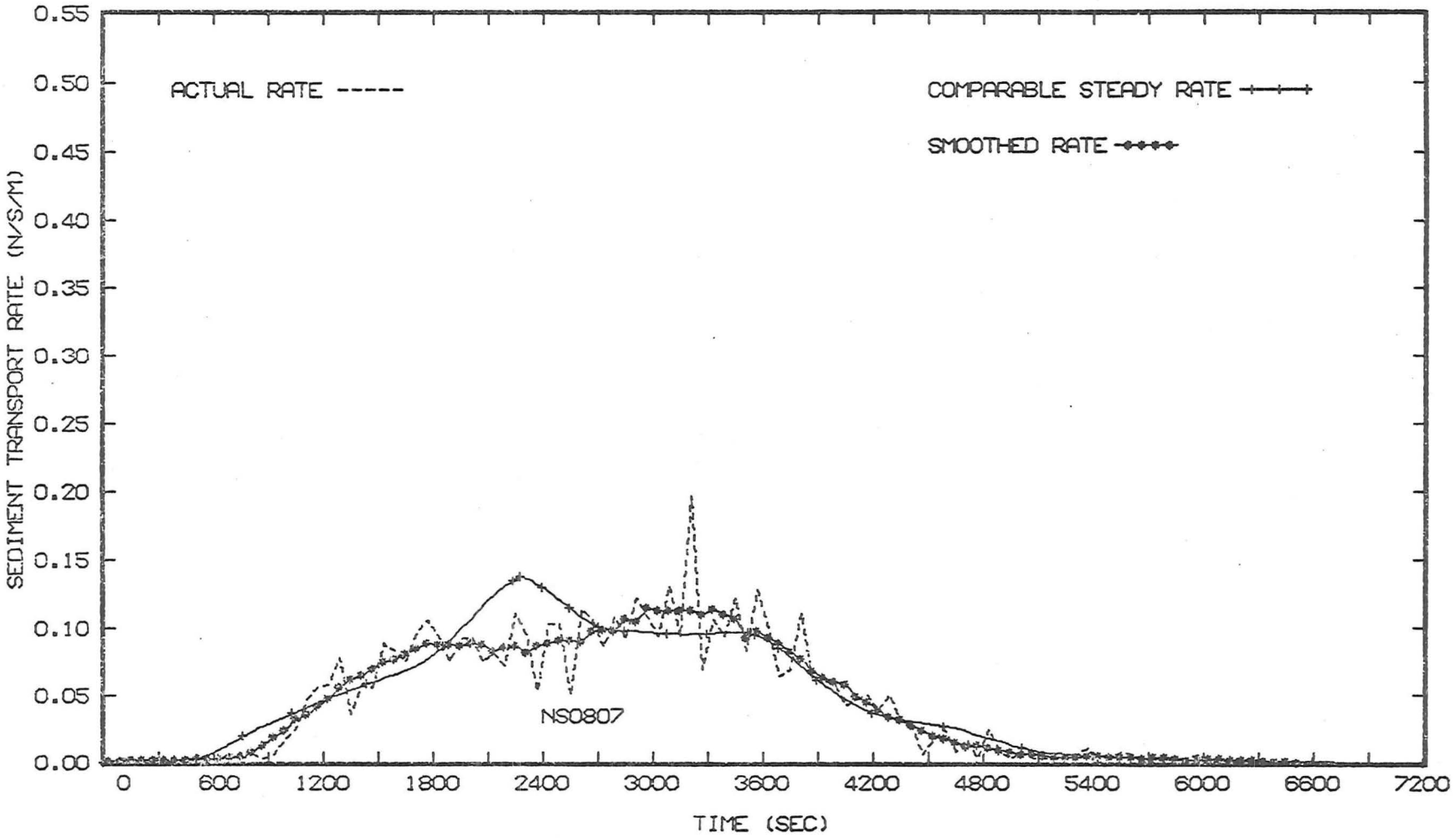

FIGURE B.2 : Comparable, Actual and Smoothed Bedload Transport Rates (NS0807)

APPENDIX C

INITIAL MOTION CRITERIA AND EQUILIBRIUM FORMULAE

C.1 INITIAL MOTION CRITERIA

(1) Shields (1936) {from White, Milli and Crabbe (1973)}

(a) $D_{50} = 2.11$ mm

$$D_{gr} = D_{50} \left[\frac{g(S_s-1)}{\nu^2}\right]^{1/3}$$

$$= 51 \text{ in this case}$$

Thus the Entrainment function value for threshold conditions according to the Shields Curve is

$$Y_c = .0435$$

and the threshold shear velocity is

$$u_{*_b} = .040 \text{ m/s}$$

(b) $D_{50} = 4.02$ mm {Griffiths (1976)}

$$D_{gr} = 95$$

$$Y_c = .056$$

$$u_{*_b} = 0.061 \text{ m/s}$$

(2) Paintal (1971a)

Paintal considered that the point of intersection of his two dimensionless transport rate curves

$$g_s^* = 6.56 \times 10^{18} Y^{16}$$

and

$$g_s^* = 13\ Y^{2.5}$$

represented the initiation of general movement. This occurred at a value of $Y_c = .05$ and $g_s^* = 10^{-2}$.

(3) Neill and Yalin (1969)

The dimensionless erosion rate N was given an arbitrary value of $N = 1.0 \times 10^{-6}$.

C.2 EQUILIBRIUM TRANSPORT FORMULAE

C.2.1 Formulae detailed in White *et al.* (1973)

(a) Einstein-Brown (1950) p.17

(b) Rottner (1959) p.28

(c) Yalin (1963) p.29

(d) Ackers and White (1972) p.41

C.2.2 Other Formulae

(a) Meyer-Peter (1948) - detailed in A.S.C.E. (1975) p. 192.

The formula in S.I. units (N/s/m) is

$$g_s^{2/3} = 1142\ q^{2/3} S_f - 194.9\ D_{50} \qquad \ldots (C.1)$$

(b) Einstein Bed Load Function (1950)

Ref. Einstein (1950)

Since mean velocities were readily calculated from experimental data, the bar-resistance chart to determine u'_{*_b} was bypassed. Instead, equation 48 in White *et al.* (1973)

$$\frac{\bar{u}}{u_{*_b}} = 5.75 \log \left[\frac{12.27\ y}{D_{65}} \cdot \left| \frac{u'_{*_b}}{u_{*_b}} \right|^2 .x\right] \qquad \ldots (C.2)$$

was used to determine u'_{*_b} by iteration.

(c) Paintal (1971b)

Shown in the form of a dimensionless graph, Y versus g_s^*, from Paintal's equation 34.

C.2.3 Prediction of Transport Rates

The transport rate predictions, using the hydraulic and sediment data from the SE Series (Table C.1), of the various equilibrium formulae listed above are shown in Table C.2.

Table C.1 : Hydraulic and Sediment Data

(corrected for side-wall effects, Williams (1970)).

q	y	$\bar{u}$	τ_o	u_{*_b}
$m^3/s/m$	m	m/s	N/m^2	m/s
.070	.116	.603	2.130	.0462
.090	.137	.657	2.487	.0499
.110	.156	.705	2.803	.0529
.130	.173	.750	3.080	.0555
.150	.190	.789	3.352	.0579
.170	.206	.825	3.604	.0600

D_{50} = 2.11 mm, S_s = 2.75, S_o = .0020, Y_c (Shields) = .0435,

$\nu = 1.11 \times 10^{-6}\ m^2/s$

Table C.2 : Transport Rate Predictions

q	g_{se} (N/s/m)							
$m^3/s/m$	A Ackers -White	B Einstein -Brown	M Meyer -Peter	E Einstein	P Paintal	R Rottner	Y Yalin	Eqn. 6.4
.07	.087	.043	-	.0063	.058	.075	.030	.036
.09	.156	.087	.010	.021	.137	.148	.085	.094
.110	.234	.140	.038	.053	.236	.235	.157	.164
.130	.325	.199	.073	.098	.355	.347	.244	.261
.150	.413	.268	.113	.141	.488	.466	.346	.389
.170	.505	.340	.156	.195	.622	.597	.455	.552

APPENDIX D

INITIAL MOTION AND EQUILIBRIUM TRANSPORT RESULTS

D.1 INITIAL MOTION

The data from the initial motion runs (IM Series) is tabulated below in Table D.1. The sidewall correction formula of Williams (1970) was used to correct the shear velocity or bed shear stress. The corrected values of the data from Griffiths (1976), for a similar initial motion study, are also included, where D_{50} = 4.02 mm.

Table D.1 : Initial Motion Results

Run No.	q $m^3/s/m$	y m	$\bar{\theta}$ ^oC	u_{*_b} m/s	Y	n $m^{-2}s^{-1}$	N x 10^{-6}	g_s N/s/m
D_{50} = 2.11 mm	S_s = 2.75	S_o = .0030	$\overline{Re}_*$ = 70					
IM0193	.017	.0411	15.1	.0344	.0327	.694	.190	9.72×10^{-6}
02	.018	.0433	16.0	.0353	.0344	.936	.247	1.44×10^{-5}
03	.020	.0459	13.7	.0363	.0364	1.03	.267	1.73×10^{-5}
04	.021	.0483	14.3	.0372	.0382	2.56	.646	4.66×10^{-5}
05	.023	.0502	15.3	.0378	.0394	2.99	.744	5.86×10^{-5}
06	.024	.0522	13.0	.0386	.0411	5.40	1.31	1.13×10^{-4}
07	.027	.0550	13.3	.0397	.0435	7.89	1.87	1.78×10^{-4}
08	.028	.0563	14.1	.0400	.0442	10.5	2.46	2.64×10^{-4}
IM0993	.030	.0601	14.5	.0414	.0473	15.8	3.59	4.43×10^{-4}

Table D.1 cont.

Run No.	q $m^3/s/m$	y m	$\bar{\theta}$ ^oC	u_{*_b} m/s	Y	n $m^{-2}s^{-1}$	N x 10^{-6}	g_s N/s/m
D_{50} = 2.11 mm S_s = 2.75 S_o = .0020 $\overline{Re}_*$ = 73.5								
IM1093	.036	.0761	16.7	.0378	.0394	3.92	.973	7.68×10^{-5}
IM1193	.038	.0777	16.8	.0381	.0401	5.54	1.37	1.16×10^{-4}
Griffiths (1976) D_{50} = 4.02 mm S_s = 2.68 S_o = .0023 $\overline{Re}_*$ = 200								
G1	.069	.117	16.2	.0497	.0373	.395	.516	-
G2	.085	.132	17.3	.0526	.0418	.969	1.20	-
G3	.095	.141	17.5	.0542	.0443	1.86	2.23	-
G4	.109	.152	17.8	.0561	.0475	4.61	5.34	-
G5	.089	.134	16.1	.0529	.0422	1.08	1.33	-
G6	.100	.143	16.4	.0545	.0448	2.91	3.47	-
G7	.075	.119	16.4	.0501	.0379	.431	.559	-
G8	.068	.112	17.0	.0487	.0358	.253	.337	-
G9	.079	.122	16.9	.0507	.0388	.600	.769	-
G10	.081	.126	16.9	.0514	.0399	.662	.837	-
G11	.116	.159	16.8	.0573	.0496	5.06	5.74	-

$$u_{*_b} = u_* \left[1 + .055(y/B^2)\right]^{-1/2} \quad \text{Williams (1970)}$$

D.2 EQUILIBRIUM TRANSPORT

The data from the SE Series is tabulated in Table D.2, for those runs which met the criteria listed in section 5.4.2.

Table D.2 : Results of SE Series

Run No.	q $m^3/s/m$	y m	$\bar{u}$ m/s	$\bar{\theta}$ ^oC	$\bar{z}_{initial}$ m	$\bar{z}_{final}$ m	g_s (input) N/s/m	g_s (output) N/s/m
SE0193	.071	.1170	.603	16.5	.0893	.0874	.032	.037
02	.087	.1354	.645	15.3	.0899	.0885	.080	.084
03	.101	.1463	.693	15.7	.0893	.0883	.133	.135
04	.116	.1597	.728	16.1	.0890	.0865	.187	.197
05	.122	.1650	.738	15.4	.0887	.0866	.223	.232
06	.131	.1743	.752	17.1	.0893	.0890	.259	.260
07	.142	.1847	.767	17.0	.0893	.0871	.316	.325
08	.142	.1843	.768	14.8	.0899	.0880	.314	.317
09	.142	.1843	.768	15.4	.0895	.0878	.314	.318
SE1093	.148	.1888	.785	15.8	.0897	.0886	.391	.396

$S_o \doteq S_f = .0020$ $D_{50} = 2.1$ mm $S_s = 2.75$

APPENDIX E

STEADY FLOW NON-EQUILIBRIUM TRANSPORT

RESULTS

E.1 MEAN STAGE LEVELS, TRANSPORT RATES AND MEAN BED LEVELS

Table E.1 Results from the ST..93 Series (x_R = 9.29 m)

Run No.	q $m^3/s/m$	$\bar{\theta}$ ^oC	Mean Stage Levels $\bar{h}$ m	t min	$\bar{h}$ m	t min	$\bar{h}$ m	t min
ST0193	.046	15.8	.1800	0	.1800	120	-	-
2	.056	17.2	.1915	10	.1916	125	-	-
3	.068	17.4	.2054	0	.2055	80	-	-
4	.082	18.5	.2209	0	.2210	17	.2211	73
5	.097	17.8	.2367	15	.2368	65	.2370	117
6	.111	18.9	.2501	0	.2504	25	.2508	75
7	.127	17.0	.2637	0	.2638	15	.2649	110
8	.140	18.9	.2740	0	.2749	20	.2756	50
ST0993	.159	18.8	.2897	9	.2921	56	-	-

$\bar{g}_s(t)$ (N/s/m) (Dry Weight)

Run No.	Time (min) 5	15	25	35	45	55	65	75	85	95	105	115
ST0193	.004		.004					.004				.004
2	.020		.021			.021				.020		.019
3	.034		.033		.033		.033		.032	.031	.029	.027
4	.061	.060		.059			.057	.055	.052	.050	.048	.047
5	.115		.114			.112		.107		.101	.098	.094

Table E.1 cont.

Run No.	Time (min) 5	15	25	35	45	55	65	75	85	95	105	115
6	.163		.161		.157		.153		.144	.135	.125	.117
7	.246		.241		.238		.217	.200	.177	.156	.135	
8	.318		.314		.305		.271	.244	.219	.189		
ST0993	.446		.428	.403	.382	.348	.314					

Table E.2 : Results from the ST..53 Series (x_R = 5.29 m)

Run No.	q $m^3/s/m$	$\bar{\theta}$ ^oC	Mean Stage Levels $\bar{h}$ m	t min	$\bar{h}$ m	t min	$\bar{h}$ m	t min
STO153	.045	16.3	.1838	12	.1838	58	-	-
2	.056	16.6	.1955	14	.1956	75	-	-
3	.067	16.0	.2097	21	.2096	117	-	-
4	.082	16.7	.2247	19	.2249	68	.2254	117
5	.097	17.6	.2400	0	.2402	27	.2409	117
6	.111	15.5	.2527	0	.2540	66	.2551	115
7	.127	16.8	.2672	0	.2677	20	.2691	99
8	.139	16.8	.2781	4	.2799	65	.2804	111
STO953	.160	17.7	.2956	0	.2965	20	.2981	53

$\bar{g}_s(t)$ (N/s/m) (Dry Weight)

Run No.	Time (min) 5	15	25	35	45	55	65	75	85	95	105	115
STO153	.006		.006		.005				.005		.004	
2	.017		.015		.016		.014		.013			.011
3	.040		.035		.030		.026		.025		.022	.020
4	.066	.065	.062		.057		.053		.045	.043	.040	.038
5	.113		.110	.100	.091		.083		.080		.078	.075
6	.164		.161		.156		.145	.137	.128	.116	.112	.104
7	.244		.238		.217	.203	.190	.177	.165	.152	.141	
8	.305		.296		.265	.248	.231	.217	.204	.193	.183	
STO953	.450		.403	.358	.325	.300	.285	.278				

Table E.3 : Results from the ST..35 Series (x_R = 3.53 m)

Run No.	q $m^3/s/m$	$\bar{\theta}$ ^oC	Mean Stage Levels $\bar{h}$ m	t min	$\bar{h}$ m	t min	$\bar{h}$ m	t min
ST0135	.046	17.8	.1859	13	-	-	-	-
2	.055	18.1	.1970	12	.1973	24	.1977	82
3	.067	19.0	.2107	7	.2114	85	-	-
4	.081	14.6	.2273	12	.2274	79	.2277	123
5	.097	16.0	.2418	22	.2429	58	.2437	122
6	.111	17.6	.2544	0	.2546	19	.2568	101
7	.127	17.5	.2694	0	.2719	65	.2731	120
8	.139	15.1	.2806	8	.2849	65	.2862	115
ST0935	.160	18.3	.2975	0	.3003	21	.3035	87

$\bar{g}_s(t)$ (N/s/m) (Dry Weight)

Run No.	Time (min) 5	15	25	35	45	55	65	75	85	95	105	115
ST0135	.004		.004									
2	.016		.015		.013		.012		.013		.012	.012
3	.034	.031	.028	.023	.021	.019	.018	.017		.015		.014
4	.063	.060	.058	.056	.054		.054		.046		.039	.036
5	.118	.115	.109	.105	.102		.099		.090	.083	.075	.064
6	.167	.165	.162	.159	.155	.149	.140	.130	.115	.104	.095	.086
7	.242	.238	.234	.225	.212	.195	.176	.161	.144	.131	.120	.111
8	.294	.286	.277	.268	.255	.243	.212	.186	.159	.138	.130	.124
ST0935	.450	.422	.378	.338	.299	.263	.235	.212	.198			

Table E.4 : Results from the ST..17 Series (x_R = 1.74 m)

Run No.	q $m^3/s/m$	$\bar{\theta}$ ^oC	Mean Stage Levels $\bar{h}$ m	t min	$\bar{h}$ m	t min	$\bar{h}$ m	t min
ST0117	.046	13.4	.1879	8	.1877	105	-	-
2	.056	15.3	.2015	8	.2019	95	-	-
3	.067	15.6	.2145	11	.2148	73	.2151	116
4	.082	16.8	.2303	17	.2309	82	.2311	114
5	.098	17.8	.2474	23	.2478	63	.2483	115
6	.111	17.2	.2601	18	.2617	63	.2619	111
7	.127	18.7	.2747	19	.2757	50	.2761	112
8	.140	15.5	.2854	13	.2873	63	.2881	113
ST0917	.160	16.6	.2970	4	.2999	20	.3051	122

$\bar{g}_s(t)$ (N/s/m) (Dry Weight)

Run No.	Time (min) 5	15	20	25	35	45	55	65	75	85	95	115
ST0117	.004			.003		.004		.003		.003	.002	.002
2	.018			.018		.018		.016		.014	.013	.010
3	.035			.035	.032	.030	.025	.022	.018	.015	.014	.014
4	.064			.061	.054	.045	.035	.030	.028	.026	.024	.021
5	.121	.111	.099	.086	.065	.059	.046	.039	.034	.030	.024	.020
6	.167	.165	.160	.151	.111	.084	.061	.055	.049	.046	.041	.035
7	.247	.234	.216	.181	.115	.090	.076	.065	.059	.054	.047	.043
8	.309	.278	.246	.188	.128	.105	.090	.079	.071	.065	.061	.058
ST0917	.452	.407	.333	.221	.164	.131	.115	.105	.096	.087	.082	.071

Table E.5 : Results from the ST..07 Series (x_R = 0.74 m)

Run No.	q $m^3/s/m$	$\bar{\theta}$ °C	Mean Stage Levels $\bar{h}$ m	t min	$\bar{h}$ m	t min	$\bar{h}$ m	t min
ST0107	.047	15.4	.1884	6	.1884	71	.1883	109
2	.056	17.1	.1995	7	.1999	72	-	-
3	.067	17.8	.2118	10	.2118	52	.2123	100
4	.082	16.1	.2282	14	.2286	69	.2288	119
5	.098	15.9	.2444	14	.2448	63	.2451	116
6	.111	16.9	.2577	10	.2583	64	.2589	113
7	.127	16.2	.2734	14	.2739	73	.2743	112
8	.140	16.0	.2853	14	.2861	54	.2854	112
ST0907	.159	16.9	.2974	4	.3003	67	.2997	92

$\bar{g}_s(t)$ (N/s/m) (Dry Weight)

Run No.	Time (min) 1	5	10	15	20	25	30	35	55	75	95	115
ST0107		.005		.004		.004		.003	.003	.003	.003	.003
2		.017	.015	.012	.013	.011		.009	.009	.006	.006	.006
3		.037	.035	.030	.025	.020	.017	.016	.013	.013	.015	.014
4		.069	.054	.039	.032	.026	.022	.022	.019	.018	.017	.018
5		.118	.096	.069	.054	.045	.036	.031	.021	.015	.012	.011
6	.170	.165	.127	.072	.053	.044	.039	.033	.024	.017	.015	.012
7	.241	.210	.135	.082	.060	.050	.048	.042	.034	.030	.025	.024
8	.293	.267	.208	.110	.083	.067	.058	.051	.035	.030	.026	.019
ST0907	.445	.371	.162	.109	.080	.060	.055	.049	.041	.034	.027	

TABLE E. 6 : MEAN BED LEVELS FOR REACH LENGTH = 9.29 M

RUN NO.	MEAN BED LEVEL ($\bar{Z}$) (M) TIME (MIN)										
ST0193	0.0898	0.0896	0.0885	0.0886	0.0883	0.0882					
	ORIG.	0.0	31.5	61.5	91.5	120.0					
ST0293	0.0907	0.0905	0.0902	0.0900	0.0897	0.0900	0.0889	0.0886	0.0878	0.0879	
	ORIG.	0.0	6.5	16.5	36.5	46.5	61.5	76.5	106.5	120.0	
ST0393	0.0902	0.0901	0.0899	0.0890	0.0890	0.0885	0.0872	0.0865	0.0863	0.0854	0.0862
	ORIG.	0.0	11.5	21.5	31.5	46.5	59.5	76.5	92.5	106.5	122.5
ST0493	0.0902	0.0888	0.0879	0.0867	0.0855	0.0862	0.0848	0.0839	0.0826	0.0822	0.0819
	ORIG.	0.0	6.5	11.5	23.5	31.5	46.5	59.5	81.5	91.5	119.5
ST0593	0.0899	0.0885	0.0871	0.0870	0.0865	0.0835	0.0826	0.0814	0.0808	0.0795	0.0793
	ORIG.	0.0	6.5	11.5	21.5	40.5	61.5	76.5	91.5	106.5	122.0
ST0693	0.0899	0.0886	0.0862	0.0858	0.0831	0.0823	0.0787	0.0778	0.0761	0.0761	
	ORIG.	0.0	6.5	11.5	16.5	31.5	46.5	91.5	106.5	120.0	
ST0793	0.0907	0.0890	0.0872	0.0853	0.0831	0.0812	0.0805	0.0788	0.0763	0.0748	0.0741
	ORIG.	0.0	6.5	12.5	17.5	32.5	46.5	63.5	76.5	91.5	106.5
ST0893	0.0903	0.0916	0.0881	0.0863	0.0848	0.0826	0.0797	0.0781	0.0742		
	ORIG.	0.0	8.5	13.5	28.5	43.5	59.5	71.5	98.0		
ST0993	0.0912	0.0919	0.0906	0.0861	0.0815	0.0788	0.0787	0.0735			
	ORIG.	0.0	6.5	11.5	16.5	31.5	46.5	60.0			

TABLE E. 7 : MEAN BED LEVELS FOR REACH LENGTH = 5.29 M

RUN NO.	MEAN BED LEVEL ($\bar{Z}$) (M) TIME (MIN)										
ST0153	0.0950	0.0942	0.0942	0.0936	0.0936	0.0935	0.0934				
	ORIG.	0.0	6.5	31.5	61.5	92.5	120.0				
ST0253	0.0951	0.0942	0.0934	0.0935	0.0932	0.0926	0.0917	0.0916	0.0913	0.0911	
	ORIG.	0.0	6.5	16.5	26.5	47.5	61.5	77.5	91.5	120.0	
ST0353	0.0946	0.0935	0.0923	0.0915	0.0903	0.0899	0.0895	0.0889	0.0876	0.0871	0.0863
	ORIG.	0.0	6.5	11.5	31.5	46.5	66.5	76.5	92.5	106.5	121.0
ST0453	0.0950	0.0931	0.0918	0.0902	0.0903	0.0893	0.0878	0.0857	0.0852	0.0838	0.0834
	ORIG.	0.0	6.5	11.5	16.5	31.5	46.5	76.5	91.5	106.5	120.0
ST0553	0.0943	0.0919	0.0909	0.0902	0.0894	0.0872	0.0861	0.0846	0.0833	0.0827	0.0818	0.0797
	ORIG.	0.0	6.5	11.5	16.5	31.5	46.5	61.5	76.5	91.5	106.5	120.0
ST0653	0.0948	0.0925	0.0909	0.0899	0.0886	0.0856	0.0832	0.0821	0.0796	0.0784	0.0773	0.0755
	ORIG.	0.0	6.5	11.5	16.5	31.5	46.5	61.5	76.5	91.5	106.5	120.0
ST0753	0.0947	0.0930	0.0891	0.0884	0.0870	0.0841	0.0818	0.0792	0.0765	0.0750	0.0738	
	ORIG.	0.0	6.5	11.5	16.5	31.5	46.5	61.5	77.5	91.5	106.5	
ST0853	0.0934	0.0924	0.0894	0.0878	0.0864	0.0831	0.0778	0.0757	0.0739	0.0725		
	ORIG.	0.0	6.5	11.5	16.5	31.5	61.5	76.5	91.5	106.5		
ST0953	0.0942	0.0928	0.0883	0.0874	0.0858	0.0805	0.0765	0.0747	0.0715			
	ORIG.	0.0	6.5	11.5	16.5	31.5	50.5	61.5	76.5			

TABLE E. 8 : MEAN BED LEVELS FOR REACH LENGTH = 3.53 M

RUN NO.	MEAN BED LEVEL ($\bar{Z}$) (M) TIME (MIN)											
ST0135	0.0957 ORIG.	0.0953 0.0	0.0946 34.5									
ST0235	0.0958 ORIG.	0.0947 0.0	0.0945 16.5	0.0935 47.5	0.0934 61.5	0.0933 76.5	0.0924 91.5	0.0922 106.5	0.0919 121.5			
ST0335	0.0953 ORIG.	0.0939 0.0	0.0931 16.5	0.0922 29.5	0.0916 51.5	0.0913 61.5	0.0901 76.5	0.0898 91.5	0.0888 106.5	0.0885 121.5		
ST0435	0.0952 ORIG.	0.0932 0.0	0.0922 6.5	0.0910 16.5	0.0895 31.5	0.0887 47.5	0.0880 61.5	0.0864 76.5	0.0855 91.5	0.0840 106.5	0.0838 121.5	
ST0535	0.0947 ORIG.	0.0930 0.0	0.0911 6.5	0.0897 11.5	0.0894 16.5	0.0882 31.5	0.0875 46.5	0.0861 61.5	0.0835 79.5	0.0815 91.5	0.0801 106.5	0.0791 121.5
ST0635	0.0950 ORIG.	0.0936 0.0	0.0916 6.5	0.0890 12.5	0.0883 16.5	0.0864 31.5	0.0833 46.5	0.0816 61.5	0.0795 76.5	0.0779 91.5	0.0767 106.5	0.0752 121.5
ST0735	0.0950 ORIG.	0.0939 0.0	0.0911 6.5	0.0884 11.5	0.0873 16.5	0.0857 31.5	0.0815 46.5	0.0783 61.5	0.0754 78.5	0.0739 91.5	0.0717 106.5	0.0704 121.5
ST0835	0.0951 ORIG.	0.0939 0.0	0.0920 6.5	0.0886 11.5	0.0879 16.5	0.0835 31.5	0.0793 46.5	0.0758 61.5	0.0734 78.5	0.0718 91.5	0.0692 106.5	0.0662 121.5
ST0935	0.0935 ORIG.	0.0924 0.0	0.0892 6.5	0.0872 11.5	0.0857 16.5	0.0790 31.5	0.0745 46.5	0.0697 61.5	0.0663 76.5	0.0629 91.5		

TABLE E. 9 : MEAN BED LEVELS FOR REACH LENGTH = 1.74 M

RUN NO.	MEAN BED LEVEL ($\bar{Z}$) (M) TIME (MIN)											
ST0117	0.0967 ORIG.	0.0963 0.0	0.0961 31.5	0.0958 61.5	0.0955 91.5	0.0952 121.5						
ST0217	0.0978 ORIG.	0.0973 0.0	0.0960 16.5	0.0950 31.5	0.0942 47.5	0.0937 61.5	0.0929 76.5	0.0923 91.5	0.0917 106.5	0.0915 121.5		
ST0317	0.0973 ORIG.	0.0962 0.0	0.0954 6.5	0.0929 16.5	0.0902 31.5	0.0883 46.5	0.0873 61.5	0.0864 76.5	0.0853 91.5	0.0843 107.5	0.0837 121.5	
ST0417	0.0985 ORIG.	0.0962 0.0	0.0935 6.5	0.0923 11.5	0.0902 16.5	0.0868 31.5	0.0843 46.5	0.0826 61.5	0.0811 76.5	0.0799 92.5	0.0790 106.5	0.0780 121.5
ST0517	0.0976 ORIG.	0.0949 0.0	0.0910 6.5	0.0883 11.5	0.0870 16.5	0.0819 31.5	0.0790 46.5	0.0770 61.5	0.0756 76.5	0.0744 91.5	0.0729 106.5	0.0725 121.5
ST0617	0.0973 ORIG.	0.0966 0.0	0.0913 6.5	0.0873 11.5	0.0840 16.5	0.0795 31.5	0.0751 46.5	0.0726 61.5	0.0713 76.5	0.0704 91.5	0.0690 106.5	0.0680 121.5
ST0717	0.0970 ORIG.	0.0955 0.0	0.0880 6.5	0.0841 11.5	0.0808 16.5	0.0745 31.5	0.0722 46.5	0.0689 61.5	0.0672 76.5	0.0659 91.5	0.0643 106.5	0.0627 121.5
ST0817	0.0965 ORIG.	0.0952 0.0	0.0864 6.5	0.0830 11.5	0.0791 16.5	0.0727 31.5	0.0689 46.5	0.0662 61.5	0.0640 76.5	0.0625 91.5	0.0607 106.5	0.0586 121.5
ST0917	0.0968 ORIG.	0.0958 0.0	0.0852 6.5	0.0795 11.5	0.0744 16.5	0.0671 31.5	0.0628 46.5	0.0592 61.5	0.0561 76.5	0.0545 91.5	0.0524 106.5	0.0505 121.5

TABLE E.10 : MEAN BED LEVELS FOR REACH LENGTH = 0.74 M

RUN NO.	MEAN BED LEVEL ($\bar{Z}$) (M) TIME (MIN)										
ST0107	0.0993 ORIG.	0.0994 0.0	0.0990 16.0	0.0986 31.0	0.0983 46.0	0.0979 61.0	0.0980 76.0	0.0979 91.0	0.0977 120.0		
ST0207	0.0965 ORIG.	0.0965 0.0	0.0936 16.0	0.0916 31.0	0.0898 46.0	0.0875 76.0	0.0872 91.0	0.0860 106.0	0.0857 120.0		
ST0307	0.0994 ORIG.	0.0974 0.0	0.0942 6.0	0.0919 11.0	0.0907 16.0	0.0888 31.0	0.0863 46.0	0.0841 61.0	0.0834 76.0	0.0817 106.0	0.0808 120.0
ST0407	0.0991 ORIG.	0.0967 0.0	0.0926 6.0	0.0898 11.0	0.0881 16.0	0.0845 31.0	0.0820 46.0	0.0809 61.0	0.0798 76.0	0.0782 106.0	0.0772 120.0
ST0507	0.0998 ORIG.	0.0988 0.0	0.0908 6.0	0.0871 11.0	0.0849 16.0	0.0800 31.0	0.0770 43.0	0.0744 64.0	0.0732 76.0	0.0719 91.0	0.0707 106.0	0.0700 120.0
ST0607	0.0988 ORIG.	0.0962 0.0	0.0856 6.0	0.0813 11.0	0.0787 16.0	0.0746 31.0	0.0718 46.0	0.0703 61.0	0.0680 76.0	0.0663 91.0	0.0660 107.0	0.0653 120.0
ST0707	0.0974 ORIG.	0.0963 0.0	0.0849 6.0	0.0792 11.0	0.0763 16.0	0.0721 31.0	0.0689 46.0	0.0674 61.0	0.0655 76.0	0.0639 91.0	0.0620 123.0	
ST0807	0.1003 ORIG.	0.0972 0.0	0.0860 6.0	0.0785 11.0	0.0750 16.0	0.0700 31.0	0.0668 46.0	0.0649 61.0	0.0629 76.0	0.0615 91.0	0.0589 120.0	
ST0907	0.1012 ORIG.	0.0982 0.0	0.0795 6.0	0.0734 11.0	0.0699 16.0	0.0673 21.0	0.0641 31.0	0.0611 46.0	0.0583 61.0	0.0557 76.0	0.0522 106.0	

E.2 MAXIMUM SCOUR HOLE DEPTH (ST...53 SERIES)

Table E.11 : Results of Maximum Scour Depths

Run No.											
	d_{max} (mm)										
	t (sec)										
ST0253	2.2	2.9	3.7	4.4	5.9	6.6	7.3	8.0	8.8	8.8	
	60	330	945	1545	2805	3645	4605	5445	6345	7200	
ST0353	3.6	5.9	7.3	8.8	11.0	12.5	13.2	13.9	14.7	15.4	16.9
	60	330	630	945	1845	2745	3945	4545	5505	6345	7260
ST0453	4.1	8.8	12.4	13.2	17.6	21.2	23.4	24.9	25.6	25.6	
	60	330	630	945	1845	2745	4545	5445	6345	7200	
ST0553	4.1	11.7	15.4	17.8	22.5	24.2	25.7	27.9	30.1	31.0	32.3
	60	330	630	945	1845	2745	3645	4545	5445	6345	7200
ST0753	2.2	15.6	22.0	25.7	32.0	35.0	37.4	40.4	42.6	44.0	
	60	330	630	945	1845	2745	3645	4605	5445	6345	
ST0953	4.4	22.0	29.4	33.0	38.2	44.0	48.4	49.9			
	60	360	660	960	1860	3000	3660	4560			

E.3 COMPARISON PROCEDURE RESULTS (SECTION 3.3.2)

Table E.12 : Results of Comparison Procedure (Figure 3.9)

	Measured		Derived		
Run No.	x m	$\bar{t}$ min	$\bar{g}_s(x,t)$ N/s/m	$\bar{u}=q/y(x,t)$ m/s	$g_{se}(x,t)$ N/s/m
ST0653	0.3	2.5	.114	.661	.096
		7.5	.045	.633	.067
		12.5	.035	.619	.052
		22.5	.012	.600	.034
		37.5	.010		-
	0.4	2.5	.129	.660	.095
		7.5	.065	.636	.070
		12.5	.050	.617	.050
		22.5	.020	.597	.032
		37.5	.013		-
ST0753	0.3	2.5	.180	.714	.178
		7.5	.063	.668	.105
		12.5	.034	.649	.082
		22.5	.022	.621	.058
		37.5	.010	.607	.040
	0.4	2.5	.239	.716	.183
		7.5	.093	.675	.114
		12.5	.049	.653	.087
		22.5	.034	.630	.063
		37.5	.014	.611	.045
ST0893	0.3	3.5	.125	.721	.191
		9.5	.058	.690	.135
		19.5	.023	.659	.093
		34.5	.016	.650	.084
	0.4	3.5	.171	.728	.208
		9.5	.072	.688	.132
		19.5	.032	.656	.090
		34.5	.021	.651	.084
ST0993	0.3	2.5	.315	.772	.332
		7.5	.067	.713	.177
		12.5	.035	.690	.135
		22.5	.018	.672	.110
		37.5	.009	.660	.095
	0.4	2.5	.391	.774	.340
		7.5	.106	.722	.193
		12.5	.049	.696	.145
		22.5	.029	.675	.113
		37.5	.014	.659	.093

Table E.12 cont.

Measured			Derived		
Run No.	x m	$\bar{t}$ min	$\bar{g}_s(x,t)$ N/s/m	$\bar{u}=q/y(x,t)$ m/s	$g_{se}(x,t)$ N/s/m
ST0907 ($g_s(x,t)$ measured	0.74	5	.371	.782	.367
		15	.109	.709	.169
		30	.055	.680	.120
		45	.044	.669	.105
		105	.025	.637	.071

Table E.13 : Dimensionless Transport Rates

$\bar{q}$	t	$\bar{g}_s/g_{se_o}$ $\bar{g}_s/g_{se}(x,t)$						
$m^3/s/m$	min	0.2 m	0.4 m	0.74 m	1.74 m	3.53 m	5.29 m	9.29 m
.159	5	.184	.540	.815	.975	.973	.970	.977
		.440	.980	1.00				
	10	.048	.153	.357	.938	.949	.957	.974
		.144	.436	.790	.998			
	15	.033	.091	.239	.878	.912	.941	.970
		.122	.310	.708	.970	.990		
	30	.014	.043	.122	.401	.774	.815	.908
		.057	.197	.504	.832	.990		
	60	.010	.020	.085	.236	.533	.628	.738
		.052	.116	.395	.690	.962	.991	
					$\bar{g}_s/g_{se_o}$			
.127	5	.266	.550	.857	.999	.996	1.001	1.008
	10	.102	.278	.554	.987	.988	.998	1.002
	15	.057	.183	.337	.947	.978	.996	.996
	30	.034	.091	.195	.583	.946	.955	.985
	60	.011	.034	.132	.283	.761	.802	.921
	90	.008	.025	.109	.205	.560	.644	.690

E.4 DUNE BEDFORM PROPERTIES

Table E.14 : Dune Heights, Wavelengths and Steepness

q ($m^3/s/m$)	y (m)	λ_d (m)	Δ_d (mm)	S_d	$\frac{\tau_o}{\tau_c}$
		1.7	7	.0041	
.068	.1164				1.60
		1.5	5.5	.0037	
		1.5	6	.0040	
	.1316	1.0	7	.0070	1.84
		-	9	-	
		1.8	11	.0061	
	.1341				1.74
		1.43	10	.0070	
		1.44	11	.0076	
.082	.1342	1.20	6	.0050	1.84
		1.70	9	.0053	
		2.0	9	.0045	
	.1360	1.3	6	.0046	1.68
		-	11	-	
		1.30	6	.0046	
	.1364	1.40	13	.0093	1.77
		1.25	7	.0056	
		1.25	13	.0104	
		1.25	12	.0096	
	.1481	1.20	13	.0108	2.01
		1.40	14	.0100	
		1.60	11	.0069	
		1.05	10	.0095	
		-	16	-	
.097	.1493	1.31	10	.0076	2.02
		1.16	9	.0078	
		1.7	13	.0076	
		1.7	13	.0076	
	.1524	0.8	10	.0125	1.89
		-	12	-	

Table E.14 cont.

q ($m^3/s/m$)	y (m)	λ_d (m)	Δ_d (mm)	S_d	$\frac{\tau_o}{\tau_c}$
		-	15	-	
	.1598				2.17
		1.59	15	.0094	
		1.30	16	.0123	
		1.15	13	.0113	
		1.0	13	.0130	
.111	.1663	1.5	15	.0100	2.10
		1.13	12	.0106	
		-	12	-	
		1.6	16	.0100	
	.1702	1.95	23	.0118	2.00
		1.1	10	.0091	
		1.33	15	.0113	
	.1755				2.34
		.87	13	.0149	
		1.25	20	.0160	
	.1765				2.21
		.98	12	.0122	
		1.05	12	.0114	
		1.35	17	.0126	
	.1768	1.53	22	.0143	2.35
		.96	12	.0125	
.127					
		1.56	18	.0115	
	.1796				2.27
		1.79	17	.0095	
		1.55	19	.0123	
	.1827				2.19
		-	14	-	
		1.45	13	.0090	
		1.68	17	.0101	
		1.10	13	.0118	
	.1838	1.18	12	.0102	2.15
		1.53	19	.0124	
		1.44	15	.0104	

Table E.14 cont.

q ($m^3/s/m$)	y (m)	λ_d (m)	Δ_d (mm)	S_d	$\frac{\tau_o}{\tau_c}$
		1.02	18	.0176	
		.84	20	.0238	
	.1858	1.12	14	.0125	2.48
		1.5	23	.0153	
		1.0	20	.0200	
	.1862	1.3	25	.0192	2.44
.140					
		1.47	26	.0177	
	.1884	1.45	23	.0159	2.41
		1.03	14	.0136	
		1.45	22	.0152	
	.1921	1.55	17	.0110	2.29
		1.20	19	.0158	
		1.07	20	.0187	
	.2049	1.08	26	.0241	2.62
		-	16	-	
		0.8	17	.0213	
	.2078				2.55
		-	20	-	
		1.47	24	.0163	
.159		1.51	24	.0159	
	.2081	1.15	30	.0261	2.66
		1.83	30	.0164	
		1.87	22	.0118	
		1.11	15	.0135	
		1.0	22	.0220	
		.95	18	.0189	
	.2085	.85	16	.0188	2.68
		.95	20	.0210	
		1.20	30	.0250	

Table E.15 : Dune Celerities

C_d mm/s	$\bar{u}$ m/s	C_d mm/s	$\bar{u}$ m/s
1.07	.580	1.75	.693
1.42	.653	1.90	.668
1.47	.600	2.06	.718
1.50	.655	2.27	.751
1.61	.655	2.34	.740
1.70	.676	2.38	.748
2.66	.715	2.85	.766

APPENDIX F

NON-STEADY FLOW NON-EQUILIBRIUM TRANSPORT RESULTS

F.1 STEP CHANGE IN DISCHARGE

Table F.1 : Temporal Lags and Transport Rate Deficits

Run No.	q $m^3/s/m$	Δq $m^3/s/m$	G_{ST} N/m	G_{SC} N/m	t^* min	Δg_s^* N/s/m
			x_R = 9.29 m			
SC0193	.046	.016	-	-	75	-
02	.056	.026	61	35	51.5	.006
03	.068	.038	70	38	35.3	.009
04	.082	.052	95	71	23.3	.006
05	.097	.067	156	92	22.3	.019
06	.111	.081	149	103	15.3	.024
07	.128	.098	197	122	13.3	.042
08	.140	.110	241	143	12.8	.064
SC0993	.160	.130	247	149	9.3	.126
			x_R = 1.74 m			
SC0217	.055	.025	55	23	51.5	.007
03	.066	.036	79	35	40.3	.017
04	.081	.051	92	46	24.8	.023
05	.096	.066	118	55	17.3	.062
06	.111	.081	158	51	15.8	.096

Table F.1 cont.

Run No.	q $m^3/s/m$	Δq $m^3/s/m$	G_{ST} N/m	G_{SC} N/m	t^* min	g_s^* N/s/m
07	.128	.098	218	78	14.8	.133
08	.140	.110	227	92	12.5	.180
SC0917	.159	.129	238	104	8.8	.258

Bedload Yields G_{ST} and G_{SC} taken between $0 \leqslant t \leqslant t^*$

Table F.2 : Change in Dune Bedform Volume ($0 \leqslant t \leqslant t^*$)

Run No.	$\bar{\Delta}_d(t^*)$ mm	$\bar{\lambda}_d(t^*)$ m	(a) Change in Dune Vol. $\Delta(\bar{\lambda}_d.\bar{\Delta}_d - D_{50})/16$ m^3/m	(b) Transported Vol. V_s m^3/m	$V_s.\frac{\bar{\Delta}_d}{D_{50}}$ m^3/m	Ratio $\frac{(a)}{(b)}$
SC0393	4	1.47	$.173 \times 10^{-3}$	2.44×10^{-3}	.0046	14.1
04	7	1.20	.367	4.51	.0160	12.3
05	10.5	1.0	.524	5.89	.0293	11.3
06	14	0.95	.706	6.57	.0436	9.3
07	17	0.94	.875	7.82	.0630	8.9
08	20	1.0	1.12	9.14	.0866	8.2
SC0993	23	1.05	1.37×10^{-3}	9.52×10^{-3}	.104	6.9

F.2 TRANSLATION WAVES

F.2.1 Comparable and Actual Transport Rates

The following figures display both the comparable steady flow transport rate curve and the smoothed translation wave transport rate hydrograph for all the successful waves routed over the five test reach lengths. Detailed tabulated results of transport rates and the comparison procedure are available on request from the Dept. of Civil Engineering, University of Canterbury.

Table F.3 : Wave Bedload Yields and Strouhal Numbers

Run No.	Wave Bedload Yield G_{NS} (N/m)	Bedload Yield Ratio G^*_{ST}/G_{NS}	Strouhal Nos. $\frac{y_c}{u_{*_b}(\max)T}$ (x 10^{-4})	Strouhal Nos. $\frac{y_c^2}{q_{max}.T}$ (x 10^{-6})
NS0893	944	1.07	1.53	3.92
06	579	1.19	2.35	5.99
04	299	1.17	4.76	12.3
02	125	1.41	9.59	24.4
07	215	1.24	1.81	6.59
05	145	1.31	2.72	9.80
03	72	1.36	5.40	19.1
NS0193	46	1.39	10.6	34.6
NS0853	839	1.14	1.61	4.31
06	538	1.23	2.42	6.45
04	278	1.26	4.86	12.8
02	106	1.72	9.79	25.9
03	76	1.31	5.61	20.7
NS0153	44	1.49	10.9	37.3

Table F.3 cont.

Run No.	Wave Bedload Yield G_{NS} (N/m)	Bedload Yield Ratio G^*_{ST}/G_{NS}	Strouhal Nos. $\frac{y_c}{u_{*_b}(max)T}$ ($\times 10^{-4}$)	Strouhal Nos. $\frac{y_c^2}{q_{max}.T}$ ($\times 10^{-6}$)
NS0835	735	1.23	1.63	4.53
06	550	1.23	2.42	6.51
04	248	1.36	5.02	13.8
02	84	2.06	10.2	28.6
07	173	1.53	1.89	7.18
03	55	1.69	5.83	22.4
NS0135	28	2.29	11.3	40.5
NS0817	557	1.32	1.57	4.35
06	393	1.30	2.39	6.66
04	226	1.40	4.88	13.4
02	74	2.31	9.74	26.2
07	170	1.36	1.84	6.94
05	113	1.45	2.75	10.3
03	45	2.12	5.56	20.8
NS0117	26	2.49	10.9	38.2
NS0807	293	1.06	1.49	4.01
06	255	1.23	2.24	5.92
04	212	1.08	4.49	11.7
02	147	1.06	9.26	23.7
07	140	1.32	1.75	6.38
05	105	1.32	2.61	9.35
03	84	1.01	5.26	18.6
NS0107	58	1.08	10.4	33.9

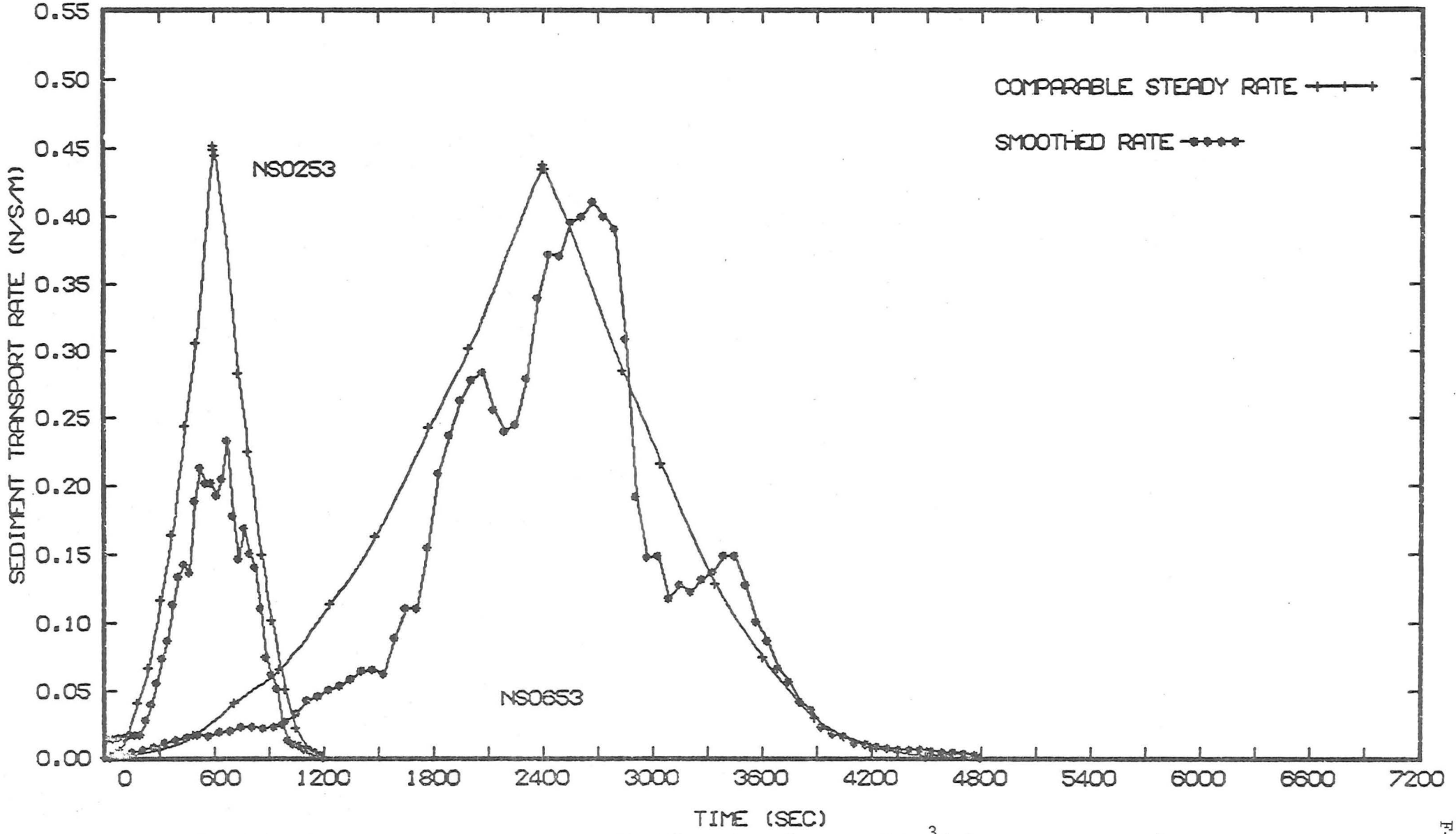

FIGURE F.1 (a) : Comparable transport rates, NS--53 series, (q_{max} = .16 $m^3/s/m$, T = 20, 80 min)

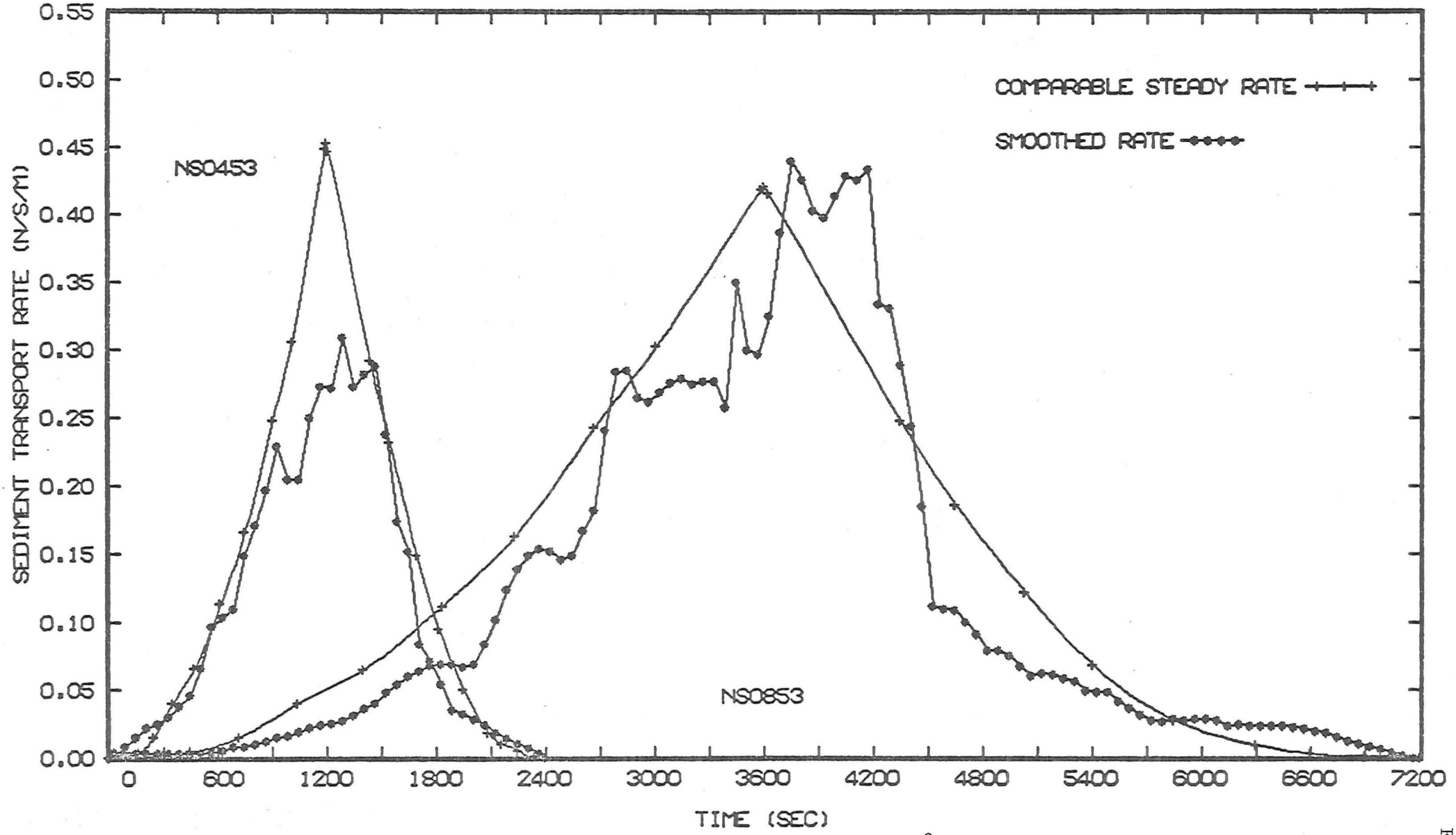

FIGURE F.1 (b) : Comparable transport rates, NS--53 series, (q_{max} = .16 $m^3/s/m$, T = 40, 120 min)

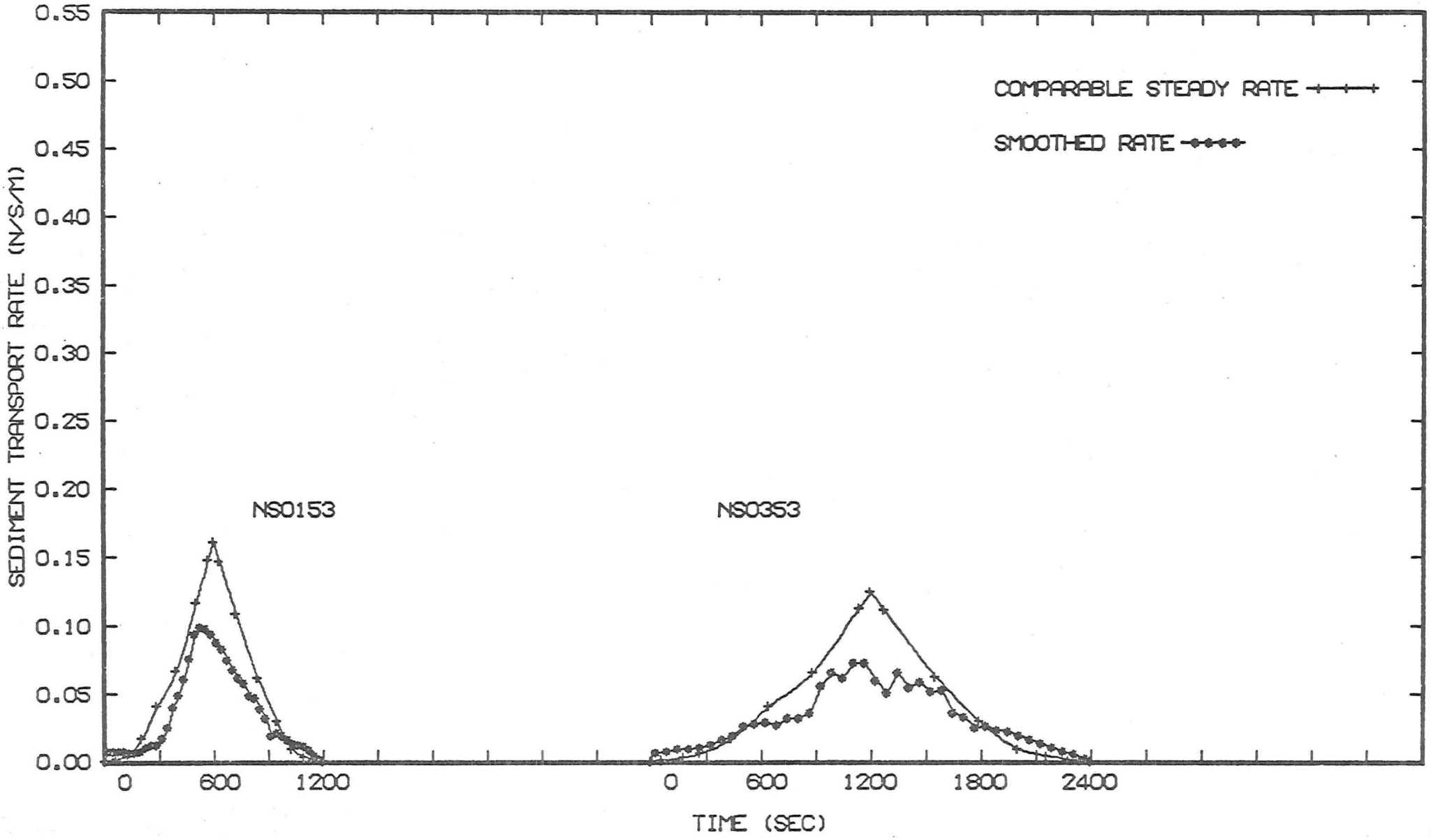

FIGURE F.1 (c) : Comparable transport rates, NS--53 series, (q_{max} = .11, .10 $m^3/s/m$, T = 20, 40 min)

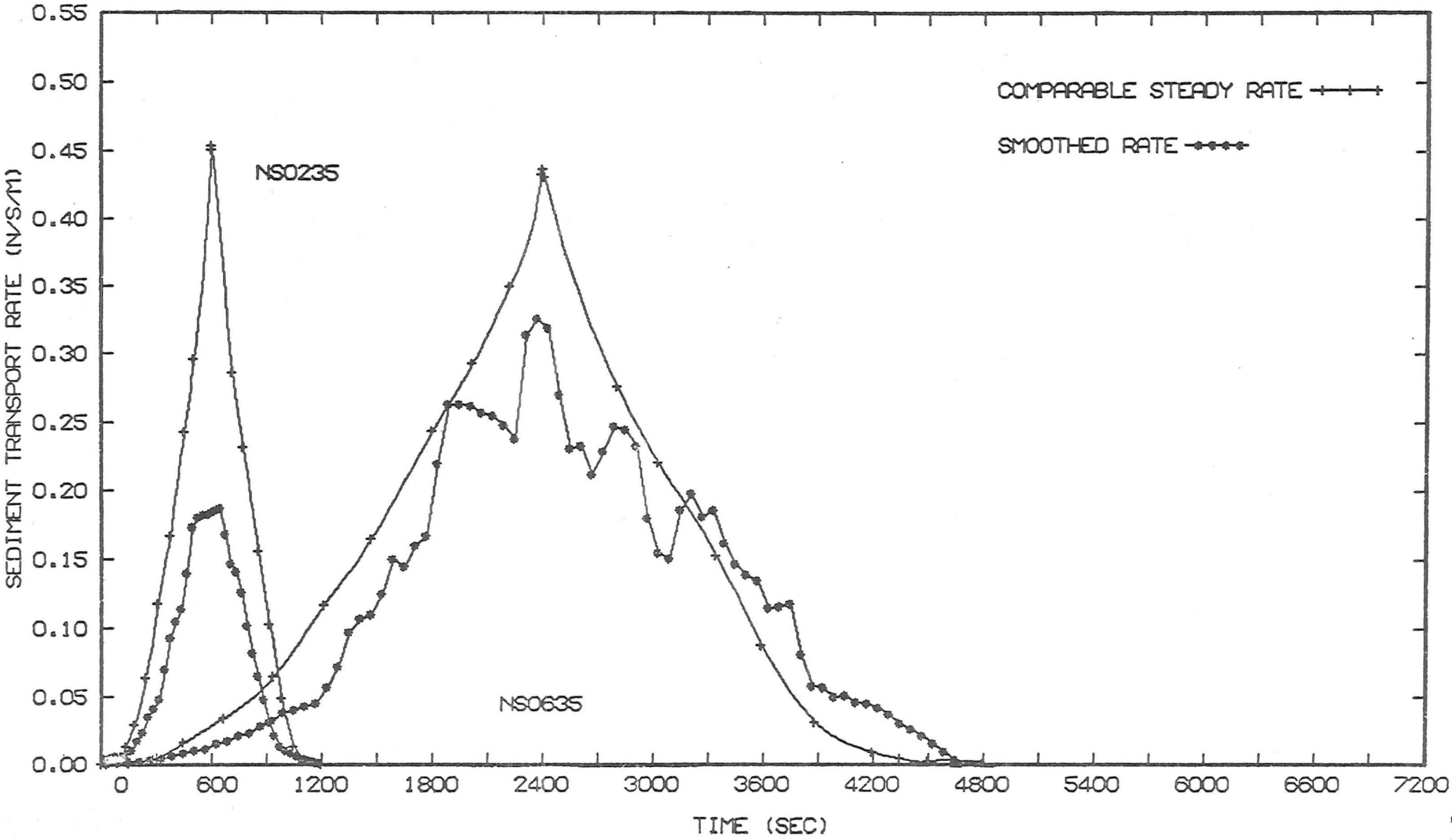

FIGURE F.2 (a) : Comparable transport rates, NS--35 series, (q_{max} = .16 $m^3/s/m$, T = 20, 80 min)

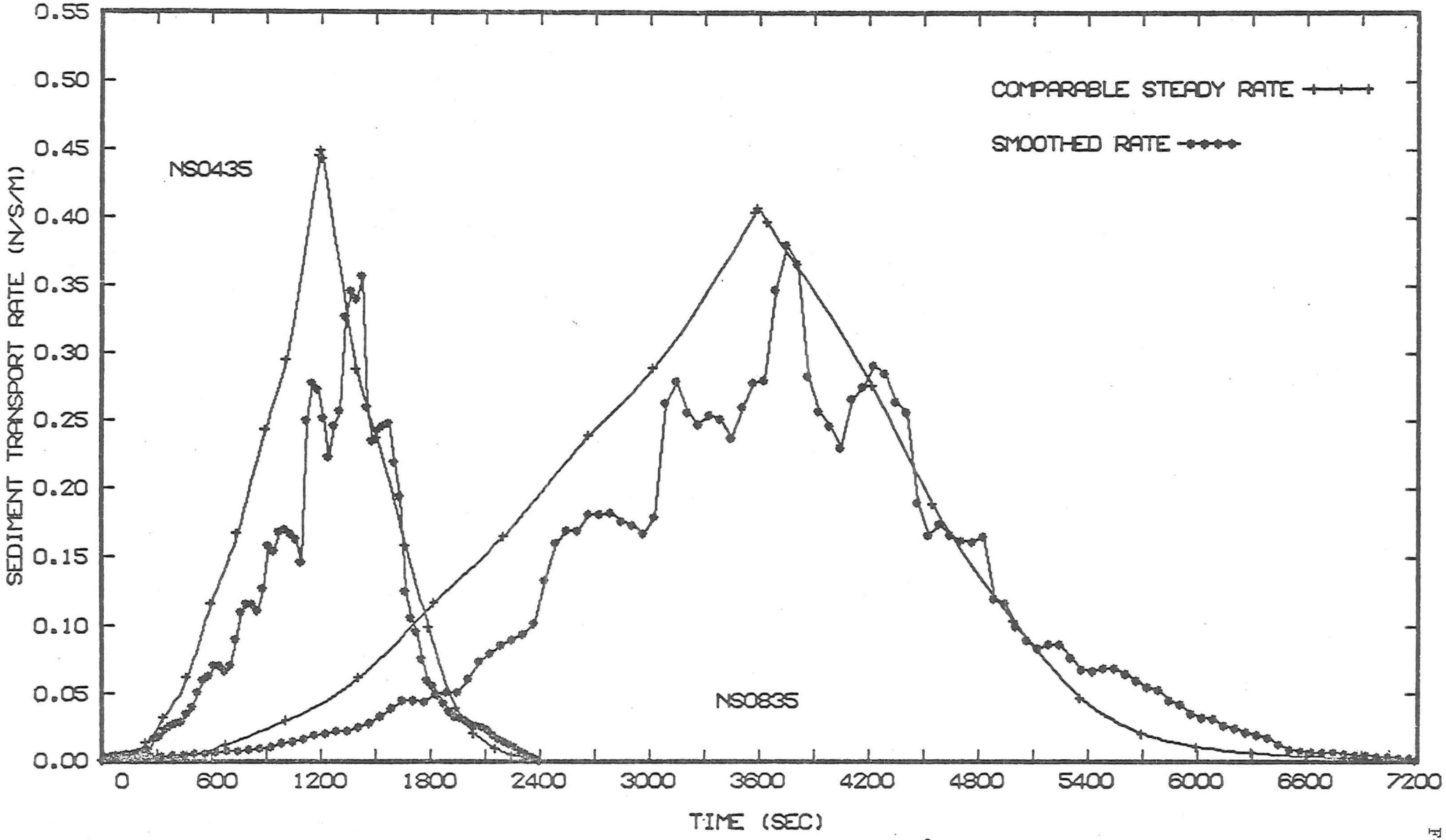

FIGURE F.2 (b) : Comparable transport rates, NS--35 series, (q_{max} = .16 $m^3/s/m$, T = 40, 120 min)

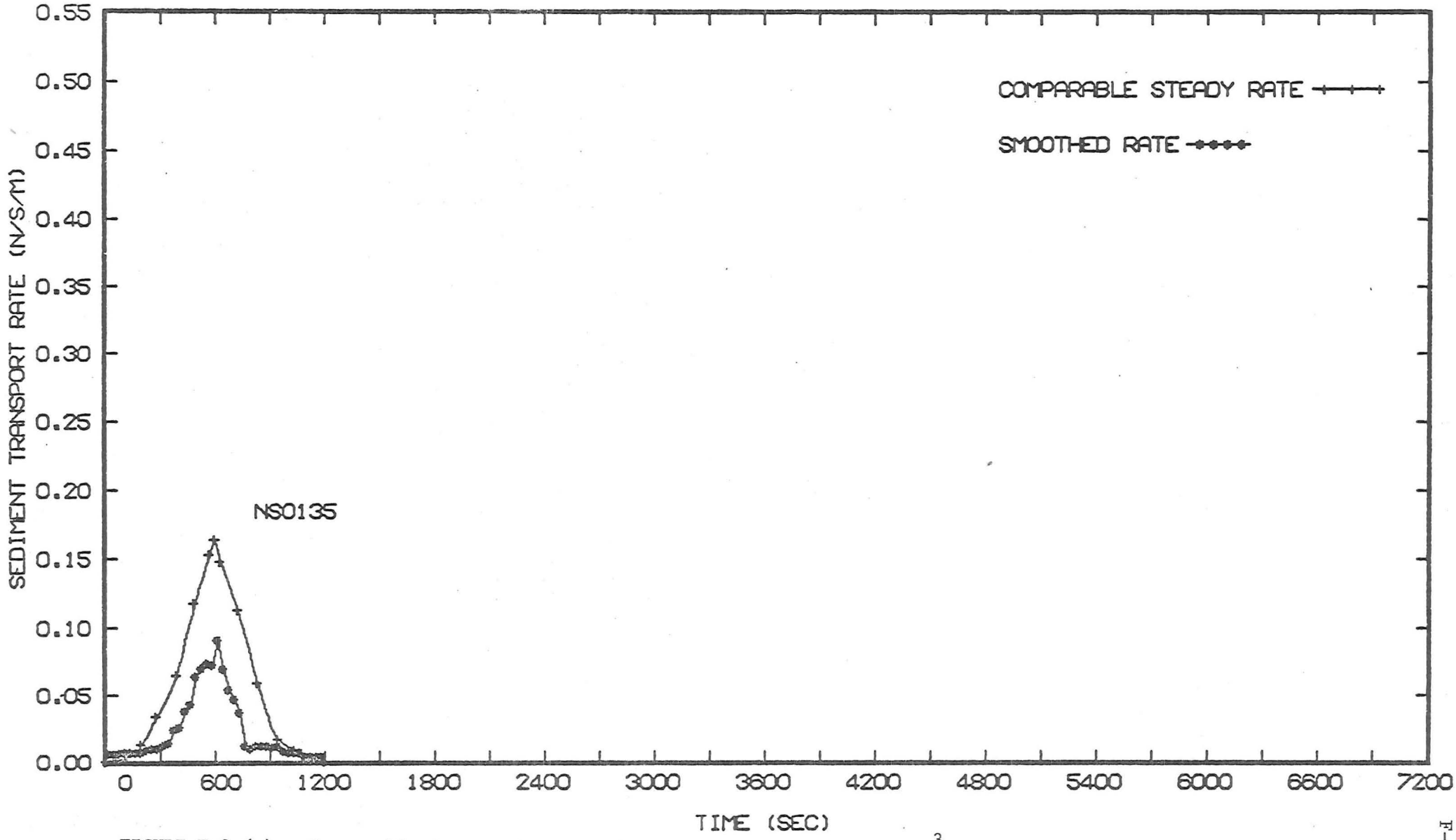

FIGURE F.2 (c) : Comparable transport rates, NS--35 series, (q_{max} = .11 m^3/s/m, T = 20 min)

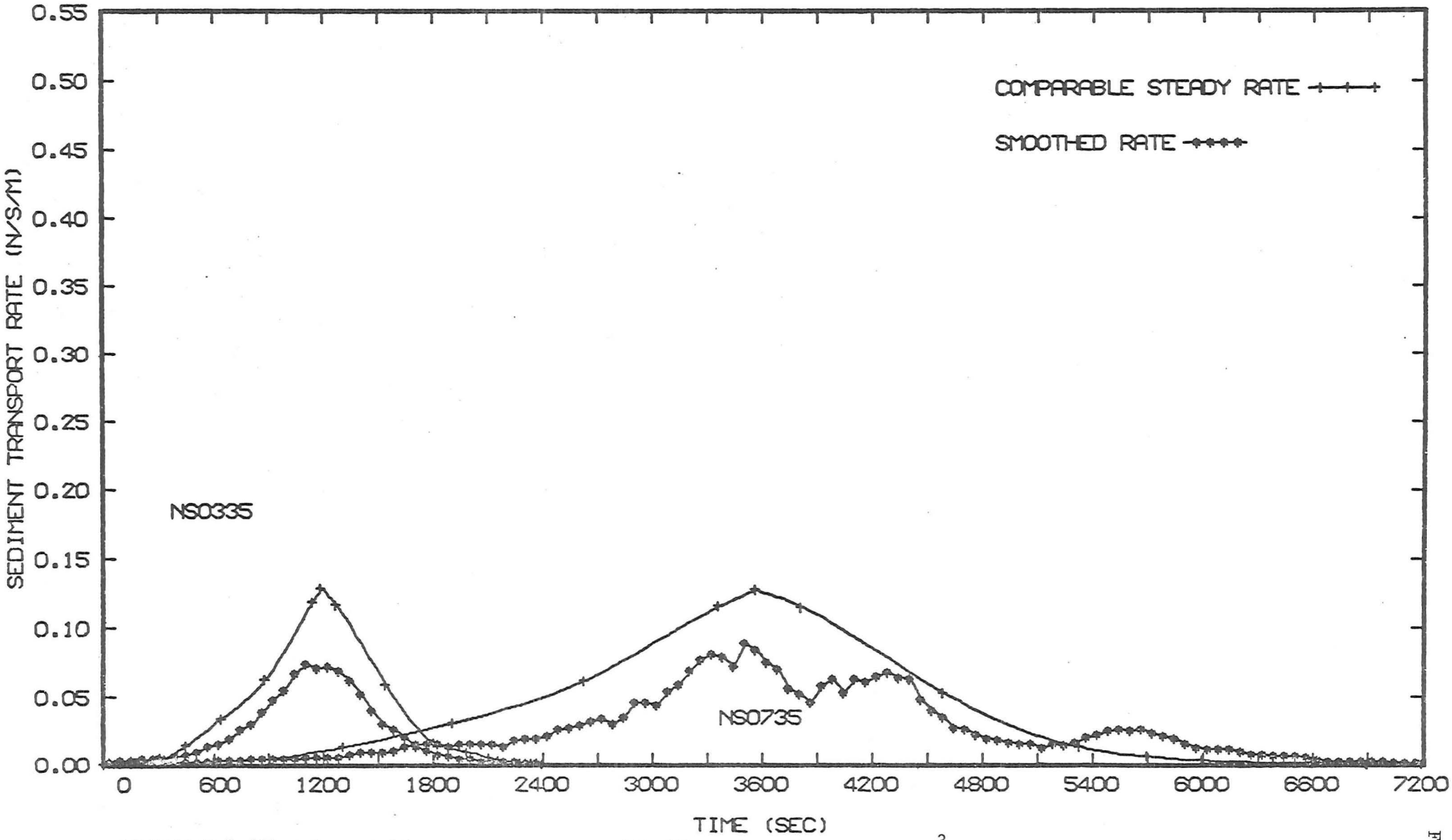

FIGURE F.2 (d) : Comparable transport rates, NS--35 series, (q_{max} = .10 m^3/s/m, T = 40, 120 min)

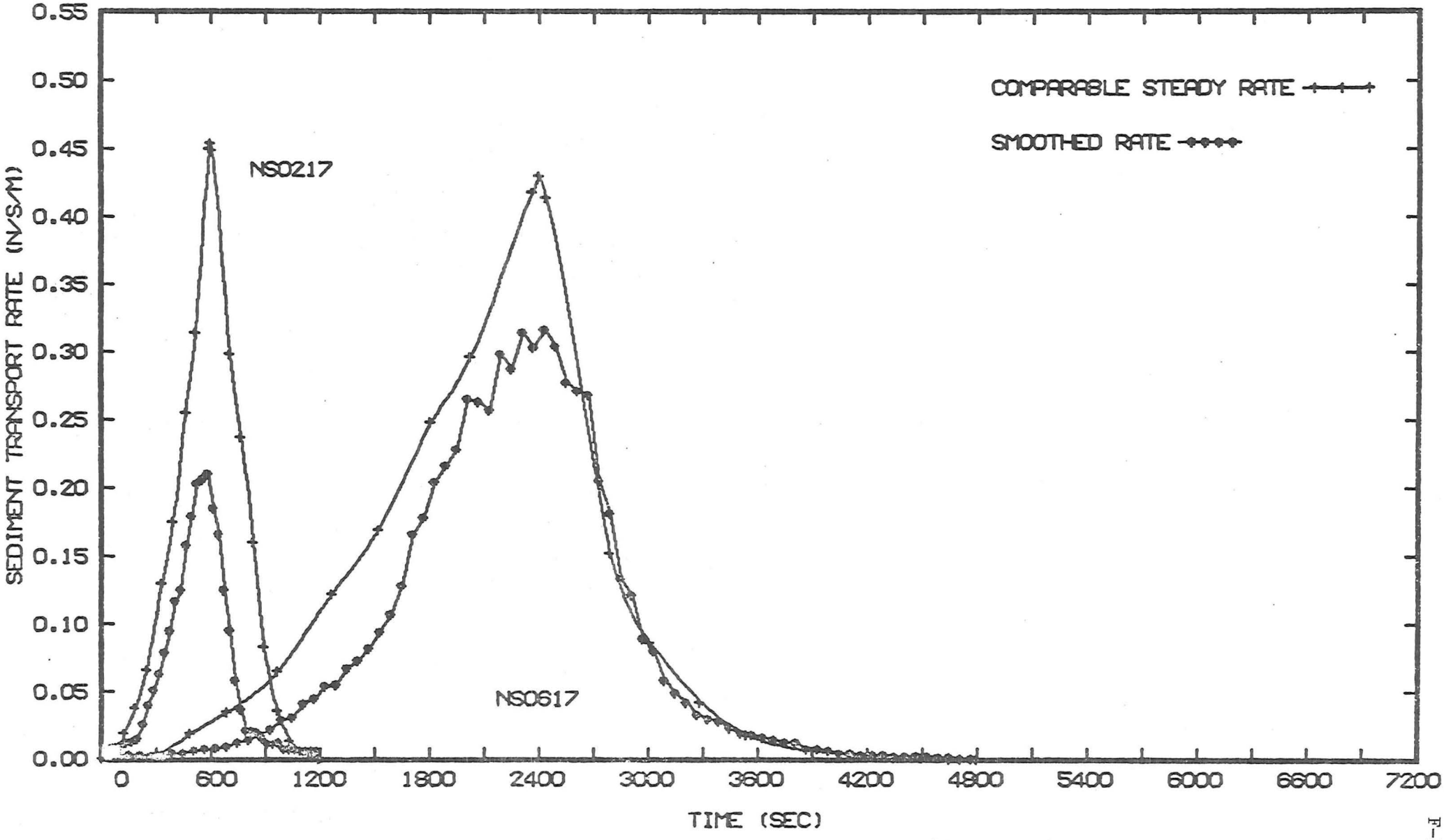

FIGURE F.3 (a) : Comparable transport rates, NS--17 series, (q_{max} = .16 $m^3/s/m$, T = 20, 80 mins)

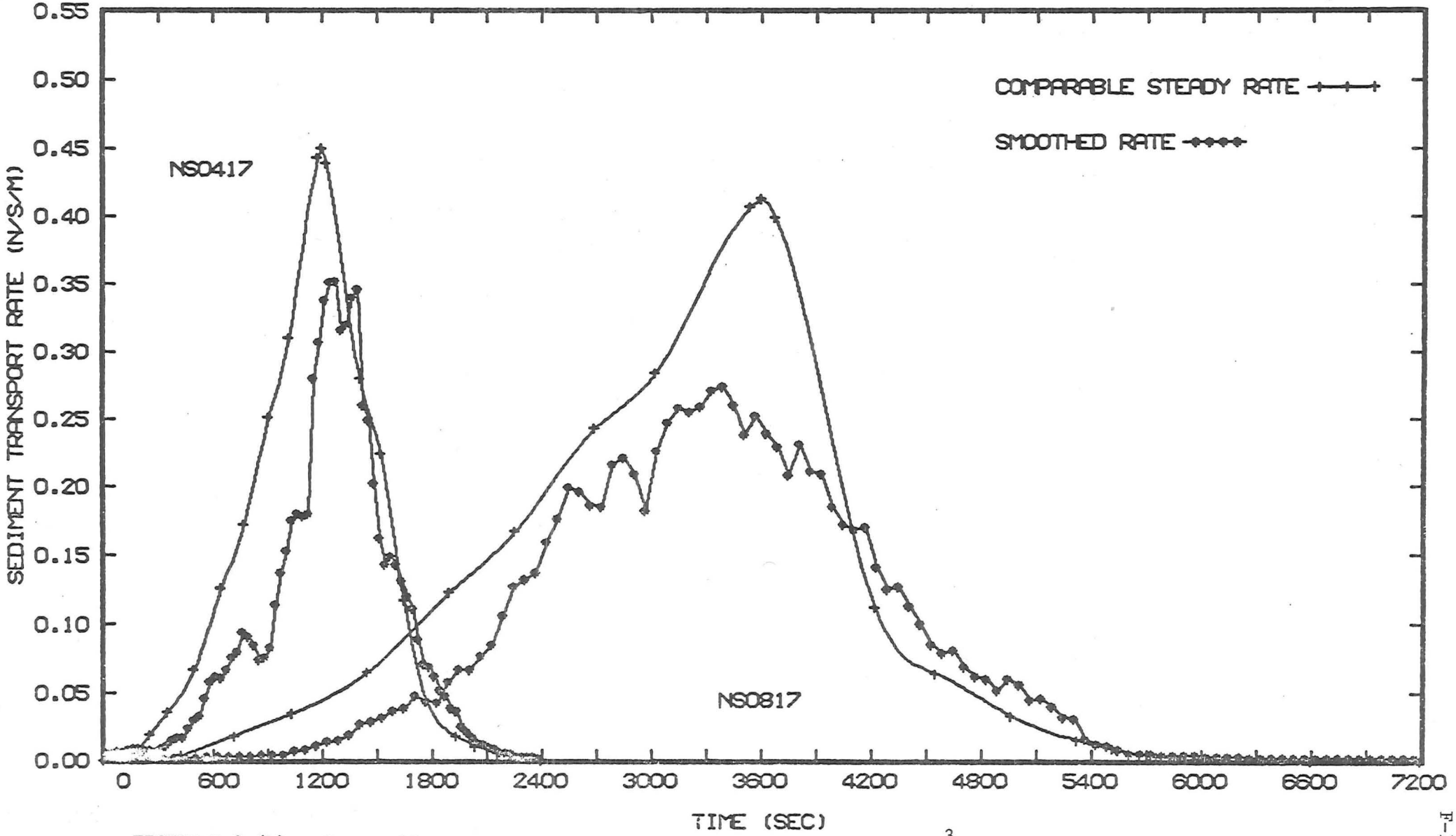

FIGURE F.3 (b) : Comparable transport rates, NS--17 series, (q_{max} = .16 m^3/s/m, T = 40, 120 min)

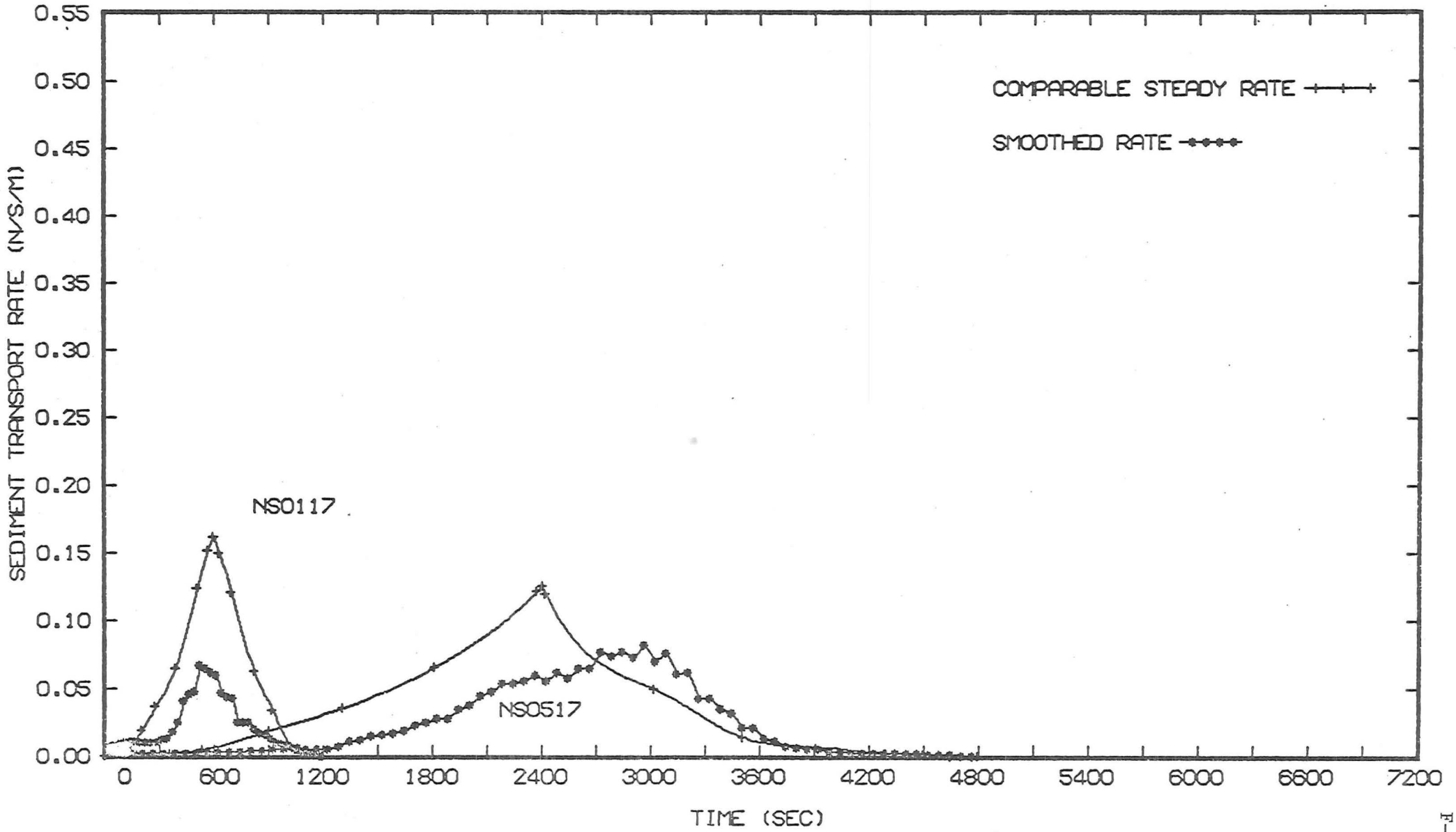

FIGURE F.3 (c) : Comparable transport rates, NS--17 series, (q_{max} = .11, .10 $m^3/s/m$, T = 20, 80 min)

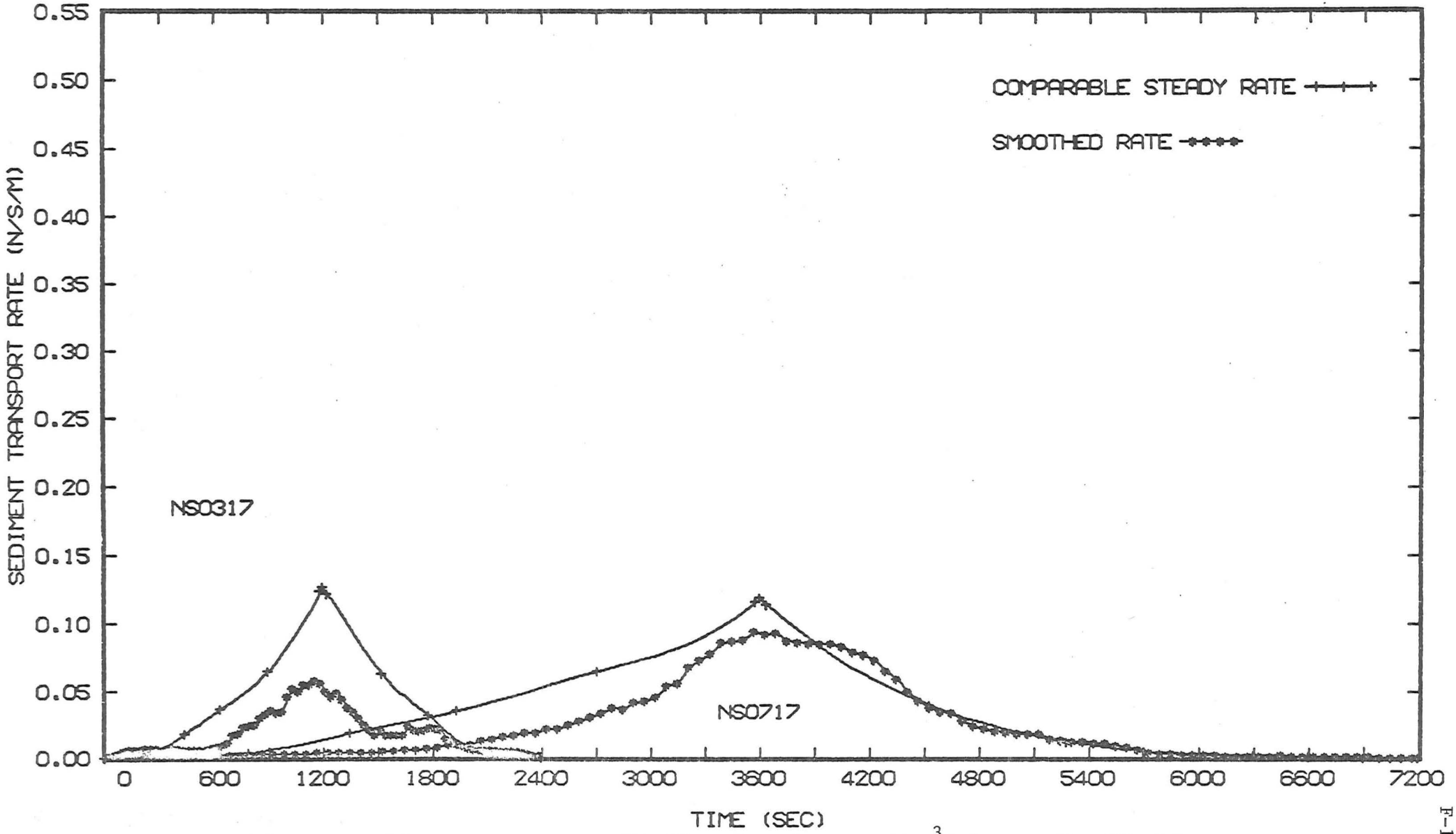

FIGURE F.3 (d) : Comparable transport rates, NS--17 series, (q_{max} = .10 m^3/s/m, T = 40, 120 min)

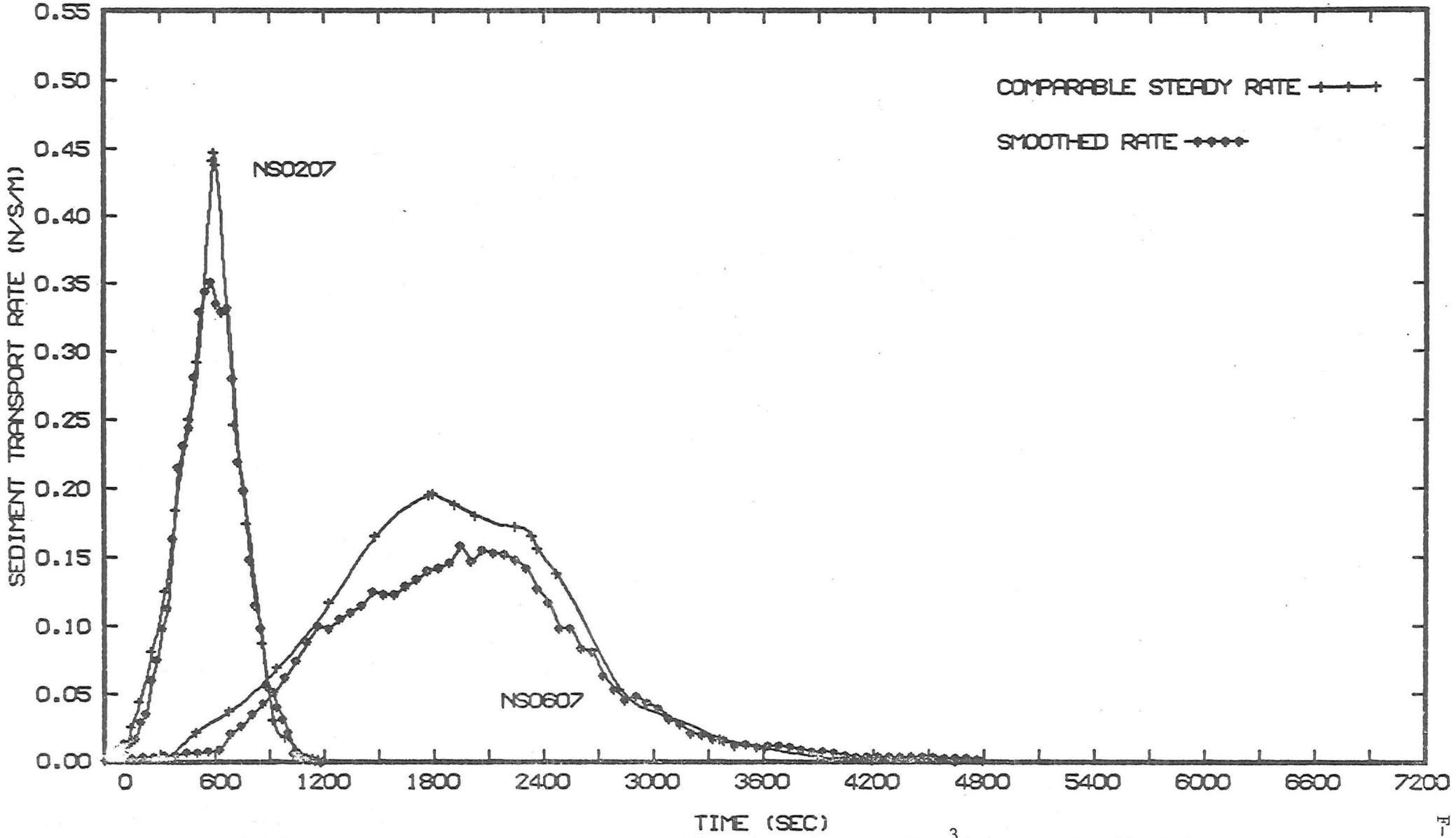

FIGURE F.4 (a) : Comparable transport rates, NS--07 series, (q_{max} = .16 $m^3/s/m$, T = 20, 80 min)

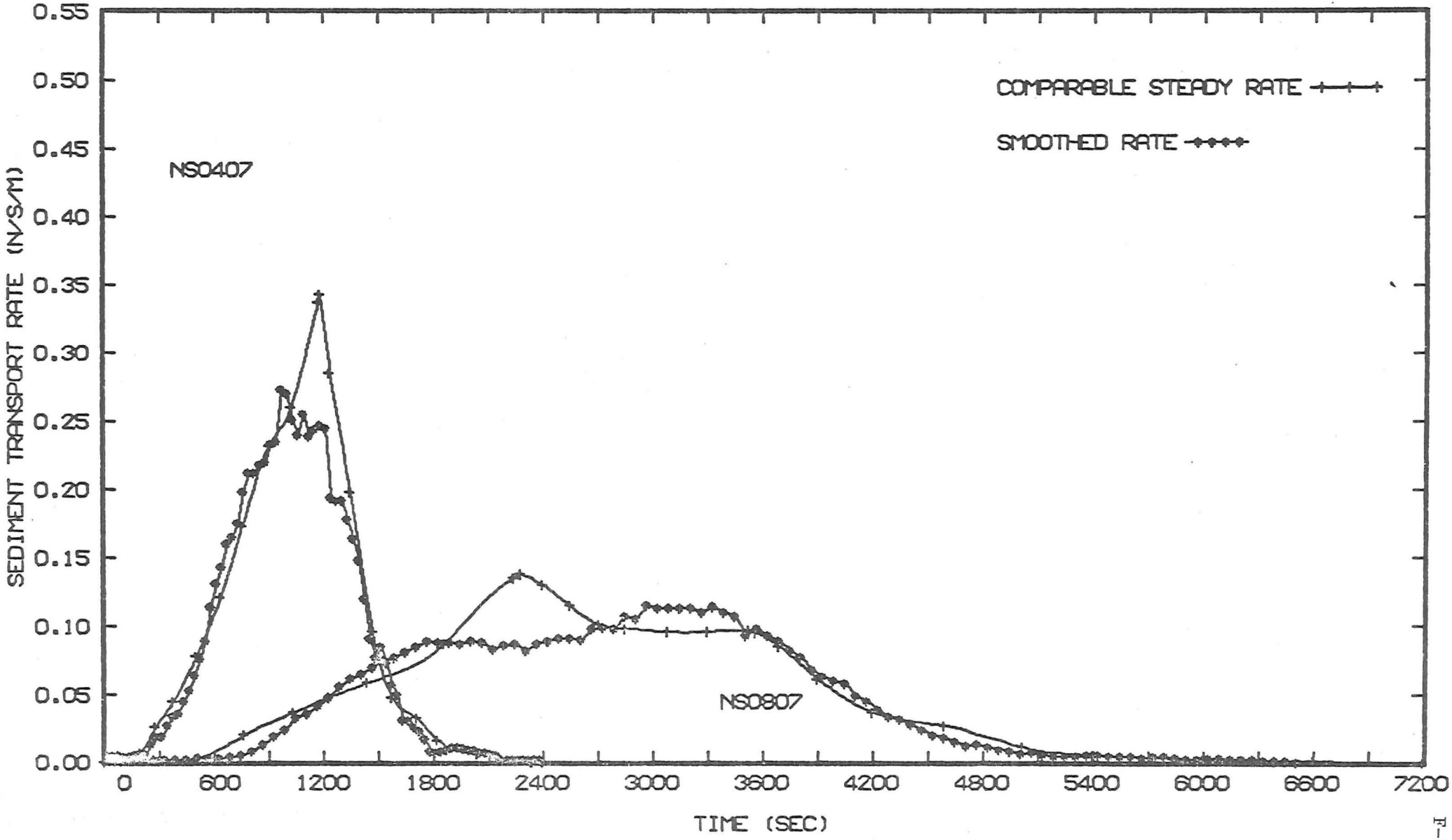

FIGURE F.4 (b) : Comparable transport rates, NS--07 series, (q_{max} = .16 $m^3/s/m$, T = 40, 120 min)

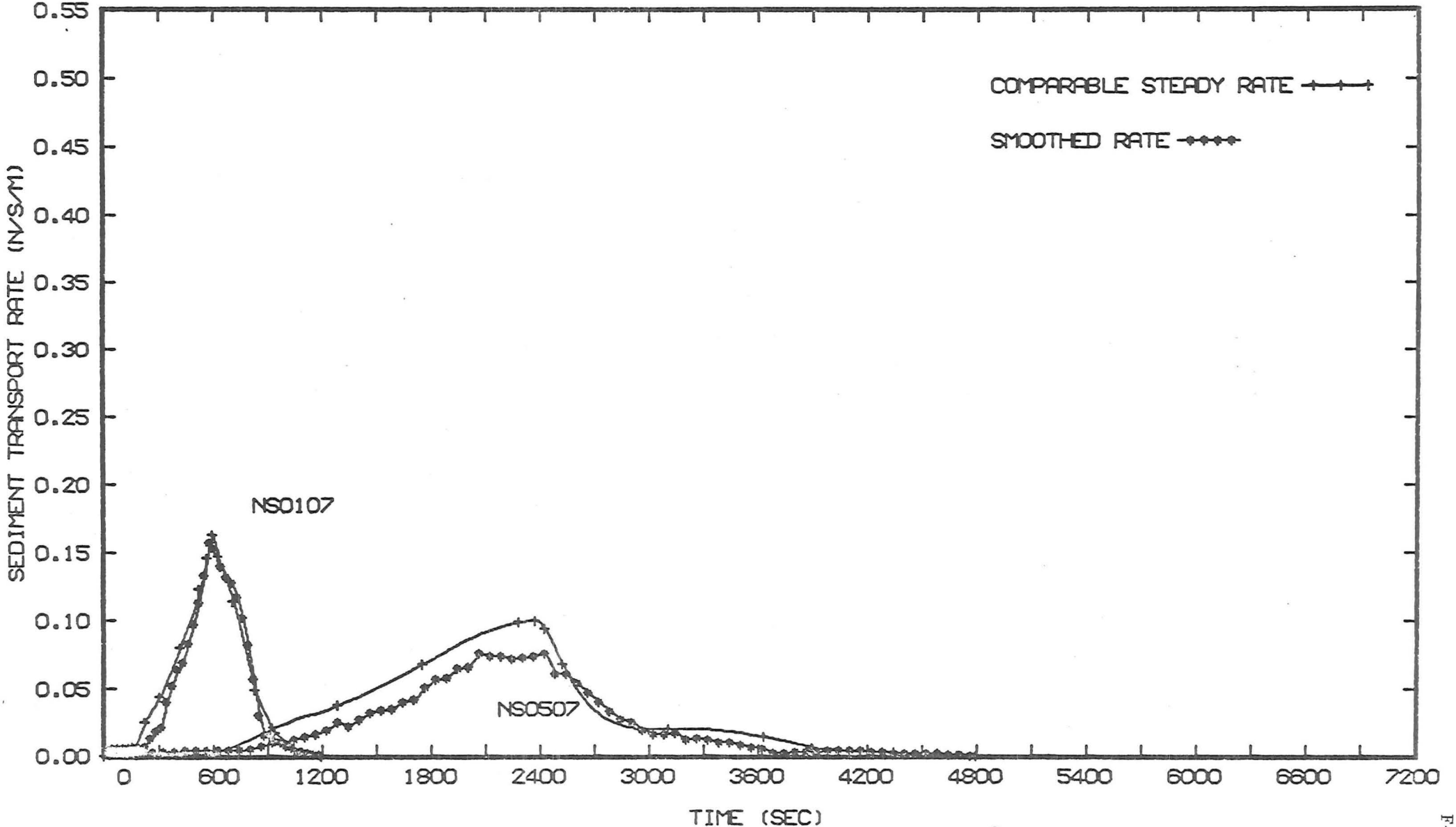

FIGURE F.4 (c) : Comparable transport rates, NS--07 series, (q_{max} = .11, .10 $m^3/s/m$, T = 20, 80 min)

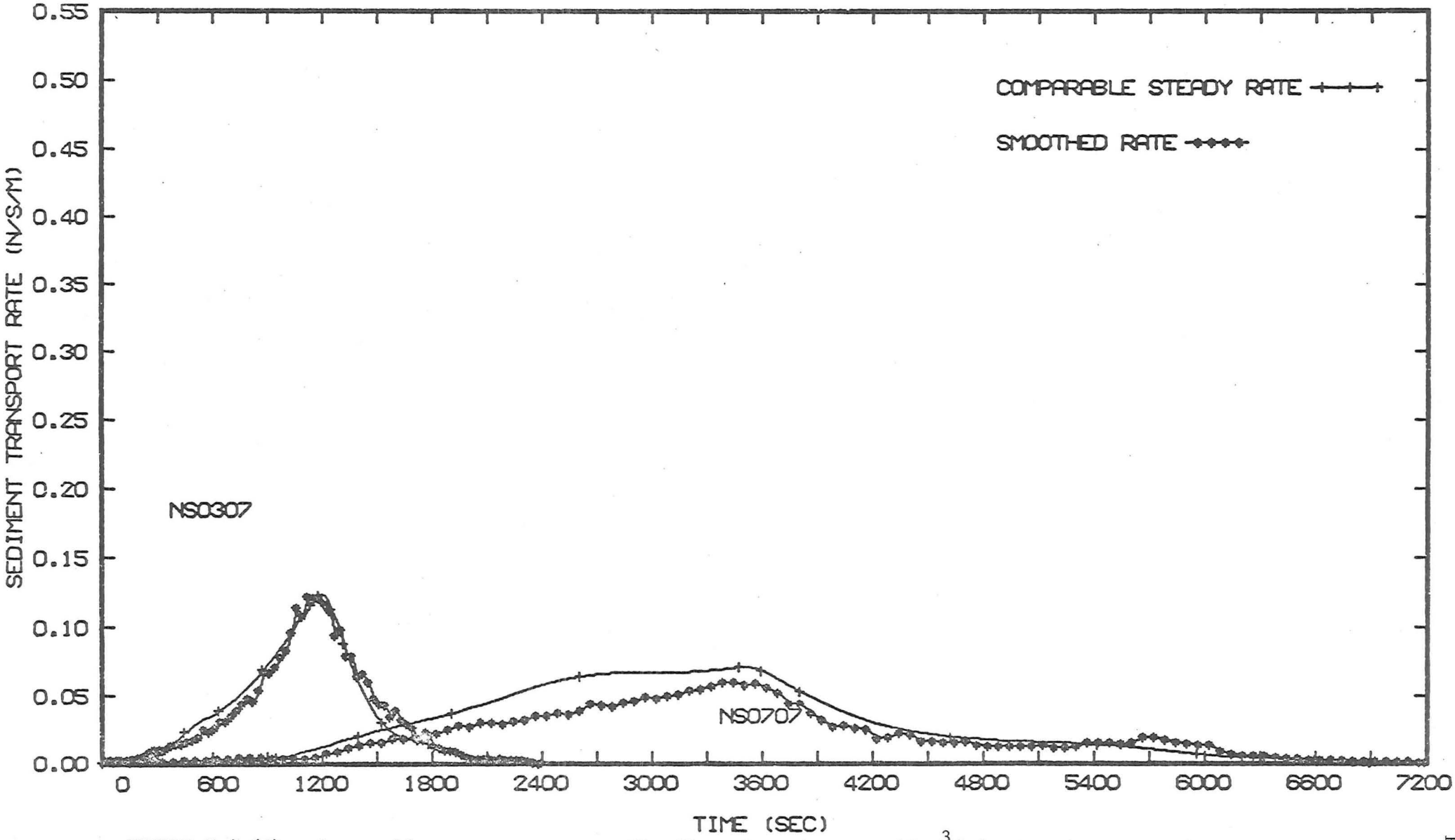

FIGURE F.4 (d) : Comparable transport rates, NS--07 series, (q_{max} = .10 $m^3/s/m$, T = 40, 120 min)

Table F.4 : Dimensionless Wave Yield and Strouhal Numbers

Run No.	$\frac{q_{max}}{q_c}$	$\frac{u_{*_b}(max).T}{y_{max}}$ $(\times 10^3)$	$\frac{G_{NS}}{D_{50}\, y_{max}\, P_s}$
NS0893	5.33	2.06	133.9
06	5.33	1.39	84.7
04	5.33	.696	43.6
02	5.33	.353	18.8
07	3.33	2.45	41.9
05	3.33	1.65	28.7
03	3.33	.827	14.4
NS0193	3.66	.404	8.9
NS2893	5.33	1.23	87.8
Griffiths (1976)			
W1	4.14	.400	10.8
W2	4.14	.793	18.7
W3	4.14	1.61	46.5
W4	2.63	.484	3.92
W5	2.63	.966	6.16
W6	2.63	1.92	17.1

F.2.2 Bedform Geometric Properties

Table F.5 : Dune Bedform Geometric Properties

← Measured →				← Comparable Steady Flow) →		
Run No.	$\bar{t}$ min	$\bar{\Delta}_d$ mm	$\bar{\lambda}_d$ m	q^{ST} $m^3/s/m$	t_1^{NS} min	$\bar{\Delta}_d^{ST}$ mm
				.068	3.0	5.0
	7	0	-	.082	4.1	8.5
	8.4	8.7	0.70	.097	5.3	11.9
				.112	6.5	14
	9.4	11.1	0.72	.127	7.7	17
	10.5	13.4	0.73	.140	8.5	20
	13.5	10.2	0.81	.159	10.0	24
NS0293	14.5	9.9	0.78	.140	11.6	20.8
	17.5	9.5	1.20	.127	12.6	17
				.112	13.7	14.2
				.097	14.9	12.5
				.082	16.0	8.8
				.068	17.1	4.8
				.068	6.0	5
				.082	8.1	8.5
	10	0	-	.097	10.5	12
	10.8	2.6	1.70	.112	12.7	14
	17	13.3	0.70	.127	15.2	17
	21.8	16.2	0.77	.140	17.1	20
	26.6	15.2	0.90	.140	23.2	21
NS0493	31.6	10.7	0.97	.127	25.2	17
	36.5	8.4	1.21	.112	27.6	14.3

Table F.5 cont.

← Measured →				← Comparable (Steady Flow) →		
Run No.	$\bar{t}$ min	$\bar{\Delta}_d$ mm	$\bar{\lambda}_d$ m	q^{ST} $m^3/s/m$	t_1^{NS} min	$\bar{\Delta}_d^{ST}$ mm
				.097	30.0	12.6
	40.0	7.2	1.14	.082	32.4	8.8
				.068	34.8	4.7
				.068	11.8	5
	16.0	0	-	.082	15.9	8.5
	21.9	8.0	0.84	.097	20.9	11.5
	31.9	14.1	0.81	.112	25.2	14.7
	36.9	13.7	0.70	.127	30.2	17.0
	41.8	15.2	0.77	.140	34.6	20.5
NS0693	46.6	14.3	1.02	.159	39.7	23.5
	53.5	13.2	1.02	.127	51.0	17.2
	61.0	14.1	1.32	.112	55.6	14.1
	71.0	9.2	1.29	.097	59.8	11.6
				.082	64.5	8.0
				.068	68.8	4.5
				.068	18.1	5
	29.5	4.3	1.32	.082	24.4	8.5
	36.3	9.7	.89	.097	31.9	11.5
	42.8	14.6	.91	.112	38.4	14.3
	49.9	13.3	1.08	.127	45.1	17.5
	55.5	15.4	.82	.140	52.1	20.3
	60.3	22.7	1.16	.159	59.5	23.6
NS0893	71.5	19.1	.92	.140	69.0	19.1
	76.3	16.6	1.07	.127	76.4	16.1

Table F.5 cont.

← Measured →				← Comparable (Steady Flow) →		
Run No.	t min	$\bar{\Delta}_d$ mm	$\bar{\lambda}_d$ m	q^{ST} $m^3/s/m$	t_1^{NS} min	$\bar{\Delta}_d^{ST}$ mm
				.112	83.3	15
	80.0	16.5	1.41	.097	89.9	12
	94.5	11.9	1.53	.082	97.0	8
				.068	103.2	4.4

Table F.6 : Dune Celerities During NS0493

t min	y m	q $m^3/s/m$	$\bar{u}$ m/s	C_d mm/s
12.5	.1608	.111	.692	3.40
				2.81
14.5	.1725	.124	.721	3.62
15.5	.1783	.131	.733	3.12
17.5	.1870	.143	.765	3.73
18.5	.1915	.150	.785	3.36
19.5	.1956	.157	.801	3.60
21.5	.1930	.150	.779	2.69
22.5	.1900	.144	.750	2.46
				2.48
26.3	.1692	.119	.706	2.39
27.5	.1610	.111	.691	1.57
30.8	.1422	.090	.633	1.13

F.2.3 Stage-Discharge Relations

Table F.7 : Stage-Discharge Curves (NS0835 and NS0235)

	Steady Flow	NS0835		NS0235	
Discharge q $m^3/s/m$	Stage h^{ST} m	Rising Stage m	Falling Stage m	Rising Stage m	Falling Stage m
.03	.163	.163	.164	.164	.171
.05	.188	.189	.190	.185	.195
.07	.211	.212	.213	.209	.218
.09	.232	.232	.233	.231	.238
.11	.251	.251	.252	.251	.257
.13	.270	.269	.272	.270	.274
.14	.279	.278	.282	.278	.282
.15	.288	.286	.289	.286	.288
.16	.296	.297	.297	.294	.294

(measured at recorder site x = 3.25 m)